A GEO-THERMOCHRONOLOGICAL STUDY OFFSHORE WEST OF IRELAND:

the timing of exhumation and magmatic activity and the nature of the basement on the Irish Atlantic Margin

PhD Thesis

2021

Rémi Rateau

Annexes 1 and 2

Trinity College Dublin
Coláiste na Tríonóide, Baile Átha Cliath
The University of Dublin

Contents

1 ANNEXE 1: DESCRIPTION OF THE U/PB, AFT/AHE RESULTS AND MISCELLANEOUS BOREHOLE STUDIES ..6

1.1 DETAILED ANALYSIS OF THE U/PB AND TRACE ELEMENT RESULTS 6
1.1.1 Goban Spur 6
1.1.2 North Porcupine High 19
1.1.3 Miscellaneous locations 29
1.2 ANALYSIS OF THE AFT AND AHE RESULTS 45
1.2.1 Goban Spur 45
1.2.2 North Porcupine High 53
1.2.3 Miscellaneous locations 73
1.3 SONIC AND VR DATA FOR EXHUMATION ESTIMATES 85
1.3.1 34/05-1 85
1.3.2 26/26-1 95
1.3.3 26/30-1 98
1.4 AGE OF THE IGNEOUS ROCKS IN BOREHOLE 35/15-1 103
1.4.1 Cuttings and logs interpretation 103
1.4.2 Age of the mafic rocks 105
1.5 34/05-1 - IGNEOUS INTRUSION(S) 107
1.5.1 Geochemical and optical anomalies 107
1.5.2 New interpretation of the logs and geological data 108
1.6 34/05-1 - AGE AND SIGNIFICANCE OF THE RED BRICK CLASTIC UNIT 115
1.7 DISCUSSION: WHICH SAMPLES ARE IN-SITU? 118
1.7.1 Introduction 118
1.7.2 C-MeBo: In-situ 119
1.7.3 C-MeBo2: Near in-situ 119
1.7.4 C-PH1 to C-PH14: In-situ 119
1.7.5 HG1 samples, C-402-1, C-402-8, C-402-11: Not in-situ 121
1.7.6 HG-2 samples, C-303-1, C-402-3: Not in-situ 121
1.7.7 C-402-4, 9 and 13: Possibly in-situ 123
1.7.8 C-204-1, C-402-6: Possibly in-situ 123
1.7.9 C-302-1: Possibly in-situ 123
1.7.10 In situ nature of the 2014 dredges - conclusions 123
1.8 REFERENCES 125

2 ANNEXE 2 - THERMAL HISTORY MODELS 129

2.1 INTRODUCTION 129
2.2 NORTHERN ZONE 130
2.2.1 13/03-1 130
2.3 CENTRAL ZONE 135
2.3.1 16/28-sb01 135
2.3.2 26/26-1 143
2.3.3 34/05-1 151

2.3.4 C-PH4-12 ..... *159*
2.3.5 C-MeBo *163*
1.1. C-MeBo2 ..... *166*
2.3.6 26/30-1 ..... *173*
2.4 SOUTHERN ZONE 180
2.4.1 Stability of the log likelihood and posterior chains *180*
2.4.2 R-24 ..... *181*
2.4.3 R-25 ..... *185*
2.4.4 R-26 ..... *186*
2.4.5 R-27 ..... *190*
2.4.6 R-28 ..... *192*

List of figures

FIGURE 1: ZIRCON AND APATITE U/PB AGES AND APATITE TRACE ELEMENT BIPLOT RESULTS FOR SAMPLE R-24 (GRANITE CLIFF 4000). 7
FIGURE 2: ZIRCON AND APATITE U/PB AGES AND APATITE TRACE ELEMENTS FOR SAMPLE R-25 (GRANITE CLIFF 4000). 9
FIGURE 3: ZIRCON AND APATITE U/PB AGES AND APATITE TRACE ELEMENTS FOR SAMPLE R-26 (GRANITE CLIFF 4000). 11
FIGURE 4: ZIRCON U/PB CONCAGE OF COMBINED SAMPLE R-24-26 (GRANITE CLIFF 4000). 12
FIGURE 5: ZIRCON AND APATITE U/PB AGES AND APATITE TRACE ELEMENTS FOR SAMPLE R-27 (MENEZ BIHAN). 14
FIGURE 6: PHOTOS OF SAMPLE R-27 WITH POSSIBLE LOCATION OF AN HYDROTHERMAL/APLITIC VEIN. 15
FIGURE 7: ZIRCON AND APATITE U/PB AGES AND APATITE TRACE ELEMENTS FOR SAMPLE R-28 (MENEZ BIHAN). 17
FIGURE 8: ZIRCON AND APATITE U/PB AGES AND APATITE TRACE ELEMENTS FOR SAMPLE R-29 (GOBAN SPUR PLATEAU). 18
FIGURE 9: ZIRCON U/PB RESULTS FOR SAMPLE R-3 (16/28-SB01). A) WETHERILL PLOTS, B) DENSITY PLOTS AND KDES 19
FIGURE 10: ZIRCON U/PB RESULTS FOR SAMPLE R-5 (16/28-SB01). A) & C) WETHERILL PLOTS, B) DENSITY PLOTS AND KDES. 20
FIGURE 11: ZIRCON U/PB RESULTS FOR SAMPLES R-7 AND R-8 (26/26-1). A) WETHERILL PLOTS, B) DENSITY PLOTS AND KDE, C) ZIRCON U/PB DENSITY PLOT AND KDE OF BASEMENT SAMPLE IN 26/26-1, THE PHMS DREDGE SAMPLES AND THE LOWERMOST DALRADIAN UNITS OF CO. MAYO. 21
FIGURE 12: APATITE U/PB AGES AND APATITE TRACE ELEMENTS FOR SAMPLE R-8 (26/26-1). 24
FIGURE 13: ZIRCON U/PB RESULTS FOR SAMPLE R-10 (34/05-1). 24
FIGURE 14: ZIRCON U/PB RESULTS FOR SAMPLE R-11 (34/05-1). 25
FIGURE 15: APATITE U/PB AND TRACE ELEMENT RESULTS FOR SAMPLE R-12-15 (34/05-1). 26
FIGURE 16: HISTOGRAMS AND KDES OF ^{206}PB/^{238}U AGES (CONCORDANT GRAINS ONLY) FROM SAMPLES R-10, R-11, R-12, R-13-14 AND R-15 (34/05-1). 28
FIGURE 17: ZIRCON U/PB RESULTS FOR SAMPLE R-12-15. 28
FIGURE 18: APATITE U/PB AND TRACE ELEMENT RESULTS FOR SAMPLE R-37 (12/13-1A). 29
FIGURE 19: ZIRCON AND APATITE U/PB AND TRACE ELEMENT RESULTS FOR SAMPLE R-1 (13/03-1). A) APATITES; B) ZIRCONS. 31
FIGURE 20: APATITE U/PB AND TRACE ELEMENT RESULTS FOR SAMPLE R-2 (13/03-1). 32
FIGURE 21: APATITE U/PB AND TRACE ELEMENT RESULTS FOR SAMPLE R-44 (18/25-2) 33

Figure 22: Sample R-68: Apatite and zircon U/Pb dating results and apatite trace element analysis. 35
Figure 23: Sample R-50: Apatite and zircon U/Pb dating results and apatite trace element analysis. 37
Figure 24: Sample R-51: Apatite and zircon U/Pb dating results and apatite trace element analysis. 38
Figure 25: Apatite U/Pb and trace element results for sample R-54 (35/13-1). 39
Figure 26: Apatite U/Pb ages and trace element results for samples R-16, R-18, R-19 combined as one sample (35/15-1). 41
Figure 27: Zircon U/Pb dating of samples R16 to R-19. 43
Figure 28: Distribution of zircon and apatite grains according to U/Pb age and samples. 44
Figure 29: AFT results for the Late Variscan granite samples. Left column: AFT age radial plot, coloured by [C]; right column: Fission track lengths. 46
Figure 30: AFT results for samples R-25, 27 and 29. Left column: AFT age radial plot, coloured by [C]; right column: Fission track lengths. 48
Figure 31: AFT results for legacy samples L-GC777-9 and L-GC777-2, after Green (2001). 55
Figure 32: AFT results for basement sample R-8 (26/26-1). Left: Radial plot colour-coded with Cl concentration. Right: confined track length density plot, KDE and MTL. 58
Figure 33: AFT results for borehole 34/05-1. a) AFT results of sample R-12-14. b) AFT results for sample R-15. ... 64
Figure 34: a) 34/05-1 Carboniferous samples AHe ages vs [U], [Th], [Sm] with AFT [U], [Th], [Sm] histograms and KDEs as background. 66
Figure 35: AFT results for sample C-MeBo (25/7-sb(MeBo)3) and C-MeBo2 (25/27-sb(MeBo)2). a) LAFT radial plots. b) Confined track lengths density plot and KDE function. 68
Figure 36: AFT results for samples C-PH1 to C-PH12 and merged sample C-PH4-12 (LAFT radial plots and confined track length density plots with KDE function) 71
Figure 37: AFT results for sample R-37 (12/13-1A). 74
Figure 38: AFT and AHe results for sample R-1 (13/03-1 Eocene sands) 74
Figure 39: AFT and AHe results for sample R-2 (13/03-1 298 Ma gabbro). 76
Figure 40: AFT results for sample R-44 (18/25-2). 78
Figure 41: AFT data for sample R-68 (26/30-1) 78
Figure 42: AFT results for a) sample R-51 and b) combined sample R-50-51. 81
Figure 43: AFT results for sample R-54 (35/13-1). 81
Figure 44: AFT results summary. a) Results per sample. b) Radial plot of combined sample R-16-19 with chlorine content for colour scale. c) Histograms and KDEs of [U], Dpar and Cl for all the grains in sample R16-19. .. 83
Figure 45: AHe results summary for samples R-17, R-18 and R-19 (35/15-1). 86
Figure 46: Pre-Cenozoic exhumation estimates of 34/05-1 based on sonic velocity. a) Cenozoic and Stephanian intervals (c. 730 and 750 m MD respectively. b) Westphalian B interval (c. 1325 m MD). 88
Figure 47: VR data for borehole 34/05-1 and surrounding wells. 91
Figure 48: Estimates of maximum temperature reached for the VR sample at 1294 m MD with a VR of 1 R_o% (34/05-1). 91

Figure 49: Estimates of maximum temperature reached for the VR sample at 1294 m MD with a VR of 1 R_o% (34/05-1). 92
Figure 50: a) Summary of exhumation estimates at the TCU from sonic velocities and VR data (34/05-1). b) Paleogeothermal gradients required to reach the maximum temperature at 1400 m MD. 94
Figure 51: Sonic-derived exhumation estimates for borehole 26/26-1. 96
Figure 52: Maximum temperatures reached by the VR samples in borehole 26/26-1. 97
Figure 53: Well 26/30 1 stratigraphy, lithology, logs and sample depths. 99
Figure 54: Exhumation estimates from sonic velocities. 100
Figure 55: VR data from 26/30-1 and surrounding wells. 102
Figure 56: Various interpretations of the igneous units from log responses and sample weight and apatite/zircon yields. Based on the apatite yield, interpretation #1 is favoured, where only the top unit is a lava flow and the underlying units are shallow intrusions. The seabed at the time of emplacement would be located at 6470 feet MD. 104
Figure 57: K-Ar results from mafic igneous samples modified after Church et al. (1981). 106
Figure 58: Thermal maturity of organic matter in well 34/05-1 from geochemical and optical studies. a) Plots of vitrinite reflectance (VR), thermal alteration index (TAI) and pyrolysis maximum temperature (T_{MAX}) vs depths. For each VR sample, the minimum, mode and maximum values are plotted. Note the anomaly in VR, TAI and T_{MAX} data between 1320 and 1400 mMD. b) Raw thermal maturity data from the geochemical report (Cailleaux and Robert, 1981). 109
Figure 59: Identification of a doleritic intrusion between 1346 and 1365 mMD in borehole 34/05-1. a) Log responses and location of sidewall cores (SWC). b) Lithology description of sidewall cores and cuttings. c) Model of contact aureoles and CLRsZ from Spacapan et al. (2020). 110
Figure 60: 34/05-1 location of doleritic intrusions between 1200 and 1488 mMD (TD). 111
Figure 61: Determination of the top and bottom boundaries of the red unit based on information from the composite log, mud log and biostratigraphical report of borehole 34/05-1. 115
Figure 62: Possible sources of areas with AFT ages > 266 Ma. 122

List of tables

Table 1: AFT and ZFT results for shallow borehole 16/28-sb01. 54
Table 2: Summary of new AFT and AHe results for well 26/26-1. 56
Table 3: AFT and AHe results for samples R-10 to R-15 (34/05-1). 61
Table 4: Borehole 35/15-1 AFT results. 82
Table 5: Exhumation estimates based on VR-derived maximum temperatures and paleogeothermal gradients. 94
Table 6: Paleo-geothermal gradients required to reach Tmax at c. 1400 m MD with an eroded column of 1.1 to 2.12 km. 94
Table 7: Tmax-based exhumation estimates (in km) for borehole 26/26-1. 97
Table 8: Geological information for all Porcupine High seabed samples, sorted out by AFT ages. 120

1 Annexe 1: Description of the U/Pb, AFT/AHe results and miscellaneous borehole studies

1.1 Detailed analysis of the U/Pb and trace element results

1.1.1 Goban Spur

1.1.1.1 Sample R-24 (Granite)

Zircon U/Pb

The 50 zircon grains yielded 39 concordant grains (78%) with a concordia age of 297.2 ± 1.5 Ma (Late Variscan) with a concordance MSWD of 0.1 (FIGURE 1A). One grain yielded an older concordant $^{206}Pb/^{238}U$ age of 409 ± 13.1 Ma (Late Caledonian). Ten grains are discordant with an age difference between $^{206}Pb/^{238}U$ and $^{207}U/^{235}U$ ages greater than 5% (FIGURE 1A).

The cores of 12 of these grains were also dated. Only seven of these cores yielded concordant ages with six cores being Late Variscan igneous cores (no difference with the rims) and one grain yielding a $^{206}Pb/^{238}U$ age of 563.2 ± 17.9 Ma (Cadomian) (FIGURE 1A).

Apatite U/Pb

The 40 grains all align on a Tera-Wasserburg discordia with a lower intercept age of 300.9 ± 4.2 Ma and a MSWD of 0.85 (Late Variscan) (FIGURE 1B). When the upper intercept of the discordia is anchored using the common lead isotopic composition derived from the Stacey and Kramers (1975) terrestrial Pb evolution model, the lower age intercept age is 306 ± 2.2 Ma (Late Variscan). The weighted mean $^{206}Pb/^{238}U$ age using this common lead isotopic composition is 305.3 ± 2.3 Ma with a MSWD of 0.98 (FIGURE 1B).

Apatite trace elements

The 40 grains are clustered in the IM domain (FIGURE 1B).

Discussion

The zircon concordia age (297.2 ± 1.5 Ma) is within error of the apatite unanchored discordia age (300.9 ± 4.2 Ma). Since the discordia is very well constrained by the large spread of isotope ratios, the unanchored age is probably more reliable than the anchored age. Since the zircon age has the smaller uncertainty, it will be used as the emplacement age of this granitoid, *i.e*. 297.2 ± 1.5 Ma (earliest Permian or Late Variscan). The Late Caledonian zircon and Cadomian core are probably inherited zircons that might be representative of the crust of this part of the Goban Spur. The presence of a Cadomian grain in particular might indicate that the Goban Spur could be underlain by peri-Gondwanan or Avalonian terranes. The small number of inherited cores or grains in the population (2

out of 52 spots including 12 cores) is in accordance with the trace element data showing that the granitoid is possibly an I or I-S-type which have usually few inherited zircons.

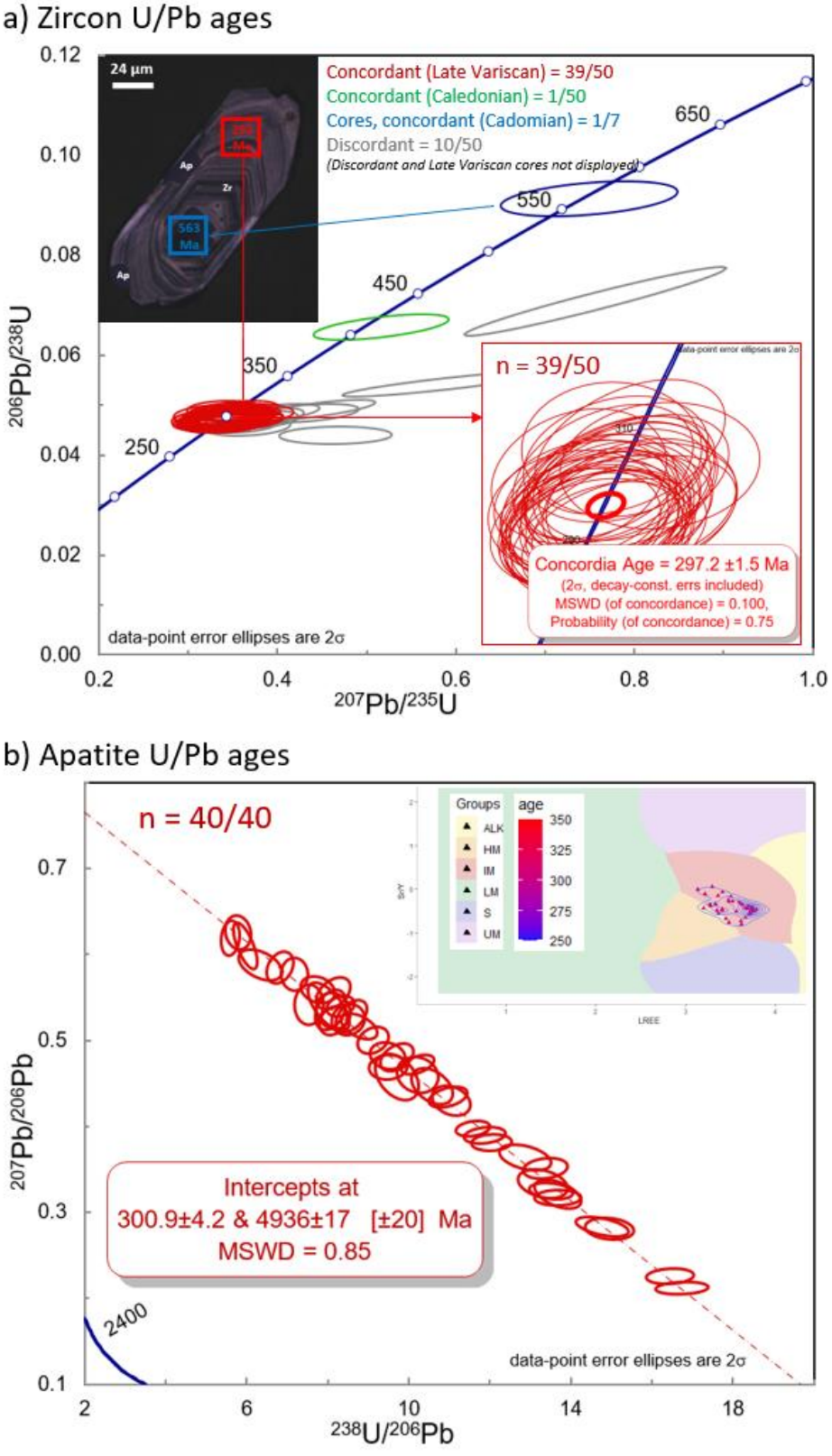

Figure 1: Zircon and apatite U/Pb ages and apatite trace element biplot results for sample R-24 (Granite Cliff 4000).

1.1.1.2 Sample R-25 (Dark crystalline rock)

Zircon U/Pb

Out of 49 analysed grains, 48 align on a discordia with an upper intercept age of 2764 ± 24 Ma (Neoarchean), a lower intercept age of -45 ± 62 Ma and with a MSWD of 1.3 (FIGURE 2A). One grain plots as an outlier possibly due to inclusion of common Pb at the time of crystallisation. 14 cores were also dated and they all plot on the 2764 Ma discordia expect one grain which plots near the outlier (FIGURE 2A).

Apatite U/Pb

Out of 40 measurements, 33 grains align on a Tera-Wasserburg discordia with a lower intercept age of 1714 ± 16 Ma and a MSWD 0.99 (Late Paleoproterozoic) (FIGURE 2B). Seven grains plot as outliers, possibly forming at least two age groups with mean ^{207}Pb-corrected ^{206}Pb/^{238}U ages of 2367 Ma (early Paleoproterozoic) and 1830 Ma (mid Paleoproterozoic) (FIGURE 2B).

Apatite trace elements

The apatites plot in the lower half of the Sr/Y-LREE space with a large spread on the x-axis (FIGURE 2B). A weak trend is visible with the older grains in the HM field and younger grains towards the LM field. Based on this trend, it is possible that the grains probably first clustered at the right extremity of the ellipse during an episode of high-grade metamorphism (possibly at 2.8 Ga?, see red circle in FIGURE 2B). Later, diffusion of LREE or LREE loss due to dissolution-reprecipitation reactions during lower-grade metamorphism shifted some of the grains left towards the LM field (possibly at 1.7 Ga?, retrograde metamorphism, see red arrow in FIGURE 2B).

Discussion

The U/Pb ages record a first crystallisation event at c. 2.7 Ga (Neoarchean) which might correspond to the age of the latest high-grade metamorphic event that has affected the rock. The apatite U/Pb ages record a later lower-grade metamorphic event at c. 1.7 Ga (Late Paleoproterozoic). The trace elements support the fact that the rock has experienced Late Paleoproterozoic retrograde metamorphism. The sample did not experienced any significant thermal effects during the Cadomian, Caledonian or Variscan orogenies, otherwise the apatite ages would have been reset).

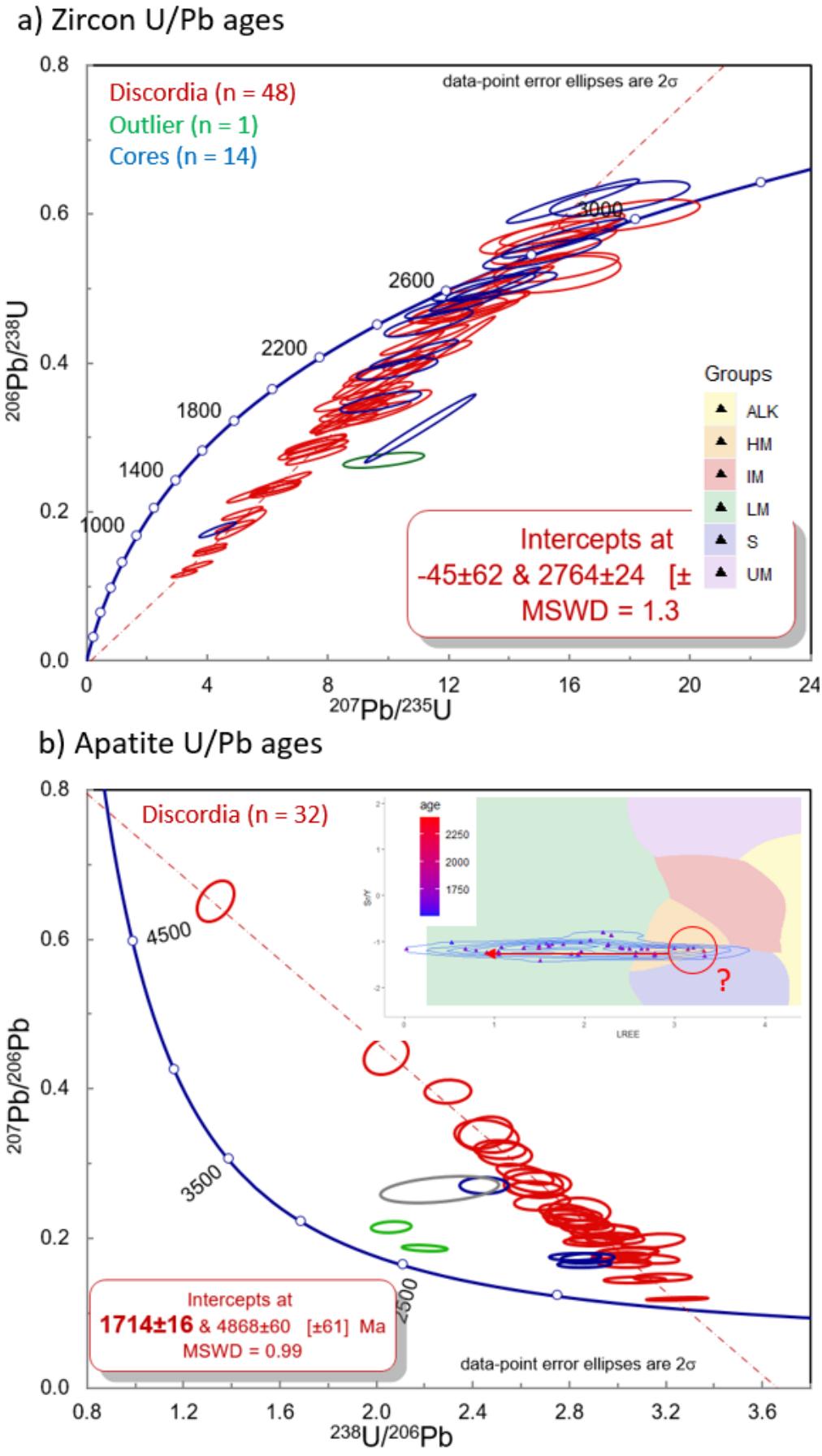

Figure 2: Zircon and apatite U/Pb ages and apatite trace elements for sample R-25 (Granite Cliff 4000).

1.1.1.3 Sample R-26 (Granite)

Zircon U/Pb

The 49 zircon grains yielded 36 concordant grains (76%) with a concordia age of 296.1 ± 1.5 Ma (concordance MSWD of 0.117) (Late Variscan) (FIGURE 3A). One grain yielded a slightly younger age of 273 ± 8 Ma. One grain yielded an older concordant $^{206}Pb/^{238}U$ age of 1769 ± 52 Ma (Late Paleoproterozoic). 12 grains are discordant with an age difference between $^{206}Pb/^{238}U$ and $^{207}U/^{235}U$ ages greater than 5% (FIGURE 3A).

The cores of 11 of these grains were also dated. Only six of these cores yielded concordant ages with three cores being Late Variscan igneous cores (no difference with the rims) and three cores yielding a Late Caledonian $^{206}Pb/^{238}U$ age (417 ± 14 Ma) and two Cadomian $^{206}Pb/^{238}U$ ages (574 ± 18 Ma and 605 ± 14 Ma) (FIGURE 3A).

Apatite U/Pb

The 40 apatites align on a Tera-Wasserburg discordia with a lower intercept age of 298 ± 12 Ma (Late Variscan) and a MSWD 2.1 (FIGURE 3B).

Apatite trace elements

Most of the grains are clustered in the IM domain (FIGURE 3B).

Discussion

Both zircons and apatites U/Pb ages demonstrate that the granite is a Late Variscan intrusion with an emplacement age of c. 296 ± 2 Ma.

The Late Caledonian, Cadomian and Late Paleoproterozoic zircon grains and cores are probably inherited zircons that might be representative of the crust of this part of the Goban Spur. The presence of a Cadomian grain in particular might indicate that the Goban Spur could be underlain by peri-Gondwanan or Avalonian terranes. The small number of inherited cores or grains in the population (6 out of 60 spots including 11 cores) is in accordance with the trace element data showing that the granitoid is probably of I-type affinity which usually have few inherited zircons due to both higher magma temperatures (with higher zircon saturation) and fewer zircons in the source region (in comparison to S-type granitoid melts) (Chew et al., 2020).

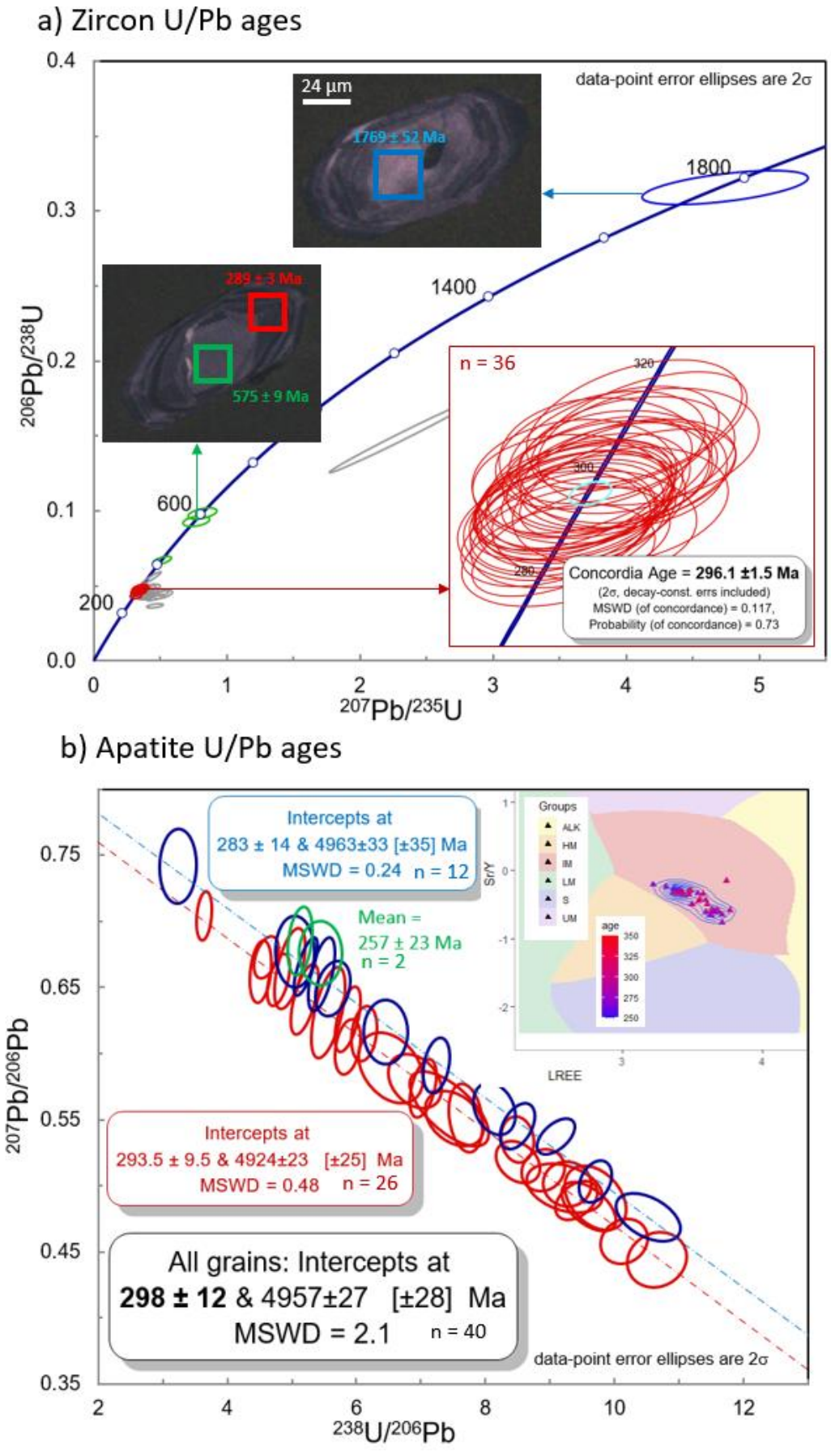

Figure 3: Zircon and apatite U/Pb ages and apatite trace elements for sample R-26 (Granite Cliff 4000).

1.1.1.4 Combined sample R-24-26 (Granite Cliff 4000 granite)

Sample R-24 and R-26 come from two different dredges that cross each other on Granite Cliff 4000, with a maximum theoretical distance between the two samples being 5 km but is probably much less. Since the samples are spatially very close and yielded similar zircon and apatite U/Pb ages, it is likely that the two samples come from the same granitic body.

The zircon U/Pb ages from the two samples can be combined to better constrain the age of the granite. The combined population contains 74 analyses yielding a concordia age of 296.7 ± 1.1 Ma (Asselian, Late Variscan) with a MSWD of 0.25 (FIGURE 4). This age will be used as the emplacement age of the Granite Clifff 4000 granite.

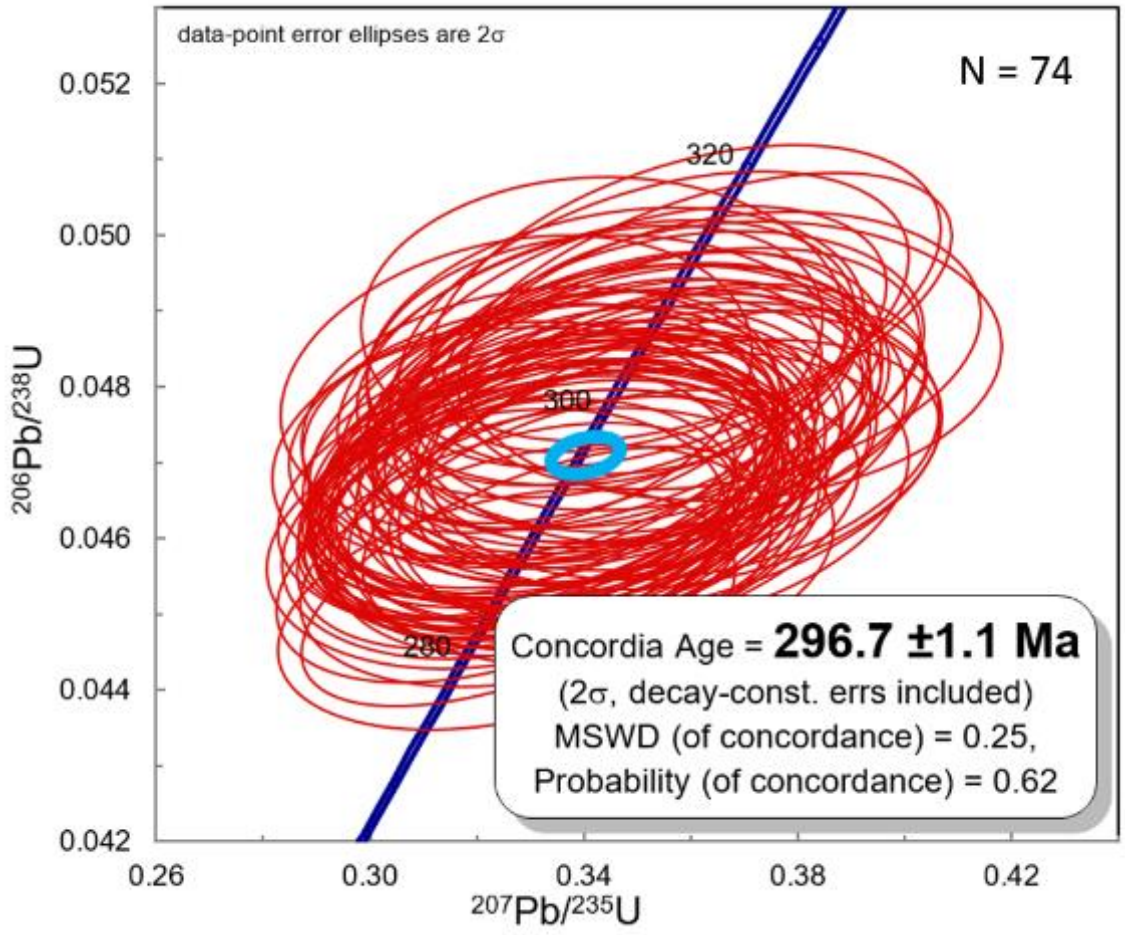

Figure 4: Zircon U/Pb ConcAge of combined sample R-24-26 (Granite Cliff 4000).

1.1.1.5 Sample R-27 (Granulite)

Zircon U/Pb

Eight of the 17 zircons yield a concordia age of 571.2 ± 7.5 Ma (Cadomian). Seven grains (four concordant and four discordant) align on a discordia with a lower intercept age of 296.9 ± 5.4 Ma while the four concordant grains yielded a concordant age of 300.1 ± 5.8 Ma (Late Variscan) (FIGURE

5A). Finally, the two remaining grains yielded concordant ages with $^{206}Pb/^{238}U$ ages of 393.9 ± 16 Ma (Late Caledonian) and 509.3 ± 20.7 Ma (possibly Early Caledonian?). Five cores were dated, four of them yielding concordant Cadomian ages and one of them being discordant (FIGURE 5A).

Apatite U/Pb

The 40 apatites align on a Tera-Wasserburg discordia with a lower intercept age of 446 ± 11 Ma (Caledonian) and a MSWD of 0.5 (FIGURE 5B).

Apatite trace elements

The grains are spread over both the HM and IM domains, with a few grains extending to the right edge of the LM domain (FIGURE 5B).

Discussion

The zircons shows that the protolith might have been an igneous rock emplaced at c. 571 Ma during the Cadomian Orogeny and thus belong to the peri-Gondwanan domain (south of the Iapetus Suture Zone), probably the northern margin of Avalonia.

The apatite data show that the rock might have also experienced Caledonian metamorphism at c. 446 Ma which corresponds to the closure of the Iapetus Ocean at the end of the Ordovician-Silurian. This metamorphic event must have been high grade as shown by numerous apatites plotting on the HM domain of the trace element biplot (FIGURE 5B).

Finally, the Late Variscan zircons cannot belong to the matrix of the rock since the apatites have not been reset by the Late Variscan Orogeny. The photographs of the sample show one clast with a white vein on one of its surface (up to a few millimetres thick) (FIGURE 6). This white rock could be a Late Variscan hydrothermal or aplitic vein from which the Late Variscan zircons come from. The thin section of this sample does not contain this vein and it is therefore impossible for now to confirm the hypothesis. Such a Late Variscan mineralization event could be related to the emplacement of the Late Variscan granitic batholiths of Menez Bihan and Granite Cliff 4000 (samples R-24, R-26 and R-28) which have similar zircon ages (288-296 Ma).

In conclusion, sample R-27 is a metamorphic rock which belongs to the Avalonian domain and was formed or metamorphosed during the Cadomian Orogeny (crystallisation of the matrix zircons) and subsequently affected by the main phase of the Caledonian orogeny (crystallisation of the apatites). At c. 297 Ma, during the Late Variscan magmatic activity, zircon-bearing veins were possibly formed from hydrothermal fluids or aplitic magmas linked to the emplacement of a granitic pluton at this location (samples R-28).

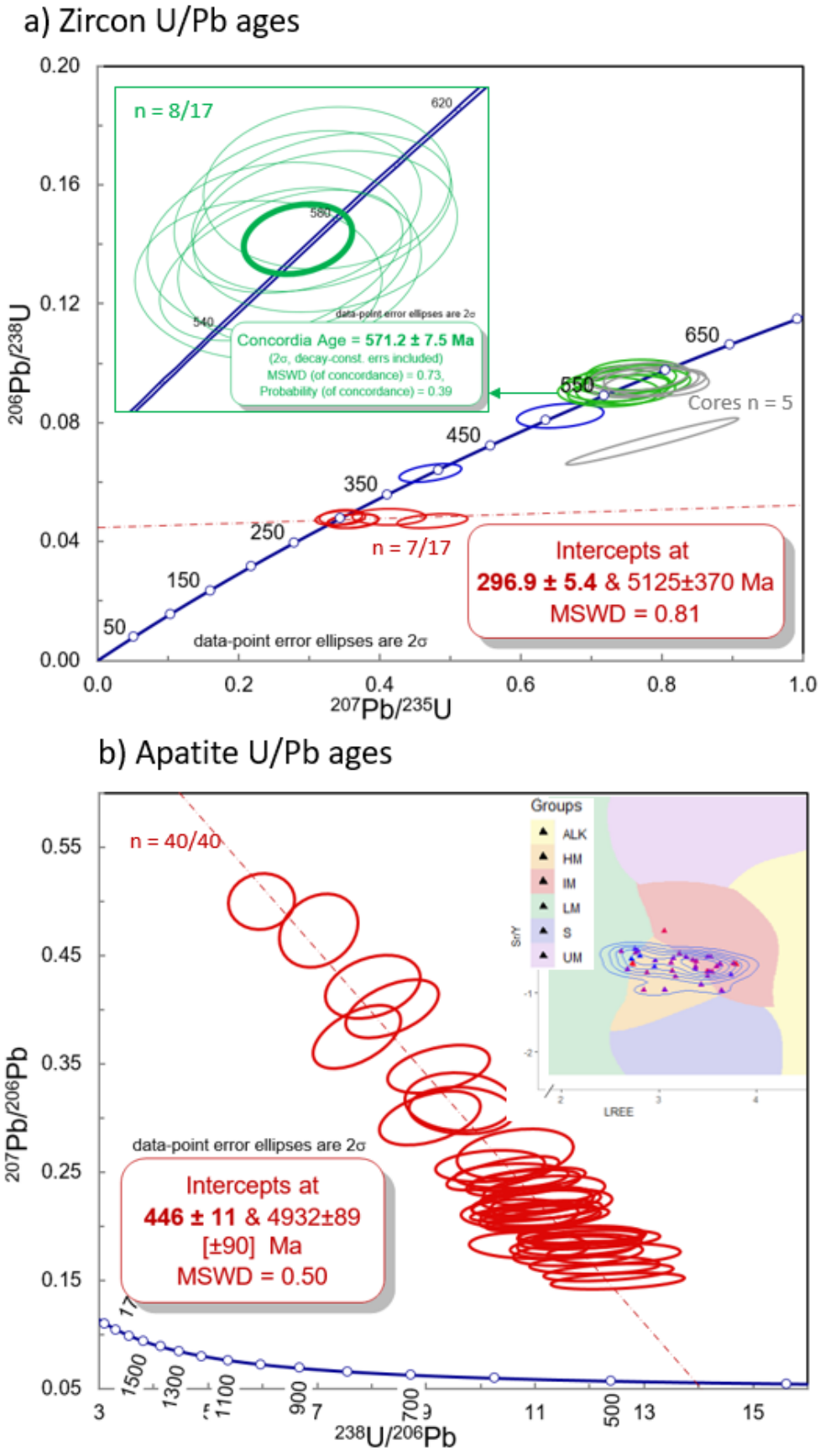

Figure 5: Zircon and apatite U/Pb ages and apatite trace elements for sample R-27 (Menez Bihan).

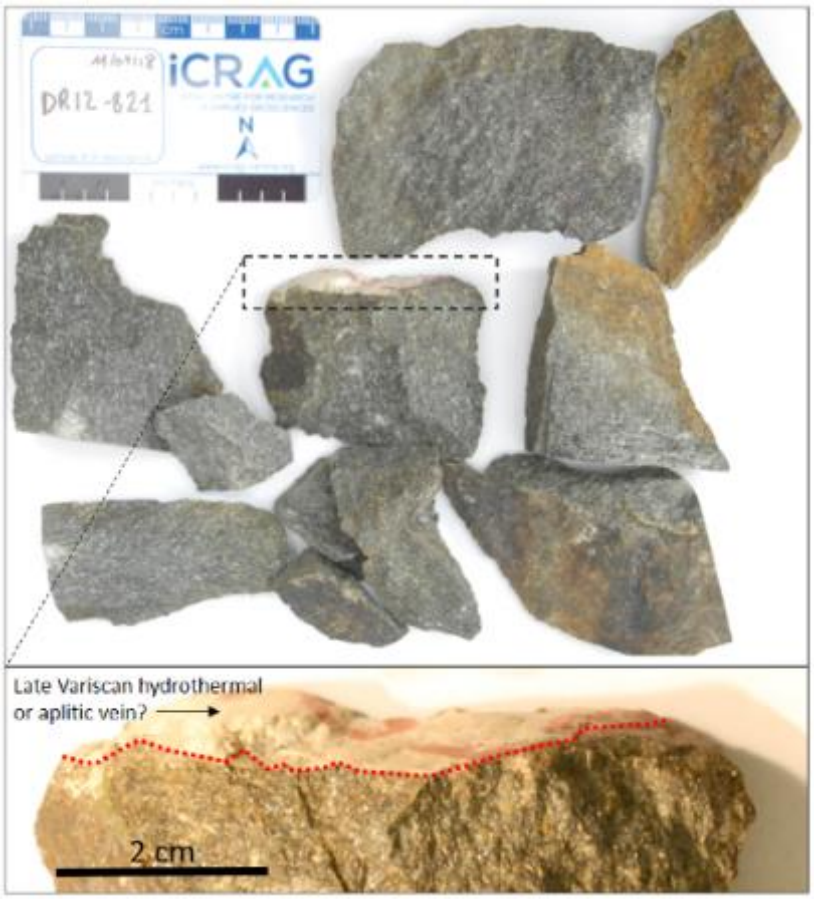

Figure 6: Photos of sample R-27 with possible location of an hydrothermal/aplitic vein.

1.1.1.6 Sample R-28 (Granite)

Zircon U/Pb

Out of the 46 zircon grains, 36 yielded concordant ages with a concordia age of 288.3 ± 1.4 Ma (Late Variscan) with a MSWD of 0.94 (FIGURE 7A). Ten grains were slightly discordant possibly due to Pb loss.

The cores of 16 grains were also dated, with 11 of them yielding a similar Late Variscan age. Three cores yielded concordant ages of 339.8 ± 12.6 Ma (Variscan), 554 ± 16.9 Ma and 613 ± 10 Ma (both Cadomian) (FIGURE 7A). The discordance of one of the two discordant cores (core of grain 33) was caused by the ablation of the Late Variscan rim for the first few seconds (which yields an age of 291 ± 6 Ma) followed by the ablation of the core itself during the last few seconds (which yields an age of c. 1155 ± 24 Ma, or late Mesoproterozoic) (FIGURE 7A).

Apatite U/Pb

Out of the 40 grains, 39 of them align on a Tera-Wasserburg discordia with a lower intercept age of 293.7 ± 9.8 Ma (Late Variscan) with a MSWD of 0.79 (FIGURE 7B).

Apatite trace elements

All the grains are clustered in the centre of the IM domain.

Discussion

Both zircons and apatites U/Pb ages demonstrate that the granite is a Late Variscan intrusion with an emplacement age of c. 288 ± 1.4 Ma (using the zircon concordia age). The Late Mesoproterozoic and Cadomian zircon cores are probably inherited zircons that might be representative of the crust of this part of the Goban Spur. The presence of a Cadomian grain in particular might indicate that the Goban Spur could be underlain by peri-Gondwanan or Avalonian terranes. However, the small number of inherited cores or grains in the population (5 out of 62 spots including 16 cores) might indicate and that little lower crustal contamination occurred. This is supported by the trace element data showing that the granitoid is possibly an I-type.

1.1.1.7 Sample R-29 (Green sandstone)

Zircon U/Pb

Out of the 117 analysed grains, 97 grains yield concordant ages ranging from 280.4 ± 8.8 Ma to 1981.7 ± 60.6 Ma. The main peaks are at c. 420 Ma (Late Caledonian, 12% of grains), c. 460 Ma (Early Caledonian, 18%), c. 570 Ma (Cadomian, 16%) and c. 1000-1600 (Mesoproterozoic, 24%), with only a few older Paleoproterozoic grains. No Archean zircons were found in the sample (FIGURE 8A).

Apatite U/Pb

Out of the eight apatites, six of them yielded Early Caledonian (Grampian) ages and the other grains yielded Cadomian ages (FIGURE 8B).

Apatite trace elements

The apatite grains plot in the LM, UM, IM and ALK domains of the biplot (FIGURE 8B), reflecting their detrital nature.

Discussion

The youngest concordant zircon age provides a maximum stratigraphic age of c. 280 Ma (late Early Permian) to the sandstone. The sandstone is therefore Middle Permian or younger. The rarity of Late Variscan zircons and absence of Late Variscan apatites from the sandstone suggest that the Late Variscan granites were likely still buried at that time.

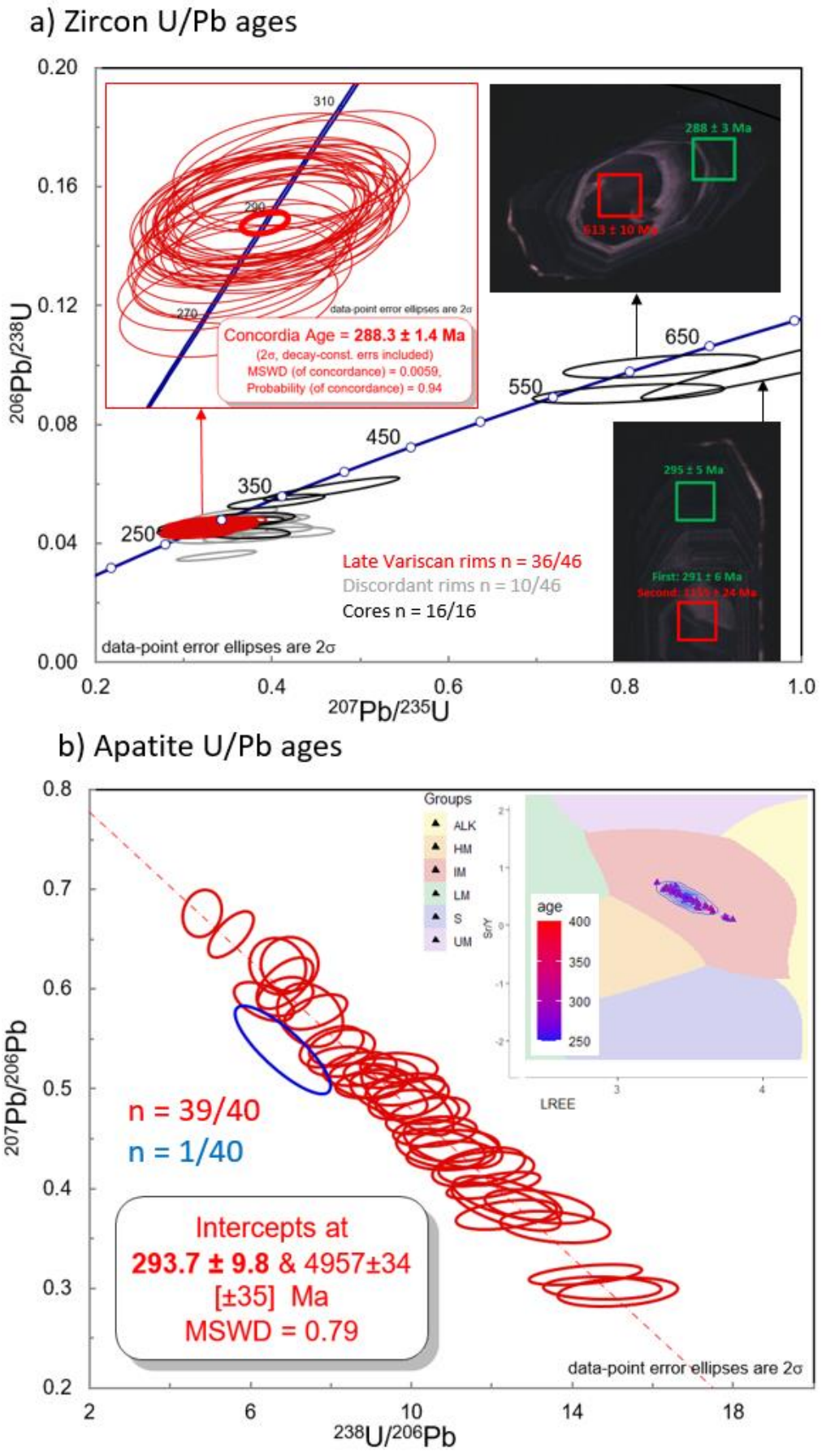

Figure 7: Zircon and apatite U/Pb ages and apatite trace elements for sample R-28 (Menez Bihan).

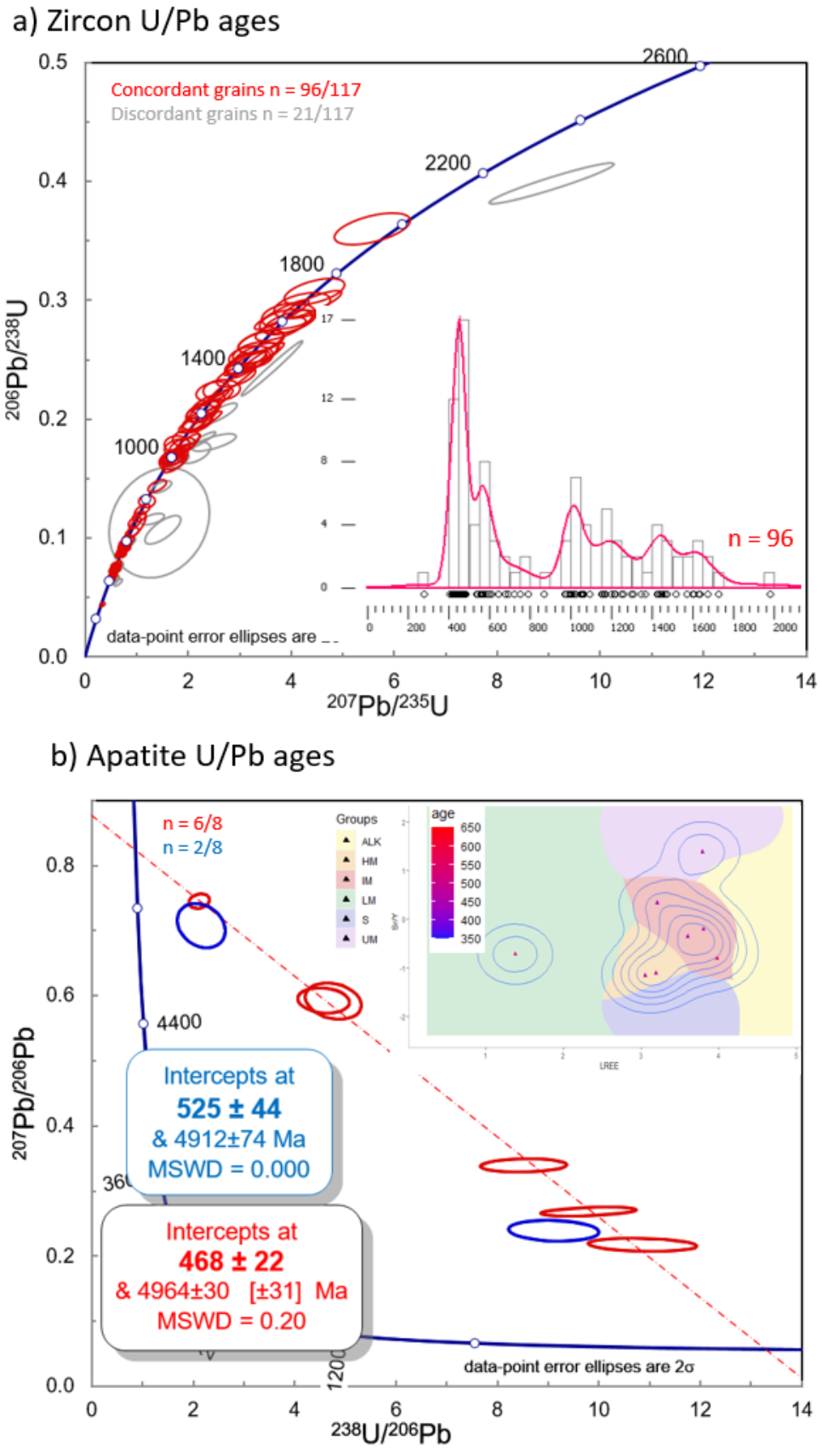

Figure 8: Zircon and apatite U/Pb ages and apatite trace elements for sample R-29 (Goban Spur plateau).

1.1.2 North Porcupine High

1.1.2.1 16/28-sb01

Analysis of 58 zircons from sample R-3 (Early-Middle Eocene) yielded 37 concordant ages ($^{207}Pb/^{235}U$ age < ± 5% of $^{206}Pb/^{238}U$ age) ranging from 62.4 ± 1.9 Ma to 2023.3 ± 53.8 Ma (FIGURE 9). The main peak is at c. 1700 Ma (Labradorian), followed by a secondary peak at c. 420 Ma (Late Caledonian) and minor peaks at 600 Ma (Cadomian) and 1050 Ma (Grenville). There is one Paleogene grain dated at 62.4 ± 1.9 Ma (FIGURE 9).

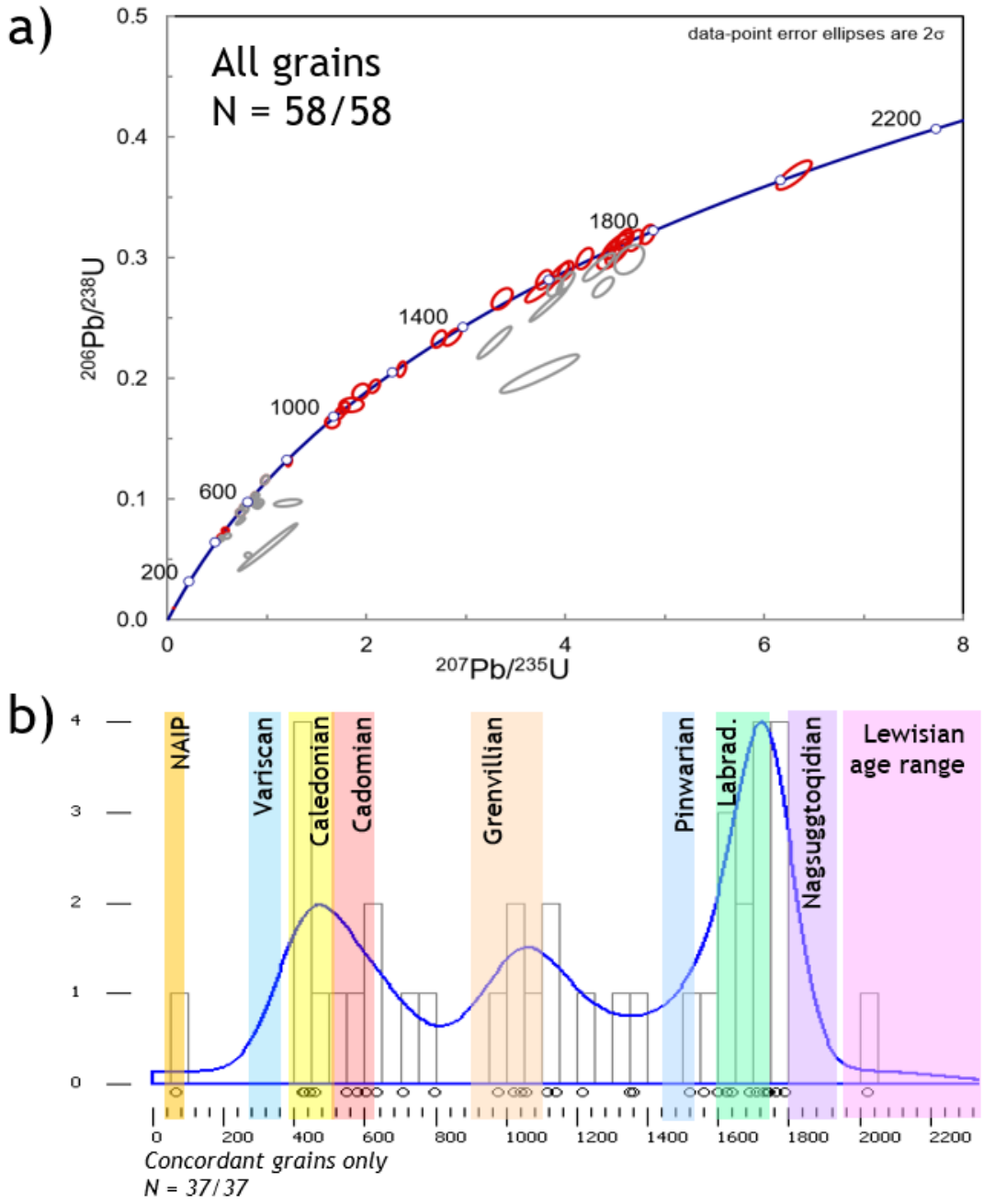

Figure 9: Zircon U/Pb results for sample R-3 (16/28-sb01). a) Wetherill plots, b) Density plots and KDEs

Analysis of 180 zircons from sample R-5 (Late Cretaceous, Cenomanian?) yielded 153 concordant ages ($^{207}Pb/^{235}U$ age < ± 5% of $^{206}Pb/^{238}U$ age) ranging from 476.4 ± 34.8 Ma to 1859.7 ± 55.6 Ma (FIGURE 10A, B). The main age peak is at c. 1.7 Ga with 116 grains (76% of the concordant grains) yielding a weighted mean $^{206}Pb/^{238}U$ age of 1721 ± 11 Ma (MSWD of 5.1) (FIGURE 10B). However, most of these grains and some of the discordant grains align on a discordia which yields an upper intercept age of 1763 ± 9 Ma and a lower intercept age of 843 ± 100 Ma (FIGURE 10C). The lower intercept uncertainty is large because the spread of isotope ratios in the grains is relatively small and most grains are concentrated towards the upper intercept.

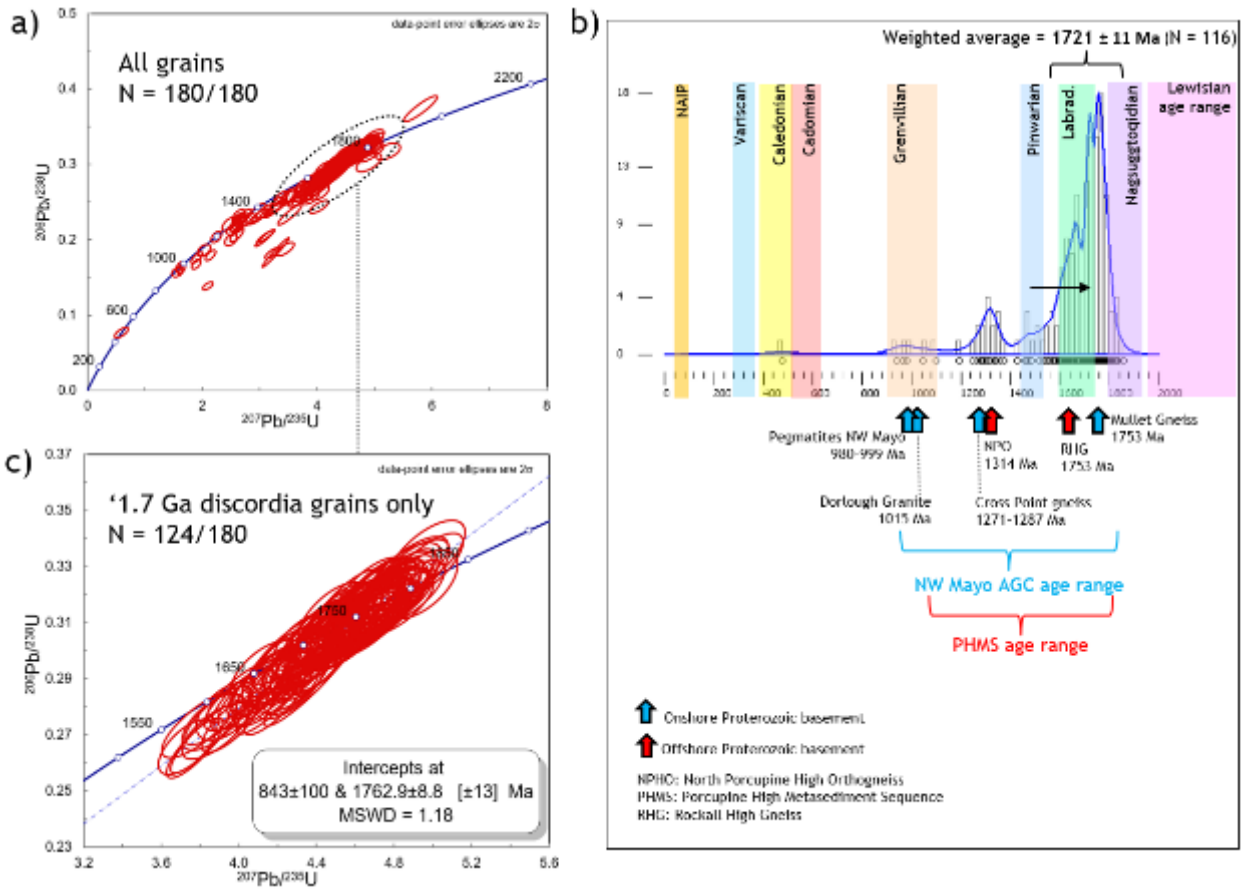

Figure 10: Zircon U/Pb results for sample R-5 (16/28-sb01). a) & c) Wetherill plots, b) Density plots and KDEs.

1.1.2.2 26/26-1

Sample R-7 (Eocene sands)

Analysis of 58 zircons yielded 37 concordant ages ($^{207}Pb/^{235}U$ age < ± 5% of $^{206}Pb/^{238}U$ age) ranging from 62.4 ± 1.9 Ma to 2023.3 ± 53.8 Ma (FIGURE 11). The main peak is at c. 1700 Ma (Labradorian), followed by a secondary peak at c. 420 Ma (Caledonian) and minor peaks at 600 Ma (Cadomian) and 1050 Ma (Grenville). There is one Paleogene grain dated at 62.4 ± 1.9 Ma (FIGURE 11).

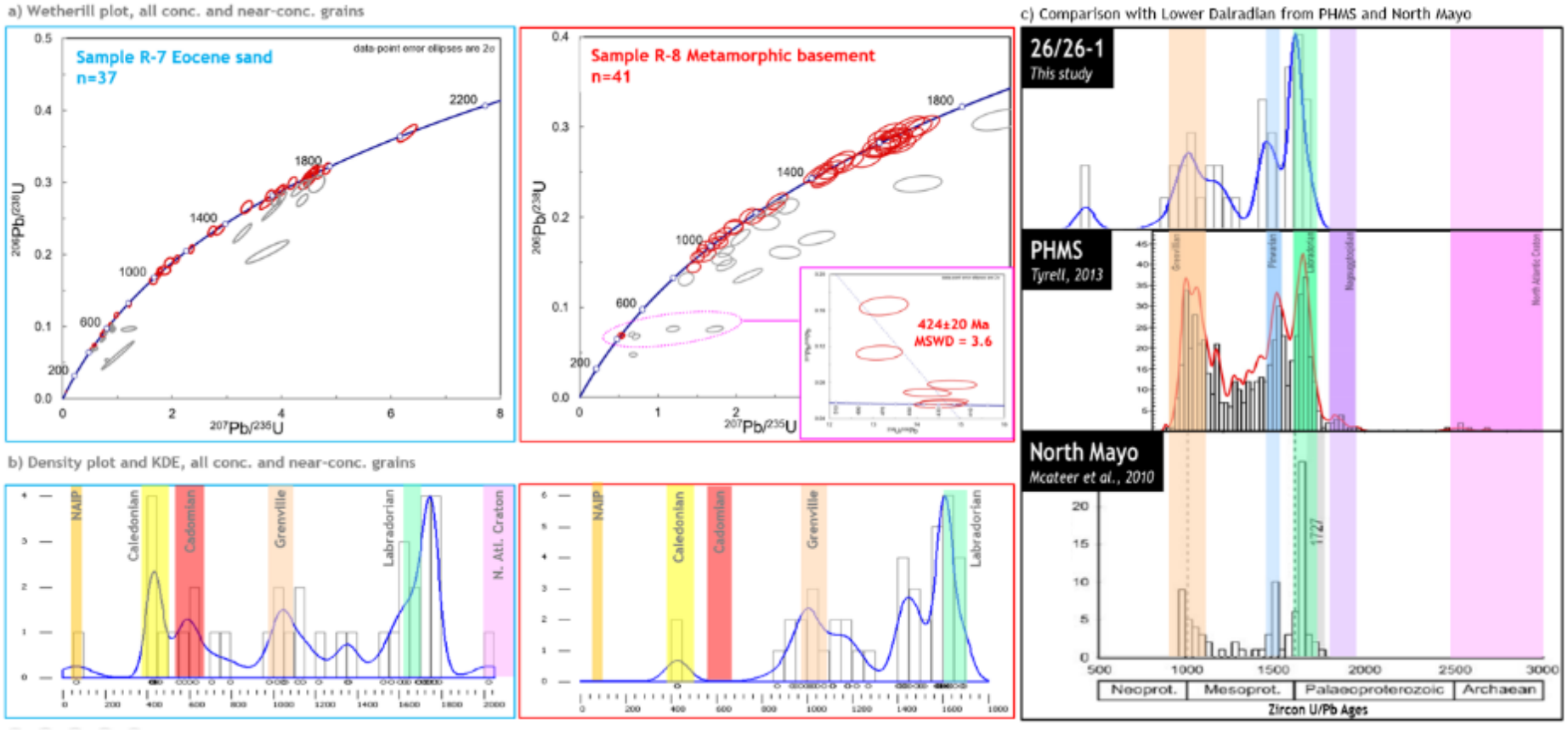

Figure 11: Zircon U/Pb results for samples R-7 and R-8 (26/26-1). a) Wetherill plots, b) Density plots and KDE, c) Zircon U/Pb density plot and KDE of basement sample in 26/26-1, the PHMS dredge samples and the lowermost Dalradian units of Co. Mayo.

Sample R-8 (Metamorphic basement)

Apatite U/Pb ages

The 65 ^{207}Pb-corrected ages range between 202.9 ± 189 Ma and 1645.2 ± 679.7 Ma. However, when plotted on a Tera-Wasserburg plot, most of the analyses (51 grains) align on one discordia while eight grains can be considered as outliers with older ages and six grains as outliers with younger ages (FIGURE 12).

The 51 grains yield an unanchored discordia age of 395.1 ± 9.6 Ma with a MSWD of 1.4. When the upper intercept of the discordia is anchored using the common lead isotopic composition derived from the Stacey and Kramers (1975) model, the lower age intercept age is 391.9 ± 5.9 Ma (Middle Devonian) (FIGURE 12).

Trace elements results

All grains, except one, plot within the HM and LM fields (high and low-grade metamorphic rocks) (FIGURE 12) which is in agreement with the nature of the rocks (schists and gneisses) and implies they are neo-crystalline metamorphic apatite and not detrital grains. The one grain that plots in the 'alkali-rich igneous rocks' field (red circle in FIGURE 12) may not have been derived from the basement rocks but could come from contamination in the drilling mud.

Zircon U/Pb ages

Analysis of 60 zircons yielded 41 concordant ages ranging from 426.3 ± 13.1 Ma to 1694.8 ± 53 Ma with a dominant peack at c. 1.6 Ga (Labradorian) and two secondary peaks at 1.05 Ga (Grenville) and 1.45 Ga and (Pinwarian) (FIGURE 11). Two concordant grains yielded a Caledonian age of c. 420 Ma. Together with four other discordant grains, they form a Tera-Wasserburg discordia with a non-anchored lower intercept of 424 ± 20 Ma (MSWD = 3.6) (FIGURE 11).

1.1.2.3 34/05-1

Sample R-10 (Paleocene-Eocene sandstone)

Apatite U/Pb ages

The two grains in this sample yielded ^{207}Pb-corrected ages of 404.8 Ma and 404.9 Ma. They are most likely detrital Caledonian apatites.

Trace element results

The two grains plot in the mafic igneous/mafic I-type granitoids (IM) and high-grade metamorphic (HM) domains.

Zircons U/Pb ages

For the Eocene sample R-10, 100 grains were ablated which yielded 99 zircon U/Pb ages. Out of the 99 zircons, 49 were concordant or near-concordant (*i.e.* here, $^{207}Pb/^{235}U$ age within ± 5 % of the $^{206}Pb/^{238}U$ age) while the remaining 50 grains were discordant.

The concordant ages range from 440.8 ± 10 Ma to 2578.5 ± 68.2 Ma with a dominant peak at c. 468 Ma (Grampian Phase of the Caledonian orogenic cycle) and smaller peaks at c. 812 Ma (Knoydartian Orogeny?), c. 1 Ga and 1.2 Ga (Grenvillian Orogeny), c. 1.6 Ga (Labradorian Orogeny) and c. 2.5 Ga (North Atlantic Craton) (FIGURE 13).

Sample R-11 (Albian? sands)

Zircons U/Pb ages

For the red unit sample R-11, 100 grains were ablated which yielded 100 zircon U/Pb ages. Out of the 100 zircons, 62 were concordant or near-concordant while the remaining 38 grains were discordant.

The ages range from 100.3 ± 3.4 Ma to 2533.8 ± 68.4 Ma with a dominant peak at c. 469 Ma (Grampian Phase of the Caledonian orogenic cycle) and smaller peaks at c. 0.9-1.2 Ga (Grenvillian Orogeny), c. 1.4 Ga and c. 2.5 Ga (North Atlantic Craton). There is only one grain younger than Caledonian, grain R-11.47 with an age of 100.3 ± 3.4 Ma (Albian-Cenomanian boundary) (FIGURE 14).

Sample R-12 to R-15 (Carboniferous clastics)

Apatite U/Pb ages

For the U/Pb data, all the Carboniferous samples have been analysed together to obtain a statistically meaningful population of grains (n=40).

The ^{207}Pb-corrected ages range between 303.8 ± 88.5 Ma and 1536.9 ± 56.9 Ma (FIGURE 15). Based on the distribution of the ^{207}Pb-corrected ages, the grains have been separated in six age groups. For groups 1 to 5, the unanchored discordia lower intercept age was calculated. An age was also calculated by iteratively anchoring the upper intercept with the Stacey and Kramers (1975) common lead value until the lower intercept age remains constant. The sixth family is composed of only one grain, so no discordia age was calculated, only the ^{207}Pb-corrected age. From youngest to oldest, the six groups have an anchored age of 319 ± 13 Ma (Westphalian, based on only 3 grains), 417 ± 11 Ma (n=15), 472.7 ± 7.1 Ma (n=14), 672 ± 36 Ma (n=5), 1057 ± 32 Ma (n=2) and 1536.9 ± 56.9 Ma (n=1) (FIGURE 15).

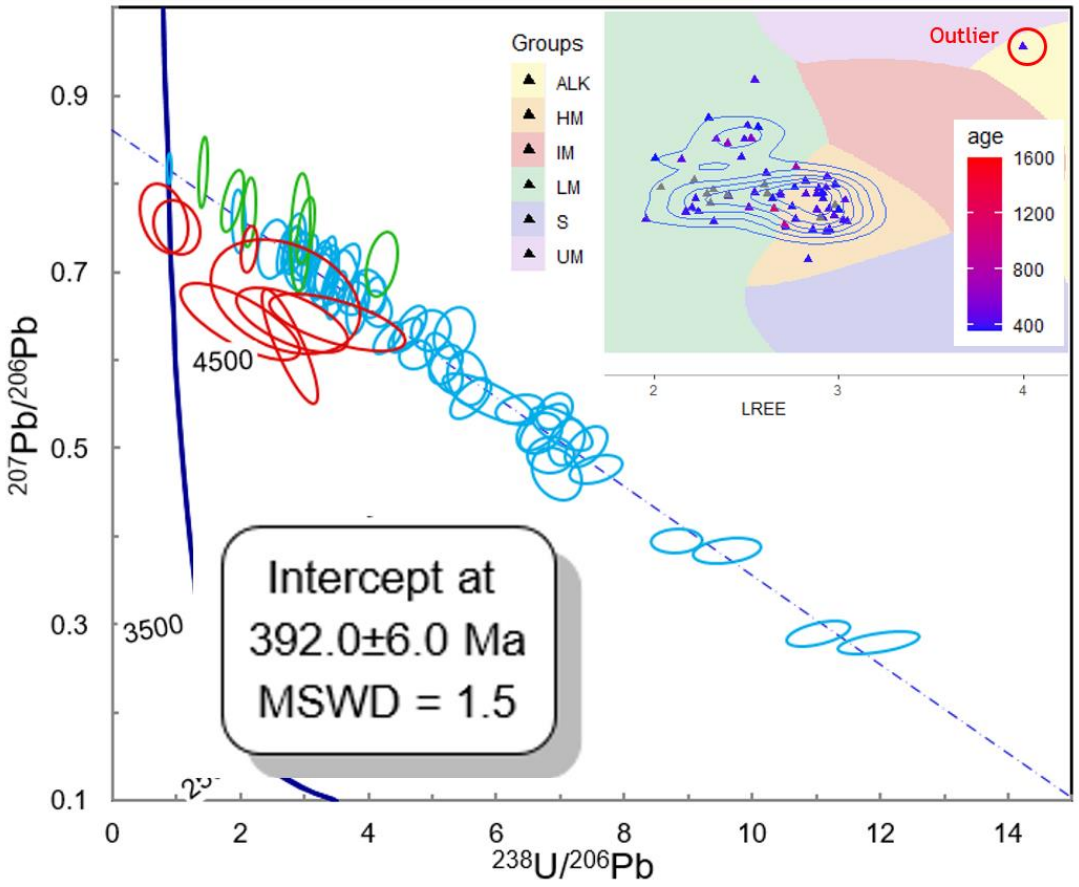

Figure 12: Apatite U/Pb ages and apatite trace elements for sample R-8 (26/26-1).

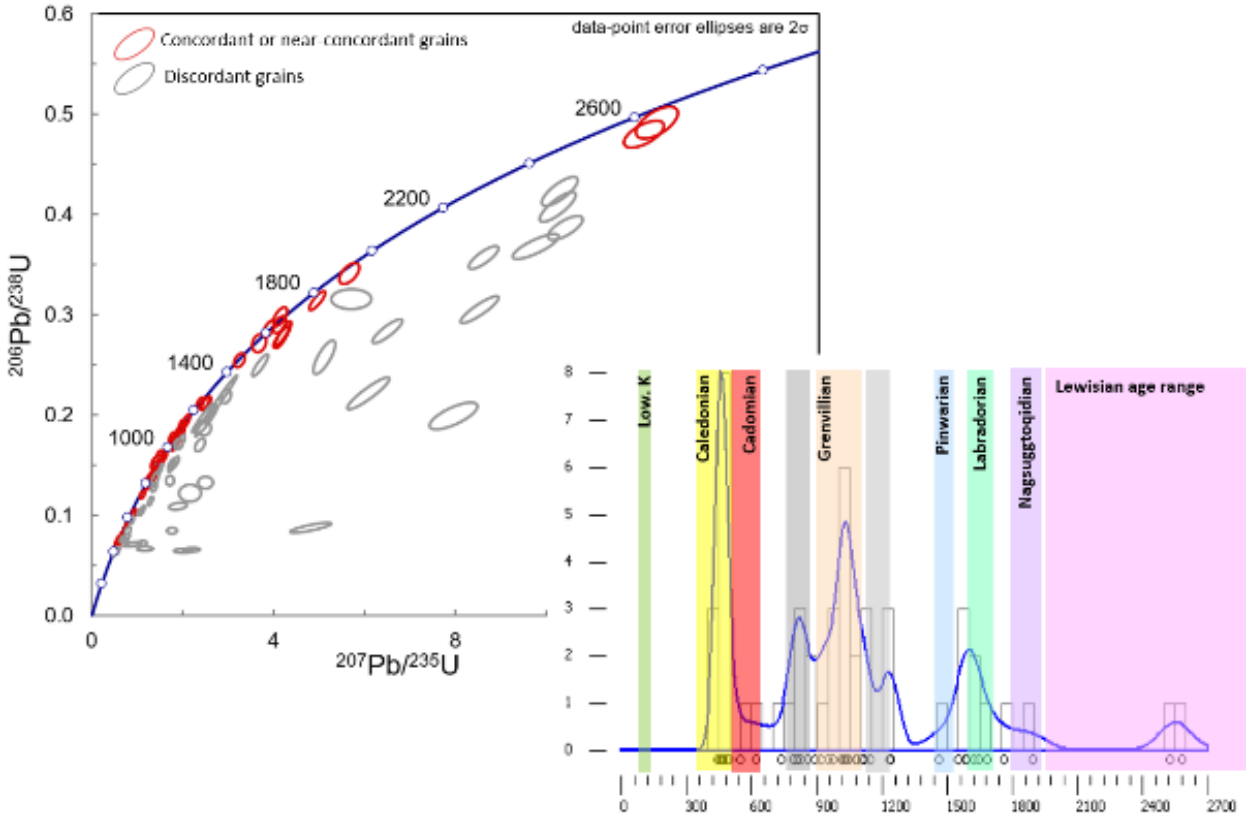

Figure 13: Zircon U/Pb results for sample R-10 (34/05-1).

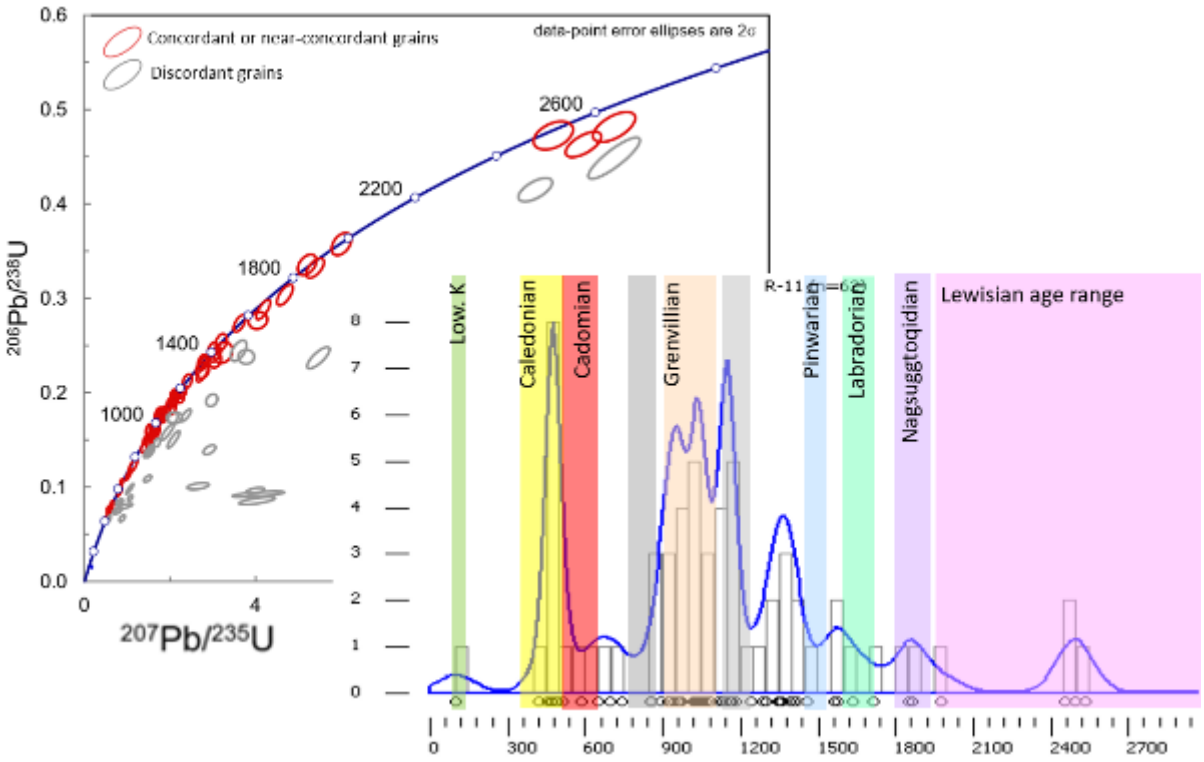

Figure 14: Zircon U/Pb results for sample R-11 (34/05-1).

Trace element results

Most of the grains plot on the mafic igneous/mafic I-type granitoids (IM), and high-grade metamorphic (HM) domains, while a few grains also plot in the LM, UM, ALK and S fields (FIGURE 15).

The three Westphalian grains are spread apart from each other in the I and LM fields of the biplot suggesting a detrital nature rather than being cogenetic grains from a syn-sedimentary magmatic event such as an ash fall. Similarly, the Caledonian and older grains also plot over a large area of the Sr/Y-LREE plot and no clear correlation is observed between grain age and source rock type.

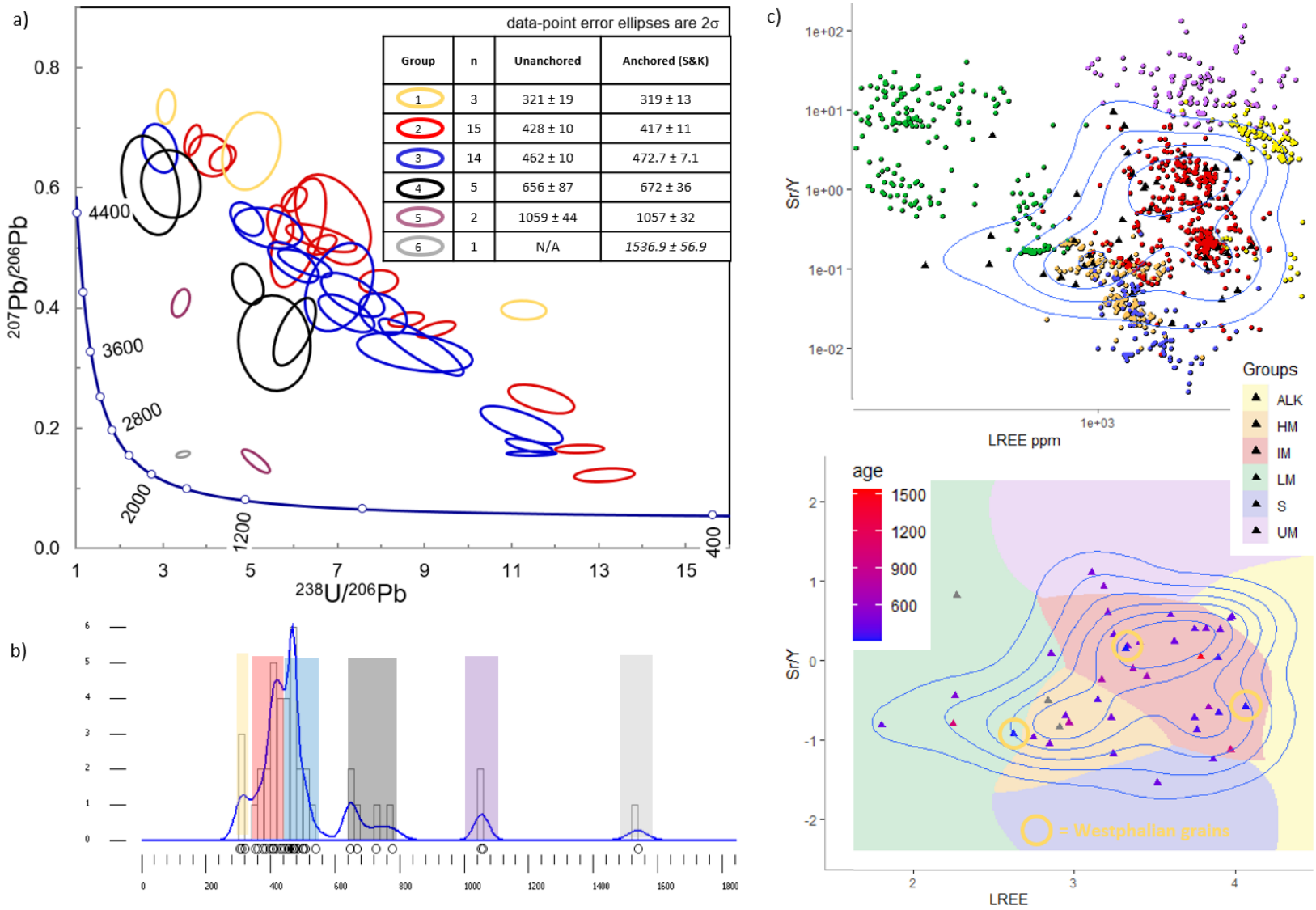

Figure 15: Apatite U/Pb and trace element results for sample R-12-15 (34/05-1).

Zircons U/Pb ages

Sample R-12

For the Westphalian D sample R-12, 100 grains were ablated which yielded 100 zircon U/Pb ages. Out of the 100 zircons, 57 were concordant or near-concordant while the remaining 43 grains were discordant. The ages range from 414.4 ± 10.6 Ma to 3259.4 ± 79.3 Ma with a dominant peak at at c. 435 Ma (Caledonian orogenic cycle) and a few very small peaks at c. 1-1.2 Ga, 1.3 Ga and 1.6 Ga and a few grains at 2.3 to 3.2 Ga (North Atlantic Craton) (FIGURE 16).

Sample R-13-14

For the Westphalian C sample R-13-14, 132 grains were ablated which yielded 132 zircon U/Pb ages with 102 concordant or near-concordant grains while the remaining 30 grains were discordant. The ages range from 305.9 ± 6.9 Ma to 2944.7 ± 96.6 Ma with a dominant peak at at c. 433 Ma (Caledonian orogenic cycle) and some smaller peaks at c. 1 Ga (Grenvillian Orogeny), 1.3 Ga, 1.45 Ga (Pinwarian), 1.6 Ga (Labradorian), 1.7 Ga and nine grains spanning 1.9 to 2.9 Ga (North Atlantic Craton) (FIGURE 16). There is only one grain younger than Caledonian with a $^{206}Pb/^{238}U$ age of 305.9 ± 6.9 Ma and a $^{207}Pb/^{235}U$ of 312.7 ± 11.3 Ma (c. Namurian to Stephanian), very close to the depositional age of 312.6 ± 2.6 Ma (Westphalian C).

Sample R-15

For the Westphalian B sample R-15, 100 grains were ablated which yielded 100 zircon U/Pb ages with 77 concordant or near-concordant grains while the remaining 23 grains were discordant. The ages range from 406.6 ± 10.6 Ma to 2776.7 ± 67 Ma with a dominant peak at c. 431 Ma (Caledonian orogenic cycle) and smaller peaks at c. 617 Ma (Cadomian), c. 1 Ga (Grenvillian), c. 1.6 Ga (Labradorian) and five grains spanning 2 to 2.8 Ga (North Atlantic Craton) (FIGURE 16).

Combined Carboniferous sample R-12-15

The Carboniferous samples can also be regrouped and treated as one sample. This combined sample comprise 332 analysed zircons with 236 concordant or near-concordant grains and 96 discordant ones. The ages range from 306 Ma to 3259 Ma. The dominant peak is at c. 429 Ma (Caledonian orogenic cycle) with secondary peaks at 1023 Ma (Grenvillian) and 1622 Ma (Labradorian) and smaller peaks at 611 Ma (Cadomian), c. 1300 Ma, c. 1480 Ma (Pinwarian), 1766 Ma and 2750 Ma (North Atlantic Craton) (FIGURE 17).

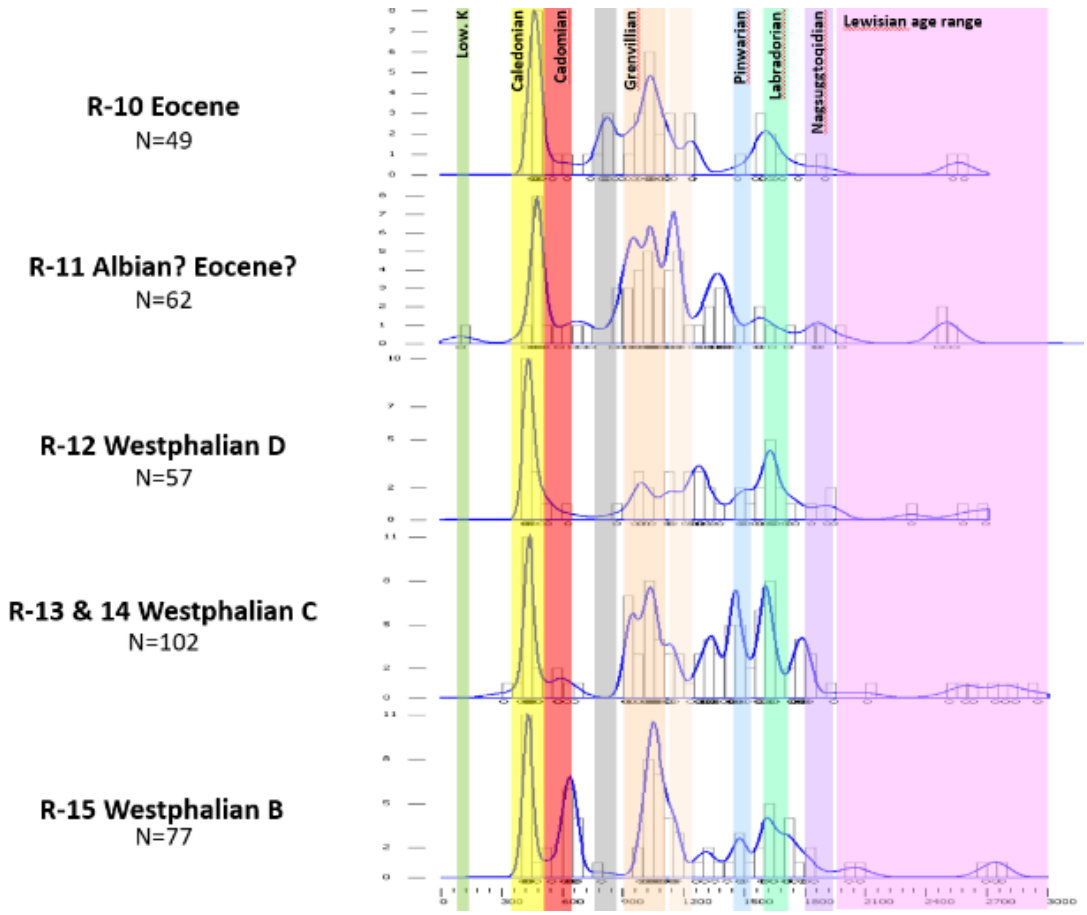

Figure 16: Histograms and KDEs of $^{206}Pb/^{238}U$ ages (concordant grains only) from samples R-10, R-11, R-12, R-13-14 and R-15 (34/05-1).

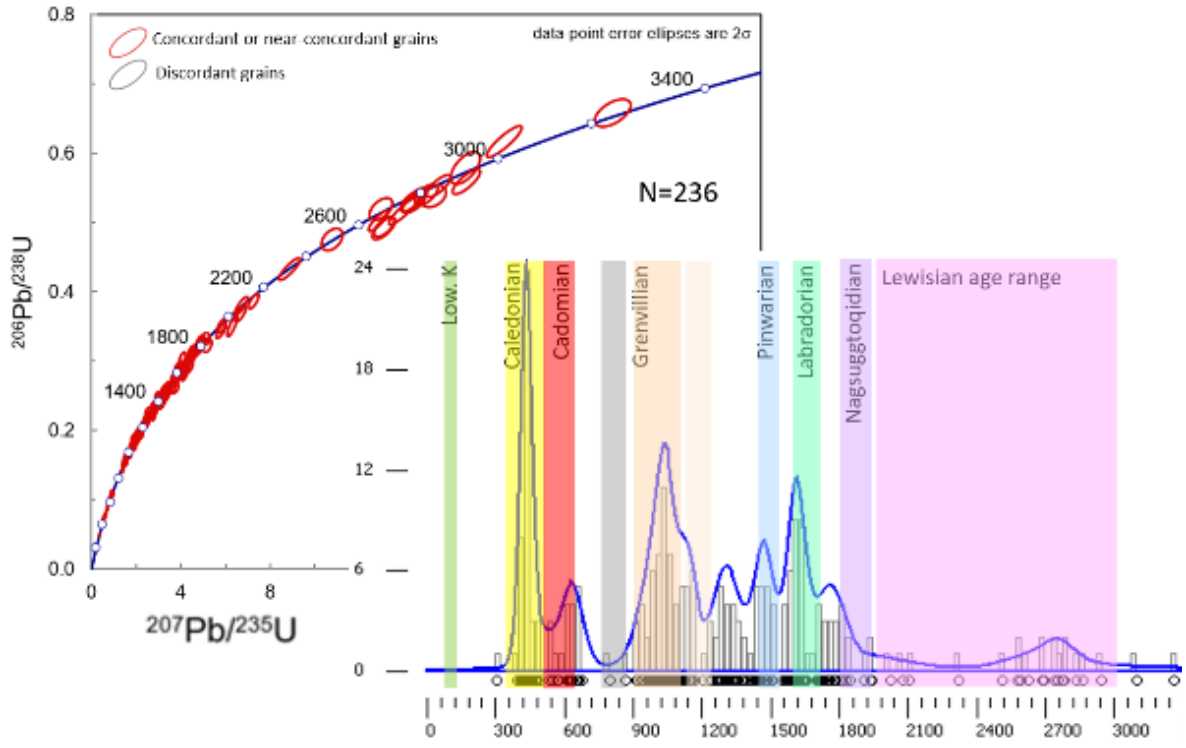

Figure 17: Zircon U/Pb results for sample R-12-15.

1.1.3 Miscellaneous locations

1.1.3.1 12/13-1A

The 64 apatite U/Pb ages ^{207}Pb-corrected ages range between 284.1 ± 20.7 Ma and 2614 ± 101 Ma. The three younger grains align on a discordia yielding an anchored age of 291.3 ± 8.4 Ma (Early Permian) and plot within the IM field of the trace element biplot, suggesting they come from a mafic igneous rock. Most of the other grains (n=51, 80%) have ages ranging from 1350 to 1925 Ma (Mesoproterozoic and Paleoproterozoic) (Figure 18).

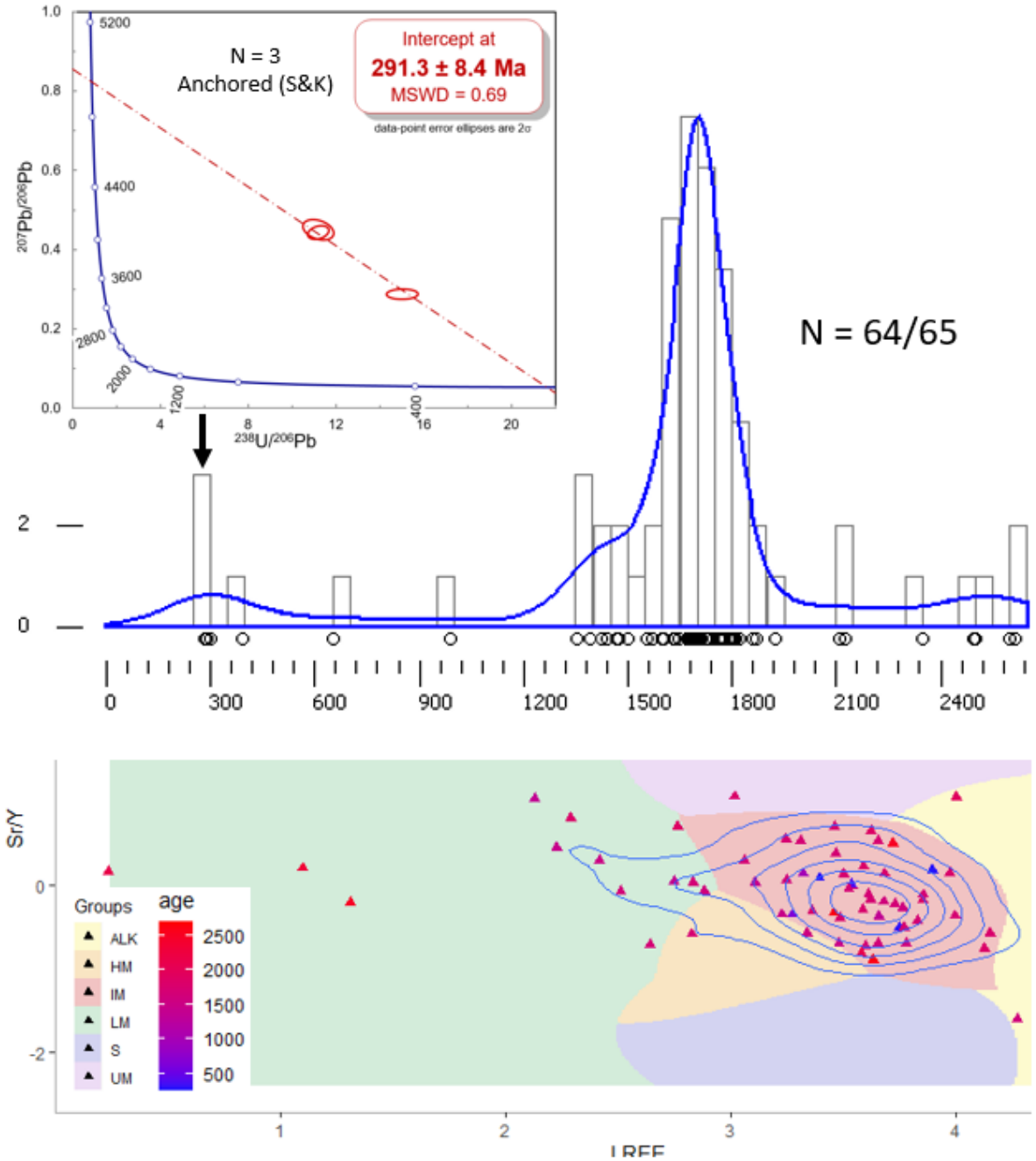

Figure 18: Apatite U/Pb and trace element results for sample R-37 (12/13-1A).

1.1.3.2 13/03-1

Sample 1 (Eocene sands)

Apatite U/Pb ages

The 73 ^{207}Pb-corrected ages range between 321.7 ± 23.7 Ma and 2728.7 ± 129.9 Ma (FIGURE 19). 13 grains (18 %) form a discordia with a lower intercept age of 333.9 ± 8.9 Ma (Visean). When these 13 grains are anchored to a common Pb value derived from the Stacey and Kramers (1975) terrestrial Pb evolution model, the lower intercept age is 336.1 ± 5.3 Ma (Visean). 27 grains (77 %) form a discordia with a lower intercept age of 424 ± 13 Ma (Late Caledonian). The remaining 33 grains (45%) are pre-Cambrian with peaks at 0.5-0.7 Ga, 0.8 Ga, 1.7-1.9 Ga and 2.7 Ga (FIGURE 19).

Trace element results

The grains plot over all the six domains of the biplot (FIGURE 19), confirming the detrital nature of the grains in the sand. When considering each age group separately, they still all plot across many different domains except the four oldest grains (>2 Ga) which all plots within the HM field (high-grade metamorphic rocks).

Zircon U/Pb ages

60 out of 97 grains are concordant with ^{206}Pb/^{238}U ages ranging from 319.6 ± 7.6 Ma to 2762 ± 72 Ma with peaks at c. 0.43 Ga (Late Caledonian), 1.1 Ga, 1.5-1.8 Ga (Labradorian) (FIGURE 19). Two grains yields Early Carboniferous ages of 320 and 340 Ma (FIGURE 19).

Sample 2 (basal gabbro)

Apatite U/Pb ages

The 123 apatite grains yield a Tera-Wasserburg non-anchored lower intercept age of 394 ± 43 Ma (Early Devonian) with a MSWD of 1.5 (FIGURE 20A). All the grains are clustered in one area of the Tera-Wasserburg plot space, indicating a very homogenous amount of common Pb in the grains. The clustering prevents the formation of a well-defined linear discordia and therefore the uncertainties on the intercepts are quite large. The weighted average ^{207}Pb-corrected age is 297.1 ± 9 Ma (FIGURE 20B). When the discordia is anchored to a common Pb value derived from the Stacey and Kramers (1975) terrestrial Pb evolution model, the lower intercept age is similar at 299 ± 9 Ma (with a final common Pb ratio anchor of 0.8555) (FIGURE 20A).

Trace element results

The grains plot mostly in the IM domain (FIGURE 21).

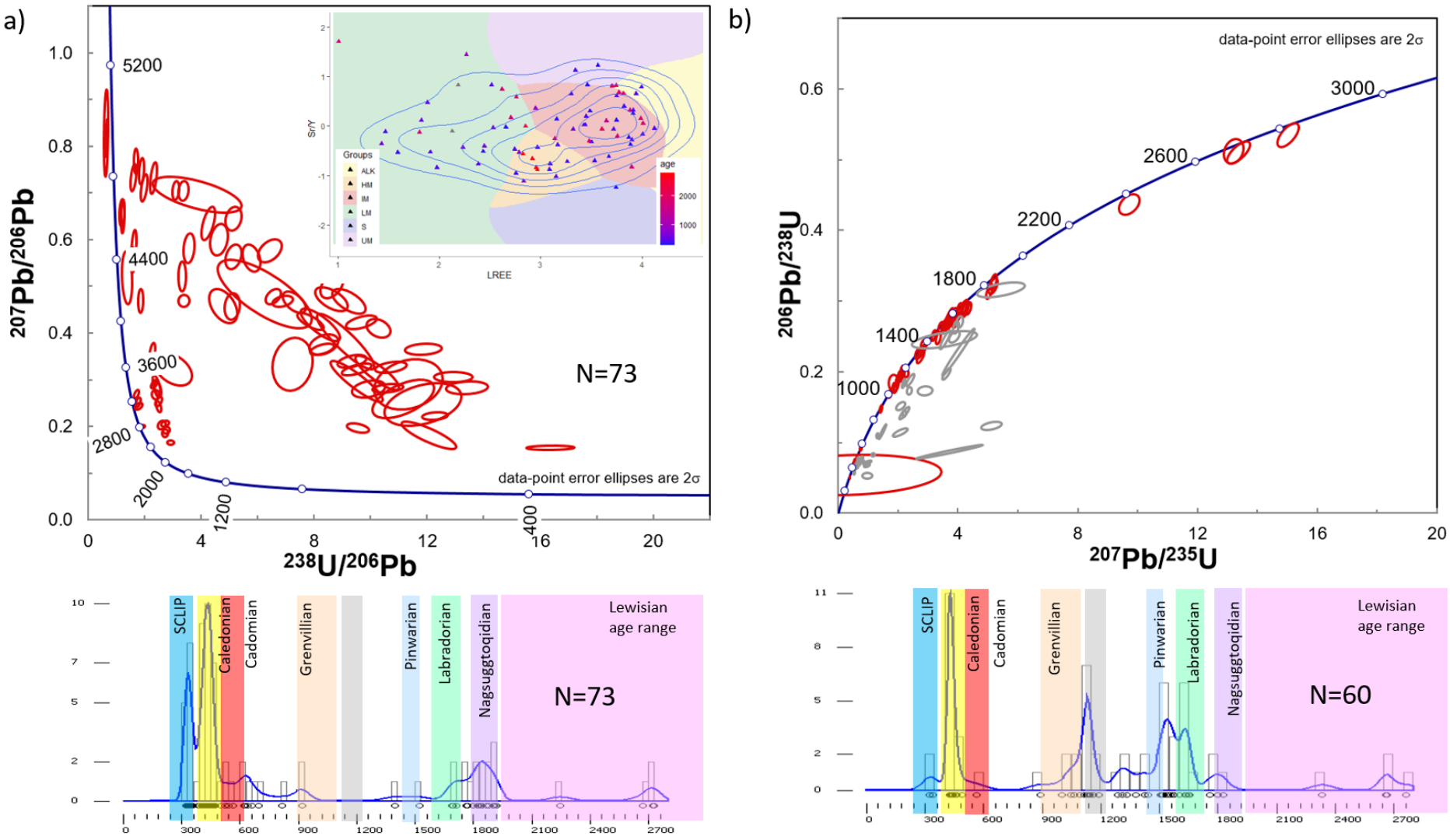

Figure 19: Zircon and apatite U/Pb and trace element results for sample R-1 (13/03-1). a) Apatites; b) Zircons.

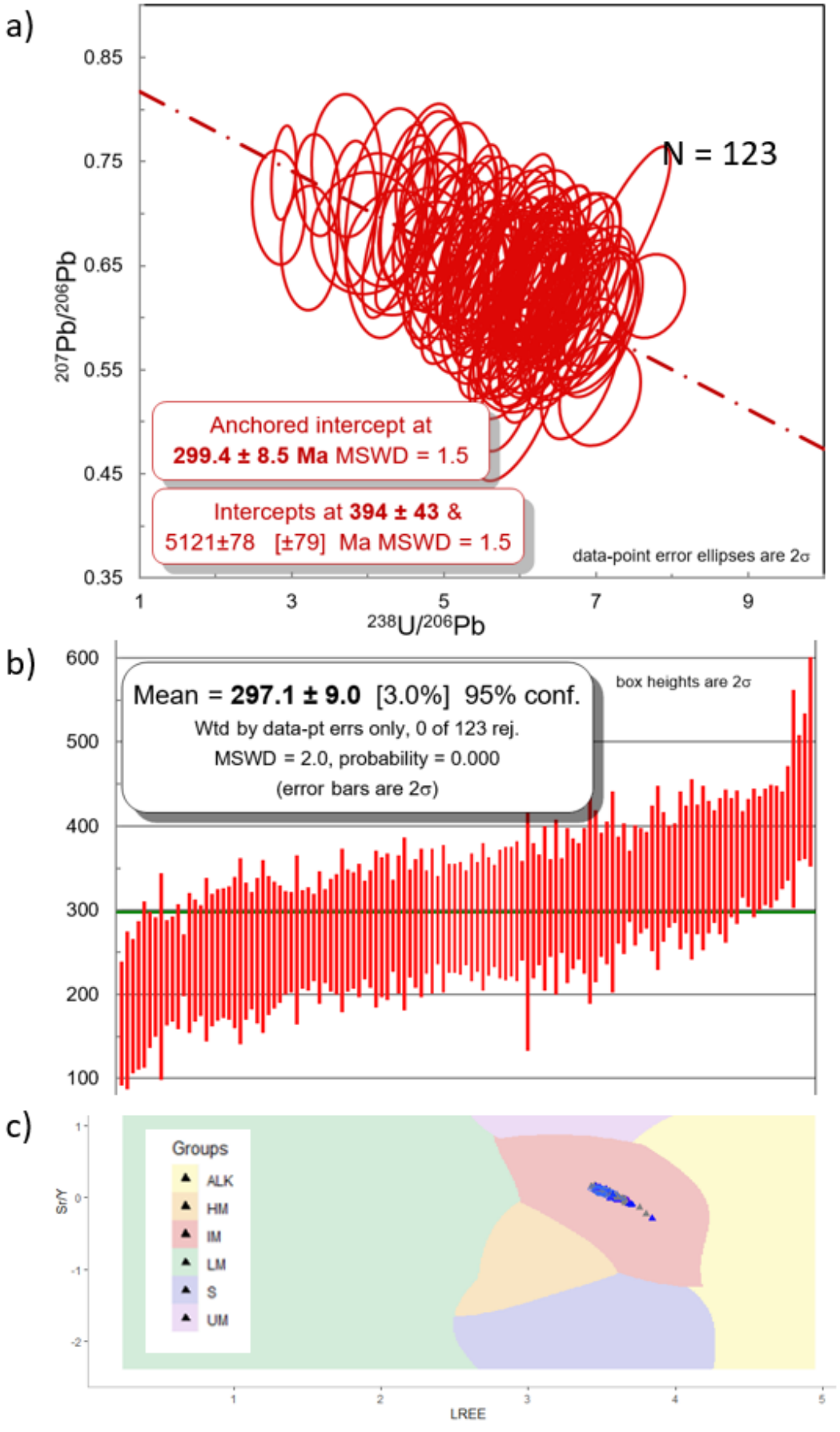

Figure 20: Apatite U/Pb and trace element results for sample R-2 (13/03-1).

Discussion

The gabbro intrudes Westphalian B-C sediments (317.1 ± 1.9 Ma) and therefore must be younger than 317 Ma, which excludes the non-anchored discordia age of 394 Ma. Therefore the weighted average ^{207}Pb-corrected age, 297.1 ± 9 Ma, will be used as the best age estimate for the rest of the study.

1.1.3.3 18/25-2

Sample 44

Apatite U/Pb ages

The 55 apatite grains yield a Tera-Wasserburg non-anchored lower intercept age of 230 ± 45 Ma (Late Triassic) with a MSWD of 1.5 (FIGURE 21A). When these 55 grains are anchored to a common Pb value derived from the Stacey and Kramers (1975) terrestrial Pb evolution model, the lower intercept age is 126 ± 20 Ma (Early Cretaceous). Similarly, the weighted average ^{207}Pb-corrected age is 129 ± 21 Ma (Early Cretaceous) (FIGURE 22A), which will be used as the best age estimate for the rest of the study.

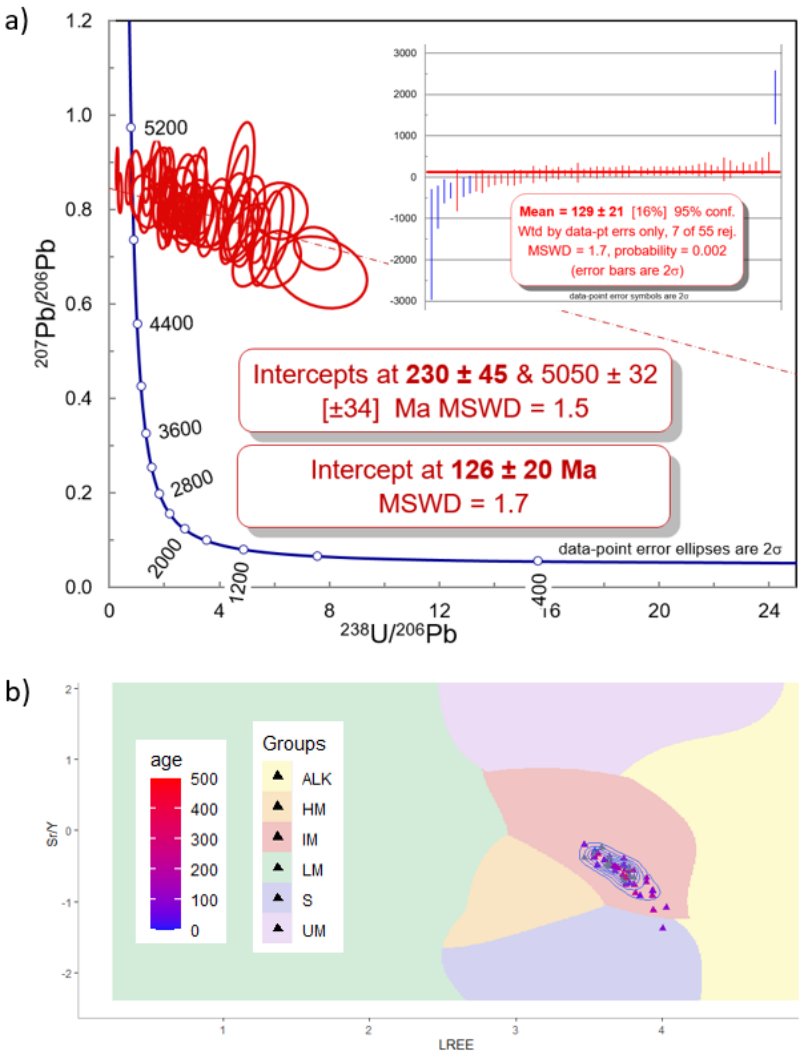

Figure 21: Apatite U/Pb and trace element results for sample R-44 (18/25-2)

Trace elements results

All the 55 apatites (except one) plot in the IM field (mafic, I-type) (FIGURE 21B).

1.1.3.4 26/30-1

Sample R-68 (Bathonian-Early Oxfordian sands)

Apatite U/Pb ages

The 131 ^{207}Pb-corrected ages range between 118.9 ± 47.1 Ma and 2575.8 ± 101.8 Ma. 68 grains (52 %) form a discordia with a lower intercept age of 156.2 ± 5.4 Ma (Kimmeridgian). When these 68 grains are anchored to a common Pb value derived from the Stacey and Kramers (1975) terrestrial Pb evolution model, the lower intercept age is 159.8 ± 3.1 Ma (Oxfordian) (FIGURE 22). 35 grains (27 %) are from a Laurentian source with ages ranging from 847 Ma to 2576 Ma with peaks at c. 0.85-1 Ga and 1.7 Ga. The remaining 28 grains are Permian (n = 8), Early Carboniferous (n = 5), Devonian (n = 9), Grampian (n = 3) and Cadomian (n = 3).

Trace elements results

Most of the 68 Late Jurassic apatites plot inside the UM (ultra-mafic) domain of the biplot. The older grains are spread out in all six domains, except the S field, without any age population being restricted to a specific source rock type (FIGURE 22).

Zircon U/Pb ages

136 out of 182 grains are concordant with ^{206}Pb/^{238}U ages ranging from 295.3 ± 6.9 Ma to 3139 ± 75 Ma. 97 grains (71 %) have a Laurentian affinity with peaks at c. 1 Ga (Grenville) and 1.7 Ga (Labradorian), with smaller peaks at c. 1.3 Ga, 1.5 Ga (Pinwarian), 1.9 Ga (Nagsuggtoqidian) and 10 Archean grains. The remaining grains are Cadomian (n = 18, 13%), Caledonian (n = 11, 8 %), Devonian (n = 1), Early Carboniferous (n = 5) and earliest Permian (n=1). The youngest concordant grain has an age of 295 ± 7 Ma (earliest Permian) (FIGURE 22).

Sample R-50 (Westphalian C sands)

Apatite U/Pb ages

The 19 grains have ^{207}Pb-corrected ages ranging between 296.3 ± 114.7 Ma and 2188.5 ± 175 Ma. 17 grains have a probable Laurentian origin with ages ranging from 1058 ± 108 Ma to 2188.5 ± 175 Ma. The two younger grains have an age of 394.9 ± 34.4 Ma (Early Devonian) and 296.3 ± 114.7 Ma (early Permian, but large uncertainty) (FIGURE 23).

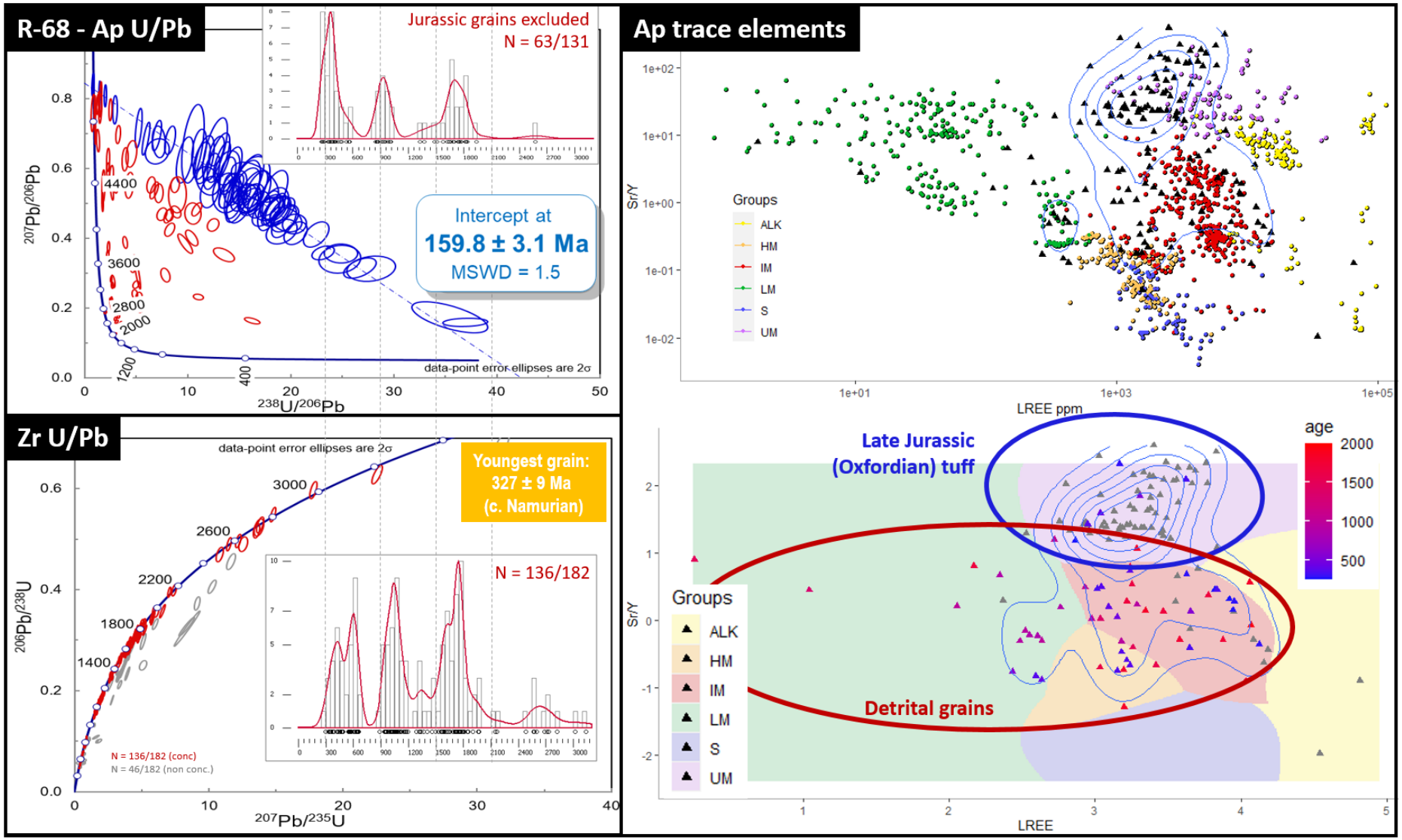

Figure 22: Sample R-68: Apatite and zircon U/Pb dating results and apatite trace element analysis.

Trace elements results

The grains plot over the IM, HM, S and UM domains (FIGURE 23).

Sample R-51 (basal granite wash and granite)

Apatite U/Pb ages

The 33 grains have ^{207}Pb-corrected ages ranging between 136.6 ± 117.1 Ma and 1846.1 ± 92.4 Ma. The majority of grains (n = 23, 70 %) have ages ranging from c. 866 to 1846 Ma. The remaining grains are Caledonian (400-453 Ma, n =6), Triassic (n = 1) and Jurassic (n = 3) (Figure 24). The six Caledonian grains align on a discordia with a lower intercept age of 415 ± 12 Ma (anchored to the common Pb value from Stacey and Kramers (1975)).

Trace element results

The three Jurassic grains plot in UM domain (as for sample R-68). Most of the Late Caledonian grains plot in the LM and HM fields. The Laurentian grains form a cluster in the IM domain with a few grains in the S, HM and LM fields with a few grains also plotting in the ALK, HM and LM domains (FIGURE 24).

Zircon U/Pb ages

40 out of 50 grains are concordant with ^{206}Pb/^{238}U ages ranging from 359.7 ± 8.8 Ma to 3177.2 ± 69.8 Ma. 28 grains (70%) have a Laurentian affinity with peaks at c. 1, 1.5 and 1.7 Ga. The remaining grains are Cadomian (n = 1), possibly Grampian-Taconic arc volcanism (497 Ma, n=1), Grampian (n = 5), Scandian (n = 3) and Devonian (n = 3). The youngest concordant grain has an age of 359.7 ± 8.8 Ma (FIGURE 24).

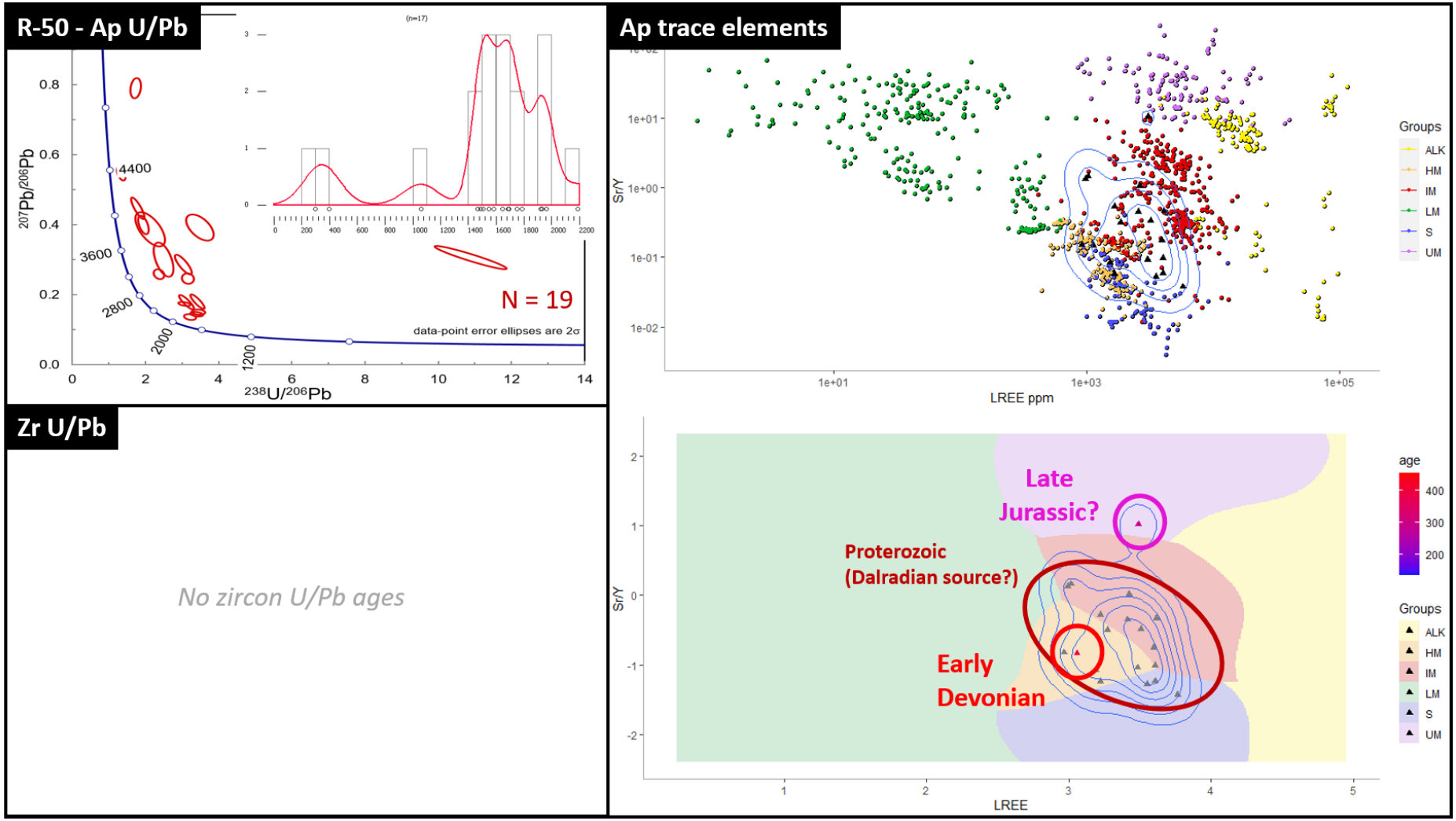

Figure 23: Sample R-50: Apatite and zircon U/Pb dating results and apatite trace element analysis.

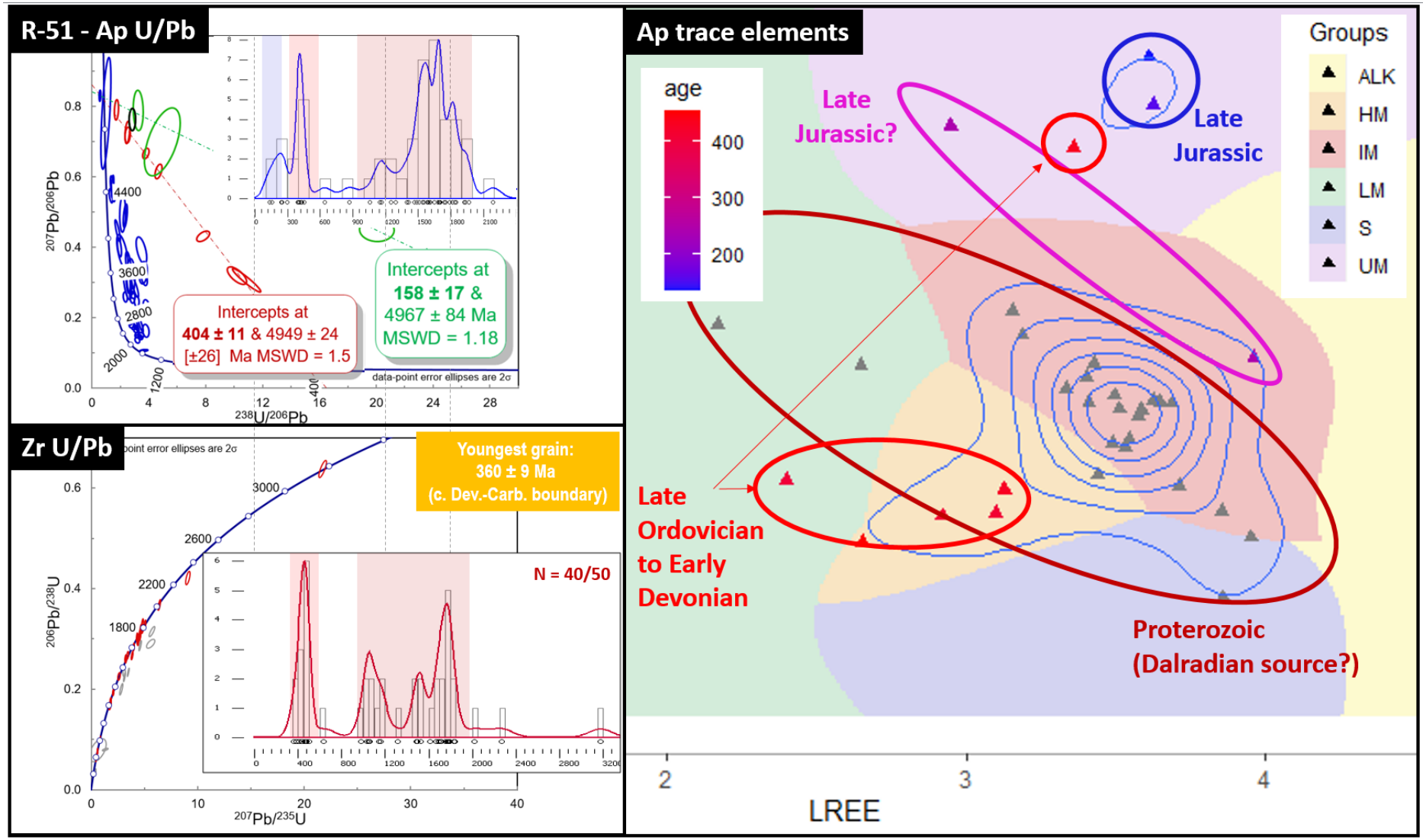

Figure 24: Sample R-51: Apatite and zircon U/Pb dating results and apatite trace element analysis.

1.1.3.5 35/13-1

Sample 54 (Oligocene dolerite sill)

Apatite U/Pb ages

The 99 apatites all plot in the upper left part of the Tera-Wasserburg plot space, suggesting a high and homogenous common Pb content. When grains with negative ^{207}Pb-corrected ^{238}U/^{206}Pb ages or positive age errors greater than 100 % are removed (leaving 64 grains, 65 %), the grains form a discordia with a lower intercept age of 69.9 ± 4.8 Ma (Latest Cretaceous-earliest Paleocene boundary). The weighted average of the 207-corrected ^{238}U/^{206}Pb age of all 99 grains yields an age of 61.6 ± 5.6 Ma (Danian-Selandian boundary) (FIGURE 25).

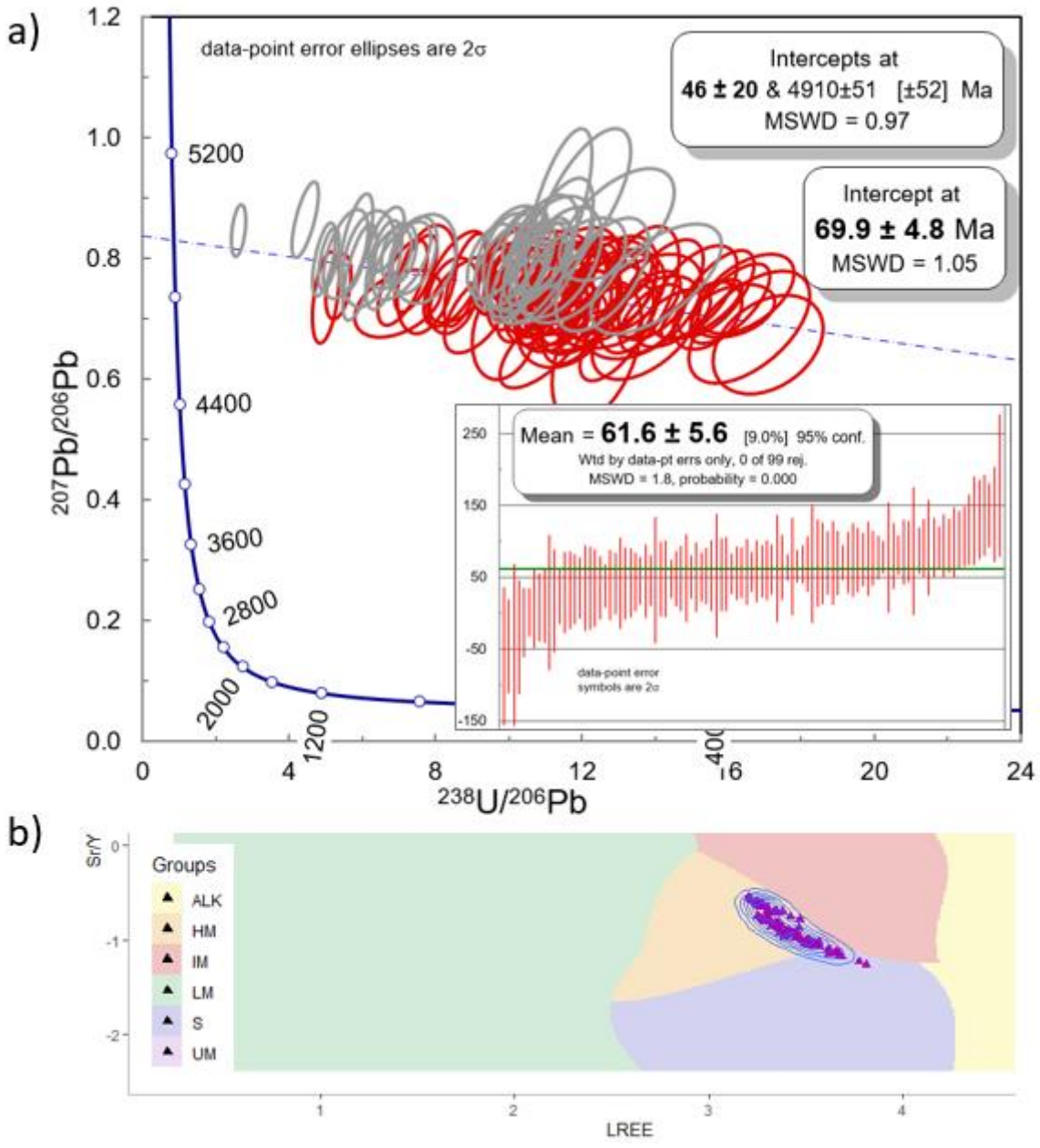

Figure 25: Apatite U/Pb and trace element results for sample R-54 (35/13-1).

Trace element results

All 99 grains plot in the right corner of the HM field (high-grade metamorphic rocks) domain and uppermost corner of the S field. However, in the training dataset, this area of the plot is underlain by numerous IM points (and no S points at all), which is more in line with the mafic nature of the dolerite.

1.1.3.6 35/15-1

Combined sample R-16-19

Apatite U/Pb ages

There are only a small number (17) of individual apatite U/Pb ages available for samples R-16 to R-19. However, they can be considered together as one population since the basalts are probably coeval or emplaced within a short period of time during the Paleocene as discussed above.

When plotted on a Tera-Wasserburg plot, the 17 grains align on two different discordia trends, reflecting two age groups (FIGURE 26A). Group 1 comprises the most apatite grains (14/17, *i.e*. 82%). They align on a discordia yielding a lower intercept age of 62 ± 18 Ma (upper Danian) with a MSWD of 1.7 (FIGURE 26B). However, based on their trace element signatures, two grains (R-16.g1j and R-19.g2) are possibly a separate detrital population or with U/Pb ages only partially reset by the Paleocene igneous event and are therefore best left out for the U/Pb age calculation. The new population of 12 grains align on a discordia yielding a lower intercept age of 76 ± 39 Ma (upper Danian) with a MSWD of 2.2. When the upper intercept of the discordia is anchored using the common lead isotopic composition derived from the Stacey and Kramers (1975) model for the time of crystallization, the lower age intercept age is 66 ± 7.5 Ma (Campanian to Paleocene,) (FIGURE 26B). The weighted average of ^{207}Pb-corrected ages, after five iterations of the correction using the common lead value from Stacey and Kramers (1975), yields an age of 68 ± 12 Ma (FIGURE 26B).

The age estimation for this group has a large uncertainty because of both the low number of grain and large uncertainty ellipses. The large ellipses are probably due to the low amount of U and Pb in these young and uranium-poor apatites ([U] = c. 3.5 ppm). Despite the large uncertainty on the age, the results show that these apatites are Paleocene apatites derived from the igneous rocks.

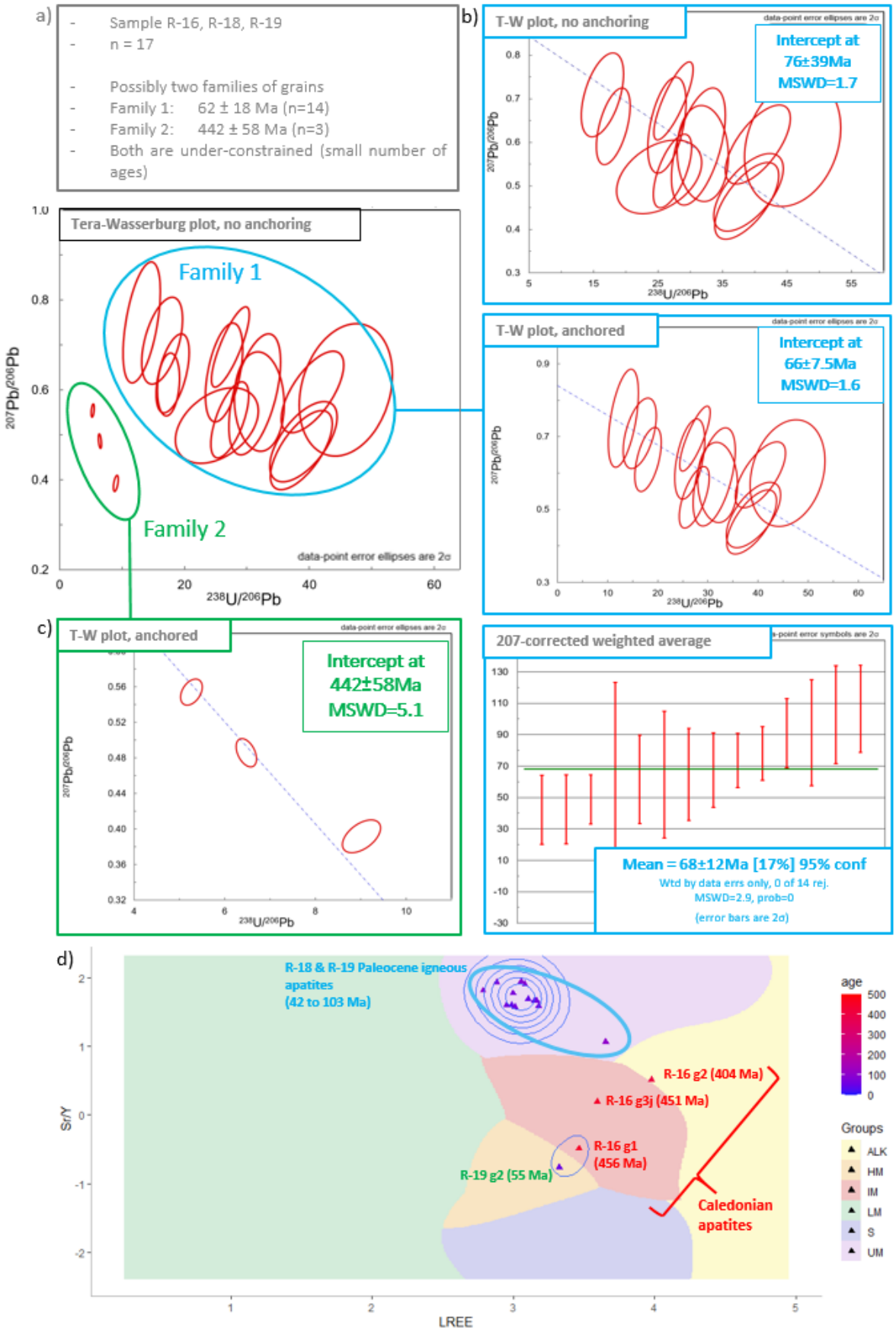

Figure 26: Apatite U/Pb ages and trace element results for samples R-16, R-18, R-19 combined as one sample (35/15-1).

Group 2 comprises only three grains but they have much smaller ellipses and align nicely on a discordia that yields an anchored lower intercept of 442 ± 58 Ma. Despite the low number of grains, there is little doubt that these three grains are detrital grains of Caledonian age (FIGURE 26C). These three grains will therefore be excluded from the AFT study since they do not come from the igneous units. This shows the power of LAFT and the dual-dating (U/Pb-AFT) of apatites when attempting fission track studies on samples with a risk of pre-sampling contamination (such as cuttings in a well) and when the targeted AFT sample has a single U/Pb age population such as crystalline igneous metamorphic bedrock samples (extraneous grains cannot be identified in detrital samples unless they are younger than the deposition age).

Apatite trace elements

The majority of grains (13/17, 76%) in samples R-16-19 plot within the UM field (FIGURE 26D). These 13 grains all have U/Pb ages within uncertainty of a Paleocene age. This result agrees very well with the basalt geochemical report that classified the rocks as mafic basalts from ultramafic parent magmas that have undergone very little amount of fractionation (Henderson, 1980). Out of the four outlier grains, three of them are the Caledonian grains identified by U/Pb dating. They plot within or near the IM field (FIGURE 26D).

Grain R-19.g2 has a Paleocene age but plots far away from the Paleocene grain cluster, in the HM domain (Figure 26d). This grain is possibly a xenocrystic apatite that were incorporated in the magma at a very late stage of emplacement which led to complete (R-19.g2) resetting of the U/Pb geochronometer while preserving their LREE and Sr/Y signatures. The uncertainty on the origin of these two grains mean they are not used for fission track interpretation purposes.

Zircon U/Pb ages

Data quality

As for the apatites, all the zircons from samples R-16 to R-19 (n=125) have been analysed as a single population. Sixteen grains with significant discordance when plotted on both either Wetherill or Tera-Wasserburg plots have been removed from the analysis. The final dataset used to calculate ages is composed of 109 concordant or near-concordant grains. Four grains displaying an apparent rim overgrowth were dated on both their rims and cores.

Paleocene zircons

The zircon $^{238}U/^{206}Pb$ ages range from 58.14 Ma to 2098.20 Ma, with dominant peaks at c. 60 Ma , 414 Ma, 596 Ma and 1063 Ma (FIGURE 27).

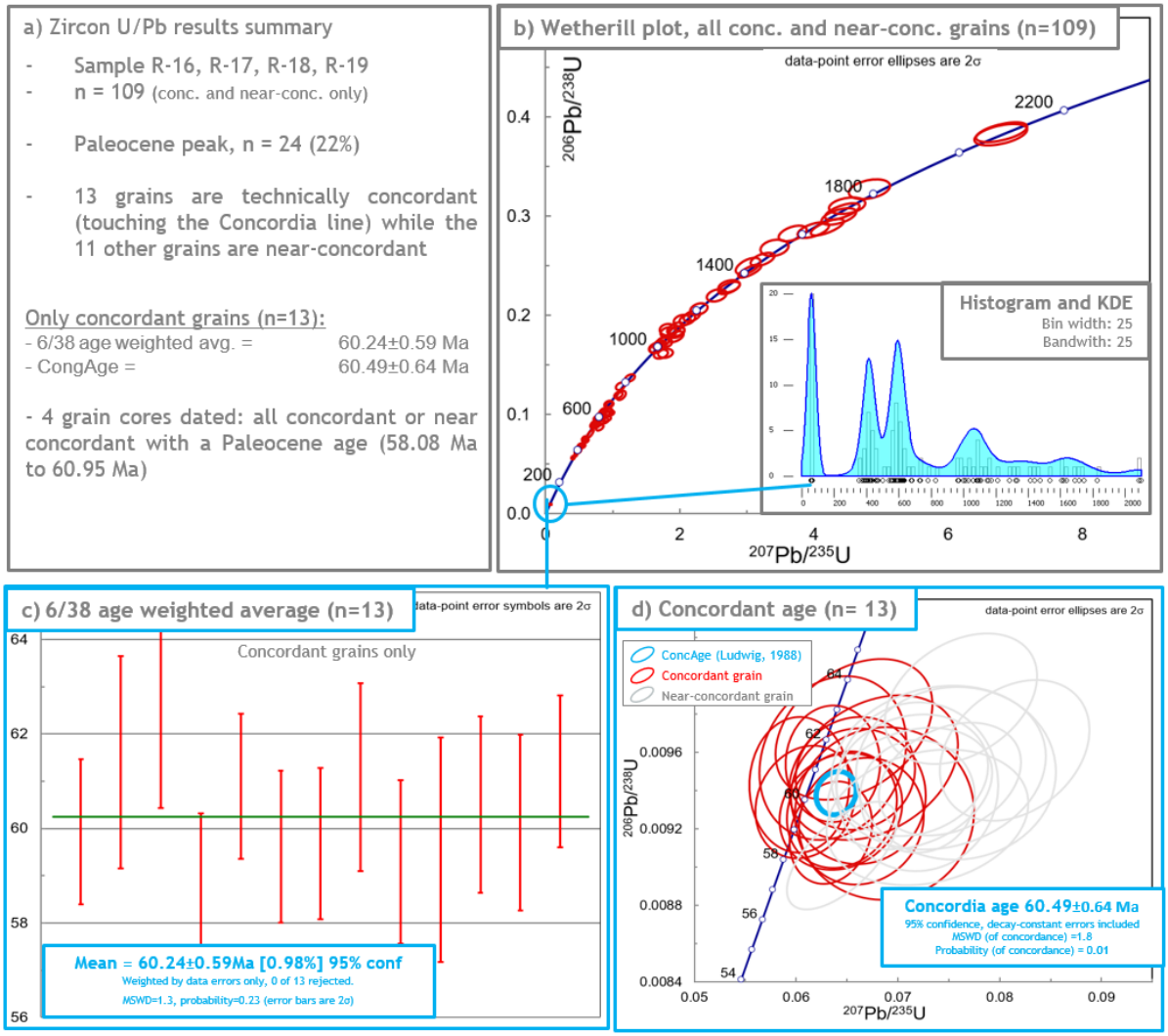

Figure 27: Zircon U/Pb dating of samples R16 to R-19.

The main peak at c. 60 Ma is composed of 24 concordant to near-concordant grains (22% of the 109 grains) with ages ranging from 58.14 to 63.38 Ma. Out of these 24 Paleocene grains, 13 grains are technically concordant (their uncertainty ellipse intersects the concordia line). The weighted average $^{238}U/^{206}Pb$ age of these concordant grains is 60.24 ± 0.59 Ma (Selandian) with a MSWD of 1.3 (FIGURE 27) while the concordia age (ConcAge, Ludwig (1998)) is 60.49 ± 0.64 Ma with a MSWD and probability of concordance of respectively 1.8 and 0.01 (FIGURE 27). The slightly discordant grains have most probably incorporated minor common lead. Four grains selected for dual core-rim dating based on their CL response yielded an identical Paleocene age for both core and rim.

Older zircons

The older grains range from 354.06 Ma to 2098.20 Ma with three dominant peaks at 414 Ma (Caledonian), 595 Ma (Cadomian) and 1063 Ma (Grenville) (FIGURE 27). The peak ages were calculated by deconvolution of multiple age components using Isoplot.

Distribution of Paleocene vs older apatites/zircons in the samples

70% of the Paleocene zircons come from the topmost sample R-16. The remaining 30% are split equally between R-17 and R-18 with no Paleocene zircons in R-19. 35% of the older detrital zircons come from R-16, 28% and 36% come from R-17 and T-18 and only one grain comes from the micro-gabbro R-19 (FIGURE 28). Only 7% of the Paleocene apatites come from the topmost sample R-16. There is no data for R-17. 71% come from R-18 and 21% come from the R-19. The three detrital Caledonian apatites all come from sample R-16 (FIGURE 28).

	Zircons			Apatites		
	Paleocene	Older	*Total*	Paleocene	Older	*Total*
R-16	14	29	*43*	1	3	*4*
R-17	3	23	*26*	?	?	*?*
R-18	3	30	*33*	10	0	*10*
R-19	0	1	*1*	3	0	*3*
Total	*20*	*83*	*103*	*14*	*3*	*17*

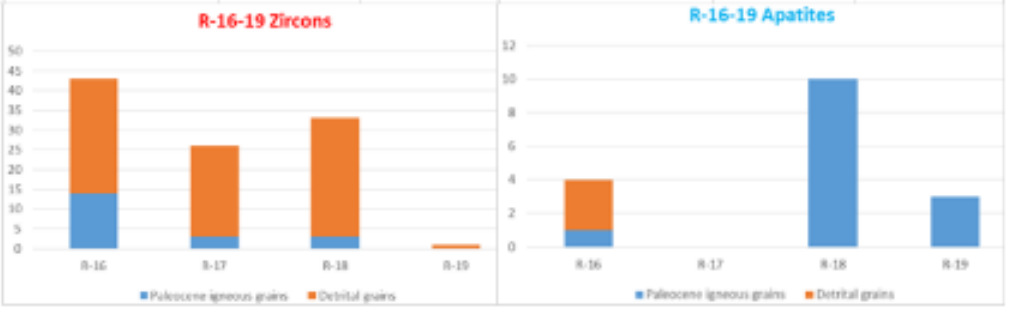

Figure 28: Distribution of zircon and apatite grains according to U/Pb age and samples.

1.2 Analysis of the AFT and AHe results

1.2.1 Goban Spur

1.2.1.1 Sample R-24 (Late Variscan granitoid)

AFT results

The 40 analysed apatites yielded 39 AFT ages ranging from 88.7 ± 13 Ma to 397.2 ± 57.4 Ma with a central age of 192 ± 9.2 (1σ) Ma (Early Jurassic) and a chi-square test <0.01 (*i.e.* the ages are overdispersed and might belong to more than one age group) (FIGURE 29).

The Cl content ranges from 0.18 to 0.38 wt% with an average of 0.26 ± 0.04 (1σ) wt%. The Dpar ranges from 1.65 to 2.16 µm with an average of 1.95 ± 0.1 (1σ) µm. The U content ranges from 13 to 124 ppm with an average of 45 ± 30 (1σ) ppm.

The lengths of 291 confined fission tracks range from 3.09 to 16.35 µm with a MTL of 12.0 ± 2.8 (1σ) µm and a unimodal distribution with a peak at 13.5-14 µm (FIGURE 29).

AHe results

Seven grains were analysed for AHe dating. Two grains had degassing issues and therefore were discarded before parent element concentration measurements. Four of the remaining grains were fully outgassed with background values during the second run suggesting no inclusions. They have raw ages of 59, 87, 90 and 95 Ma and F_T-corrected ages of 87, 130, 136 and 136 Ma (Cretaceous; Valanginian to Coniacian).

One grain (R-24.g7) was still leaking some helium during the second heating run (but only c. 0.34% of first run value) and third run (0.05% of first run value), suggesting that it might contain some inclusions. This grain yielded an AHe raw age of 173 Ma and a F_T-corrected age of 221 Ma (Late Triassic). It is likely that the much older age of this grain is caused by extraneous helium from the inclusions as suggested by the leaking helium. This grain will not be used for thermal history interpretation and modelling.

The ages do not show the expected correlations with either damage intensity (eU) or diffusion domain size (grain size, Req). The younger grain for example has both a small size and the highest eU, which should result in an older age (FIGURE 29).

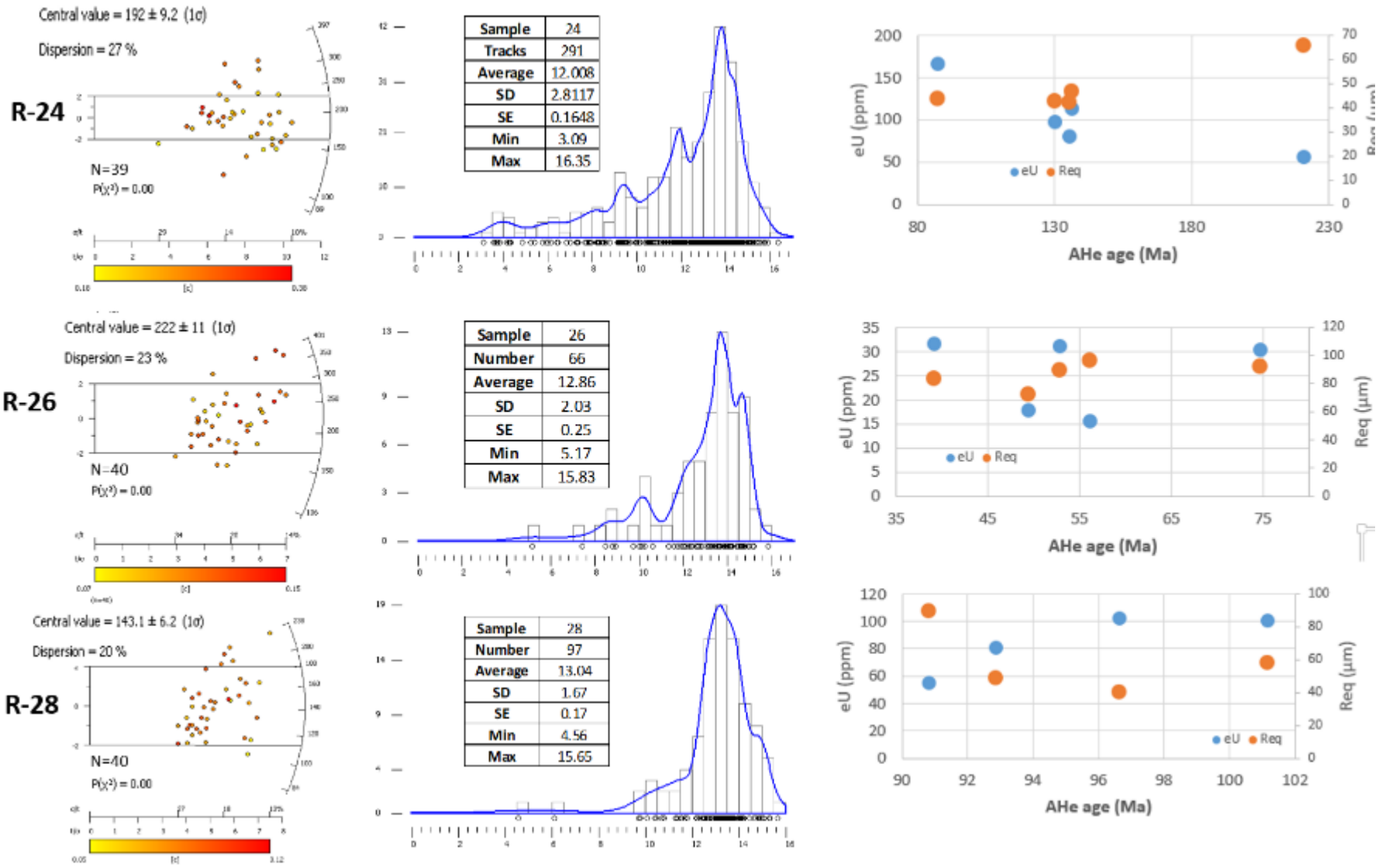

Figure 29: AFT results for the Late Variscan granite samples. Left column: AFT age radial plot, coloured by [C]; right column: Fission track lengths.

Based on the absence of clear correlations between eU, Req and AHe ages, only the three grains which form an age cluster at 130-136 Ma (Hauterivian-Valanginian) are estimated to be trustworthy due to the repeatability of the age. The younger grain will not be used for thermal history interpretation and modelling.

Discussion

The younger AHe ages (Early Cretaceous) in comparison to the AFT age (Early Jurassic) and the presence of small track lengths suggest that the sample spent a significant amount of time in the PAZ and PHeRZ (rather than cooling down quickly) during the Jurassic and Cretaceous.

1.2.1.2 Sample R-25 (Archean metamorphic rock)

AFT results

The 40 analysed apatites yielded 40 AFT ages ranging from 14.9 ± 10.6 Ma to 97.1 ± 37.1 Ma with a central age of 41.8 ± 2.5 (1σ) Ma, a chi-square test of 0.6 (*i.e.* the ages are not overdispersed and probably belong to only one age group) (FIGURE 30).

The Cl content ranges from 0.06 to 0.29 wt% with an average of 0.12 ± 0.05 (1σ) wt%. The Dpar ranges from 1.16 to 1.91 µm with an average of 1.52 ± 0.16 (1σ) µm. The U content ranges from 1.2 to 141 ppm with an average of 20 ± 22 (1σ) ppm.

The length of only two confined fission tracks could be measured (11.8 and 14.5 µm) (FIGURE 30).

AHe results

Seven grains were analysed for AHe dating. One grain had degassing issues and therefore was discarded before parent element concentration measurement and only six AHe ages were obtained.

One grain only had a good degassing during the first run (grain R-25-g.3) and yielded background He concentrations during the repeat run. The other five grains had He leaks during the repeat runs (>2% for grains 4 and 5 and < 0.6% for grains 1, 2 and 6).

Grain 5 yielded an implausible raw age of 883 Ma. Its parent element concentrations are much smaller than for the five other grains (e.g. [U] 1 ppm vs 12-30 ppm) which is the cause for the very old age. This grain will not be used for thermal history interpretation.

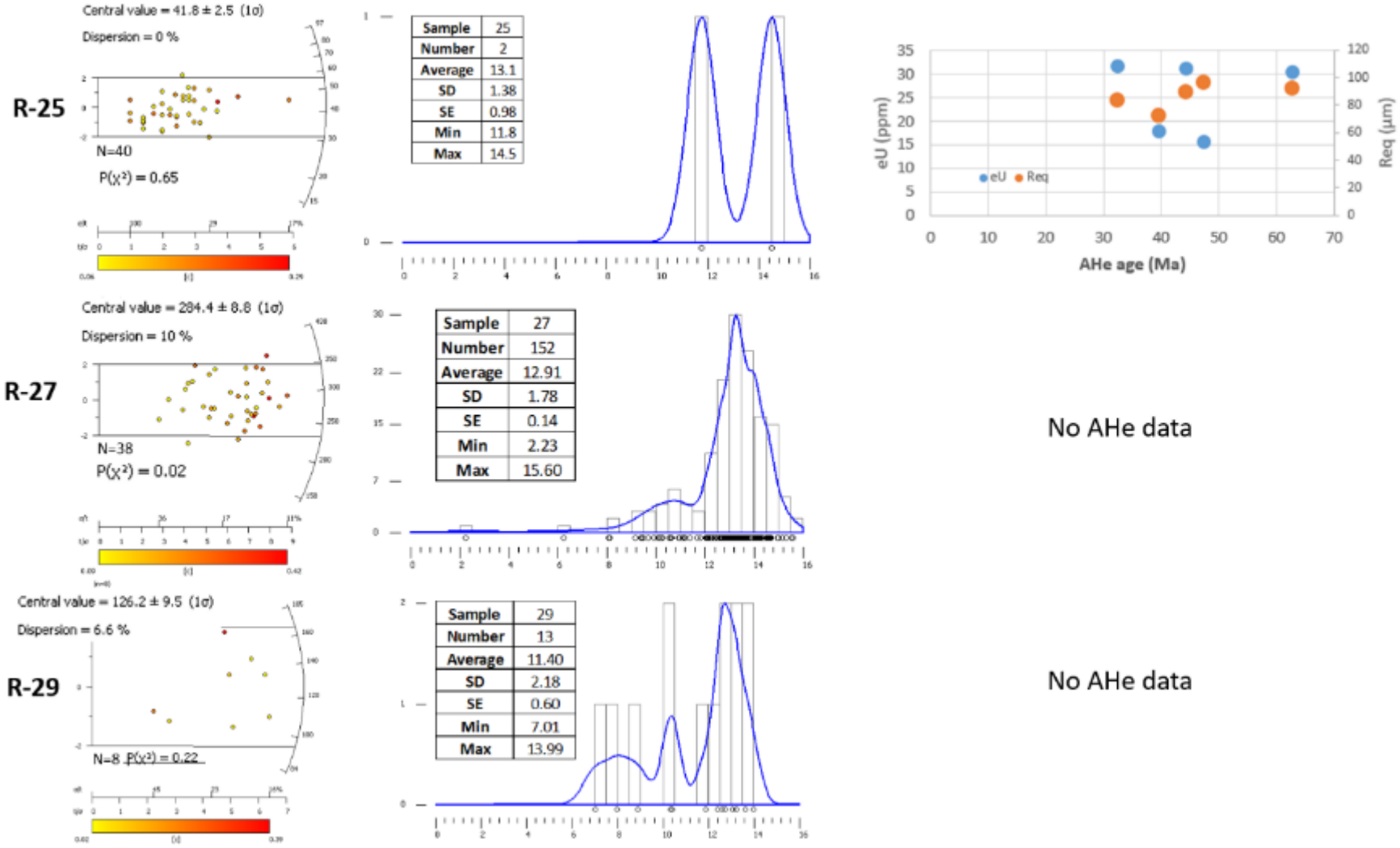

Figure 30: AFT results for samples R-25, 27 and 29. Left column: AFT age radial plot, coloured by [C]; right column: Fission track lengths.

The five other grains yielded raw ages of 32, 40, 44, 47 and 63 Ma (c. Paleocene-Eocene) and F_T-corrected ages of 39, 49, 53, 56 and 75 Ma (Late Cretaceous-Middle Eocene). Grain 3 which had perfect He degassing provides the most trustworthy age at 40 Ma (49 Ma when F_T-corrected). Together with grains 4 and 6 they form an age cluster at 49-56 Ma (F_T-corrected, Early Eocene/Ypresian). The grain with the oldest raw age (63 Ma) is also geologically implausible since the AFT central age is 41.8 ± 2.5 Ma which is an approximate upper limit to the possible AHe ages.

The five grains do not show the expected correlations between AHe ages and Req or eU (FIGURE 30). However, when only the cluster of three grains are considered, they is a positive correlation between ages and Req (FIGURE 30).

Discussion

Both the AFT central age (c. 42 Ma, Lutetian) and AHe cluster age (c. 49-56 Ma, Ypresian) are very close suggesting that the sample cooled down quickly through both the PAZ and PHeRZ at some point during the Early-Middle Eocene. The AHe ages are slightly older than the AFT age which could be due to either:

- An inaccurate AFT age due to the low number of counted tracks per grain (Ns), or;
- Inaccurate AHe ages due to extraneous He or non-representative F_T-correction (e.g. inaccurate geometry simplification)

However, the mismatch is small and the uncertainty on the timing of the cooling event is limited to a few millions of years (Ypresian-Lutetian).

1.2.1.3 Sample R-26 (Late Variscan granite)

AFT results

The 40 analysed apatites yielded 40 AFT ages ranging from 105.9 ± 35.9 Ma to 401.4 ± 60.6 Ma with a central age of 222 ± 11 (1σ) Ma, a chi-square test of <0.01 (*i.e.* the ages are overdispersed and might belong to more than one age group) (FIGURE 29).

The Cl content ranges from 0.07 to 0.15 wt% with an average of 0.11 ± 0.02 (1σ) wt%. The Dpar ranges from 1.35 to 1.96 µm with an average of 1.69 ± 0.12 (1σ) µm. The U content ranges from 6 to 35 ppm with an average of 19 ± 8 (1σ) ppm.

The lengths of 66 confined fission tracks range from 5.2 to 15.8 µm with a MTL of 12.9 ± 2.0 (1σ) µm (FIGURE 29).

AHe results

Six grains were analysed for AHe dating. Only one grain yielded a background helium concentration during the repeat run (grain 6). The other grains yielded higher concentration (from 0.06% to 2.4% of the first run) and one of them (grain 5) continued to yield high He concentration even at the third run suggesting the presence of helium-rich inclusions in the mineral.

The six grains yielded raw AHe ages of 45, 82, 84, 85, 236 and 280 Ma and F_T-corrected ages of 63, 104, 111, 112, 280 and 365 Ma (Early Paleocene to Late Devonian). The oldest grains are outliers and have raw AHe ages which are older than the AFT central age which is geologically implausible. These two grains probably contain extraneous He from inclusions.

Three grains form an age cluster at 104-112 Ma (F_T-corrected, Albian). They all have similar size (Req 57 to 68 µm) and eU (52-62 ppm). The youngest grain is grain 6 which is the only grain which did not leak any He during repeat runs (it is therefore the most trustworthy grain). However, this grain is an outlier in comparison to the other three grains (raw age of 45 Ma vs 82-85 Ma). This grain is smaller (Req 48 µm) which could explain the younger age (smaller diffusion domain), however it has a much higher eU and radiation damage (152 ppm) which should lead to an older age (FIGURE 29).

In conclusion, the AHe results show a cluster of Albian ages but also a grain with a reliable but much younger age (Danian) which could be due to its smaller size (although its high eU content would probably counterbalance this effect).

Discussion

The younger AHe ages (Albian) in comparison to the AFT age (Late Triassic) and the presence of small track lengths suggest that the sample spent a significant amount of time in the PAZ and PHeRZ (rather than cooling down quickly) during the Mesozoic.

The AHe ages appear to be a bit younger (Albian) than in sample R-24 (Valanginian-Hauterivian), while the AFT central age appears to be slightly older (Late Triassic vs Early Jurassic). Since both samples come from two dredges crossing each other and probably from the same Late Variscan granitoid body, it is unlikely that the differences in AFT and AHe data result primarily from a different thermal history. Rather, it is more likely that the differences come from inaccuracies in both the AFT and AHe data.

Both sample R-24 and R-26 demonstrate that the Late Variscan granitoid of Granite Cliff 4000 was exhumed and brought to surface probably gradually during mainly the Jurassic and Early Cretaceous.

1.2.1.4 Sample R-27 (Cadomian? granulite)

AFT results

The 40 analysed apatites yielded 38 AFT ages ranging from 157.7 ± 37.8 Ma to 437.8 ± 97.2 Ma with a central age of 284.4 ± 8.8 (1σ) Ma (Early Permian), a chi-square test of 0.01 (*i.e.* the ages are not overdispersed and might belong to one age group only) (FIGURE 30).

The Cl content ranges from 0.09 to 0.41 wt% with an average of 0.20 ± 0.09 (1σ) wt%. The Dpar ranges from 1.62 to 2.44 µm with an average of 2.02 ± 0.18 (1σ) µm.

The lengths of 152 confined fission tracks range from 2.23 to 15.6 µm with a MTL of 12.91 ± 1.78 (1σ) µm (FIGURE 30).

AFT results for legacy sample L-DR12-B21

The analysis of the granulite sample L-DR12-B21 by Fügenschuh et al. (2003) yielded an AFT central age of 211.6 ± 10.3 Ma (Late Triassic) with a chi-square test of 0.44. The 101 measured track lengths have a MTL of 12.98 ± 1.30 (1σ) µm.

AHe results

No apatite grains suitable for AHe dating were found for this sample.

Discussion

Despite being measured on the same clast, the central age found in this study (284 Ma) is significantly older than the central age of the legacy study by Fügenschuh et al. (2003) (212 Ma). The MTL however values are very similar. The poor repeatability of the AFT central age cannot be explained without further analyses of the clast. However, the analysis of Fügenschuh et al. (2003) was done on 16 apatite grains only, while the analysis on R-27 was done on 40 grains which theoretically should result in a more reliable central age and therefore will be used for thermal history interpretation in this study. At the very least, it can be concluded that the AFT central age for this granulite sample is Permian-Triassic, which is much older than the central age of the other sample from Menez Bihan.

The AFT central age and presence of small track lengths indicate that the sample experienced a protracted cooling through the PAZ during the Late Carboniferous-Early Permian.

The AFT central age (284 ± 9 Ma) is very similar to the age of the zircons believed to come from a vein (297 ± 5 Ma) that could be linked to the emplacement of the Late Variscan granites of Granite Cliff 4000 (296-297 Ma) and Menez Bihan (288 Ma). Therefore, it is possible that the exhumation of this granulite occurred at the same time than the emplacement and cooling of the granite intrusion. For this to be the case, it requires the granulite to be significantly above the Menez Bihan granite intrusion for it to cool down below 60 °C while the granite is cooling down.

1.2.1.5 Sample R-28 (Late Variscan granitoid)

AFT results

The 40 analysed apatites yielded 38 AFT ages ranging from 84.4 ± 22.9 Ma to 238.0 ± 40.7 Ma with a central age of 143.1 ± 6.2 (1σ) Ma (Berriasian), a chi-square test <0.01 (*i.e.* the ages are overdispersed and might belong to more than one age group) (FIGURE 29).

The Cl content ranges from 0.05 to 0.12 wt% with an average of 0.08 ± 0.02 (1σ) wt%. The Dpar ranges from 1.46 to 1.93 µm with an average of 1.74 ± 0.11 (1σ) µm.

The lengths of 97 confined fission tracks range from 4.56 to 15.65 µm with a MTL of 13.04 ± 1.67 (1σ) µm (FIGURE 29).

AHe results

Seven grains were analysed for AHe dating. One grain could not be degassed properly and therefore AHe ages for only six grains were obtained. Two grains (grains 3 and 5) yielded background He values during the repeat runs, the four other grains (1, 2, 6 and 7) leaked He (0.11 to 3.23% of the first run) suggesting the possible presence of inclusions.

One grain yielded an implausible raw age of 1247 Ma, probably due to anomalous parent element concentration measurement (e.g. [U] 3ppm vs 42-103 ppm for the other grains). This grain will not be used for thermal history interpretation.

The five other grains yielded raw AHe ages of 10, 63, 66, 76 and 76 Ma. The youngest grain is an outlier in term of age but also in term of parent element concentration with a higher [U] (103 ppm vs 42-76 ppm) and a much higher [Th] (1158 ppm vs 44-95 ppm) in comparison to the four other grains. The 40 AFT apatite grains yielded [U] ranging from 10 to 66 ppm with an average of 25 ppm, which is in agreement (within error) with the [U] of the four other grains (Figure 29). The younger AHe age, higher U, Th and Sm concentration and much higher Th/U ratio clearly separate this grain from the four other grain. The origin of the difference is unknown. This grain will not be used for thermal history interpretation.

The four remaining grains have F_T-corrected ages of 91, 93, 97 and 101 Ma (c. Turonian-Cenomanian) and they include the two grains with no He leaks (most reliable grains) which corresponds to the two oldest ages (97-101 Ma, Albian-Cenomanian boundary).

These four grains show a positive correlation between AHe ages and eU, indicating that radiation damage might be the cause of some of the age dispersion. However, there is no clear correlation between AHe ages and grain size for these four grains (FIGURE 29).

Discussion

The younger AHe ages (c. Cenomanian) in comparison to the AFT age (c. Berriasian) and the presence of small track lengths suggest that there was a gradual (rather than sudden) cooling down through the the PAZ and PHeRZ during the latest Jurassic and Early Cretaceous.

1.2.1.6 Sample R-29 (Post-Early Permian green sandstone)

AFT results

The eight analysed apatites yielded eight AFT ages ranging from 83.6 ± 29.9 Ma to 185.4 ± 38.7 Ma with a central age of 143.1 ± 6.2 (1σ) Ma (Early Cretaceous), a chi-square test <0.01 (*i.e.* the ages are overdispersed and might belong to more than one age group) (FIGURE 30).

The Cl content ranges from 0.05 to 0.12 wt% with an average of 0.08 ± 0.02 (1σ) wt%. The Dpar ranges from 1.46 to 1.93 µm with an average of 1.74 ± 0.11 (1σ) µm.

The lengths of only 13 confined fission tracks range from 7.01 to 13.99 µm with a MTL of 11.4 ± 2.18 (1σ) µm. There are not enough tracks to derive meaningful thermal history information from them (FIGURE 30).

AHe results

No apatite grains suitable for AHe dating were found for this sample.

Discussion

There are not enough AFT ages to derive reliable thermal history information from this sample because the individual FT age dispersion is large.

The young AFT central age could either be the result of an old sandstone (e.g. Devonian) that was buried and then exhumed during the Mesozoic, possibly with partial annealing of tracks inherited from the source or else a younger sandstone (e.g Cretaceous or even Tertiary) that contain AFT ages inherited from the sources. The shape of the confined track length distribution could help discriminate between a detrital *vs* reset sample but for this sample there are only 13 confined track lengths which is not enough to be used for such purpose.

1.2.2 North Porcupine High

1.2.2.1 16/28-sb01 (Table 1 and Figure 31)

Sample L-GC777-1 (Depositional age: Middle Eocene 37.8-47.8 Ma)

The two apatites yielded AFT ages of 0 ± 74.8 Ma and 92.8 ± 55 Ma and a MTL of 12.16 ± 0.16 µm (the central age is not provided since it is meaningless with only two ages). The AFT age of 0 Ma is due to the absence of tracks in this grain (Ns = 0).

Sample L-GC777-9 (Depositional age: Middle Eocene 37.8-47.8 Ma)

Legacy AFT results

The 20 grains yielded AFT ages ranging from 67.6 ± 21.5 Ma to 450.4 ± 137 Ma, a central age of 180.6 ± 21.1 Ma (Early Jurassic) and a chi-square test P-value <0.01 (*i.e.* the ages are overdispersed and probably belong to more than one age group). The 82 confined track lengths measured for these grains have a MTL of 13.68 ± 1.06 µm (1σ) with a modal peak at 13-15 µm (TABLE 1 AND FIGURE 31).

The results of Green (2001) show that this sample have not experienced high temperatures above c. 100 °C and the tracks have not been completely annealed since the time of deposition in the Middle Eocene.

Legacy ZFT results

The 11 zircons from the Middle Eocene sample L-GC777-9 yielded a pooled fission track age of 260 ± 43 Ma.

Table 1: AFT and ZFT results for shallow borehole 16/28-sb01.

AFT Results

Sample	Depth		n	Ns	Ni	Area	U/Ca	$P(\chi^2)$	Central Age	±1σ	Tracks	MTL	SD	SE	Inverse?	
	m MD	*m BSB*				*cm²*			*Ma*	*Ma*		*µm*	*µm*	*µm*	*FTA*	*FTL*
L-GC777-1	41	41	2	4	16	n/a	n/a	0.14	57.3	33.1	2	12.16	0.16	0.11	No	No
L-GC777-9	60.5	61	20	366	422	n/a	n/a	<0.01	180.6	21.1	82	13.68	1.06	0.16	Yes	Yes
R-3	89	89	1	8	n/a	1.43E-05	4.25E-02	n/a	126.8	45.3	1	6.70	0.00	0.00	No	No
R-4	136.5	136.5	0	-	n/a	-	n/a	n/a	-	-	-	-	-	-	No	No
R-5	147	147	1	43	n/a	2.64E-05	1.50E-01	n/a	104.5	16.7	1	12.9	0	0	No	No
L-GC777-2	147	147	17	445	640	n/a	n/a	0.51	161.7	11.3	43	13.31	1.51	0.17	Yes	Yes

ZFT Results (Green, 2000)

Sample	Grains	Age	±1σ	Age type
		Ma	*Ma*	
L-GC77-9	11	260	23	Pooled age
L-GC77-2	7	245	43	Central age

Note on L-GC777-1

The two ages in sample L-GC777-1 corresponds to the younger part of the range of ages in sample L-GC777-9 (which has two ages below 100 Ma at 67.6 ± 21.5 Ma and 72.8 ± 42.1 Ma). Therefore, the two (young) ages in sample L-GC777-1 are probably just caused by random sampling of the younger part of the dispersed range of AFT ages of the Middle Eocene sandstone. In other words, they do not represent a separate Cenozoic thermal event.

Sample R-3 (Depositional age: Early-Middle Eocene – 37.8-56 Ma)

The single dated grain in this sample yielded an AFT age of 126.8 ± 45.26 Ma and one confined track length of 6.7 µm. No qualitative interpretation can be derived from only one grain.

Sample R-4 (Depositional age: Early Eocene)

This sample did not yield any apatite grains.

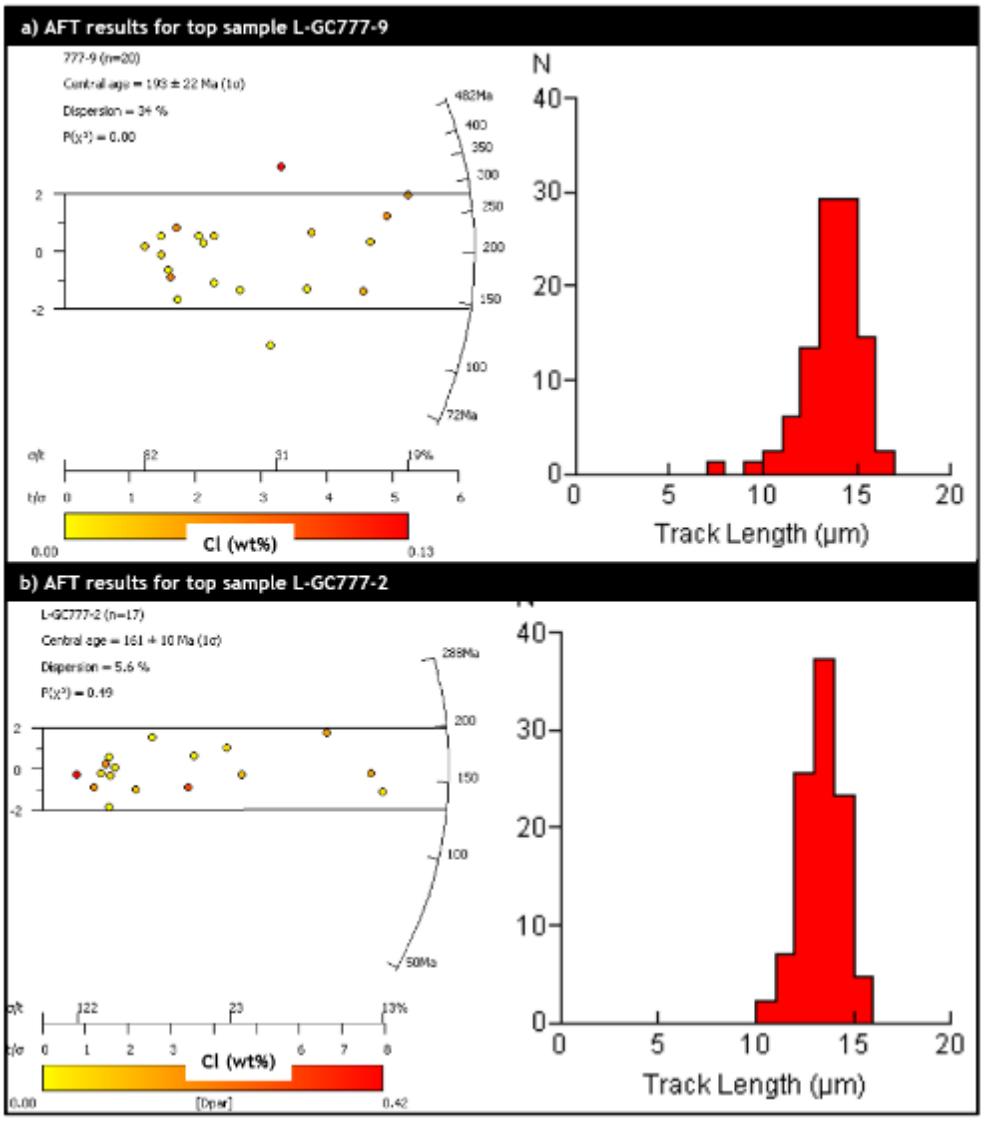

Figure 31: AFT results for legacy samples L-GC777-9 and L-GC777-2, after Green (2001).

Sample R-5 (Depositional age: Late Cretaceous 66-100.5 Ma)

The single dated grain in this sample yielded an AFT age of 104.5 ± 16.7 Ma and one confined track length of 12.9 µm. No qualitative interpretation can be derived from only one grain.

Sample L-GC777-2 (Depositional age: Late Cretaceous 66-100.5 Ma)

Legacy AFT results

The 17 grains yielded AFT ages ranging from 50.6 ± 32.2 Ma to 287.8 ± 111.7 Ma, a central age of 161.7 ± 11.3 Ma (Late Jurassic) and a chi-square test P-value of 0.51 (*i.e.* the ages are not overdispersed and probably belong to one age group only). The 43 confined track lengths measured for these grains have a MTL of 13.31 ± 1.51 µm (1σ) with a modal peak at 13-14 µm (TABLE 1 AND FIGURE 31).

The results of Green (2001) show that this sample has not experienced high temperatures above c. 100 °C and the tracks have not been completely annealed since the time of deposition in the Late Cretaceous.

Legacy ZFT results

The seven zircons from the Late Cretaceous sample L-GC777-2 yielded a pooled age of 266.6 ± 27.7 Ma (Green, 2001).

1.2.2.2 26/26-1 (Table 2 and Figure 32)

Sample R-7 (Eocene)

No apatites were found in this sample.

Table 2: Summary of new AFT and AHe results for well 26/26-1.

a) AFT Results

Sample	Depth		n	Ns	Area	U/Ca	P(χ^2)	Central Age	±1σ	Tracks	MTL	SD	SE	Inverse?	
	m MD	*m BSB*			*cm²*			*Ma*	*Ma*		*µm*	*µm*	*µm*	*FTA*	*FTL*
7	695	381	*0*	-	-	-		-	-	-	-	-	-	-	-
8	724	410	62	1443	1.44E-03	0.062620958	<0.01	160.6	6.1	65	11.20	2.20	0.27	Yes	Yes

b) AHe Results

Sample	Grain	Shape in GFTC		Length W	Diameter Max	Diameter Min	S/V	R_{eq}	Weight	Temp.	[^{238}U]	[^{232}Th]	[^{147}Sm]	eU	Th/U weight	[He]	Degassing	Raw Age	Error	F_T	Correc. age	Error
		Geometry	*GFT**	*µm*	*µm*	*µm*		*µm*	*g*	*°C*	*ppm*	*ppm*	*ppm*	*ppm*		*nmol/g*		*Ma*	*Ma*		*Ma*	*Ma*
R-8	3	Hexagonal prism	2P	209	112	109	0.050	59.5	3.98E-06	33	8	8	210	11	1.0	3.6	Lack of heat	58	9	0.758	77	12
	5	Hexagonal prism	2P	250	108	99	0.050	59.8	4.67E-06	33	17	8	288	21	0.5	8.8	Small leak?	75	11	0.759	99	15
	1	Hexagonal prism	1B	324	173	163	0.032	92.6	1.80E-05	33	7	1	302	9	0.2	5.0	Ok	93	14	0.843	111	17
	2	Hexagonal prism	2B	340	161	143	0.034	87.1	1.60E-05	33	5	2	312	7	0.4	4.6	Small leak?	103	15	0.834	124	19
	4	Hexagonal prism	1T1B	190	148	132	0.043	70	6.80E-06	33	18	3	462	21	0.2	12.3	Ok	101	15	0.795	127	19

Sample L-PB1 (Eocene)

McCulloch (1993) obtained only four 4 FT ages for this sample with a pooled age of 254.8 ± 100.8 Ma (Late Permian) and a Chi-square test P-value 0.4 (*i.e.* the ages are not overdispersed and probably belong to one age group only). There are no confined track lengths for this sample.

McCulloch (1993) results show that the Eocene interval has not been subjected to temperatures above c. 120 °C since the Early or Middle Eocene and that the thermochronological information contained in the apatite grains reflect the thermal history of the sand source area(s).

Sample L-PB2 (Hauterivian)

McCulloch (1993) obtained 13 FT ages for this sample with a pooled age of 240.8 ± 62.4 Ma (Middle Triassic) and a Chi-square test P-value of 0.5 (*i.e.* the ages are not overdispersed and probably belong to one age group only). The 25 confined tracks have a MTL of 11.24 ± 2.39 µm (1σ) and a modal peak at c. 12-13 µm.

McCulloch (1993) results show that the Hauterivian interval has not been subjected to temperatures above c. 120 °C since the Hauterivian and that the thermochronological information contained in the apatite grains reflect the thermal history of the sand source area(s).

Sample L-PB3 (Tournaisian)

McCulloch (1993) obtained only five FT ages for this sample with a pooled age of 170.8 ± 60.2 Ma (Aalenian) and a Chi-square test P-value <0.05 (*i.e.* the ages are statistically overdispersed). The confined tracks have a MTL of 11.36 ± 2.04 µm (1σ).

McCulloch (1993) results show that the Tournaisian interval experienced tempeartures above c. 120 °C after sediment deposition between the Tournaisian and the Middle Jurassic but not since the Middle Jurassic. The low modal peak and MTL of the confined tracks indicate that the sample must have experienced temperatures above c. 60 °C since the Jurassic and probably in recent times.

Sample L-PB4 (Basement)

McCulloch (1993) obtained 16 FT ages for this sample with a pooled age of 162.2 ± 26 Ma (Oxfordian) and a Chi-square test P-value 0.55 (*i.e.* the ages are not overdispersed and probably belong to one age group only). The confined tracks have a MTL of 11.72 ± 1.54 µm (1σ) and a modal peak at c. 12-13 µm.

Sample R-8 (Basement)

AFT results

This sample yielded 65 FT ages ranging from 18 Ma to 606 Ma. Three grains with a FT age of 18 Ma, 479 Ma and 606 Ma are considered geologically implausible and outliers and are therefore excluded. In nearby well 34/05-1, several grains with near-Paleogene FT ages have been rejected because they are believed to have been reset by the igneous activity (thermal conduction in the contact aureole or hot hydrothermal fluids). In this borehole, one grain with a FT age of 69 Ma could potentially have been affected by such igneous activity. However, this grain age is not a clear outlier like the grains in 34/05-1, therefore it has not been discarded and the young age is attributed to statistical dispersion only.

The screened population (excluding the three outliers mentioned just above) consists of 62 grains with FT ages ranging from 69.8 Ma to 319.1 Ma with a Chi-square test P-value <0.01 (*i.e.* overdispersed)

and a central age of 160.6 ± 6.1 Ma (1σ) (Oxfordian) (FIGURE 32). The lengths of 65 confined tracks range from 2.8 to 15.3 µm with an arithmetic average (MTL) of 11.2 ± 2.2 µm (1σ) and a modal peak at c. 12-13 µm (FIGURE 32).

These results show that this basement sample did not experience temperatures above c. 120 °C since at least the Upper Jurassic. The low modal peak and MTL of the confined tracks indicate that the sample must have experienced temperatures above c. 60 °C since the Jurassic (more probably in recent times, i.e. a few tens of millions of years).

The grains have a very low chlorine content ranging from 0 to 0.05 wt% with an average and median of c. 0.03 wt%. They also have Dpar ranging from 1.36 to 1.9 µm with an arithmetic mean of 1.6 µm. These kinetic proxies indicate that the grains are very homogenous and no significant annealing behaviour should be observed between the grains.

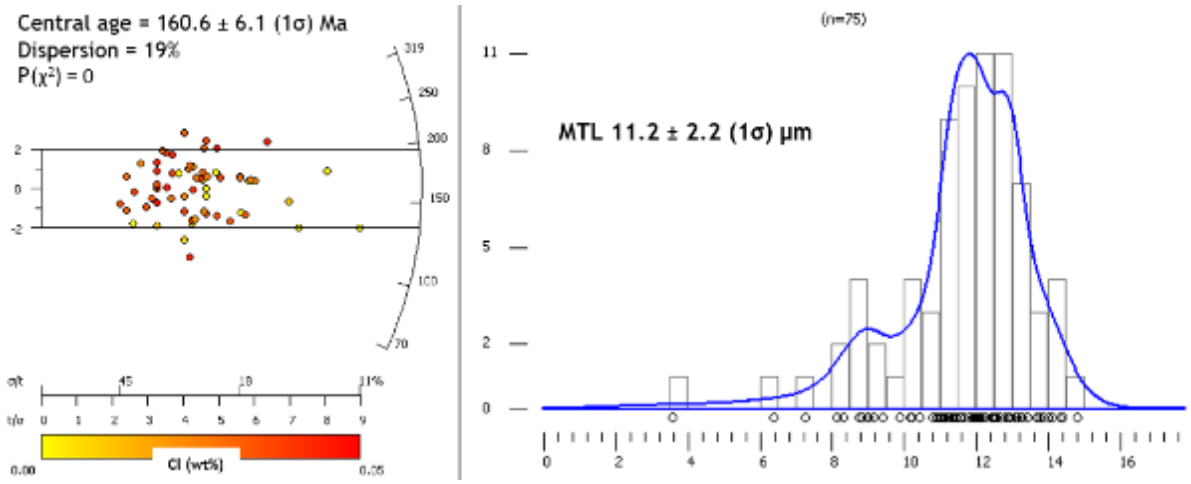

Figure 32: AFT results for basement sample R-8 (26/26-1). Left: Radial plot colour-coded with Cl concentration. Right: confined track length density plot, KDE and MTL.

AHe results

Five grains were analysed for AHe analysis. Two grains (R-8.1 and 4) were fully outgassed with background values during the second run suggesting no inclusions. They have raw ages of 93 and 101 Ma and F_T-corrected ages of 111 Ma (Albian) and 127 Ma (Barremian).

Two grains (R-8.2 and 5) were properly heated but their second run showed helium values above the background values measured from blanks (respectively 1 and 1.4% of first run values). This could indicate the presence of helium trapped in inclusions and a slight overestimation of the AHe age (*i.e.* the age should be slightly younger). However their raw AHe ages of respectively 103 Ma and 75 Ma are actually close to the ages of the two grains mentioned above and they could be considered as representative grains. But since the 'leaky' grains R-8.2 and R.8.5 have very similar S/V and eU

(respectively 0.034 and 7 ppm and 0.05 and 21 ppm) as the 'good' grains R-8.1 and R-8.4 (respectively 0.0032 and 9 ppm and 0.043 and 21 ppm), they will not be used for thermal history inverse modelling (TABLE 2).

The last grain, R-8.3, experienced a possible lack of laser heating (no visible glow of the Pt tube) resulting in a possibly not fully degassed grain and therefore an underestimation of the true age (*i.e.* the true age should be older). Indeed, the grain has a raw age of 58 Ma and a F_T-corrected age of 77 Ma (Campanian). This age is the youngest of the five ages and could be due the hypothesized partial degassing. The second run yielded helium concentration significantly above background blank values which is in accordance with helium still remaining in the grain. Consequently, this grain has been discarded.

Age dispersion

The four grains with reliable ages have corrected ages ranging from 99 to 127 Ma (early Cenomanian to Barremian) which is a somewhat small range (*i.e.* small dispersion) for AHe ages.

Taken as a whole, the grains do not show the expected correlations between S/V and eU vs AHe ages. However, when only the two most reliable grains are considered the oldest grain has indeed a higher eU content and a larger size (which both leads to higher retention of helium and therefore older ages) than the younger grain. Based on this observation, grain R-8.5 is particularly anomalous since it has a similar S/V and eU than grain R-8.4 but a much younger age (75 Ma vs 101 Ma).

Based on their perfect degassing and normal relationship between their size and radiation damage compared to their AHe ages, only grains R-8.1 and R-8.4 will be used for thermal history inverse modelling.

Sample L-PB5 (Basement)

McCulloch (1993) obtained 20 FT ages for this sample with a pooled age of 164.3 ± 18.6 Ma (Callovian) and a Chi-square test P-value 0.65 (*i.e.* the ages are not overdispersed and probably belong to one age group only). The confined tracks have a MTL of 11.81 ± 1.87 µm (1σ) and a modal peak at c. 11-12 µm.

1.2.2.3 34/05-1

Sample R-10 (Eocene sands)

The two apatites of R-10 yielded AFT ages of 99.5 ± 16.5 Ma and 179.4 ± 37.2 Ma (Table 3). The very low number of grains prevents the calculation of a meaningful central age. These two ages are older than the stratigraphic age of the host sandstone (Paleocene-Eocene, 50 ± 16.1 Ma, Cohen et al. (2020)) and indicate that the grains were never completely reset after deposition. In other words, the

Paleocene-Eocene interval (and the overlying Cenozoic section) never experienced temperature over c. 120 °C.

Sample R-11

As discussed above, no AFT ages were obtained for this sample due to the very poor apatite yield and quality for this sample.

Sample R-12

Two grains yielded AFT ages of 135.7 ± 18.2 Ma and 207.3 ± 34 Ma and 19 track lengths in the range of 7.3 to 14.1 µm with a mean track length of 11.9 ± 1.82 µm (1σ) (TABLE 3). The very low number of grains prevents the calculation of a meaningful central age. The low number of confined tracks prevents them being used used for inverse modelling. The two ages are younger than the stratigraphic age of the sample (Westphalian D, 306.5 ± 1.5 Ma), indicating that they spent some time in the PAZ and experienced a certain amount of track annealing.

Five grains were analysed for AHe analysis. Three grains were fully outgassed with background values during the second run suggesting no inclusions. They have raw ages of 33, 47 and 898 Ma and F_T-corrected ages of 59, 79 and 1770 Ma. The age of the last grain (R-12.1) is geologically implausible.

Two grains (R-12.2 and 5) experienced a possible lack of laser heating (no visible glow of the Pt tube) resulting in a possibly not fully degassed grain. The first grain has a raw age of 60 Ma and a F_T-corrected age of 101 Ma, older than the two good grains, which suggest that it was probably fully outgassed. The second grain (R-12.5) has an implausible raw age of 1556 Ma (F_T-corrected age of 2739 Ma).

The two grains with very old ages have significantly different eU values (2-3 ppm) than the three other grains with plausible geological ages (eU = 41-176 ppm).

Table 3: AFT and AHe results for samples R-10 to R-15 (34/05-1).

a) AFT Results

Sample	Depth		n	Ns	Area	U/Ca	$P(\chi^2)$	Central Age	±1σ	Tracks	MTL	SD	SE	Inverse?	
	m MD	m BSB			cm^2			Ma	Ma		µm	µm	µm	FTA	FTL
10	695	381	2	70	6.23E-05	0.08872934	0.02	130	27	3	13.18	1.36	0.79	No	No
11	724	410	0	-	-	-	-	-	-	-	-	-	-	No	No
12	925	611	2	105	3.96E-05	0.163171201	0.04	164	24	19	11.86	1.82	0.42	No	No
12-14	1050	734	31	1107	0.000576	0.117338511	<0.01	165.8	8.4	77	11.63	1.90	0.22	No	No
			29	1082	0.000535	0.12	<0.01	168.5	7.7	75	11.59	1.92	0.22	Yes	Yes
13	1055	741	21	730	0.000368	0.121875993	<0.01	166	11	39	11.50	2.16	0.35	No	No
14	1165	851	8	272	0.000169	0.096710739	0.03	167	16	19	11.66	1.29	0.30	No	No
15	1457.5	1144	11	277	0.000246	0.117276108	0.02	110	13	10	11.52	2.14	0.68	Yes	No
			9	103	0.000218	0.034194478	0.90	136	14	9	13.18	-	-	Yes	No

b) AHe Results

Sample	Grain	Shape in GFTC		Length	Diameter		S/V	R_{eq}	Weight	Temp.	$[^{238}U]$	$[^{232}Th]$	$[^{147}Sm]$	eU	Th/U weight	[He]	Degassing	Raw Age	Error	F_T	Correc. age	Error
				W	Max	Min																
		Geometry	GFT*	µm	µm	µm		µm	g	°C	ppm	ppm	ppm	ppm		nmol/g		Ma	Ma		Ma	Ma
12	4	Hexagonal prism	1P1F	135	56	48	0.098	30.7	7.70E-07	27.3	15	89	1131	41	6.1	7.9	Ok	33	5	0.558	59	9
	3	Hexagonal prism	2F	109	65	59	0.089	33.9	9.80E-07	27.3	57	470	1993	176	8.3	47.3	Ok	47	7	0.601	79	12
	2	Ellipsoid	N/A	104	72	59	0.082	36.5	7.40E-07	27.3	41	71	477	60	1.7	20.2	Lack of heat	60	9	0.6	101	15
	1	Hexagonal prism	1P1F	109	57	37	0.110	27.2	5.10E-07	27.3	1	11	10	3	18.9	16.6	Ok	898	135	0.507	1770	266
	5	Hexagonal prism	2F	98	59	54	0.097	30.9	7.40E-07	27.3	1	8	6	2	11.8	22.8	Lack of heat	1556	233	0.568	2739	411
15	1	Hexagonal prism	2B	84	69	62	0.090	33.3	8.50E-07	42.4	3	46	736	17	16.5	1.6	Ok	15	2	0.598	25	4
	4	Hexagonal prism	2F	208	66	58	0.080	37.7	1.88E-06	42.4	1	34	337	11	29.2	2.3	Ok	36	5	0.633	57	9
	3	Hexagonal prism	2F	117	78	68	0.076	39.5	1.50E-06	42.4	3	291	591	74	91.5	15.4	Ok	37	6	0.653	57	9
	5	Hexagonal prism	2F	114	80	71	0.075	40	1.54E-06	42.4	20	242	607	79	12.1	23.7	Ok	53	8	0.658	81	12
	2	Hexagonal prism	2F	124	76	67	0.076	39.2	1.51E-06	42.4	0	5	8	1	44.1	10.7	Ok	1320	198	0.651	2027	304

**GFT = Type of prism terminations used in the Alpha Ft-ejection factor software of Gautheron et al.*

Sample R-13

Twenty one FT ages were obtained for this sample ranging from 79 Ma to 733 Ma with a Chi-square test P-value <0.01 (*i.e.* overdispersed) and a central age of 165 ± 11 Ma (1σ). The lengths of 39 confined tracks range between 3.6 and 14.8 µm (asymmetric unimodal distribution) with a mean track length of 11.5 ± 2.2 µm (1σ) (TABLE 3). The AFT age is younger than the stratigraphical age of 310.9 Ma and the MTL is shorter than c. 15 µm indicating that the sample spent a certain amount of time in the PAZ.

Sample R-14

This sample yielded eight FT ages ranging from 116 Ma to 300 Ma and a central age of 167 ± 16 Ma (1σ). The lengths of 19 confined tracks range between 8.3 and 13.3 µm (asymmetric unimodal distribution) with a mean track length of 11.7 ± 1.3 µm (1σ) (TABLE 3). The AFT age is younger than the stratigraphical age of 310.9 Ma and the MTL is shorter than c. 15 µm indicating that the sample spent a certain amount of time in the PAZ.

Three grains were analysed from sample R-13 and R-14. The grains were perfectly outgassed with second runs yielding helium values equal to background values. However, the UCL team reported that the file containing the ICP-MS results was corrupted and all isotope dilution data were lost for these three grains.

Sample R-15

This sample yielded 11 FT ages ranging from 77 Ma to 285 Ma and a central age of 110 ± 13 Ma (1σ). The lengths of 15 confined tracks range between 6.5 and 14.4 µm with a mean track length of 11.5 ± 2.1 µm (1σ). The sample have grains with low chlorine content ranging from 0 to 0.3 wt% with an average of 0.14 wt% and a median of 0.11 wt% and an average Dpar of 1.8 µm (TABLE 3 AND FIGURE 33).

Two grains with an AFT age of 76.9 ± 10.6 Ma and 79.6 ± 8.9 Ma appear as outliers on the radial plot. They have a younger age, a lower uncertainty and a higher chlorine content than the other nine grains (radial plot in FIGURE 33). When assuming that the ages are a mixture of two age groups, the radial plot yields two central ages, one for the two young grain at 80.1 ± 7.1 Ma and one for the older grains at 136 ± 15 Ma.

The two grains with young AFT ages have possibly been reset by a Paleogene igneous intrusion. As discussed above, a Paleogene igneous intrusion is suspected to exist just below the TD (Total Depth) of the well at 1488 m MD. Alternatively, these two grains could also be cavings from the vicinity of the intrusion identified above in the well.

If these two grains were completely reset because of the thermal aureole of a nearby igneous intrusion, then the other grains of the same sample could also have experienced temperatures high enough to partially anneal their fission tracks. If a large number of confined fission track lengths was available for this sample, the shape of its track length distribution could give some information about the presence or absence of a recent annealing event. The partial annealing of tracks would result in a shift of the modal peak to the left and a smaller peak of unannealed long tracks. However, no such large number of tracks is available for R-15.

In a basin with significant igneous activity such as the Porcupine Basin, any sample could potentially be affected by an unrecognized igneous intrusion in the vicinity of the sample. So despite the risk of partial annealing due to igneous activity, the nine grains in sample R-15 will be used for thermal history inverse modelling with the assumption that the FT data is due to burial only. The usual threshold to accept a sample as an input data for thermal history modelling is 10. However, due to the added value of modelling several samples at different depths, this sample with only nine grains will be used as input data for inverse modelling.

The AFT central age (excluding the volcanic-affected grains) is younger (136 ± 15 Ma) than the stratigraphical age of 314.9 Ma and the MTL is shorter than c. 15 µm indicating that the sample spent a certain amount of time in the PAZ.

Five grains were analysed for AHe analysis. All five grains were fully outgassed with second runs yielding helium values similar to blank values. They yielded raw ages of 15, 36, 37, 53 and 1320 Ma and F_T-corrected ages of 25, 57, 57, 81 and 2027 Ma. The last age is geologically implausible.

Similarly to sample R-12, the grain with a very old age has a eU value (1 ppm) that is significantly lower than the rest of the grains (11 to 79 ppm).

Sample R-12-14

All the Carboniferous samples yield relatively few AFT ages and confined track length measurements. Interpretation of fission track data and inverse modelling require a minimum amount of ages and confined tracks in order to be statistically meaningful. As individual samples, only sample R-13 has enough FT ages (>=10) and track lengths (>=25) to be interpreted and modelled. But since there is no apparent stratigraphic unconformity in the Carboniferous section, it is possible to merge several samples in one, as long as the depths range of such combined sample is not too large (otherwise the sample temperature range, and therefore annealing history would be too large to pool together).

Here, it is possible to merge together samples R-12, R-13 and R-14 as one combined sample named R-12-14. The combined sample have a depth range of 870-1230 m which for a geothermal gradient of

28 °C.km^{-1} corresponds to a maximum temperature range of 10 °C. This temperature range is low enough to not have a major impact on the annealing behaviour of the grains within the sample.

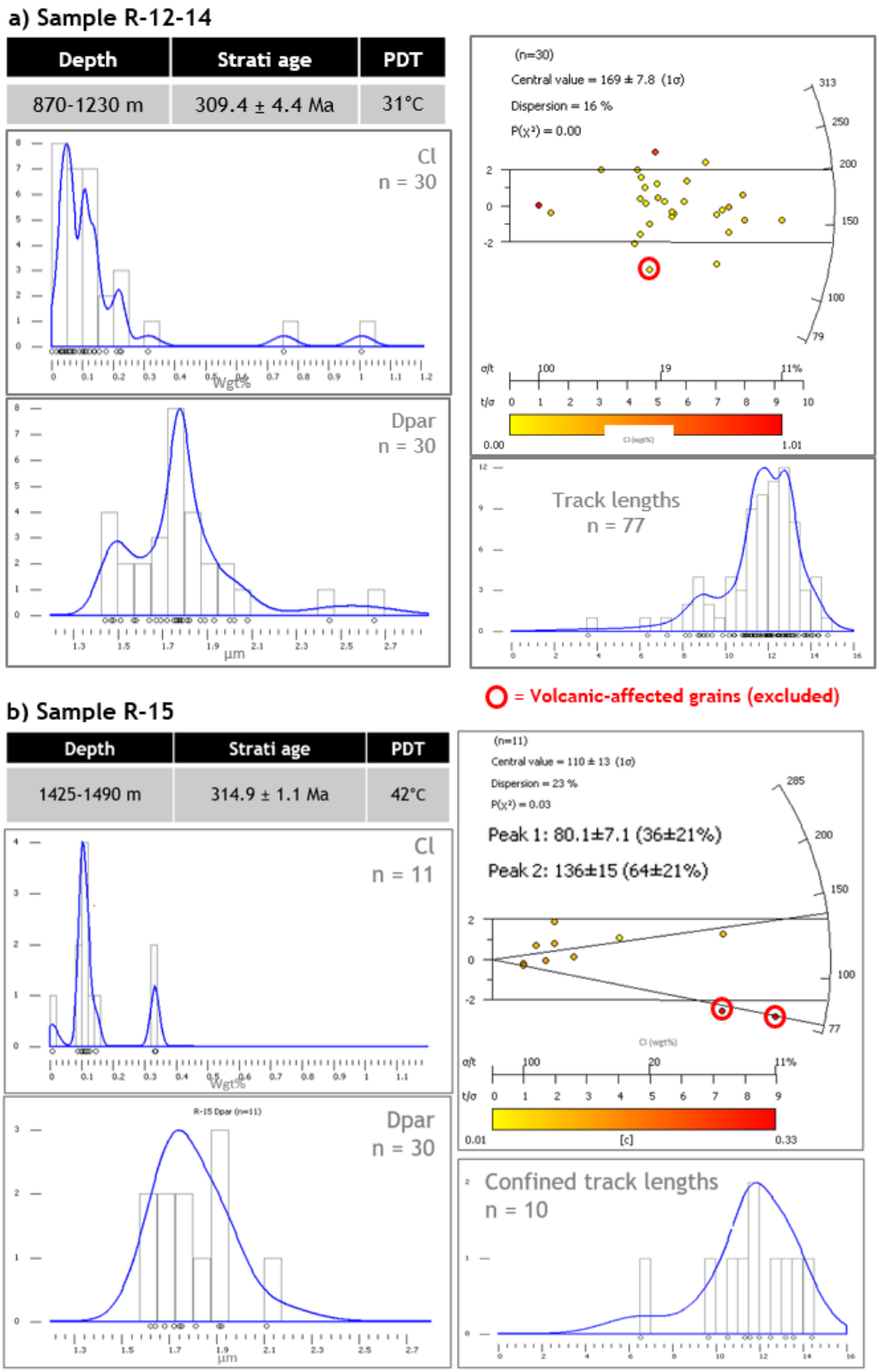

Figure 33: AFT results for borehole 34/05-1. a) AFT results of sample R-12-14. b) AFT results for sample R-15.

The stratigraphic age of the sample is Westphalian C-D (309.4 ± 4.4 Ma). It has 31 AFT ages ranging from 79 Ma to 733 Ma with a central age of 165.8 ± 8.4 Ma (1σ).

The oldest grain (grain R-13.g1) has an AFT age of 734 ± 736 Ma. The geologically implausible old FT age and the very large error are both caused by a very low uranium content for this grain (0.08 ppm) and the very low number of counted tracks (n = 1). Consequently this grain will be excluded from the dataset.

The youngest grain (R-13j.g4) has an AFT age of 78.7 ± 16.5 Ma, which is similar to the two grains in R-15 (76.9 ± 10.6 Ma and 79.6 ± 8.9 Ma) but it does not plot as a significant outlier on the radial plot.

The grain comes from sample R-13 (depth interval 1010-1100 m MD). As discussed above, an intrusion might be present at 967.5 m MD and have affected the reflectance of the vitrinite at 1048.6 m MD. The intrusion that has affected the reflectance, whether it is the suspected one at 967.5 m MD or another one nearby, could have annealed some apatites located very close to the intrusion. Consequently, as for R-15, this grain will be excluded from the dataset.

The resultant population comprises 29 grains ranging from 101 Ma to 313 Ma with a central age of 169 ± 7.8 Ma. There are 77 confined lengths ranging from 3.6 to 14.8 µm with a MTL of 11.6 ± 1.9 µm (1σ). The sample has grains with a low chlorine content ranging from 0 and 1 wt% with an average of 0.16 wt%, a median of 0.1 wt % and an average Dpar of 1.8 µm (TABLE 3 AND FIGURE 33). This narrow range implies that the annealing behaviour of all the grains in this sample should be similar.

AHE age dispersion

Taken as a whole, there is a large dispersion in F_T-corrected ages from 59 Ma to 2739 Ma for R-12 and from 25 Ma to 2027 Ma for R-15. However, three grains have geologically implausible old ages.

Anomalous [U] and [Sm]

The three anomalously old grains have much lower eU values (1-3 ppm) than the rest of the grains (11-176 ppm). In order to gauge the plausibility of the low eU values, it is possible to look at the uranium, thorium and samarium content derived from the fission track data (FIGURE 34A).

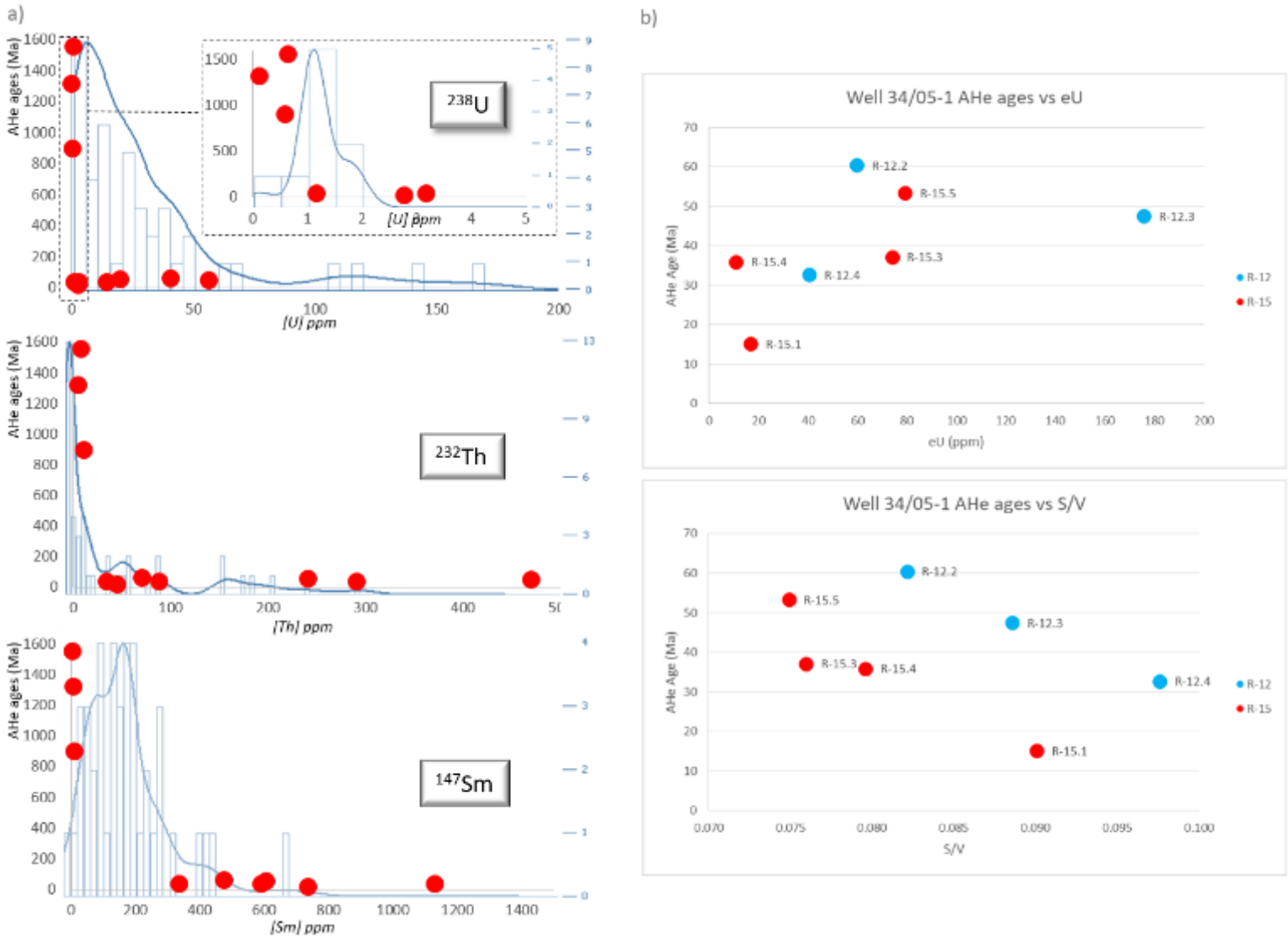

Figure 34: a) 34/05-1 Carboniferous samples AHe ages vs [U], [Th], [Sm] with AFT [U], [Th], [Sm] histograms and KDEs as background.

Uranium and thorium concentration of the FT grains show that it is possible for the Carboniferous apatites to have single-digit concentrations for these elements. However, the samarium concentration of the three AHe outliers falls outside the range of concentration of the AFT dataset. Only one AFT grain out of 42 yields similar low U, Th and Sm concentrations: Grain R-13.g1 with [U] = 0.08 pp, [Th] = 0.03 ppm and [Sm] = 16.3 ppm. But even this grain has samarium concentration more than 50% higher than the AHe anomalous grain with the highest Sm concentration (9.9 ppm). This grain falls within the low- and medium-grade metamorphic and metasomatic rocks domain on the Sr/Y vs LREE biplot (FIGURE 15). Apatites from low- to medium-grade metamorphic rocks are often depleted in U, Th and REE (therefore of Sm) due to these trace elements being concentrated in co-genetic epidotes (Henrichs et al., 2018).

It is therefore possible that these grains with anomalous ages are actually metamorphic apatites with very low concentration of parent isotopes. The anomalous old ages could then be due to excess helium from small inclusions in the grains. These grains will therefore not be used for interpretation and modelling of thermal histories.

When ignoring the anomalous grains, the remaining grains have ages ranging from 33 Ma to 60 Ma for R-12 and from 15 Ma to 53 Ma for R-15.

AHe ages vs eU and S/V

The raw ages of samples R-12 and R-15 have a weak positive correlation with eU and a negative correlation with S/V (FIGURE 34B). Both correlations imply that helium diffusion in these grains was partially influenced by radiation damage (eU proxy) and grain size (S/V proxy). Consequently, the inverse modelling of grains with different sizes and eU should help better constrain the range of possible thermal histories.

1.2.2.4 Porcupine High Dredges

Sample C-MeBo (in-situ Mesoproterozoic orthogneiss, NPHO)

The sample yielded 15 AFT ages ranging from 69.3 ± 13.8 Ma to 775.5 ± 148.9 Ma, a central age of 157 ± 27 Ma (1σ) (Late Jurassic) and a chi-square test P-value <0.01 (i.e. the ages are overdispersed and might belong to more than one age group) (FIGURE 35A). The 102 confined track lengths measured for these grains have a MTL of 13.03 ± 1.21 µm (1σ) with a modal peak of c. 14 µm (FIGURE 35B).

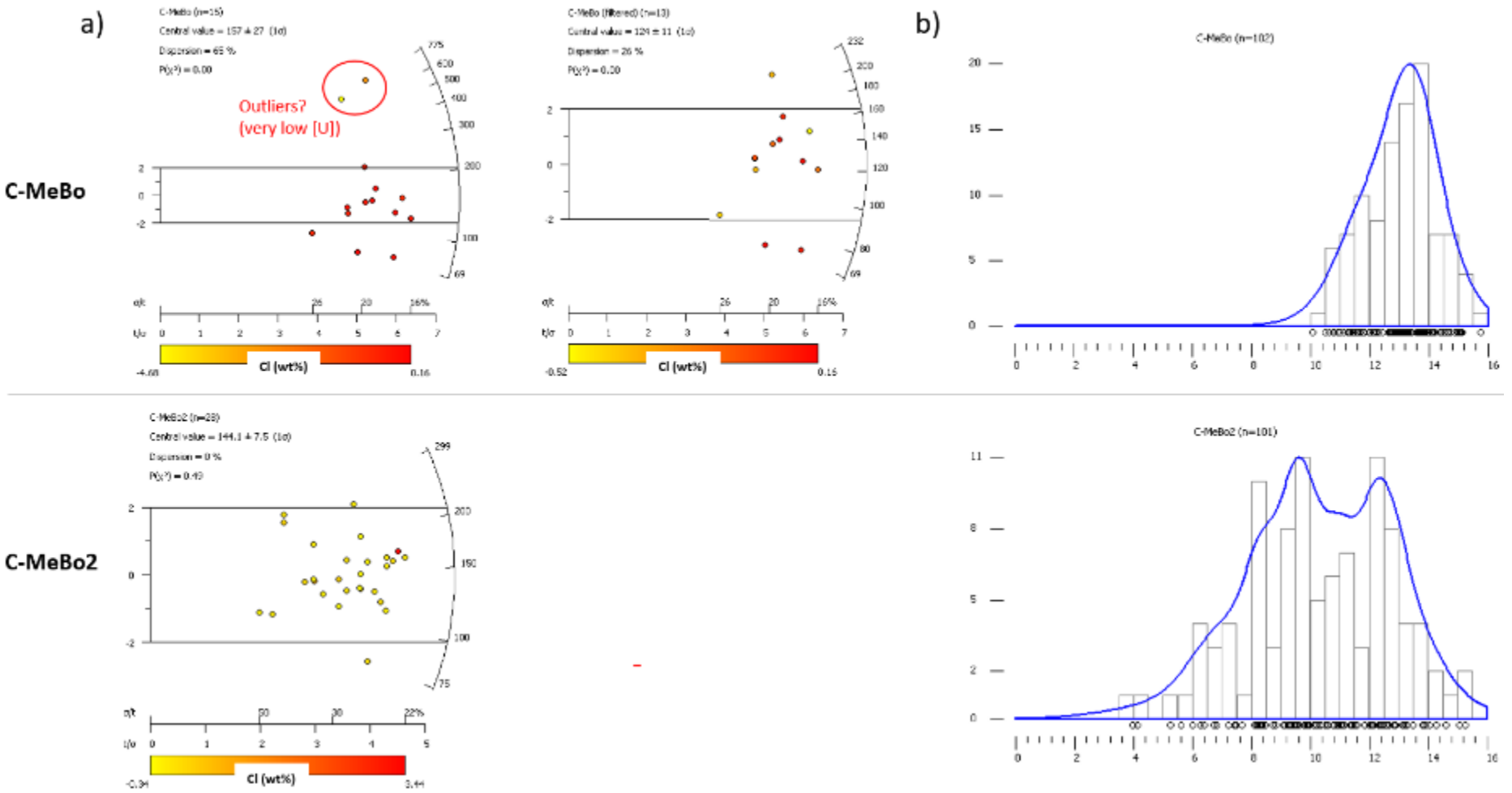

Figure 35: AFT results for sample C-MeBo (25/7-sb(MeBo)3) and C-MeBo2 (25/27-sb(MeBo)2). a) LAFT radial plots. b) Confined track lengths density plot and KDE function.

However, two grains have very old AFT ages (>700 Ma) and plot as outliers on the radial plot (FIGURE 35A). These two grains have a similar number of counted tracks than the other grains but a much lower uranium content (U/Ca ratio of c. 0.02 *vs* a range of 0.09-0.45 and an average of c. 0.19 for the 13 other grains). If these two grains are excluded, the population of 13 grains yields a younger central age of 124 ± 11 Ma (1σ) (Aptian) (FIGURE 35A).

Three grains were analysed for AHe dating. They have raw ages ranging from 144 to 151 Ma and F_T-corrected ages ranging from 186 to 197 Ma (Early Jurassic). The age dispersion is small.

The F_T-corrected AHe ages are slightly older than the AFT ages. This could be due to several reasons such as:

1. Apatites with high α-recoil damage due to a slow cooling history and high concentration of U-Th-Sm: the high level of radiation damage increases He retention to the point that the AHe closure temperature is greater than the AFT closure temperature (Flowers and Kelley, 2011).
2. Uranium-rich inclusions (e.g. zircons) (Vermeesch et al., 2007),
3. Unidentified zonation in AFT grains (Vermeesch, 2017), or
4. Sub-optimal sampling of the age population leading to ages that are not representative of the entire population. This is particularly the case for AHe dating where the number of dated grains per sample is often < 10 (Green and Duddy, 2018) and for LAFT dating, which is often associated with large age dispersions (Ketcham et al., 2018b), therefore requiring a larger number of dated grains than commonly dated.

One or several of these reasons could be the cause of the age mismatch in this sample. In any case, it is likely that the AFT and AHe ages are similar, which indicates that the sample probably passed quickly through the PAZ and the PHeRZ during the Jurassic. Since the AFT central age is based on only 15 grains with a large age dispersion while there is little age dispersion for the AHe ages (but only three grains), it is possible that the true AFT age is somewhere between 157 Ma (the AFT age) and 190 Ma (the AHe age).

Sample C-MeBo2 (in-situ? Late Caledonian deformed granite)

The sample yielded 28 AFT ages ranging from 75.3 ± 19 Ma to 299 ± 122.7 Ma, a central age of 144 ± 7.5 Ma (1σ) (Cretaceous-Jurassic boundary) and a chi-square test P-value of 0.42 (i.e. the ages are not overdispersed and probably belong to one age group) (FIGURE 35A). The 101 confined track lengths measured for these grains have a MTL of 10.29 ± 2.45 µm (1σ) with a bimodal distribution with peaks at c. 9.5-10 µm and 12-12.5 µm (FIGURE 35B). The bimodal distribution implies that the sample spent some time in the PAZ at c. 60-120 °C after a period of cooling below 60 °C.

Four grains were analysed for AHe dating. They have raw ages ranging from 25 to 71 Ma and FT-corrected ages ranging from 34 to 107 Ma, with two grains with similar ages of 51 and 57 Ma (Early Eocene) which is similar to the average age for the four grains (62 Ma). The age dispersion might be partially explained by radiation damage since there is a positive correlation between age and eU (9, 25, 38 and 53 ppm for respectively 34, 51, 57 and 107 Ma). Grain size is not a cause of age dispersion since the oldest ages are associated with the smaller grains. The AHe ages suggest that the sample went through the PHeRZ at some point during the Paleocene-Eocene.

Sample C-PH1 (PHMS)

The sample yielded 20 AFT ages ranging from 103 ± 23.9 Ma to 401.3 ± 165 Ma, a central age of 142 ± 7.8 Ma (1σ) (Jurassic - Cretaceous boundary) and a chi-square test P-value of 0.1 (i.e. the ages are not overdispersed and probably belong one age group only). The 101 confined track lengths measured for these grains range from 2.08 to 14.92 µm with a MTL of 9.69 ± 3.01 µm (1σ) with a bimodal distribution with peaks of c. 9.5-10 µm and c. 12-13 µm (FIGURE 36).

Sample C-PH4 (PHMS)

The sample yielded 24 AFT ages ranging from 81.3 ± 36.5 Ma to 248.1 ± 72 Ma, a central age of 184 ± 12 Ma (1σ) (Early Jurassic) and a chi-square test P-value of 0.1 (*i.e.* the ages are not overdispersed and probably belong one age group only). The 118 confined track lengths measured for these grains range from 3.52 to 14.43 µm with a MTL of 9.86 ± 3.01 µm (1σ) with a bimodal distribution with peaks of c. 9.5-10 µm and c. 12-14 µm (FIGURE 36).

Four grains were analysed for AHe dating. They have raw ages ranging from 66 to 130 Ma and FT-corrected ages ranging from 98 to 172 Ma without any cluster of similar ages. The large age dispersion might be partially explained by radiation damage since there is a positive correlation between age and eU (7, 15, 28 and 40 ppm for respectively 98, 110, 148 and 172 Ma) but not by grain size since there is no clear correlation between size and ages.

The AFT and AHe ages suggest that the sample went through the PAZ and PHeRZ during the Jurassic to Early Cretaceous and then remained below c. 40 °C until the present-day.

Sample C-PH5 (PHMS)

The sample yielded 21 AFT ages ranging from 125.8 ± 30 Ma to 248.1 ± 72 Ma, a central age of 194 ± 11 Ma (1σ) (Early Jurassic) and a chi-square test P-value of 0.05 (i.e. the ages are not overdispersed and probably belong one age group only). The 114 confined track lengths measured for these grains range from 3.77 to 14.5 µm with a MTL of 9.79 ± 2.86 µm (1σ) with a modal peak at c. 12-13 µm but also a large number of lengths forming a plateau in the range of c. 5.5 to 11.5 µm (FIGURE 36).

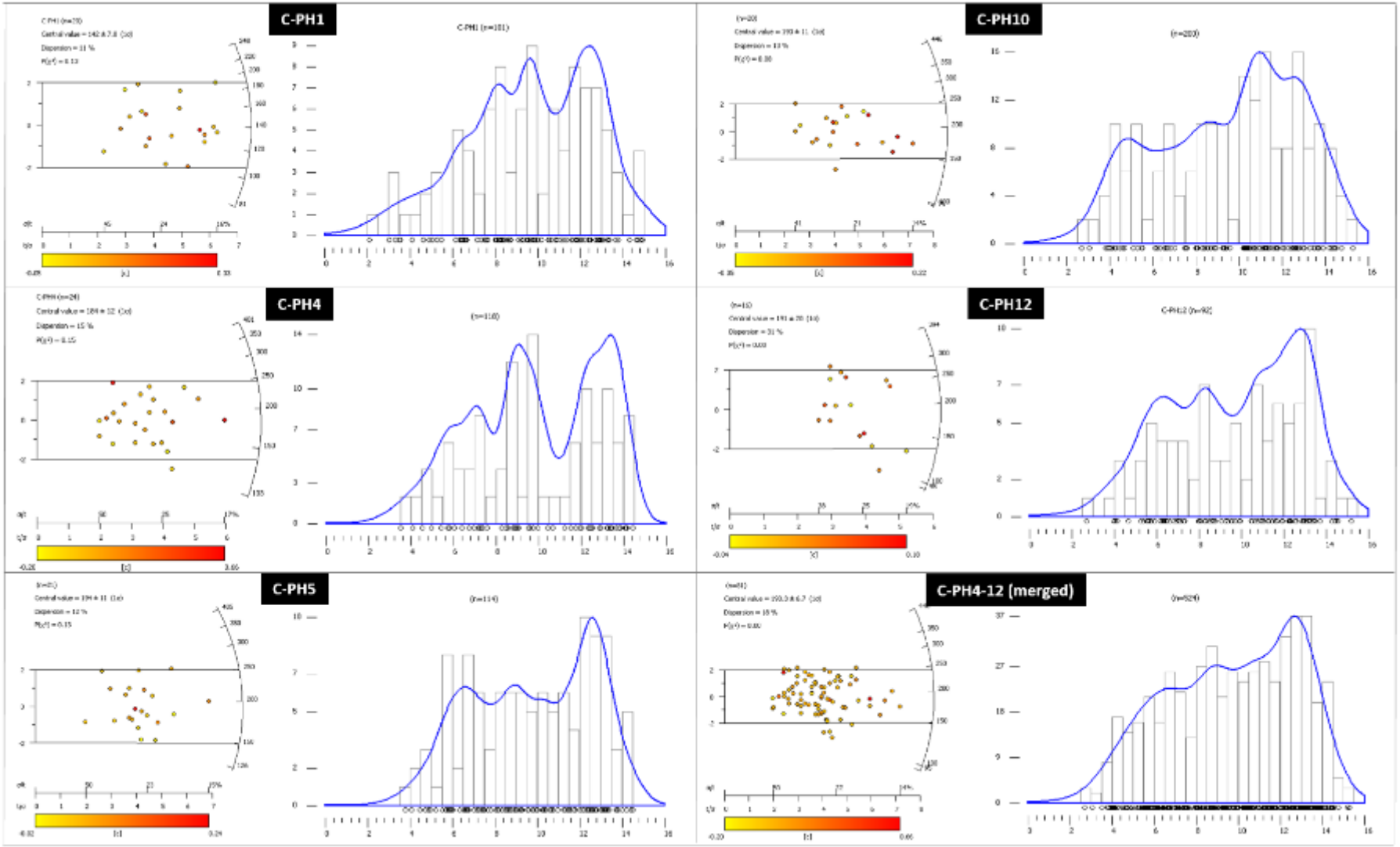

Figure 36: AFT results for samples C-PH1 to C-PH12 and merged sample C-PH4-12 (LAFT radial plots and confined track length density plots with KDE function).

Three grains were analysed for AHe dating. They have raw ages ranging from 86 to 129 Ma and FT-corrected ages ranging from 115 to 162 Ma (Late Jurassic-Early Cretaceous) without any cluster of similar ages. The large age dispersion might be partially explained by radiation damage since there is a positive correlation between age and eU (6, 9 and 13 ppm for respectively 115, 129 and 162 Ma) but not by grain size since there is no clear correlation between size and ages.

Sample C-PH10 (PHMS)

The sample yielded 20 AFT ages ranging from 98.2 ± 24.1 Ma to 446.1 ± 182.8 Ma, a central age of 194 ± 11 Ma (1σ) (Early Jurassic) and a chi-square test P-value of 0.06 (*i.e.* the ages are not overdispersed and probably belong one age group only). The 200 confined track lengths measured for these grains range from 2.69 to 15.30 µm with a MTL of 9.58 ± 3.26 µm (1σ), a modal peak at c. 11-13 µm but also a large number of lengths forming a plateau in the range of c. 4 to 11 µm (FIGURE 36).

Sample C-PH12 (PHMS)

The sample yielded 16 AFT ages ranging from 94.8 ± 21.5 Ma to 393.9 ± 131.9 Ma, a central age of 191 ± 20 Ma (1σ) (Early Jurassic) and a chi-square test P-value of 0.07 (*i.e.* the ages are not overdispersed and probably belong one age group only). The 92 confined track lengths measured for these grains range from 2.7 to 15.19 µm with a MTL of 9.72 ± 3.08 µm (1σ), a modal peak at c. 13 µm but also a large number of lengths in the range of c. 6 to 13 µm (FIGURE 36).

Combined sample C-PH4-12

As discussed above, samples C-PH4 to C-PH12 have very similar ages and MTLs and C-PH4 and C-PH5 have also very similar range of AHe ages. Only sample C-PH1 is quite different with a much younger AFT central age. Therefore, the four similar samples (C-PH4 to C-PH12) probably experienced the same thermal history and since they are relatively close spatially, they can be merged as one combined sample representative of the summit of the northern part of the Porcupine High.

The combined sample, named C-PH4-12 contains 81 grains with a central age of 190.3 ± 6.7 Ma (Early Jurassic) and a chi-square test P-value <0.01 (*i.e.* the ages are overdispersed and might not belong to one age group only). The 524 confined track lengths measured for these grains range from 2.69 to 15.30 µm with a MTL of 9.71 ± 3.09 µm (1σ), a modal peak at c. 13 µm but also a large number of lengths forming a plateau in the range of c. 7 to 13 µm (FIGURE 36). The seven FT-corrected AHe ages range from 98 to 172 Ma (Early Cretaceous-Middle Jurassic).

Sample C-204-1 to C-402-11

No detailed description of these samples is given as they will not be used for thermal history modelling (see section 1.7).

1.2.3 Miscellaneous locations

1.2.3.1 12/13-1A

Sample R-37 (Permo-Triassic volcanoclastic sandstone)

The 24 AFT ages range from 73.3 to 459 Ma with a central age of 185 ± 19 Ma (Early Jurassic) and a chi-square test value <0.01 (*i.e.* the ages are over-dispersed and might belong to more than one age group) (FIGURE 37). The 59 measured confined track lengths range from 3.37 to 15.51 µm with a MTL of 10.33 ± 2.25 (1σ) µm and a bimodal distribution with peaks at c. 10 and 12 µm.

1.2.3.2 13/03-1

Sample R-1 (Eocene sands)

AFT results

The 72 AFT ages range from 61.8 to 354.3 Ma with a central age of 163.3 ± 7.2 Ma (Middle-Late Jurassic) and a chi-square test value <0.01 (*i.e.* the ages are over-dispersed and might belong to more than one age group) (FIGURE 38A). The 194 measured confined track lengths range from 2.2 to 16.1 µm with a MTL of 11.2 ± 2.44 (1σ) µm and a bimodal distribution with peaks at c. 10 and 13 µm (FIGURE 38A). The grains have a chlorine content ranging from 0 to 0.9 wt% with an average of 0.16, a median of 0.1 wt% and a mode of c. 0.03 wt%. They also have Dpar values ranging from 0.85 to 2.4 µm with a normal distribution centred on the mean of 1.72 µm (FIGURE 38A). These kinetic proxies indicate that the grains are moderately homogenous and no significantly different annealing behaviour should be observed between the grains.

AHe results

Ten grains were analysed for AHe analysis. Seven grains (R-1.1-4 and R-1.8-10) were fully outgassed with background values during the second run suggesting no inclusions, while one grain (R-1.5) had a small helium leak that suggests that its age might be slightly younger than calculated. Two grains (R-1.6 and 7) leaked a significant amount of helium during repeat runs, suggesting the presence of inclusions and therefore are not used for AHe age calculation or modelling. The eight grains have raw ages ranging from 7 to 1105 Ma and F_T-corrected ages of 9 Ma (Late Miocene) to 160 Ma (Late Jurassic) (FIGURE 38B).

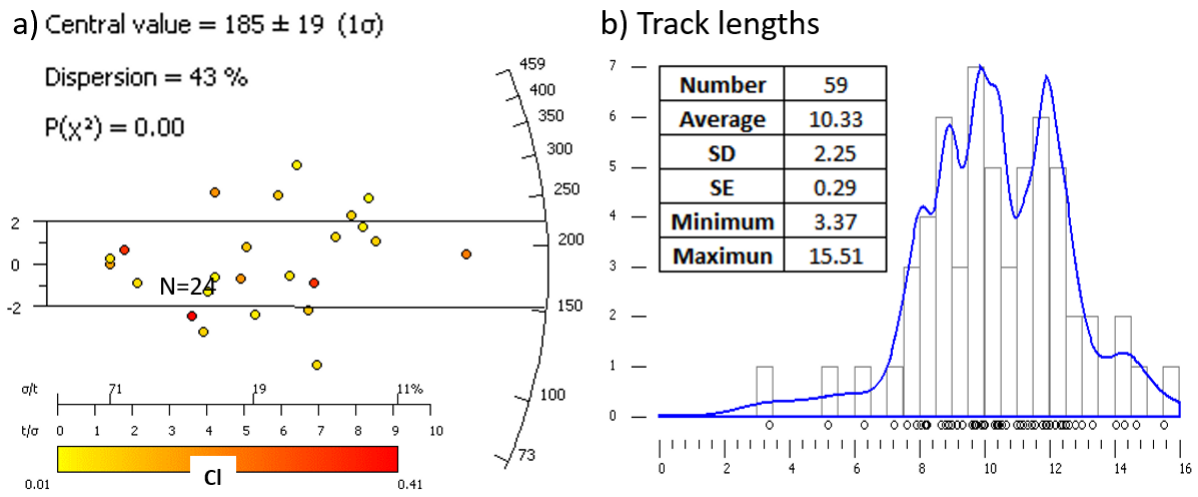

Figure 37: AFT results for sample R-37 (12/13-1A).

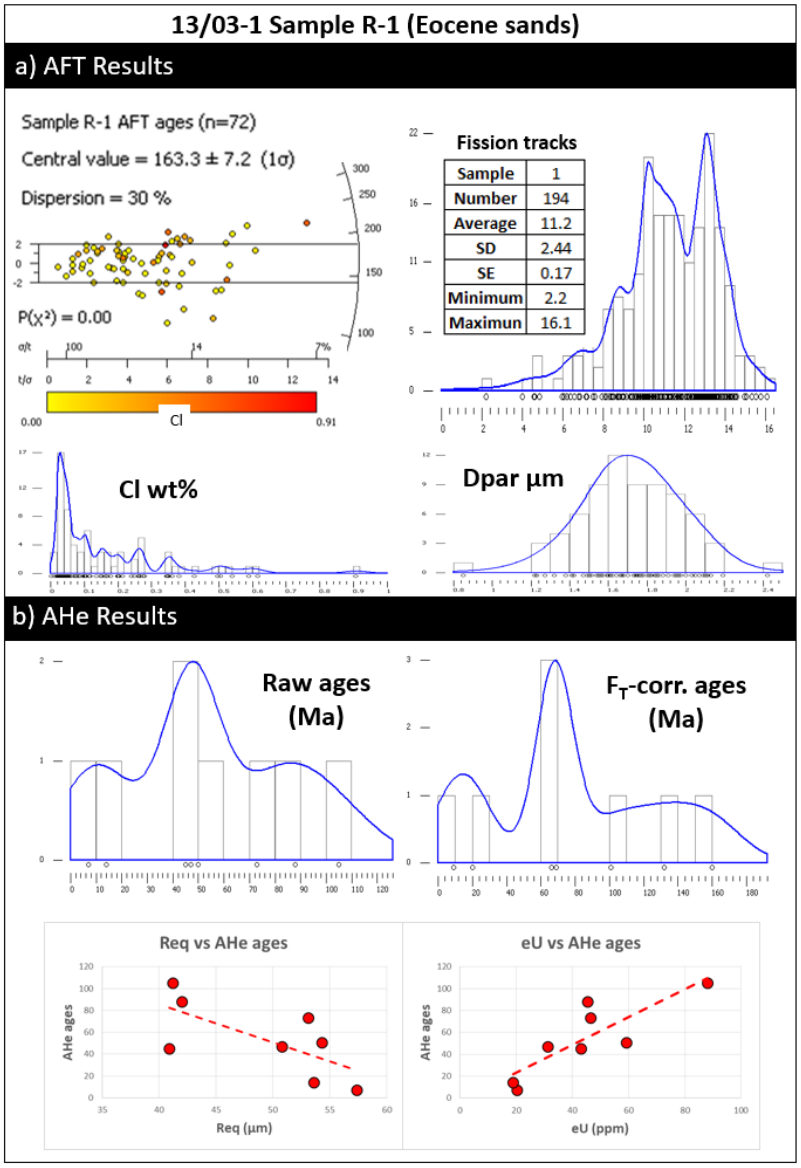

Figure 38: AFT and AHe results for sample R-1 (13/03-1 Eocene sands).

AHe age dispersion

This sample has a large AHe age dispersion. There is positive correlation between [eU] and raw AHe ages, suggesting that part of the dispersion is probably related to radiation damage in the grains. There is a negative correlation between size of the grains (proxy R_{eq}) and AHe ages, suggesting that the dispersion cannot be explained by the difference in grain size (FIGURE 38B). Due to the significant age dispersion and correlation with [eU], all eight grains will be used in the modelling.

Sample R-2 (297 Ma gabbro)

AFT results

The 123 AFT ages range from 34.6 to 353 Ma with a central age of 166.3 ± 8.4 Ma (Middle-Late Jurassic) and a chi-square test value <0.01 (*i.e.* the ages are over-dispersed and might belong to more than one age group) (FIGURE 39A). Only one confined track length could be measured due to the low uranium content of the grains (average 1.7 ppm, FIGURE 39A). The grains have a chlorine content ranging from 0.09 to 0.75 wt% with an average of 0.21, a median of 0.19 wt%. They also have Dpar ranging from 1 to 2.2 µm with a normal distribution centred on the mean of 1.71 µm (FIGURE 39A). These kinetic proxies indicate that the grains are very homogenous and no different annealing behaviour should be observed between the grains.

AHe results

Four grains were analysed for AHe analysis. All four grains were fully outgassed with background values during the second run suggesting no inclusions. They have raw ages ranging from 9 to 16 Ma and F_T-corrected ages of 13 to 23 Ma (Early-Middle Miocene) (FIGURE 39B).

AHe age dispersion

This sample has a small AHe age dispersion and the grains have a similar size and eU content (FIGURE 39B). All four grains will be used for age interpretation and modelling.

Sample L-D1 (297 Ma gabbro)

The 29 AFT ages yielded a central age of 183 ± 19.2 Ma (Early Jurassic) and no confined track lengths could be measured (McCulloch, 1993). The central age is older than the central age of sample R-2 but their 1σ uncertainties overlap in the 164-175 Ma range (Middle Jurassic).

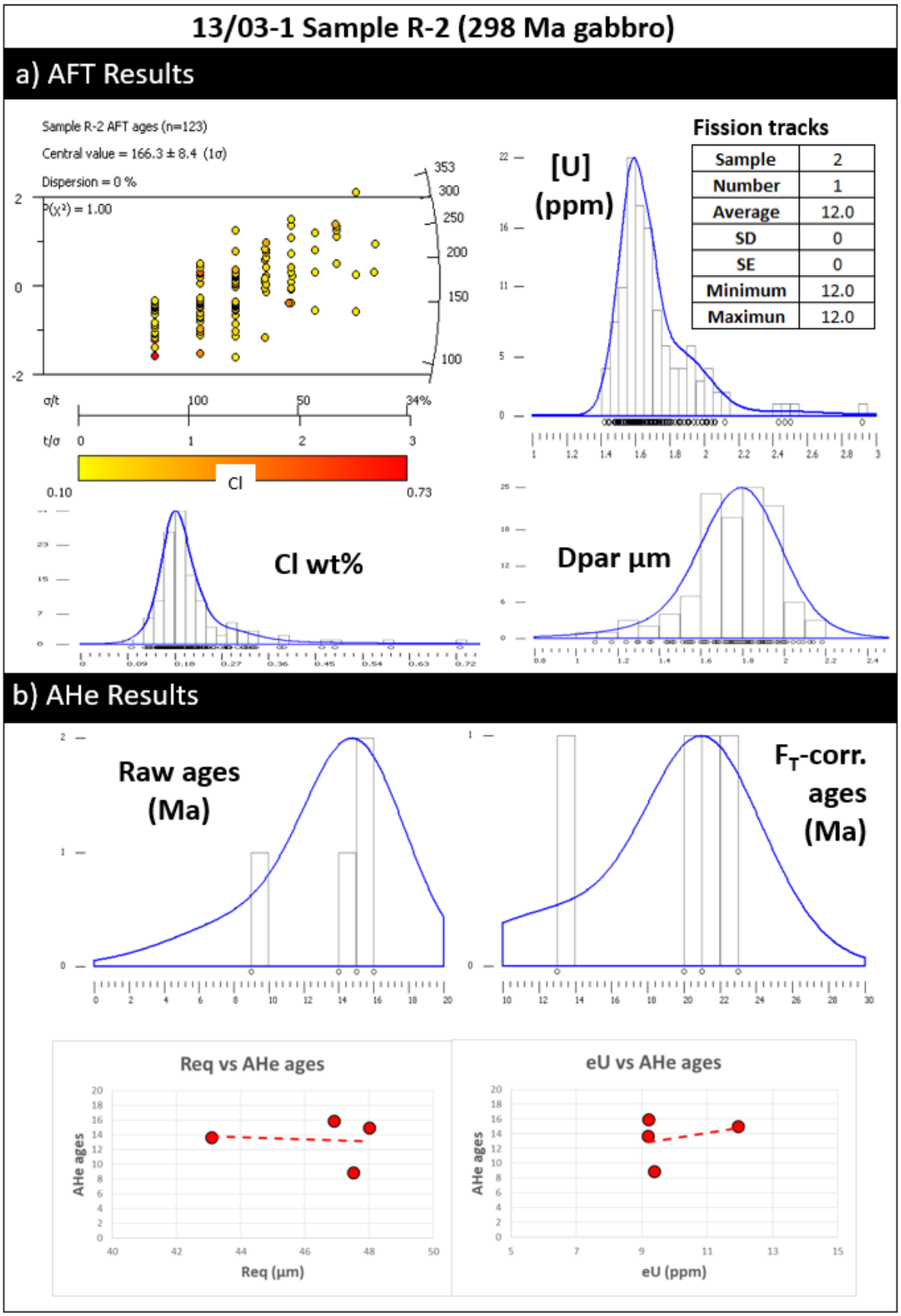

Figure 39: AFT and AHe results for sample R-2 (13/03-1 298 Ma gabbro).

1.2.3.3 18/25-2

Sample R-44 (undated intrusion)

The 34 AFT ages range from 30.4 to 319 Ma with a central age of 177 ± 21 Ma (Early-Middle Jurassic) and a chi-square test value of 0.99 (*i.e.* the grains probably belong to one age group only). Only one confined track length could be measured, probably due to the low uranium content of the grains (average 1.7 ppm) combined with their young crystallisation age (FIGURE 40).

1.2.3.4 26/30-1

Sample R-68 (Bathonian-Early Oxfordian sands)

The 75 AFT ages range from 33.6 to 656.7 Ma with a central age of 185.1 ± 8.8 Ma and a chi-square test value <0.01 (*i.e.* the ages are over-dispersed and might belong to more than one age group) (FIGURE 41A).

The detrital and volcanic (Jurassic) grains can be distinguished based on their trace element composition. In comparison to the volcanic grains, the detrital grains have a higher U concentration (mean [U] of 18 ppm *vs* 7 ppm), a higher Cl concentration (mean [Cl] of 0.24 wt% *vs* 0.08 wt%) and smaller Dpar (range of 1-2 µm with a mean of 1.7 µm *vs* 1-6 µm with a mean of 3 µm) (FIGURE 41A). In contrast to the igneous grains, the detrital grains experienced a pre-depositional thermal history, therefore it is better to consider them as two separate groups for thermochronological interpretation and modelling.

The detrital grains (n = 41) have AFT ages ranging from 66 to 372 Ma with a central age of 173 ± 10 Ma (Aalenian, Middle Jurassic) with a chi-square test value <0.01 (*i.e.* the ages are overdispersed and might belong to more than one age group) (FIGURE 41B). The 28 track lengths range from 1.57 to 14.27 µm and have a MTL of 10.63 ± 2.89 µm (1σ). The distribution appears to be bimodal with a main peak at c. 12.5 µm and a secondary one at c. 9.5 µm. However, this could be an artefact due to the small size of the population (n = 28) (FIGURE 41B).

The Jurassic volcanic grains (n = 34) have AFT ages ranging from 34 to 656 Ma with a central age of 205 ± 16 Ma (Rhaetian, latest Triassic) with a chi-square test value <0.01 (*i.e.* the ages are overdispersed and might belong to more than one age group) (FIGURE 41C). Only five confined track lengths could be measured. They range from 8.7 to 15.1 µm with a MTL of 12.89 µm and three out of the five lengths are > 14 µm suggesting that the volcanic grains might have longer track lengths than the detrital grains.

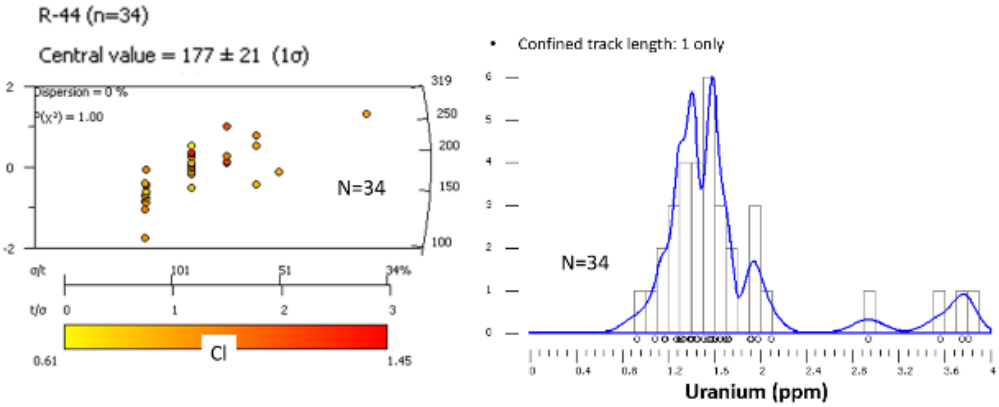

Figure 40: AFT results for sample R-44 (18/25-2).

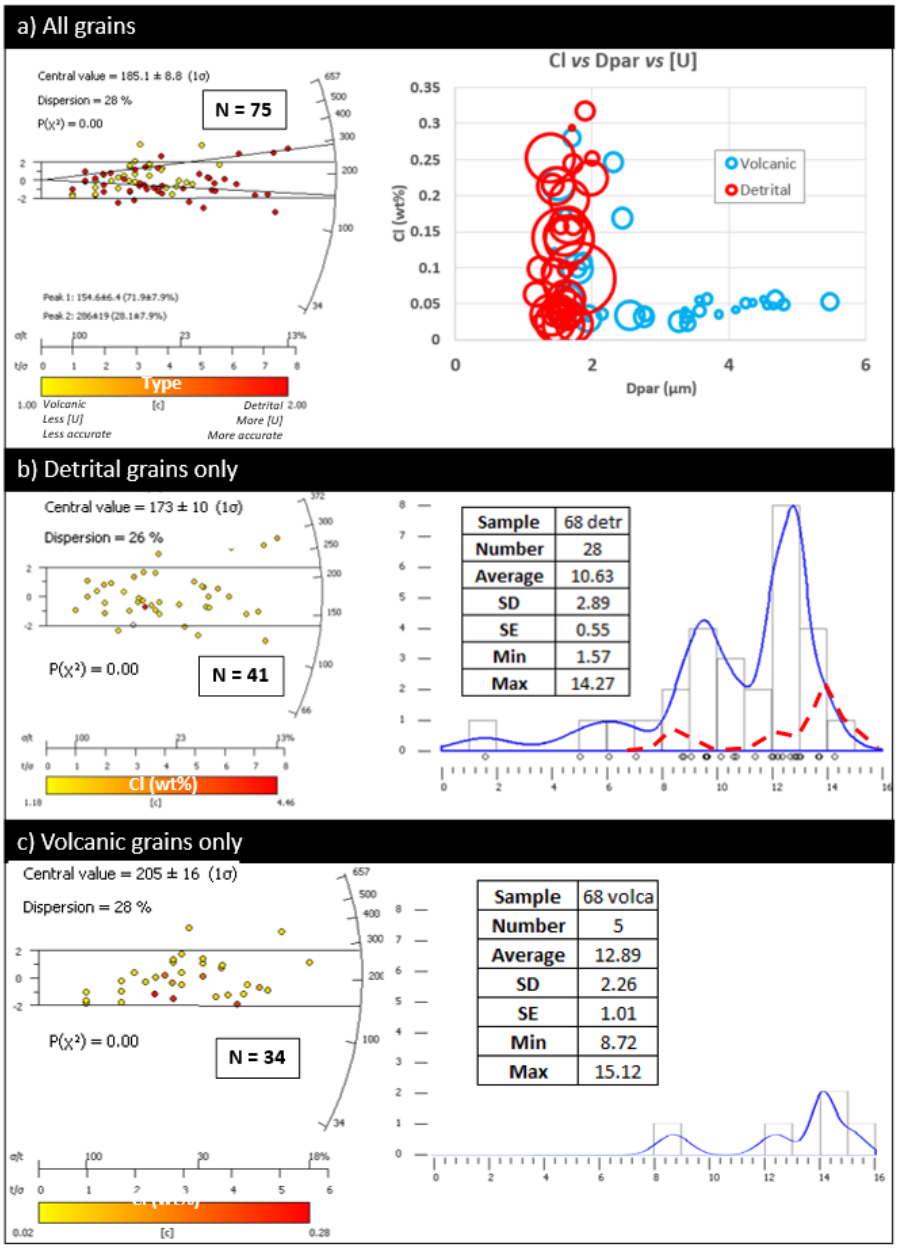

Figure 41: AFT data for sample R-68 (26/30-1).

The AFT age of the volcanic grains (205 ± 16 Ma) is slightly older than the crystallisation age (160 ± 3 Ma), suggesting that the true AFT central age should be c. 160 Ma and that the grains have not been reset since crystallisation and deposition during the Bathonian-Oxfordian. The smaller number of track lengths is probably due to their younger age and lower [U] in comparison to the detrital grains. The presence of one small track length (8.7 µm) indicates some amount of annealing post-deposition, although the preponderance of long track lengths > 14 µm could point towards the opposite conclusion. The grains have long Dpar lengths which is often indicative of slow annealing (Donelick et al., 2005) and therefore could contribute to the presence of long track lengths in the grain in comparison to the detrital grains. However, most of the grains have an unexpectedly very low Cl content which is usually correlated with shorter Dpar and faster annealing, although not always (Donelick et al., 2005).

The detrital grains have an AFT central age (173 ± 10 Ma) slightly older than the depositional age (162.8 ± 5.5 Ma) suggesting that the sample spent a certain amount of time within the PAZ but never experienced temperatures greater than c. 120 °C. This was expected based on the VR data. The bimodal track length distribution points toward a protracted episode of reburial from near-surface temperatures to temperatures within the PAZ, followed by exhumation to near-surface temperature again.

The very low number of track lengths for the volcanic grains preclude their use for thermal history inverse modelling. Only the population of detrital grains will be used as input data for the modelling.

Sample R-50 (Westphalian C sands)

Only two AFT ages could be obtained, 70.8 ± 16.2 Ma and 84.6 ± 34.9 Ma (Late Cretaceous).

Sample R-51 (Westphalian C? granite wash and in-situ Caledonian granite)

The 15 AFT ages range from 31.8 to 427.5 Ma with a central age of 151 ± 23 Ma (Tithonian, Late Jurassic) and a chi-square test value <0.01 (*i.e.* the ages are overdispersed and might belong to more than one age group) (FIGURE 42A). The 11 confined track lengths range from 7.39 to 13.96 µm with a MTL of 11.28 ± 1.64 µm with an apparent peak at c. 10.5 µm (FIGURE 42A).

The AFT central age (151 Ma) is younger than the depositional age of the granite wash (older than c. 310 Ma), suggesting that the sample experienced temperatures greater than c. 120 °C after deposition. Despite the low number of track lengths, the apparent peak at 10.5 µm and low MTL of 11.28 µm suggest that the sample experienced a protracted cooling history through the PAZ.

Even though the sample comprises apatites from two lithologies with a different pre-Carboniferous thermal history (the *in-situ* granite and the Carboniferous granite wash above), the c. 150 Ma AFT age

implies that any tracks inherited from these two different thermal histories were subsequently removed.

Combined sample R-50-51 (Westphalian C sands, granite wash and granite)

Since sample R-50 and R-51 are only c. 30 m apart in depth and have few AFT ages, it is possible to merge them as one combined sample to improve the size of the AFT age population. The new combined sample has 17 AFT ages ranging from 31.8 to 427 Ma with a central age of 141 ± 20 Ma (1σ) and a chi-square test value <0.01 (*i.e.* the ages are over-dispersed and might belong to more than one age group) (Figure 42b). The 11 confined track lengths range from 7.39 to 13.96 µm with a MTL of 11.28 ± 1.64 µm with an appaarent peak at c. 10.5 µm (FIGURE 42B). This sample will be used for the thermal history modelling.

1.2.3.5 35/13-1

Sample R-54 (undated intrusion)

The 38 AFT ages range from 20.6 to 124.7 Ma with a central age of 66.8 ± 8.6 Ma (latest Cretaceous-earliest Paleocene) and a chi-square test value of 1 (*i.e.* the grains probably belong to one age group only). No confined track lengths could be found for this sample, probably due to the very low uranium content (average of 1.8 ppm) (FIGURE 43).

1.2.3.6 35/15-1

Sample R-16

As discussed in section 0, one grain (R-16j.1) might be a xenocryst with a partially reset U/Pb age of 106.5 ± 27.8 Ma. This grains yield an AFT age of 100.2 ± 50.3 Ma and has an uranium concentration of 3.9 ppm (TABLE 4). If the grain is indeed a xenocryst, then the fission tracks should have been completely annealed and the FT data from this grain could be used for FT interpretation. However, the grain could also be an allochthonous grain coming from another source than the basalts. Due to this uncertainty, it is safer not to include this grain in the FT dataset used to derive thermal history information for this sample.

The three other grains in that sample are Caledonian detrital grains. One of them yield a Paleogene AFT age of 44.8 ± 12.1 Ma while the two other grains yield Jurassic AFT ages of 183 ± 35.7 Ma and 186.5 ± 35.6 Ma. Fission tracks are completely annealed within tens of minutes at temperature of 400°C (Green et al., 1986) so any *in-situ* or xenolithic apatites in the Paleocene basalts (with temperatures of magma emplacement probably in the range of c. 1050 - 1200 °C, Harris and Allen III (2008) and Deschamps et al. (2014)) would have Paleocene AFT ages.

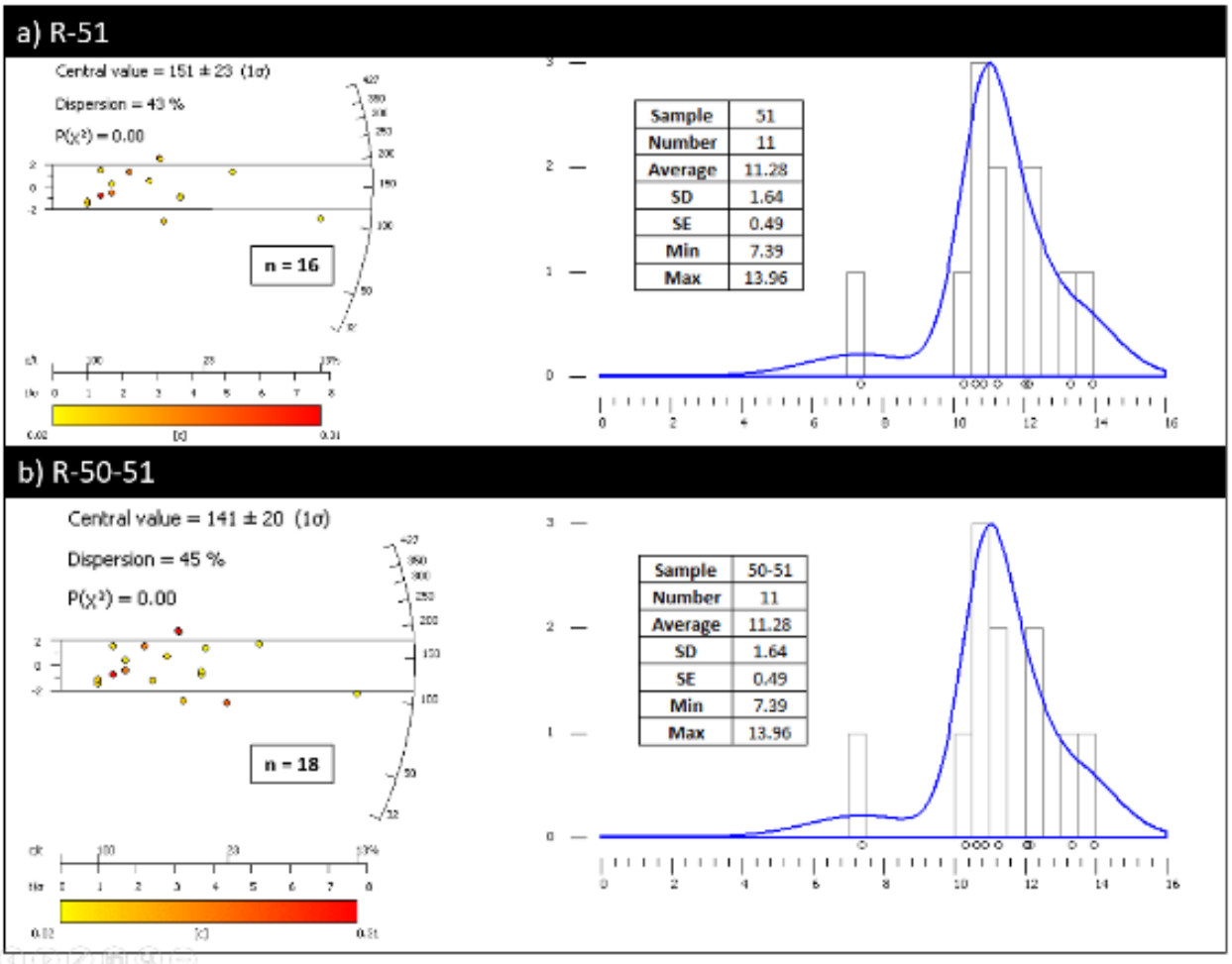

Figure 42: AFT results for a) sample R-51 and b) combined sample R-50-51.

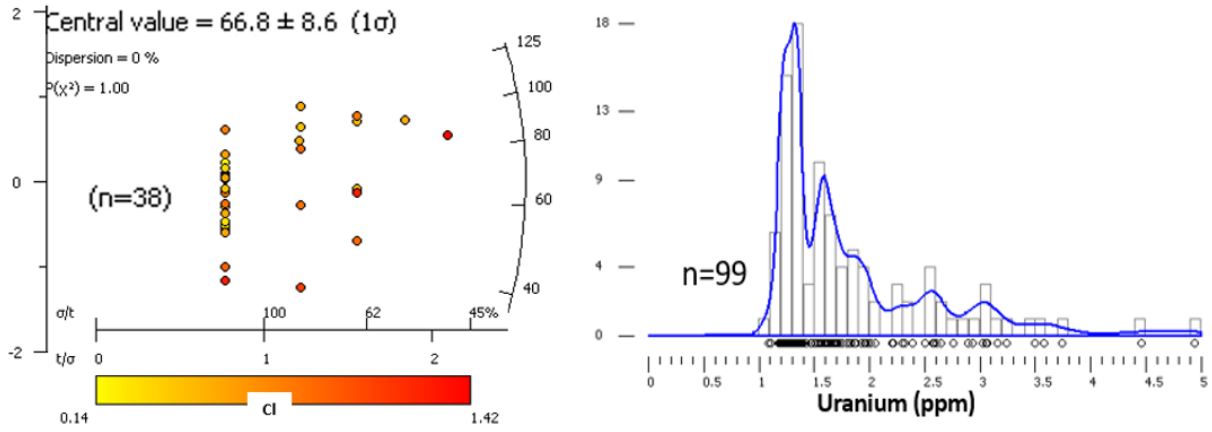

Figure 43: AFT results for sample R-54 (35/13-1).

Consequently, the first grain with an AFT age of 44.8 ± 12.1 Ma could potentially be a xenolithic grain in the Paleocene basalt or another Paleocene igneous unit from the overlying conglomerate. Conversely, the two other grains with Jurassic AFT ages are necessarily allochthonous grains (not from the basalts). However, single LAFT age can seldom be interpreted on their own due to the large inaccuracy of the dating method (Ketcham et al., 2018a), particularly for young grains with low uranium content.

In conclusion, none of the four apatite grains in sample R-16 can be used for fission track analysis and thermal history interpretation of this depth interval.

Table 4: Borehole 35/15-1 AFT results.

Sample	Depth	Seabed	Grains	Ns	Area	U/Ca*Ω	U/Ca	P(χ2)	Central Age	±1σ	Tracks	MTL	SD	SE
	m BSB	*m MSL*	n		*cm2*				*Ma*	*Ma*		*µm*	*µm*	*µm*
R-16	1632.2	310.9	4	75	7.06E-05	6.37E-06	9.03E-02	<0.01	115	36	6	11.54	0.55	0.22
R-17	1670.3	310.9	0	-	-	-		-	-	-	-	-	-	-
R-18	1746.5	310.9	9	33	2.60E-04	4.46E-06	1.72E-02	0.88	76	13	1	13.33	-	-
R-19	1862.3	310.9	3	11	1.07E-04	1.31E-06	1.22E-02	0.99	81	25	0	-	-	-
R-20	2630.4	310.9	0	-	-	-	-	-	-	-	-	-	-	-
R-16-19	1759	310.9	13	48	3.87E-04	6.15E-06	1.59E-02	0.98	79	11	N/A	N/A	N/A	N/A

Sample R-17

The AFT mount for this sample was lost and no AFT data is available for this sample.

Sample R-18

The U/Pb data show that all nine apatites are Paleocene in age and most certainly come from the basaltic unit. The AFT ages range between 39.7 and 116.3 Ma with a central age of 76 ± 13 Ma. Only one confined track length with a length of 13.33 µm was recorded. The grains have an average uranium concentration of 3.5 ppm.

Sample R-19

The U/Pb data show that all three apatites are Paleocene in age and almost certainly come from the basaltic unit. The AFT ages range between 77.7 and 83.4 Ma with a central age of 81 ± 25 Ma. No confined track lengths were found in these apatites. These three grains have an average uranium concentration of 2.6 ppm.

Combined sample R-18, R-19

Few AFT ages have been obtained for these samples due to a combination of 1) poor apatite yield, 2) poor quality of grains (too small or too fractured to be counted and ablated), 3) grain loss during laser ablation (the mounts were probably over-polished) and 4) extraneous grains. All samples have less than ten AFT ages which does not allow derivation of a statistically meaningful central age.

The difference between the average depth of the shallowest (R-18) and deepest sample (R-19) with Paleocene igneous apatites is only 180 m, which at the present-day geothermal gradient of 35.3°C/km corresponds to a difference of temperature of 6.4 °C. Since there are so few AFT ages for these samples and they have a small difference in temperature, it is possible to combine them as one sample (hereby named R-18-19) comprising 11 AFT ages ranging from 39.7 Ma to 104.3 Ma with a central age of 77 ± 12 Ma and an average uranium concentration of 3.5 ppm (TABLE 4 AND FIGURE 44A,B).

AHe results

Sample R-16

The apatite grains for sample R-16 were too low in quality to be analysed for AHe dating (either too small, or damaged or with inclusions). The LA-ICP-MS results (undertaken post-AHe grain selection) show that any grain that would have been sent for analysis would have had a high probability of being extraneous.

a)	Grains	Central age	[U]	Lengths
R-16	1?	100 ± 50 Ma	3.9 ppm	Not enough lengths (due to low U, young age)
R-17	Lost mount			
R-18	9	76 ± 13 Ma	3.5 ppm	
R-19	3	81 ± 25 Ma	2.6 ppm	
R-20	0	N/A	N/A	
R-18-19	11	77 ± 12 Ma	3.3 ppm	

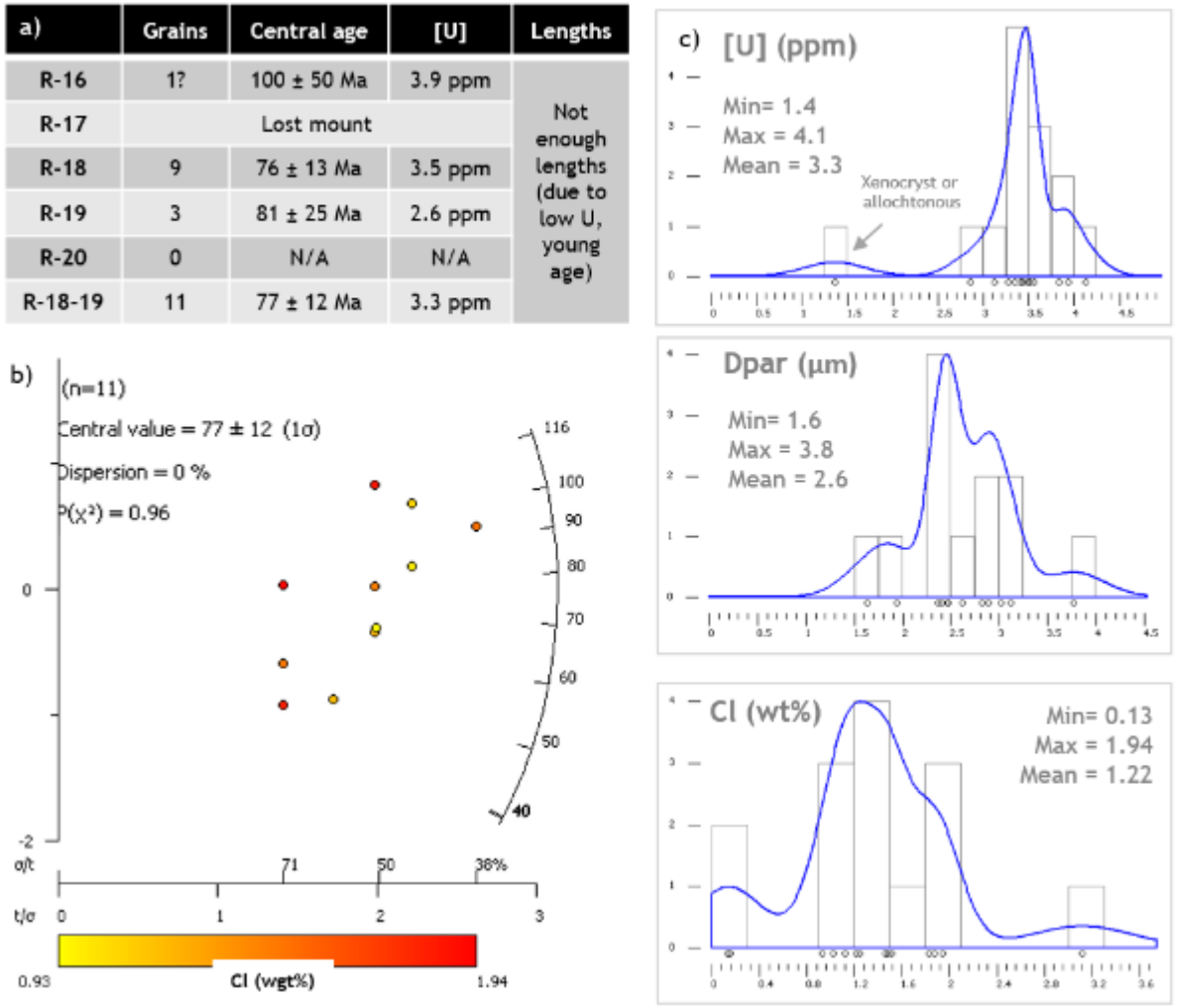

Figure 44: AFT results summary. a) Results per sample. b) Radial plot of combined sample R-16-19 with chlorine content for colour scale. c) Histograms and KDEs of [U], Dpar and Cl for all the grains in sample R16-19.

Sample R-17

Five grains were analysed for AHe analysis. Three grains were fully outgassed with helium values close to background values during the second run, suggesting no eU-rich inclusions such as zircons. They have raw ages of 26, 27 and 38 Ma and F_T-corrected ages of 36, 38 and 52 Ma (FIGURE 45).

Another grain (grain R-17.1) continued to outgas a very small amount of ^{4}He during the second run above background values suggesting the possible presence of U-Th-rich inclusions in the grain. The second run was only c. 1.9% the amount of the first run and so is small enough to be ignored. The grain yielded a raw age of 33 Ma, which is in agreement with the first three ages.

One grain experienced a possible lack of laser heating, resulting in a possibly not fully degassed grain. This grain has a raw age of 16 Ma, younger than the three good grains, which could suggest that it was not fully degassed.

Sample R-18

Five grains were analysed for AHe analysis. Three grains were fully outgassed with background values during the second run suggesting no inclusions. They have raw ages of 0, 0 and 51 Ma and F_T-corrected ages of 0, 0 and 62 Ma (FIGURE 45).

Another grain continued to outgas a very small amount of ^{4}He during the second run above background values suggesting the possible presence of U-Th-rich inclusions in the grain. The second and third runs were only c. 1.3% and 0.6% the amount of the first run and so can be ignored. The grain yielded a raw age of 12 Ma and a F_T-corrected age of 15 Ma.

One grain experienced a possible lack of laser heating (despite three repeat runs), resulting in a grain that was possibly not fully degassed. This grain has a raw age of 0 Ma, similar to two of the good grains. All four runs (the initial main run and the three repeat runs) yielded helium values similar to blank values but no glow was observed on the Pt tube. An orange-yellow glow of the Pt tube during laser heating indicates that the temperature reaches c. 500 to >1000 °C. An absence of glow could be due to either 1) a lack of heating (for example due to laser energy being reflected by a curved surface) or else 2) heating is successful but the colour of the glow does not appear on the camera screen due to wavelength filtering (for example by the sapphire glass of the sample cell or a camera filter. Each repeat run was placed to a different location of the Pt tube, to reduce the likelihood of laser beam reflection by a curved surface. Although it is possible that no significant heating was achieved for these four attempts, it is more likely that at least one of them achieved normal heating temperatures but the glow was not visible due to wavelength filtering. Therefore, the grain was probably heated by temperatures high enough to fully remove all the helium. The observed values, similar to blank values,

indicate that no helium was present in this grain before heating (AHe age of 0 Ma), which is in agreement with the two other grains with an AHe age of 0 Ma.

Sample R-19

Four grains were analysed for AHe analysis. Three grains were fully outgassed with background values during the second run suggesting no inclusions. One grain experienced a possible lack of laser heating during the first grain, but the second run was fine and yielded background values demonstrating the grain was fully outgassed during the first run. They yield raw ages of 0, 0 and 51 Ma and F_T-corrected ages of 0, 1, 11 and 118 Ma with F_T-corrected ages of 0, 2, 17 and 190 Ma (FIGURE 45).

1.3 Sonic and VR data for exhumation estimates

1.3.1 34/05-1

TCU exhumation estimates

Using the legacy data, the amount of uplift and erosion associated with the TCU can be estimated using both a compaction-based method (sonic velocities) and a temperature-based method (VR) (Corcoran and Doré, 2005). Both methods yield estimates of the amount of uplift and erosion but no information about the timing of such uplift.

Sonic velocity-derived exhumation estimates

Sonic velocity is primarily controlled by 1) lithology and 2) compaction. With increasing depth of burial, a sediment will become more compacted and therefore its sonic velocity will increase. An abrupt change in sonic velocity across an unconformity often indicates that a portion of sediments have been eroded. The amount of eroded sediments can be estimated by comparing the sonic velocities below the unconformity to reference values calculated for this specific lithology and often for a specific basin (*e.g.* Corcoran and Mecklenburgh (2005) for the Slyne Basin and Ware and Turner (2002) for the Irish Sea Basin).

In borehole 34/05-1, such an abrupt change is observed at the VU, with the sonic velocity recording a shift from c. 1900-2100 m.s-1 in the red unit to c. 2500-3000 $m.s^{-1}$ in the uppermost Carboniferous sediments, suggesting that a certain amount of material has been eroded.

Sample	Grain	Shape in GFTC		Length	Diameter		S/V	R_{eq}*	Weight	Temp.	$[^{238}U]$	$[^{232}Th]$	$[^{147}Sm]$	eU	Th/U weight	[He]	Degassing	Raw Age	Error	F_T	Correc. age	Error
		Geometry	GFT*	W	Max	Min																
				µm	µm	µm		µm	g	°C	ppm	ppm	ppm	ppm		nmol/g		Ma	Ma		Ma	Ma
R-17	4	Hexagonal prism	2F	166	87	77	0.065	46.2	2.64E-06	68	1	3	4	2	3.2	0.2	Lack of heat	16	2	0.699	24	4
	2	Hexagonal prism	2F	235	94	83	0.057	52.2	4.36E-06	68	0	2	4	1	3.6	0.1	Ok	26	4	0.73	36	5
	3	Hexagonal prism	2F	227	84	71	0.064	46.6	3.26E-06	68	1	3	2	1	3.7	0.2	Ok	27	4	0.699	38	6
	1	Hexagonal prism	2F	329	86	75	0.060	50.1	5.04E-06	68	1	2	2	1	2.5	0.2	Small leak	33	5	0.718	47	7
	5	Hexagonal prism	2F	320	90	78	0.058	52.2	5.40E-06	68	0	1	1	1	3.8	0.2	Ok	38	6	0.729	52	8
R-18	2	Hexagonal prism	2F	167	96	84	0.060	50.2	3.24E-06	71	4	7	90	6	1.7	0.0	Lack of heat	0	0	0.721	0	0
	3	Hexagonal prism	1P1F	191	78	70	0.069	43.7	2.19E-06	71	4	4	57	5	1.1	0.0	Ok	0	0	0.679	0	0
	4	Hexagonal prism	1P1F	157	76	67	0.082	36.7	1.92E-06	71	4	6	68	6	1.3	0.0	Ok	0	0	0.664	0	0
	5	Hexagonal prism	1P1F	192	146	135	0.043	70.2	6.88E-06	71	4	4	58	5	1.0	0.3	Small leak	12	2	0.796	15	2
	1	Hexagonal prism	2F	219	163	143	0.037	80.2	1.22E-05	71	2	1	1	2	0.5	0.6	Ok	51	8	0.821	62	9
R-19	3	Hexagonal prism	2F	165	65	57	0.083	36.1	1.45E-06	75	6	9	134	9	1.6	0.0	Ok	0	0	0.62	0	0
	1	Hexagonal prism	2F	145	80	70	0.071	42.1	1.95E-06	75	2	11	914	9	5.1	0.1	Ok	1	0	0.672	2	0
	2	Hexagonal prism	2F	209	63	56	0.083	36.4	1.74E-06	75	2	12	987	10	5.4	0.8	Ok	11	2	0.621	17	3
	4	Hexagonal prism	2F	221	63	55	0.082	36.6	2.20E-05	75	0	0	0	0	-920.9	0.0	Ok	118	18	0.622	190	29

*F_T and R_{eq} from Alpha Ft-ejection factor calculator (Gautheron *et al.*, 2012)

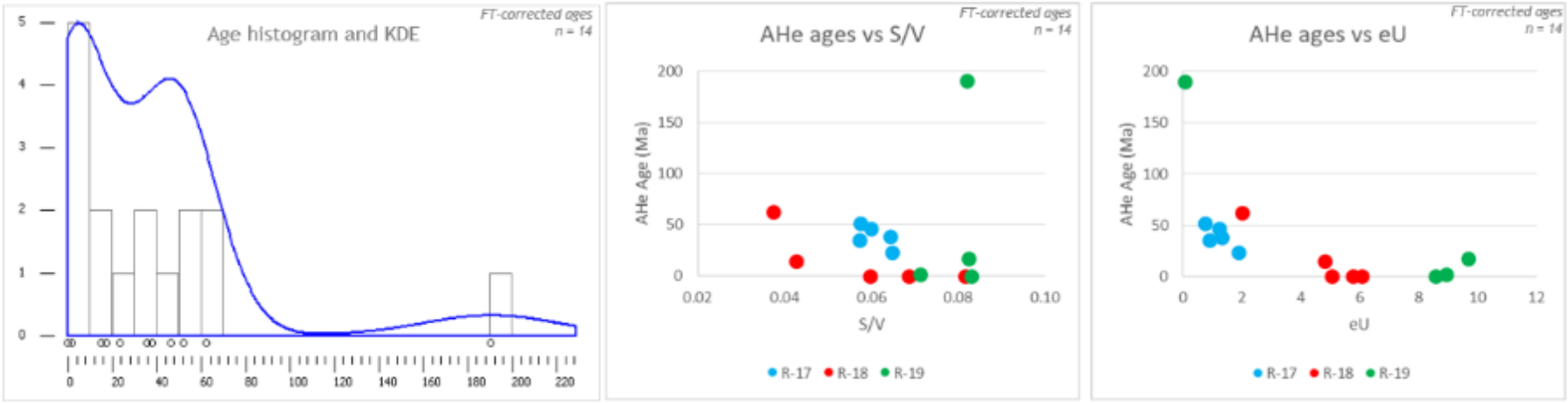

Figure 45: AHe results summary for samples R-17, R-18 and R-19 (35/15-1).

A detailed sonic velocity-based exhumation study based on newly constructed reference compaction curves for offshore West of Ireland and suitable for the sediments in borehole 34/05-1 is not part of the scope of this study. However, a rough estimate of the thickness of eroded sediments at the Paleogene-Carboniferous unconformity can be obtained by using the reference compaction curve of Corcoran and Mecklenburgh (2005). The reference compaction curve was constructed by calculating a best-fit curve through sonic velocity values from Jurassic, Cretaceous and Cenozoic shales from the Porcupine, and Rockall basins plotted *versus* depth below seabed (BSB) (FIGURE 46). Although there are no Carboniferous sediments in the dataset, the Mesozoic sediments could correspond to most of the eroded material and the basins used for the reference dataset are the ideal basins to use for borehole 34/05-1 (*i.e.* they are the closest basins deep enough to derive meaningful compaction data).

The uppermost Carboniferous sediments, which are at a present-day depth of c. 750 m MD or c. 436 m BSB. They are mostly composed of siltstones and sandstones with occasional shales and coals. These lithologies do not compact with burial as much as the shales which have been used to derive the curve. The sonic log at this depth averages 100 $\mu s.ft^{-1}$. However, the thin interval of shales seems to be associated with sonic values reaching 120 $\mu s.ft^{-1}$ (*i.e.* slower velocities). Therefore this value of 120 $\mu s.ft^{-1}$ will be used as the best estimate of shale velocity for the Carboniferous sediments just below the unconformity.

Using the reference curve, this sonic value corresponds to a depth of c. 3200 ft BSB, or 975 m BSB (FIGURE 46). Using the envelope of the entire dataset, minimum and maximum estimates of c. 1500 ft and c. 7000 ft BSB can be estimated, corresponding respectively to 457 m and 2134 m BSB (FIGURE 46A). The maximum burial that lead to the maximum compaction visible in these sediments now would have occurred before the deposition of the Paleocene to Recent sediments. Therefore the sediments between the sample depth (750 m MD) and the TCU (735 m MD), *i.e.* 15 meters thick, corresponds to preserved Carboniferous section that has not been eroded. This preserved thickness can be subtracted from the paleo-depth estimates to derive the amount of sediments eroded before Cenozoic sedimentation. This yields an estimated amount of eroded materials in the range of 442 to 2119 m with a best case estimate of 960 m (FIGURE 46A). For comparison, the claystones just above the unconformity (at c. 730 m MD or 416 m BSB) yield a best-case estimate of -110 m of eroded sediments, which means that the sonic velocity of these sediments do not require a deeper burial than the present-day burial and that no or little erosion must have occurred above them (FIGURE 46A).

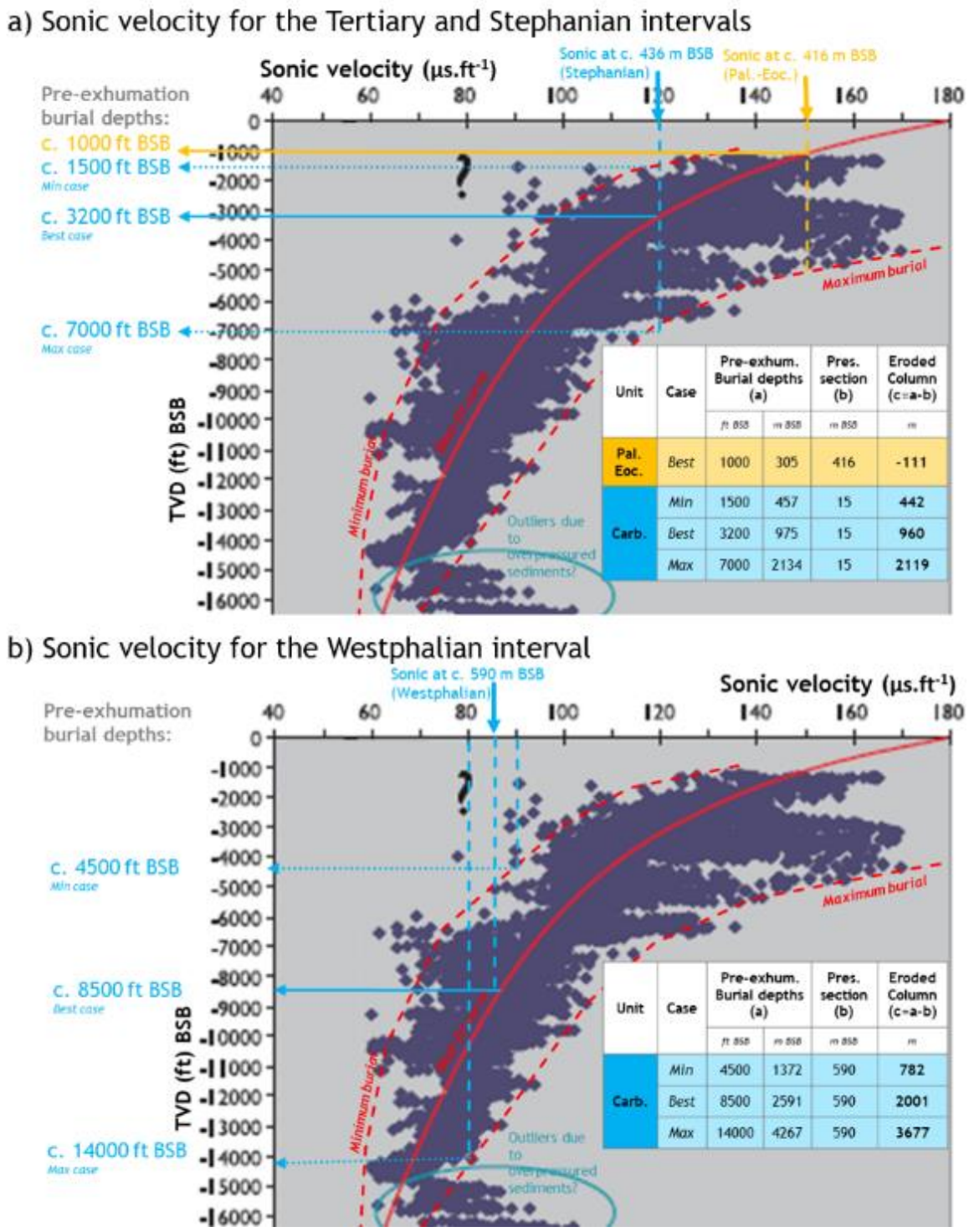

Figure 46: Pre-Cenozoic exhumation estimates of 34/05-1 based on sonic velocity. a) Cenozoic and Stephanian intervals (c. 730 and 750 m MD respectively. b) Westphalian B interval (c. 1325 m MD).

Using a similar approach, the sonic velocities at c. 1350 m MD in the older Westphalian sediments yield minimum and maximum exhumation estimates of 782 and 3677 m with a best case of 2001 m (FIGURE 46B).

However, these values should only be seen as rough estimates since the reference dataset did not include Carboniferous shales and since the Carboniferous sediments in 34/05-1 are dominated by siltstones and sands. However, it does show that probably at least a few hundred meters of Mesozoic sediments might have been removed before the deposition of the Cenozoic continental deposits.

VR-derived exhumation estimates

Introduction

Vitrinite reflectance data can be converted to maximum temperatures, paleogeothermal gradients and exhumation estimates, albeit with large uncertainties (Corcoran and Doré, 2005).

The presence in Ireland of Carboniferous samples that have experienced maximum temperatures in excess of 350 °C (e.g. Westphalian rocks in the Munster Basin, Blackmore (1995)) or reverse gradients (e.g. Slievecallan Borehole, Goodhue and Clayton (1999)) have shown that some of the Carboniferous maturity data cannot be satisfactorily explained with burial alone and that other mechanisms such as advective heating, possibly related to Variscan intrusions, could be dominant in some areas (Graham, 2009). In such cases, these anomalous VR datasets cannot be used to derive exhumation estimates.

However for borehole 34/05-1, the normal increase of VR with depth from c. 0.8 to 1.1 R_o%, the associated maximum temperatures (<175 °C, see below) and the obvious cause for anomalous high VR (igneous intrusion) do not support the presence of anomalous adjective heating or anomalous VR gradients at this location. Consequently, the VR dataset is judged suitable for exhumation estimates.

34/05-1 VR dataset

As already discussed earlier, the geochemical report present a series of vitrinite reflectance (VR) measurements with values increasing from 0.8-0.9 R_o% at c. 800 m MD to 1 R_o% at c. 1300 m and 1.1 % at c. 1400 m MD. The interval between c. 1320 and 1390 m MD yields higher VR values of 1.3 R_o% at 1330.2 m and 1.85 R_o% at 1372.5 m MD which the authors of the VR study interpret as caused by a volcanic intrusion nearby, which was confirmed with the discovery of an 18 meters thick igneous intrusion between 1346 and 1364 m MD. Similarly, the deepest VR sample at 1471 m MD yields a wide range of values up to 5.7 % (FIGURE 47).

Carboniferous paleogeothermal gradients

Using the R_o vs maximum temperature (T_{max}) relationship of Barker (1988), Corcoran and Clayton (2001) derived an average Carboniferous paleo-geothermal gradient (CPG) of 92.5 °C.km^{-1} with a 95% confidence interval of 57.2-127.8 °C.km-1 (FIGURE 48). However, using the reference curves between VR, depth BSB and geothermal gradient from Suggate (1998), it seems that the curve that best fit the

VR data of 34/05-1 (not including the points affected by the intrusion) is the one corresponding to a CPG of c. 30 °C.km-1 (dotted blue line in FIGURE 48).

A CPG of 60 or 90 °C.km-1 does not fit the data properly (FIGURE 48), unless the VR from the shallower samples have been greatly overestimated due to, for example, the correction applied to correct for high level of fluorescence (Cailleaux and Robert, 1981). It is however unlikely that all three shallow samples have been overestimated. Moreover, the VR data from the Carboniferous section of nearby well 26/26-1 also shows similar VR values for these depths (FIGURE 47).

Regionally, Corcoran and Clayton (2001) found that the Carboniferous basins of onshore and offshore Ireland had an average CPG of 60 °C.km-1 (FIGURE 48). Based on these observations, the CPG in well 34/05-1 is estimated to be 60 ± 30 °C.km-1 (FIGURE 48).

VR to T_{max}

The VR sample with possibly the least ambiguity is at 1398.9 m MD which is from a core and therefore cannot include any caving materials or other contamination from the mud. This sample has a VR value of 1.1 R_o%. Using the VR model of Barker (1988), this reflectance of 1.1 R_o% corresponds to a maximum temperature (T_{max}) of 155.8 °C (FIGURE 49A), which is similar to the value obtained from the Easy%Ro model of Sweeney and Burnham (1990), i.e. c. 158 °C (FIGURE 49B). The Basin%Ro model of Nielsen et al. (2017) yields a Tmax of c. 171 °C (FIGURE 49B). This value can be seen as a maximum value since for VR values in the range of 130-190 °C, the model of Nielsen et al. (2017) always yields the highest temperature in comparison to all other commonly used models (compare all common model curves on FIGURE 49B). Based on these models, we estimate the minimum and maximum temperature to be respectively 156 °C and 171 °C. The best-case estimate is calculated using the mean of the minimum and maximum, which yields a temperature of 163.5 °C. In conclusion, the maximum temperature reached by the VR sample is estimated to be 163.5 ± 7.5 °C (FIGURE 49C).

Exhumation estimates

Using both estimations of the CPG and T_{max} of the sample at 1398.9 m MD (and assuming that the sample reached its maximum temperature during the Carboniferous-Early Permian and not during the Mesozoic-Cenozoic which has a lower paleo-geothermal gradient), it is possible to calculate the thickness of sediments eroded. Using the mean case as an example, for the sample to reach a Tmax of 163.5 °C with a CPG of 60 °C.km-1, it must have been buried under 2.7 km of sediments. The sample is at a depth of 1398.9 m MD while the TCU is at a depth of 735 m MD, meaning only 664 m have been preserved from erosion and 2.1 km have been removed (TABLE 5). Using the minimum and maximum estimates of Tmax and the CPG, the minimum and maximum amount of eroded material is respectively 1.1 and 5 km (TABLE 5).

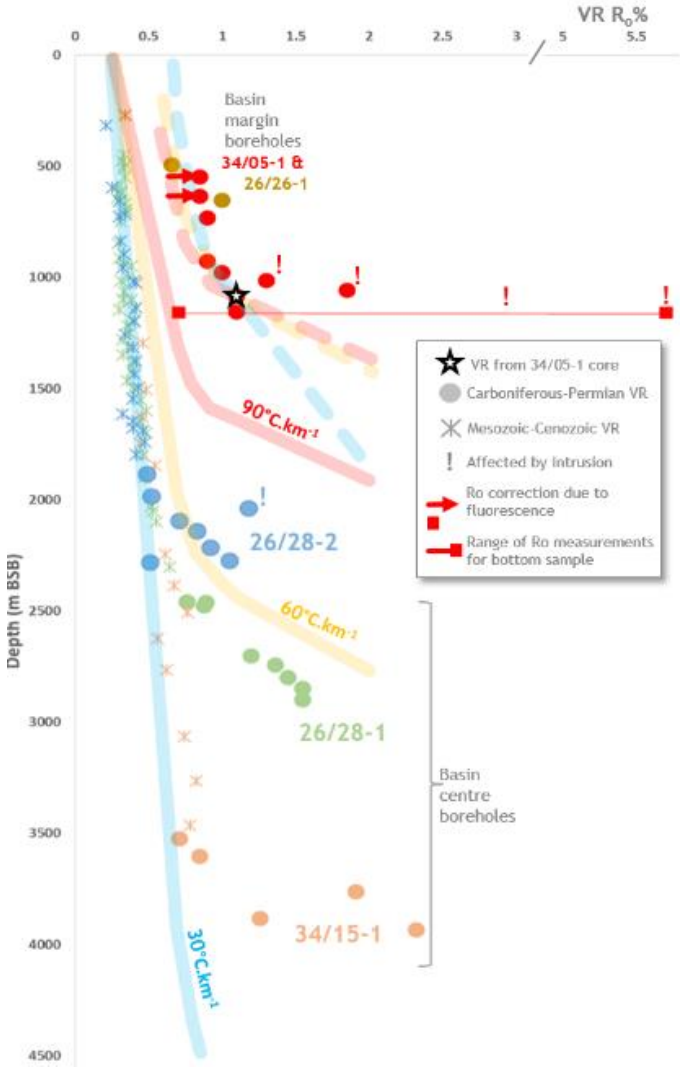

Figure 47: VR data for borehole 34/05-1 and surrounding wells.

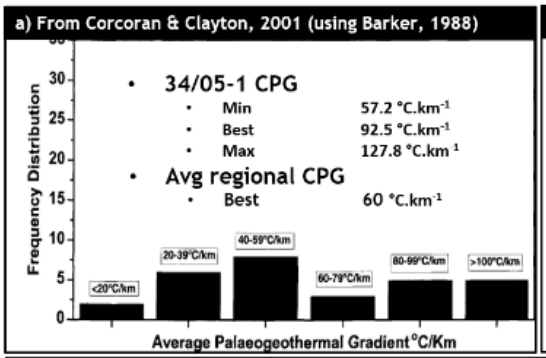

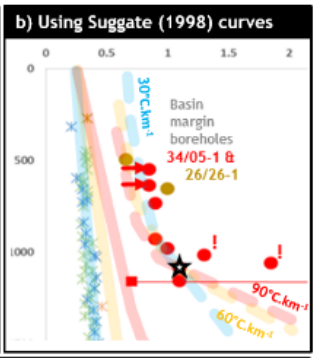

c) CPG estimates summary	Min	Best	Max
Corcoran & Clayton, 2001: 34/05-1 (a)	57.2	92.5	127.8
Corcoran & Clayton, 2001: Regional CPG (a)	11.9	60	119
Suggate, 1998 (b)	<30	c. 30	c. 90
This study	30	60	90

Figure 48: Estimates of maximum temperature reached for the VR sample at 1294 m MD with a VR of 1 R$_o$% (34/05-1).

a) T_{max} from Ro after Barker, 1988 (as used in Corcoran & Clayton, 2001)

- $\ln(R_o) = 0.0096(T_{max}) - 1.4$
- $T_{max} = \frac{\ln(R_o)+1.4}{0.0096}$
- For $R_o = 1$ then $T_{max} = 155.8$ °C

b) VR vs T_{max} from Basin%R_o and Easy%R_o models

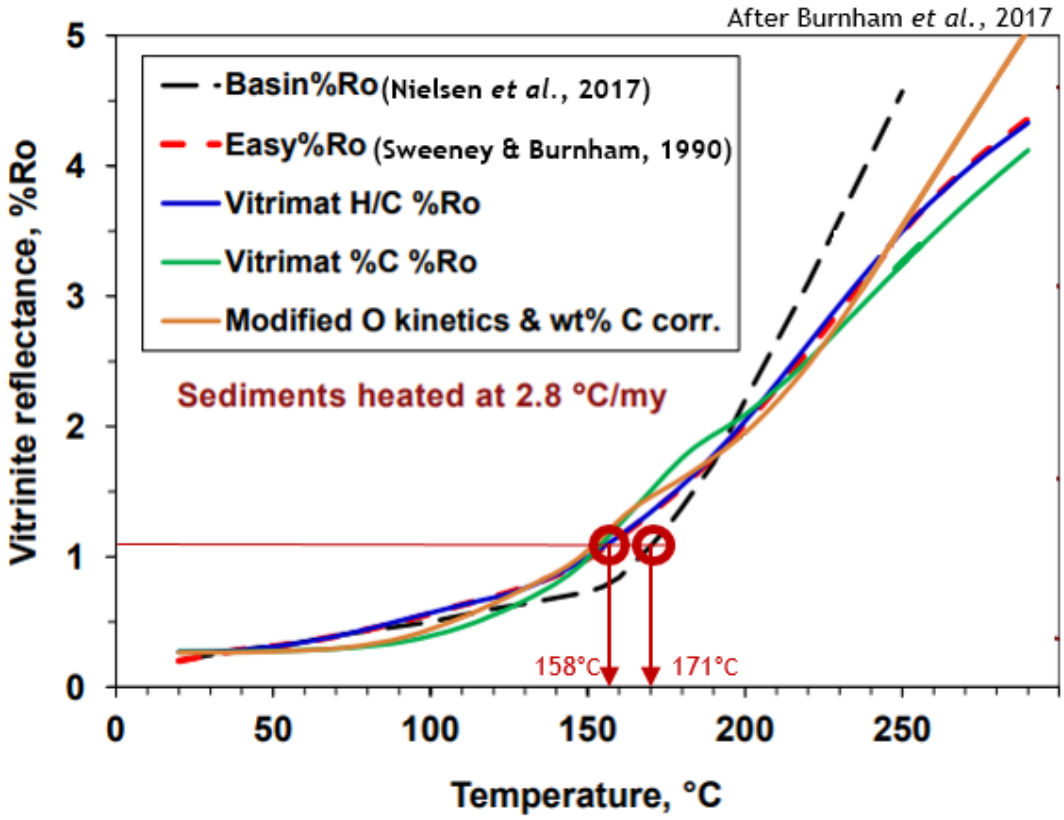

c) Estimates summary

	Min	Best	Max
Barker, 1988	155.8 °C		
Easy%Ro / Basin%Ro	158 °C	-	171 °C
This study	**156** °C	**163.5** °C	**171** °C

Figure 49: Estimates of maximum temperature reached for the VR sample at 1294 m MD with a VR of 1 R_o% (34/05-1).

Comparison of sonic- and VR-derived exhumation estimations

The sonic-derived estimates of eroded sediments range between c. 400-2100 m for the Stephanian interval and between 800-3700 m for the Westphalian interval. The VR estimates range between 1100-5000 m with a best case scenario of c. 2100 m, which is similar to the best case estimate of the deeper sonic interval and the maximum estimate of the shallower sonic interval (FIGURE 50A).

Broadly, when combining both sonic and VR estimates, it is likely that the maximum thickness of eroded sediments would be c. 4000 m (FIGURE 50B), because greater thicknesses would be hard to reconcile with the observed amount of compaction. Similarly, the minimum thickness would be c. 1000 m (FIGURE 50B), since a lower thickness would require very high geothermal gradient above 100 °C.km-1. The most likely thickness estimate is c. 2000 m, based on the best estimate from the deeper sonic interval and VR data and the fact that this thickness would require a paleogeothermal gradient of c. 60 °C.km-1 (FIGURE 50B), which is the average CPG of Corcoran and Clayton (2001).

The core sample at 1398.9 m MD, with a T_{max} of 163.5 ± 7.5 °C, can be used to back-calculate the geothermal gradients that could yield these minimum, most likely and maximum thickness of eroded sediments. For example, to reach a temperature of 156, 163.5 and 171 °C with 2000 m of eroded material (which is the most likely estimate, so 2664 m when adding the preserved 664 m of Carboniferous sediments above the sample), it requires a CPG of respectively 58.5, 61.4 and 64.2 °C.km^{-1}. The same approach on the minimum and maximum exhumation estimates (1000 and 4000 m) yields a minimum and maximum CPG of respectively 33 °C.km^{-1} and 103 °C.km-1 (FIGURE 50B).

Table 5: Exhumation estimates based on VR-derived maximum temperatures and paleogeothermal gradients.

Tmax °C	CPG °C.km^{-1} 30	60	90
156	4.5 km	1.9 km	1.1 km
163.5	4.8 km	2.1 km	1.2 km
171	5 km	2.2 km	1.2 km

Table 6: Paleo-geothermal gradients required to reach Tmax at c. 1400 m MD with an eroded column of 1.1 to 2.12 km.

Tmax °C	Exhum. (km) 2.12	1.61	1.10
156	56 °C/km	68.6 °C/km	88.4 °C/km
163.5	58.7 °C/km	71.9 °C/km	92.7 °C/km
171	61.4 °C/km	75.2 °C/km	96.9 °C/km

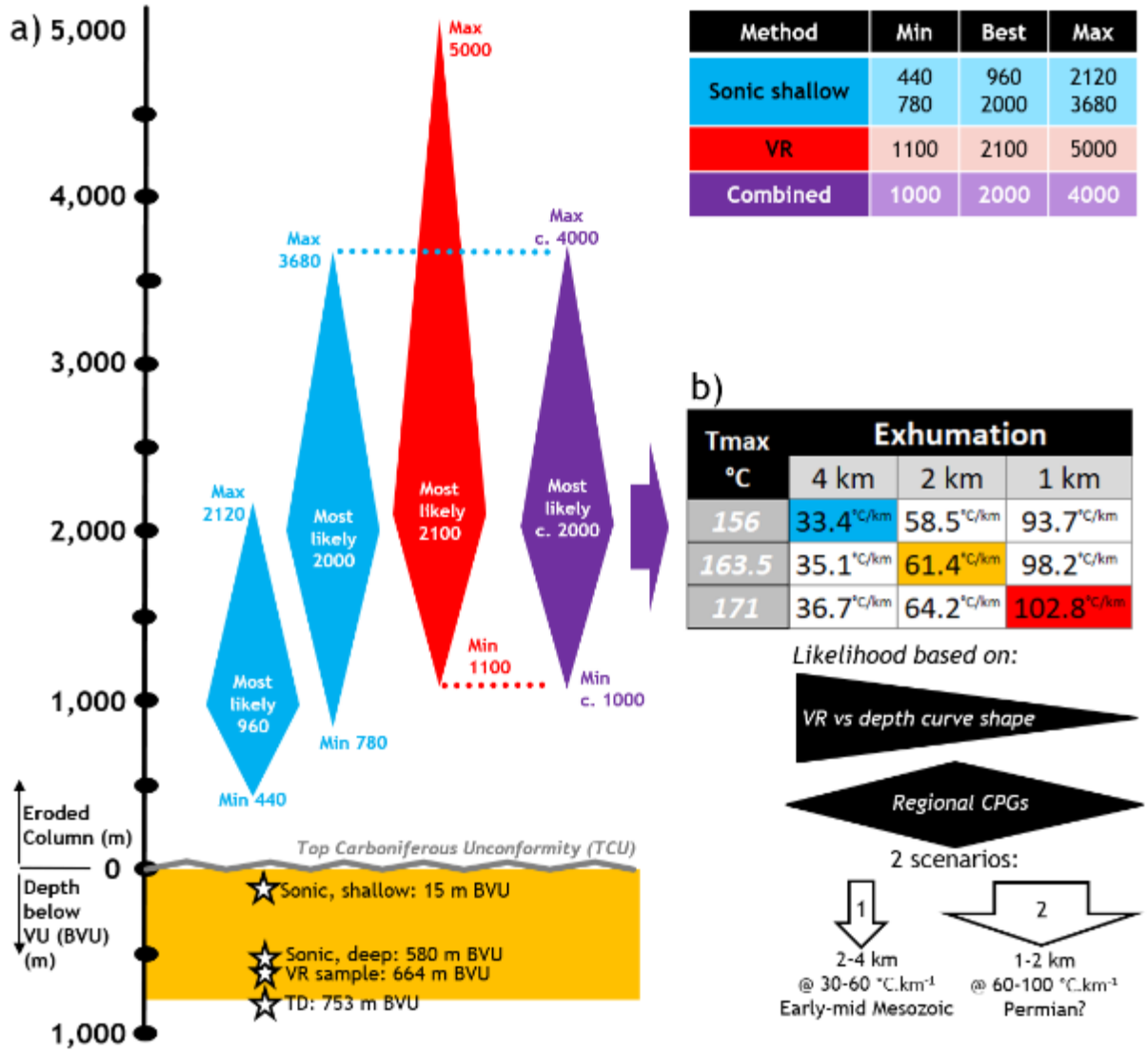

Figure 50: a) Summary of exhumation estimates at the TCU from sonic velocities and VR data (34/05-1). b) Paleogeothermal gradients required to reach the maximum temperature at 1400 m MD.

1.3.2 26/26-1

The same methodology used for borehole 34/05-1 (SECTION 1.3.1) is also used here for 26/26-1.

Sonic velocity-derived exhumation estimates

For this borehole, shallow (c. 800 mMD) and deep (c. 1070 mMD) non-sandy intervals within the Carboniferous were selected for sonic velocity analysis. For each interval, a minimum, mid and maximum sonic velocity value was selected based on the general trend of the sonic log for the Carboniferous interval (FIGURE 51A).

The shallow sonic data at 800 mMD yield a minimum estimate of c. 300 m, a maximum of c. 3000 m and a mid-case of c. 1100 m of eroded sediments. The deeper sonic data at 1070 mMD yield a minimum estimate of c. 800 m, a maximum estimate of c. 4900 m and a mid-case estimate of 2600 m (FIGURE 51B). Combining the two estimates yield a minimum estimate of c. 300 m, a maximum estimate of c. 3900 m and a mid-case estimate of c. 2100 m.

VR-derived exhumation estimates

VR data

Three VR measurements are available at 644 mMD (c. 0.34%), 871 mMD (0.66%) and 1033 mMD (c. 1%) (FIGURE 52A) but only the measurement at 871 mMD is reliable as there was not enough vitrinite materials in the two other samples (Van der Veen, 1981).

Conversion from VR to Tmax

Using the VR model of Barker (1988), this reflectance of 0.66% corresponds to a Tmax of 102.6°C (FIGURE 52B). The Basin%R_o model of Nielsen et al. (2017) yields a T_{max} of c. 135°C, which can be seen as a maximum estimate (FIGURE 52C). Using 100°C and 135°C as minimum and maximum estimates, the mid-case temperature is 117.5°C (FIGURE 52C).

Exhumation estimates

The best case estimate for the paleogeothermal gradient that could have affected the sample when it reached its maximum temperature is defined as the average gradient during the Carboniferous as calculated by Corcoran and Clayton (2001), *i.e*. c. 60°C.km^{-1}. The minimum estimate is defined as the present-day geothermal gradient, *i.e.* c. 28°C.km^{-1}, while the maximum is defined as 92°C.km^{-1} to create a triangular probability distribution centred on the mid case while falling within the range of possible paleogeothermal gradients during the Carboniferous (Corcoran and Clayton, 2001).

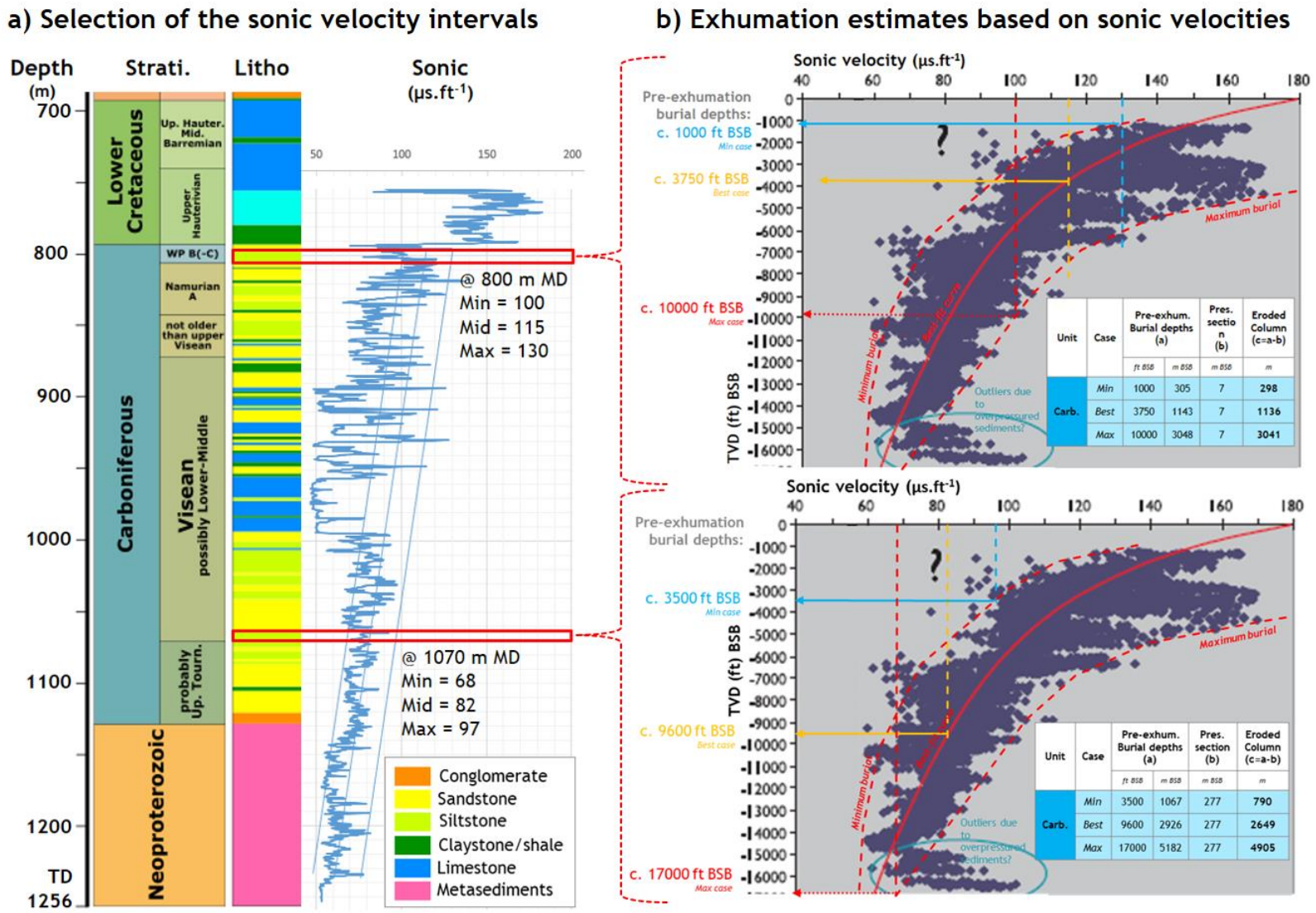

Figure 51: Sonic-derived exhumation estimates for borehole 26/26-1.

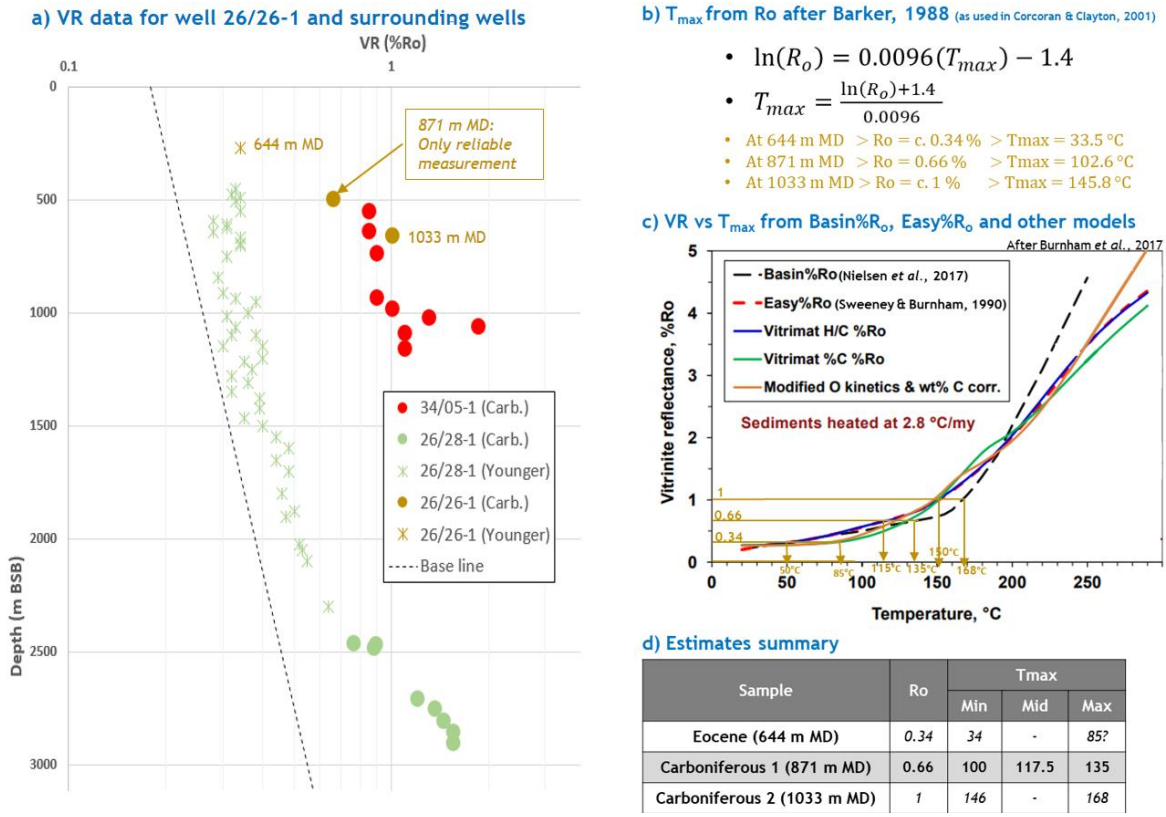

Sample	Ro	Tmax		
		Min	Mid	Max
Eocene (644 m MD)	*0.34*	*34*	-	*85?*
Carboniferous 1 (871 m MD)	0.66	100	117.5	135
Carboniferous 2 (1033 m MD)	*1*	*146*	-	*168*

Figure 52: Maximum temperatures reached by the VR samples in borehole 26/26-1.

Using this range of gradients, the maximum temperature reached by the VR sample at 871 mMD would have been obtained by the burial under a minimum of 1 km of sediments, a maximum of 4.7 km of sediments and mid case estimate of 1.9 km of sediments (TABLE 7).

Table 7: Tmax-based exhumation estimates (in km) for borehole 26/26-1.

		Geothermal gradient °C.km-1		
		28	*60*	*92*
Tmax °C	*135*	4.8	2.3	1.5
	117.5	4.2	2.0	1.3
	100	3.6	1.7	1.1
Minus preserved Carboniferous section: - 0.078 km		**4.7**	2.2	1.4
		4.1	**1.9**	1.2
		3.5	1.6	**1.0**

Discussions

Comparison of sonic- and VR-derived exhumation estimations

Broadly, when combining both sonic and VR estimates, it is likely that the absolute maximum thickness of eroded sediments would be c. 5000 m (**ERROR! REFERENCE SOURCE NOT FOUND.**A), because greater thicknesses would be hard to reconcile with the observed amount of compaction. Similarly, the minimum thickness would be c. 1000 m (**ERROR! REFERENCE SOURCE NOT FOUND.**A), since a lower thickness would require a very high geothermal gradient above 135°C.km-1. The best-case estimate is

ranging around 2000-2500 m, which is in between the best-case estimates of the VR (1900 m) and one of the sonic estimates (2649 m) (**ERROR! REFERENCE SOURCE NOT FOUND.**A). These estimates corresponds to paleogeothermal gradients of respectively c. 135°C.km-1 (minimum thickness), 20°C.km-1 (maximum thickness) and 52°C.km-1 (best case) (**ERROR! REFERENCE SOURCE NOT FOUND.**B).

In conclusion, based on the VR-sonic data, the pre-Cretaceous exhumation associated with the TCU is estimated to be c. 2000 ± $^{3000}_{1000}$ m with associated paleogeothermal gradients of c. 60 ± $^{75}_{40}$°C.km^{-1}.

Timing and regional significance

Two end-member scenarios are envisaged that could explain the data: 1) Peak temperatures were reached during the Late Carboniferous-Permian, associated with high geothermal gradients and lower denudation (1-2 km), or; 2) Peak temperatures reached during the Early Mesozoic rifting, associated with low to medium geothermal gradients and higher amount of pre-rift burial and syn-rift denudation (2-5 km).

1.3.3 26/30-1

1.3.3.1 Sonic velocity and VR-based exhumation estimates

Sonic velocity (compaction)

A detailed sonic velocity-based exhumation study based on newly constructed reference compaction curves for offshore West of Ireland and suitable for the sediments in borehole 26/30-1 is not part of the scope of this study. However, a rough estimate of the thickness of sediments required to produce the observed sonic velocities can be obtained by using the reference compaction curve of Corcoran and Mecklenburgh (2005). The reference compaction curve was constructed by calculating a best-fit curve through sonic velocity values from Jurassic, Cretaceous and Cenozoic shales from the Porcupine, and Rockall basins plotted *versus* depth below seabed (BSB) (FIGURE 54A). Although there are no Carboniferous sediments in the dataset, the Mesozoic sediments could correspond to most of the eroded material and the basins used for the reference dataset are the ideal basins to use for borehole 26/30-1 (*i.e.* they are the closest basins deep enough to derive meaningful compaction data).

Five claystones were selected for pre-exhumation burial estimates: 1) 2350 ft (Kimmeridgian), 2) 3100 ft MD (Early Kimmeridgian-Oxfordian), 4100 ft MD (Early Oxfordian-Callovian), 4956 ft MD (Westphalian C) and 5310 ft MD (Westphalian C) (FIGURE 53).

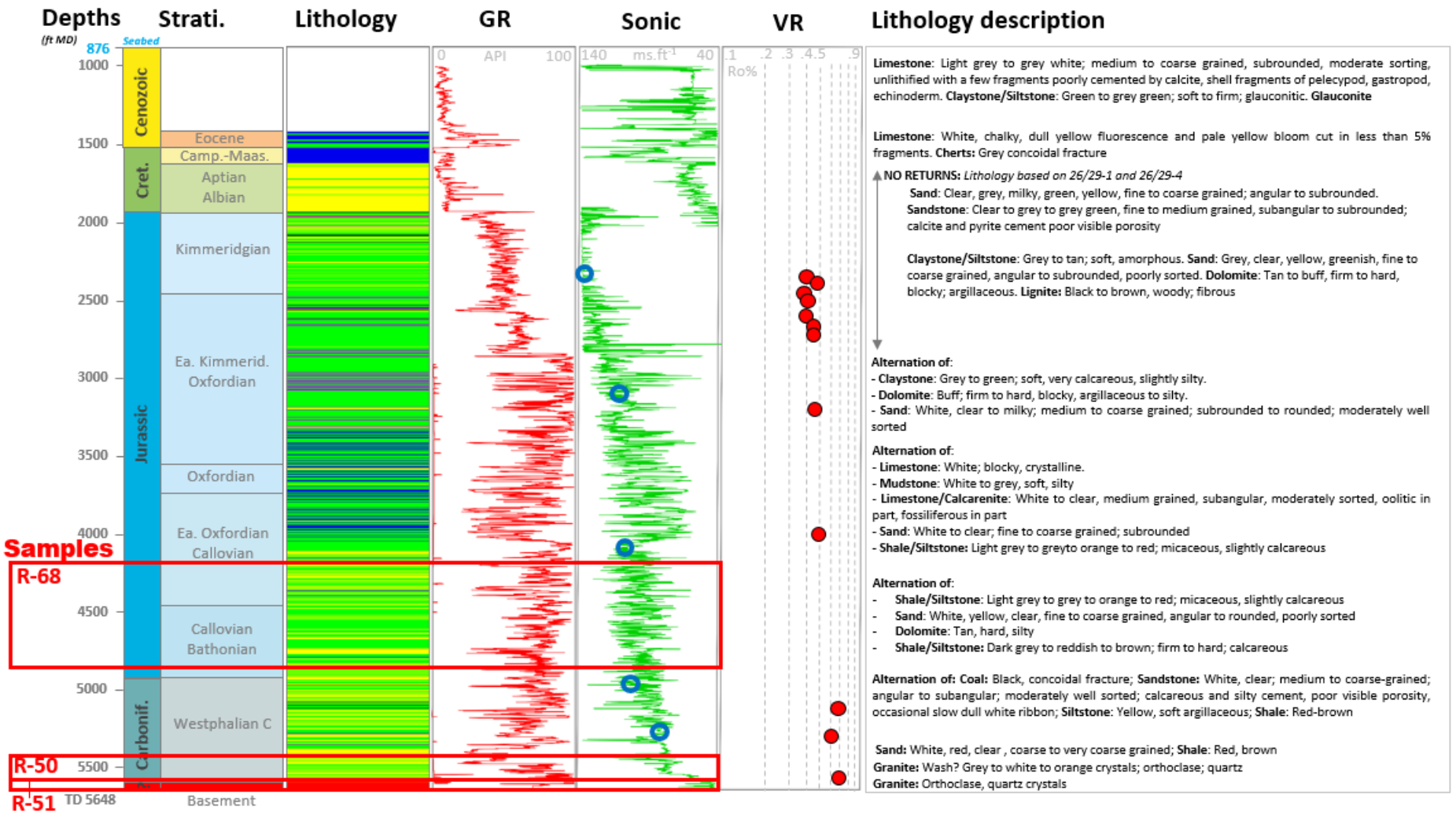

Figure 53: Well 26/30 1 stratigraphy, lithology, logs and sample depths.

a)

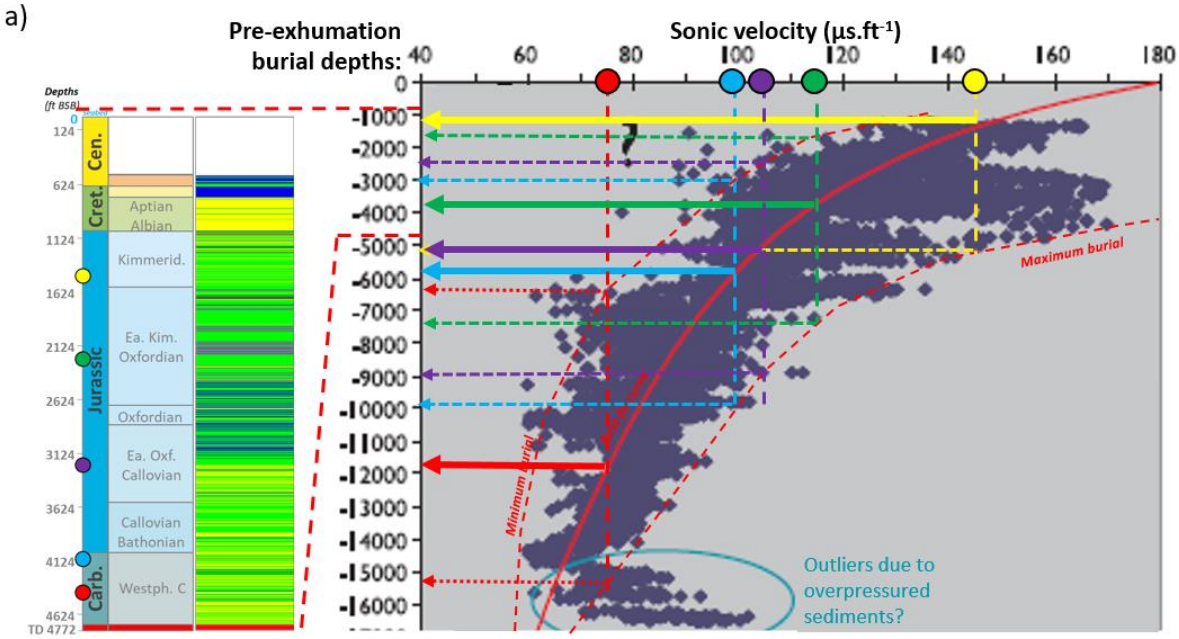

b)

	Claystone depth	Seabed depth	Depth BSB	Sonic	Pre-exhumation depths Min *ft*	Best *ft*	Max *ft*	Min minus present-day	Max possible erosion *ft*	*m*
●	2350	876	1474	145	1200	1300	5200	274	3726	1136
●	3100	876	2224	115	1600	3800	7400	624	5176	1578
●	4100	876	3224	105	2500	5100	9000	724	5776	1761
●	4956	876	4080	99.63	3000	5900	10000	1080	5920	1804
●	5310	876	4434	74.83	6300	11800	15200	-1866	10766	3281

Figure 54: Exhumation estimates from sonic velocities.

Using the reference compaction curve, it can be seen that the present-day burial (depth BSB) of the first four claystones falls within the range of pre-exhumation burial estimates (FIGURE 54). This indicates that no exhumation is required to explain the observed velocities. The deepest claystone, however, does require an additional 500 m (at the minimum) of burial in comparison to the present-day burial (FIGURE 54). This could be explained by either the presence of an unconformity within the Carboniferous (Westphalian C) unit or else the presence of sediments with a different compaction behaviour.

The maximum pre-exhumation depth can be used to calculate the maximum thickness of sediments that could have been above each claystone unit (since a higher thickness would yield unrealistic sonic velocities). For the first four claystones, the maximum sediment thickness corresponds to an additional c. 1-2 km of sediments on top of the existing sediments.

In conclusion, the lack of significant shifts in sonic velocities in the borehole does not allow the identification of unconformities associated with significant erosion. Moreover, the velocities are compatible with the present-day burial suggesting that the samples might be at their maximum burial depths which would erase any previous difference in compaction.

Vitrinite reflectance (temperature)

Introduction

Vitrinite reflectance data can be converted to maximum temperatures, paleogeothermal gradients and exhumation estimates, albeit with large uncertainties (Corcoran and Doré, 2005).

The presence in Ireland of Carboniferous samples that have experienced maximum temperatures in excess of 350°C (e.g. Westphalian rocks in the Munster Basin, Blackmore (1995)) or reverse gradients (e.g. Slievecallan Borehole, Goodhue and Clayton (1999)) have shown that some of the Carboniferous maturity data cannot be satisfactorily explained with burial alone and that other mechanisms such as advective heating, possibly related to Variscan intrusions, could be dominant in some areas (Graham, 2009). In such cases, these anomalous VR datasets cannot be used to derive exhumation estimates.

However for borehole 26/30-1, the normal increase of VR with depth from c. 0.4 to 0.67 R_o% (Figure 55a) and the associated maximum temperatures (<110°C, FIGURE 55B) do not support the presence of anomalous adjective heating or anomalous VR gradients at this location. Consequently, the VR dataset is judged suitable for exhumation estimates.

26/30-1 VR dataset

The geochemical report (Doran et al., 1982) presents a series of vitrinite reflectance (VR) measurements with values increasing from 0.4 R_o% at 2342 ft MD to 0.67 R_o% at 5590-5620 ft MD (FIGURE 53 AND FIGURE 55A).

VR to Tmax

The maximum temperature experienced by each sample can be calculated using the VR model of Barker (1988). The results are presented in Figure 55b and show that the present-day temperatures are too low to have produced the VR values of the Jurassic and Carboniferous samples, suggesting that either these samples were buried deeper, or else were subjected to a higher paleo-geothermal gradient.

Exhumation estimates

Using the present-day estimated geothermal gradient (33°C.km^{-1}), the Tmax would be reached with an additional 1 km of burial (best estimate for the average of all VR-derived temperatures). Using a paleo-geothermal gradient twice greater (which could have occurred during the main phase of rifting

and associated magmatism during the Late Jurassic-Early Cretaceous), the Tmax would be reached with only 200 m of additional sediment burial.

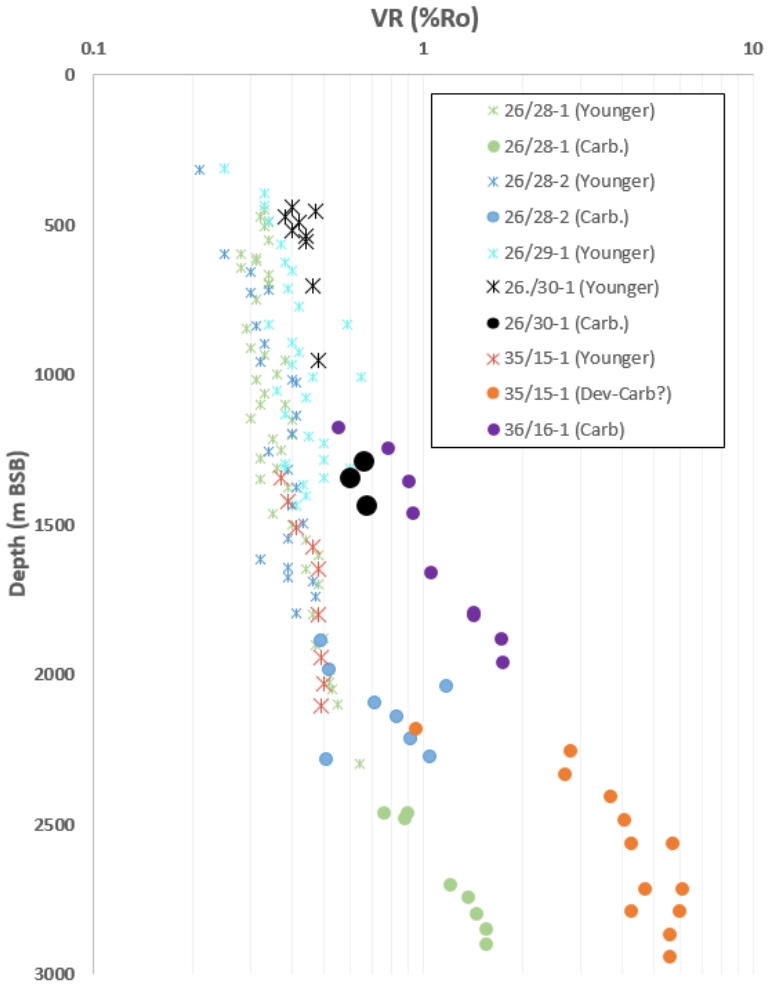

Figure 55: VR data from 26/30-1 and surrounding wells.

The Tmax values of the Jurassic and Carboniferous samples imply that they were buried to deeper depths than presently. One of the VR samples can be used to estimate exhumation estimates at various unconformities. The deepest Jurassic VR sample is at a depth of 4015 ft MD or 3819 ft BSB (below sea bed). The Base Cretaceous Unconformity is at a depth of 1930 ft, so there are 635 m of Jurassic sediments above this sample. The calculated Tmax of this sample is 69°C. With a paleo-surface temperature of 10°C and a paleogeothermal gradient of 33°C, the sample would have reached this Tmax if buried under 1.8 km of sediments, which would require the erosion of c. 1.1 km of sediments above the preserved Jurassic succession.

The paleogeothermal gradient might have been higher at the time of erosion. A maximum of 50°C.km^{-1} is estimated by Szymanski et al. (2016) for the modern rift of the Red Sea, which can be sued an estimate for the paleogeothermal gradient during main phase of rifting of the Porcupine Basin. With a paleogeothermal gradient of 50°C, only 550 m of eroded sediments would be required. The same

calculations can be done if the eroded sediments are associated with the Base Eocene Unconformity instead (at 1523 ft). The required amounts of erosion would then be c. 1km and 420 m respectively.

Discussion

The Tmax values of the Jurassic and Carboniferous samples imply that they were buried to deeper depths than presently. The eroded sediments would probably be associated with either the Base Aptian Unconformity or the Base Eocene Unconformity. The thickness of eroded sediments is estimated to c. 200 m to 1 km depending on the paleogeothermal gradient prior to exhumation.

Discussion and conclusion

Exhumation estimates

The VR data indicate that the Jurassic and Carboniferous sediments were in the past buried deeper than their present-day burial depths. The eroded sediments would most probably associated with the main unconformities in the borehole, *i.e.* the Base Aptian Unconformity (BAU) and/or the Base Eocene Unconformity (BEU). Eroded sediments associated with the BAU would be Kimmeridgian to Aptian in age, while eroded sediments associated with the BEU would be Maastrichtian to Eocene in age. 200 m to 1000 m of these sediments is estimated to have been eroded during the Early Cretaceous and/or during the Paleocene-Eocene. These estimates fall within the range of maximum thickness of eroded sediments derived from the sonic velocity data (1-2 km).

The exhumation associated with the Jurassic-Carboniferous Unconformity cannot be quantified due to the overprinting associated with post-Jurassic burial.

AFT annealing

Based on the VR data (and supporting sonic velocity data), it can be deduced that the AFT ages from the Jurassic and Carboniferous sediments have not been fully reset since deposition. However, apatites from samples deeper than c. 3000 ft (*i.e.* with Tmax greater than c. 60°C) probably resided in the PAZ for some time and experienced some amount of annealing.

1.4 Age of the igneous rocks in borehole 35/15-1

1.4.1 Cuttings and logs interpretation

The cuttings show that most of the mafic units are fine grained and described as basalt by the operator exploration geologist. However part of a unit at c. 7250-7350 ft is fine to medium-grained and described as a micro-gabbro. Based on the grain size (texture), the basalt units could either be lava flows or shallow intrusions while the micro-gabbro is most likely a shallow intrusion (FIGURE 56).

The top igneous unit between 6421 and 6469 ft is “rusty brown stained” and is “cemented by yellow to olive yellow and rusty red, limonitic matrix” (Gerneck et al., 1980), indicating that the basalt has probably been exposed to subaerial weathering. The second main unit between 6500 and 6650 ft does not have any description of its cuttings. The third one, between 6760 and 6928 ft, does not contain any sign of weathering. Based on this weathering pattern, the first unit is most likely a lava flow rather than a shallow intrusion. On the other hand, the third unit is more likely a shallow intrusion than a lava flow.

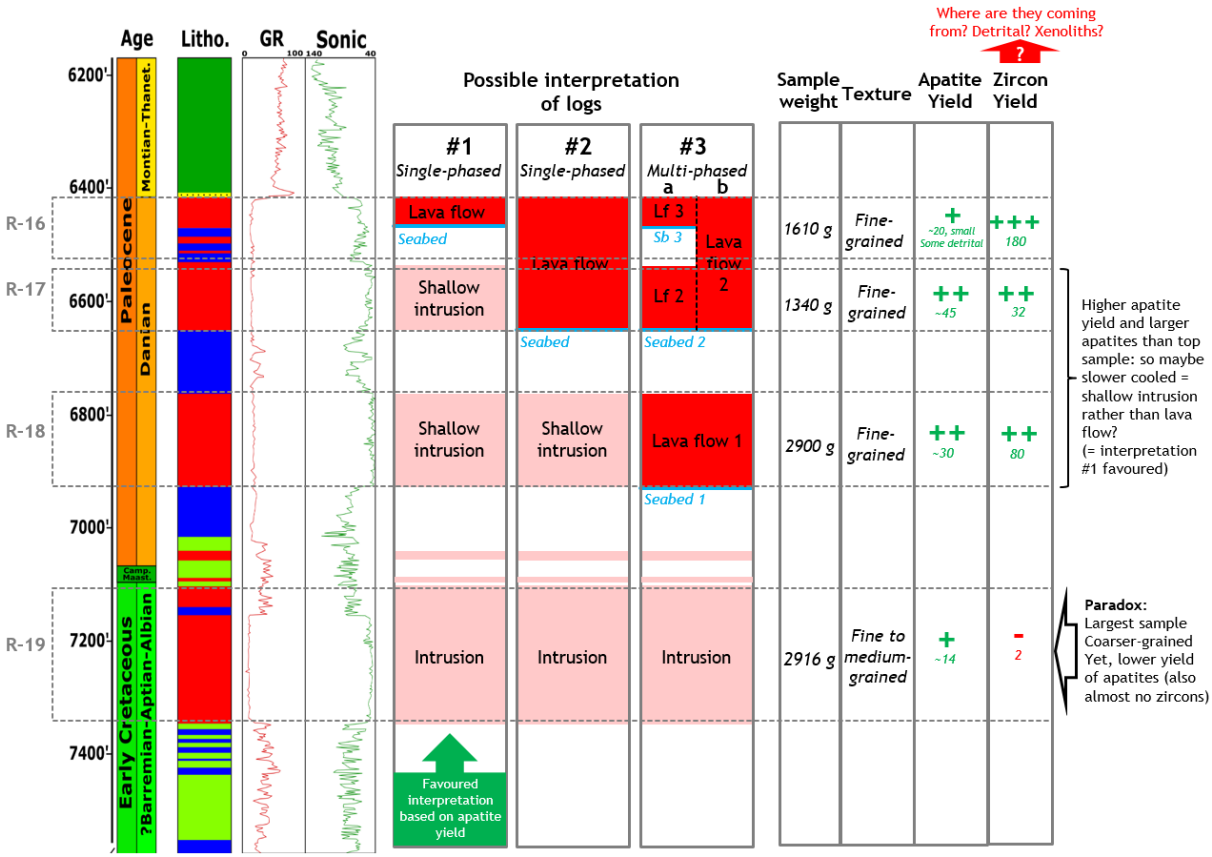

Figure 56: Various interpretations of the igneous units from log responses and sample weight and apatite/zircon yields. Based on the apatite yield, interpretation #1 is favoured, where only the top unit is a lava flow and the underlying units are shallow intrusions. The seabed at the time of emplacement would be located at 6470 feet MD.

Also the first and second unit, separated by some interbeds of limestones and basalts according to the composite log (Gerneck et al., 1980), could actually be one single lava flow. In that case, the carbonate cuttings could come from above as cavings or be xenoliths / sedimentary septa in the basalt (FIGURE 56).

Based on the log responses and the cuttings, it is difficult to come to a more definitive conclusion about the mode of emplacement of these igneous units *(i.e.* extrusives *vs* shallow intrusives).

1.4.2 Age of the mafic rocks

1.4.2.1 Stratigraphic relationships

Assuming that the topmost basalt is a lava flow and the underlying ones are shallow intrusions, the composite log indicates that this lava flow was emplaced at the top of a pile of Danian sediments (61.6-66 Ma) and was overlain by Montian-Thanetian sediments (FIGURE 56). However, the biostratigraphic report diverges from the composite log and reports a "Middle Paleocene – Thanetian" *[sic]* age for this top basalt (Church et al., 1981). The biostratigraphy consultants were also the ones who undertook the K-Ar study described below. It is possible that their attribution of the topmost basalt to the Thanetian might have been influenced by their results.

In the former case (lava emplaced on top of Danian sediments and overlain by Montian-Thanetian sediments), the Montian is equivalent to the upper Danian (De Geyter et al., 2006) so the lava flow would be upper Danian in age, *i.e.* 61.6 Ma or a few millions of years older. In the latter case (Middle Paleocene – Thanetian), the lava flow would probably be early Thanetian in age, *i.e.* 59.2 Ma or a few millions years younger.

A conservative estimate of the age of the lava flow is therefore Paleocene in age (56-66 Ma). This defines the absolute minimum and maximum ages. The most likely age is basal Thanetian to upper Danian (c. 59-62 Ma).

1.4.2.2 K-Ar dating

The well operator commissioned a K-Ar dating study of some of the igneous samples (Church et al., 1981). They obtained a range of ages becoming older with depth, from 46 ± 2.9 Ma to 58.1 ± 1.8 Ma (FIGURE 57). They proposed that this pattern reflects a decrease in alteration (and associated argon loss) from the altered top of a lava flow to less altered lava flow core and/or deeper intrusions. In consequence, they estimated that the best age for this suite of igneous rocks was the one from their deepest sample, yielding an age of 58.1 ± 1.8 Ma (Thanetian). This dating seems to support the interpretation of the topmost basalt as being Thanetian in age rather than upper Danian. However, the deepest sample used as the best age estimate could also have experienced small amount of argon loss and therefore this age should be seen as a minimum age (*i.e.* it could be slightly older than 58.1 Ma).

Sample Number	Sample Depth	Method	K_2O (%)	Atmospheric Contamination (%)	V/M	Apparent age and error (Ma)	Trends: Age	Trends: Weathering, alteration = argon loss
1	6464-6508	K-Ar T.R. 60/120	0.135 0.135 0.135	90.8 90.3 91	2.03E-4 2.16E-4 2.34E-4	46.1 ± 2.9 48.9 ± 3.2 52.9 ± 3.6		
2	6530-6626	K-Ar T.R. 60/120	0.104 0.104 0.104	91.3 90.8 91.2	1.9E-4 1.88E-4 1.84E-4	55.7 ± 3.8 55.2 ± 3.6 54 ± 3.6		
3	6760-6927	K-Ar T.R. 60/120	0.206 0.206 0.206	81.6 80.5 82.2	3.95E-4 3.98E-4 3.87E-4	58.5 ± 1.8 58.9 ± 1.8 57.3 ± 1.9		
4	7155-7347'	K-Ar T.R. 60/120	0.108 0.108 0.108	75.1 71.8 72.2	2.02E-4 2.03E-4 2.06E-4	57 ± 1.8 57.3 ± 1.8 58.1 ± 1.8		
V/M = Volume of radiogenic argon-40(mm)³ NTP per weight of sample (g). *K-Ar ages are calculated using the IUGS recommended constants (Steiger & Jäger, 1977)*						Best estimate according to analysts		

Figure 57: K-Ar results from mafic igneous samples modified after Church et al. (1981).

Nature and age of the igneous rocks

The igneous rocks in the Danian, Upper and Lower Cretaceous sediments are picritic basalts with abundant calcic plagioclases (An_{55-84}) and magnesian olivines (Fo_{75-87}) (Henderson, 1980). The chemistry of the basalts shows that the parent magmas were ultramafic and probably originated from the astenospheric upper mantle. The basalt textures and mineral alterations show that the mafic magma was emplaced near, or on, the seafloor and cooled very quickly. The geochemistry of the magma shows that it is a small part of a much larger igneous activity in the region (the North Atlantic Igneous Province) and is very similar to some picritic rocks found in the igneous centres of the British – Irish Paleogene Igneous Province (BPIP) (Henderson, 1980).

If the biostratigraphic interpretation (as presented in the composite log) is correct, then the lava flow is upper Danian in age and therefore the K-Ar age is underestimating the true age, probably due to argon loss. On the other hand, if the K-Ar age is correct, then the lava flow must have been emplaced within Thanetian sediments, which is supported by the biostratigraphy report (which was accompanied by the K-Ar data) (see detailed discussion in ANNEX 1 SECTION 4.1).

Without additional information, the former interpretation is the most likely since it relies on the composite log stratigraphy and has a plausible explanation for the younger K-Ar age (argon loss as shown by age trend in all the samples). The latter interpretation is also plausible but more dating (ideally by the $^{40}Ar/^{39}Ar$ method) would be needed to better characterize the age of this mafic volcanism phase. Based on the similarities in petrography, mineralogy and geochemistry and K-Ar ages, the different basaltic units are probably coeval and cogenetic (*i.e.* emplaced at the same time from the same magma). However, a multi-phased magmatism within a short period of times of a few

millions of years cannot be totally excluded. A longer period is very unlikely since a change in mineralogy and chemistry as well as a wider K-Ar age range would be expected.

Both the stratigraphic relationships and K-Ar dating confirm that the igneous activity in borehole 35/15-1 is Paleocene in age and is part of the early phase (pre-break-up) of magmatism of the North-East Atlantic Igneous Province (Wilkinson et al., 2017). The magma was derived from the mantle (linked to the proto-Icelandic plume) and was emplaced in the Paleocene as a very hot and fluid magma on top of the paleo-seafloor (lava flow) as well as thin intrusions just underneath the seabed. The magma was probably emplaced as a single event or within a very short period of time and cooled very quickly, except for some slower-cooled flow cores and/or shallow intrusions.

1.5 34/05-1 - Igneous intrusion(s)

According to the composite log, no igneous intrusion has been encountered in the borehole (Croisile, 1980). However, several thermal anomalies reported in the geochemical report are attributed by the authors to the presence of igneous intrusions in the vicinity of the borehole (Cailleaux and Robert, 1981) and are listed below.

1.5.1 Geochemical and optical anomalies

1.5.1.1 Thermal Alteration Index

The thermal alteration index (TAI) increases slightly from 2.5 at the top of the well to almost 3 at c. 1300 mMD but then records a sharp increase to 4+ at 1340.5 mMD and then 4.5 at 1366 m. The TAI then records lower values of 3+ and 3 at 1381 and 1398.9 mMD separated by a higher value of 4.5 at 1390.5 mMD (FIGURE 58). The authors of the geochemical report suggest that the fluctuations might be caused by the proximity of a volcanic intrusion not penetrated by the borehole (Cailleaux and Robert, 1981).

1.5.1.2 Pyrolysis maximum temperature

Similarly, below 1330.2 mMD, the maximum temperature derived from pyrolysis determinations (T_m) suddenly increases from values between 440 and 455°C to values between 465 and 470°C (FIGURE 58), which the authors also attribute to the proximity of a volcanic intrusion (Cailleaux and Robert, 1981). However, they attribute the high T_m values below 1445 mMD to caving from somewhere between 1330 and 1400 mMD (Cailleaux and Robert, 1981), probably because of the presence of a VR sample at 1400 mMD that appears not affected by intrusion-derived heating (FIGURE 58).

1.5.1.3 Vitrinite reflectance

Modal values of vitrinite reflectance (VR) for the Carboniferous section remains between 0.7 and 1.1 R_o% between 779 and 1472 mMD, except for a deviation at 1330.2 mMD and 1372.5 mMD with modal values of respectively 1.3 and 1.85 R_o% (FIGURE 58).

Single measurements of VR at 1350 and 1366 mMD yield recorded values of respectively 4 and 4.75 R_o%. Anomalous VR values are also found in the deepest VR sample at 1471 mMD where they range from 0.7 to 5.7 R_o% with c. 26 measurements above 2 R_o% (FIGURE 58).

The authors of the geochemical report believe that the samples with anomalous modal VR values of 1.3 and 1.85 R_o% are *in-situ* and results from the thermal effect of an igneous intrusion in the vicinity of the well. However, they interpret the high VR measurements in the bottom sample at 1471 mMD as due to caving from the interval c. 1320-1380 mMD (Cailleaux and Robert, 1981). They do not explain their reasoning but this interpretation is probably based on the presence of low VR values in this sample (c. 1-1.1 R_o%) and also the presence of a VR sample from the core (therefore *in-situ*) at 1397-1400.75 mMD with a uniform and narrow population of VR measurements averaging 1.1 R_o% (FIGURE 58).

1.5.1.4 Coke texture

The geochemical report also notes the presence of a population of "strongly anisotropic natural cokes" at 1372.5 mMD (FIGURE 58), which can only be produced with very high temperatures such as the presence of an igneous intrusion in the vicinity (Cailleaux and Robert, 1981).

1.5.1.5 Conclusions

Based on these observations the authors conclude that the interval between 1320 and 1400 mMD was thermally affected by an igneous intrusion located nearby but not encountered in the borehole

1.5.2 New interpretation of the logs and geological data

For the interval 1320-1400 mMD, the composite log shows an alternation of siltstones, claystones, coals and a sandstone between 1346 and 1364 m. However, this sand is actually most likely a doleritic intrusion as shown by a series of observations described below.

1.5.2.1 GR and sonic velocity

The unit between 1346 and 1364 mMD has a low and blocky gamma ray (GR) and a high sonic velocity response (FIGURE 59A), which is consistent with a clean sandstone but is also typical of a dolerite intrusion (Smallwood and Maresh, 2002).

a)

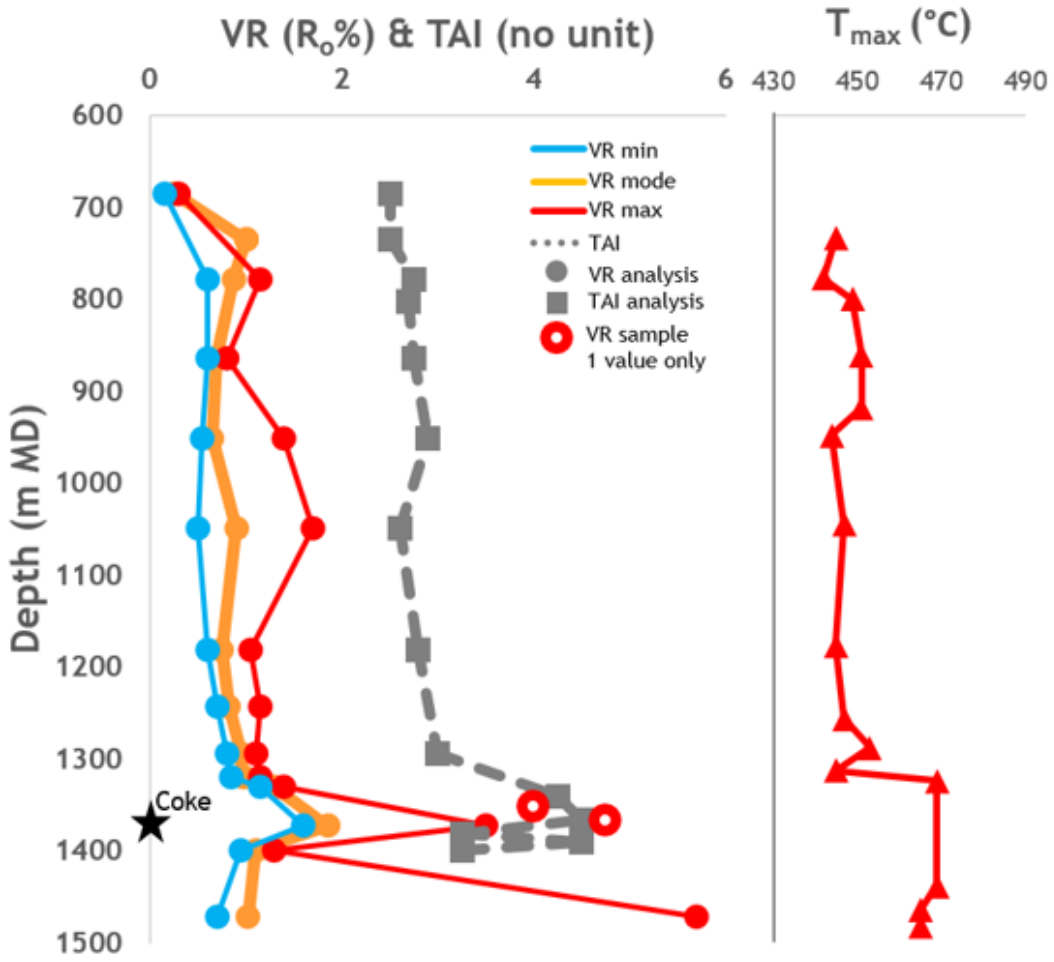

b)

Sample		VR (R$_o$%)					TAI	Tm (°C)	T$_{max}$ (°C) *Barker, 1988*
Type	Depth	Range	Min	Avg mode	Max	VR remarks			
Cuttings	685	0.15-0.3	0.15	0.25	0.3	Mud products?	2.5		1.4
SWC	735	1	1	1	1	1 value only	2.5	445	145.8
SWC	779	0.6-1.15	0.6	0.875	1.15	N/A	2.75	442	131.9
SWC	801.7	N/A	N/A	N/A	N/A	N/A	c.2.7	449	N/A
SWC	864	0.6-0.8	0.6	0.7	0.8	V & Fluorescent	2.75	451	108.7
SWC	920.5	N/A	N/A	N/A	N/A	N/A	N/A	451	N/A
SWC	951	0.55-1.4	0.55	0.65	1.4	0.8-0.9 eq.	2.9	444	101.0
SWC	1048.6	0.5-1.7	0.5	0.9	1.7		2.6	447	134.9
SWC	1066	N/A	N/A	N/A	N/A	N/A	N/A	No reading, S2 too low	N/A
SWC	1181.4	0.6-1.05	0.6	0.75	1.05	V or B (Fluorescent)	2.8	445	115.9
SWC	1242.7	0.7-1.15	0.7	0.825	1.15	N/A	N/A	N/A	125.8
SWC	1261.8	N/A	N/A	N/A	N/A	N/A	N/A	447	N/A
SWC	1294	0.8-1.1	0.8	0.95	1.1	N/A	3	453	140.5
SWC	1318.9	0.85-1.15	0.85	0.975	1.15	N/A	N/A	445	143.2
SWC	1330.2	1.15-1.4	1.15	1.3	1.4	N/A	N/A	469	173.2
SWC	1340.5	N/A	N/A	N/A	N/A	N/A	4+	N/A	N/A
Cuttings?	1350	4	4	N/A	4	1 value only	N/A	N/A	N/A
SWC	1366	4.75	4.75	N/A	4.75	1 value only	4.5	No reading, S2 too low	N/A
SWC	1372.5	1.6-1.95 (3.5)	1.6	1.85	3.5	N/A	N/A	N/A	209.9
SWC	1381	N/A	N/A	N/A	N/A	N/A	3+	N/A	N/A
SWC	1390.5	N/A	N/A	N/A	N/A	N/A	4.5	No reading, S2 too low	N/A
Core	1398.875	0.95-1.3	0.95	1.1	1.3	N/A	3-3+	N/A	155.8
Cuttings?	1445	N/A	N/A	N/A	N/A	N/A	N/A	469	N/A
Cuttings	1472	0.7-5.7	0.7	1.025	5.7	N/A	N/A	465	148.4
Cuttings?	1489	N/A	N/A	N/A	N/A	N/A	N/A	465	N/A

Figure 58: Thermal maturity of organic matter in well 34/05-1 from geochemical and optical studies. a) Plots of vitrinite reflectance (VR), thermal alteration index (TAI) and pyrolysis maximum temperature (T_{max}) vs depths. For each VR sample,

the minimum, mode and maximum values are plotted. Note the anomaly in VR, TAI and T_{max} data between 1320 and 1400 mMD. b) Raw thermal maturity data from the geochemical report (Cailleaux and Robert, 1981).

a) Log responses between 1332-1380 m MD

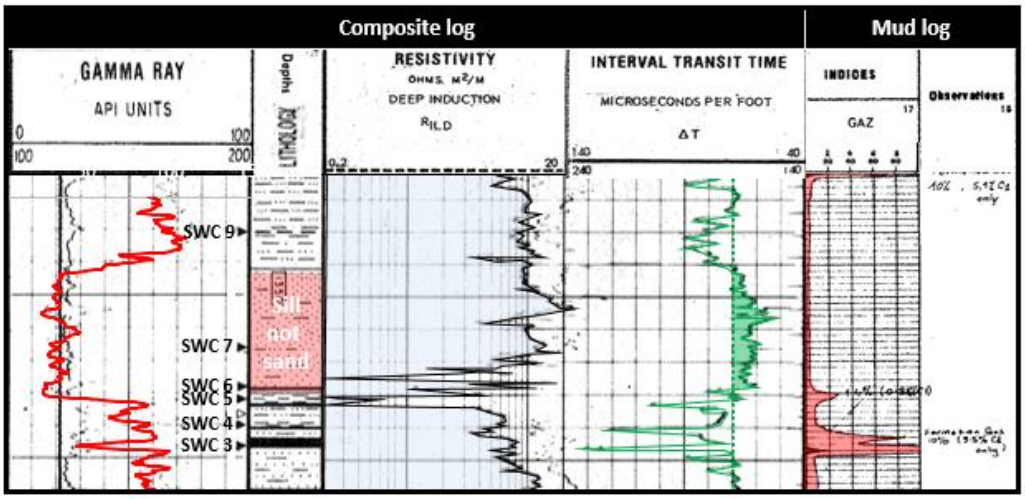

b) Contact aureola and CLRsZ for sills intruded in organic-rich units (Spacapan et al., 2019)

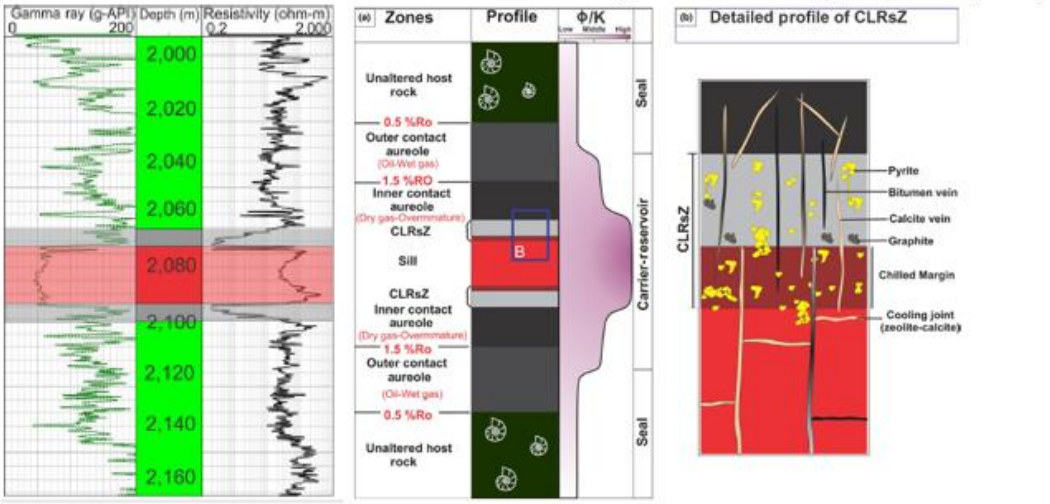

c) Lithology description of sidewall cores and cuttings fr interval 1330-1380 m MD

Lithology from sidewall cores (SWCs)

SWC	Depth	Rec.	Description
9	1340.5	50%	CLAYSTONE: Medium grey, firm, locally slightly silty, slightly dolomitic along partings
7	1358.8	30%	SILTSTONE: Medium grey-green, grey, mottled, argillaceous, very calcareous, micaceous, tight
6	1364.7	50%	SANDSTONE: Grey green, very silty, very fine, subangular, poorly sorted, well cemented with calcite veins and biotite
5	1366	100%	CLAYSTONE: Dark grey, with silty laminae, slightly dolomitic along partings
8	1368.5	0%	EMPTY BULLET
4	1370	70%	CLAYSTONE: Dark grey, firm, becoming fissile, slightly silty, micromica. with finely dispersed carbonaceous material, slightly dolomitic
3	1372.5	50%	COAL: Black, soft, with plant remains, bleeding gas

Lithology from cuttings (mud log)

Depth	Description
c. 1330	SILTSONE: Light, grey, mottled, locally carbonaceous, becoming dark grey, carbonaceous with traces of pyrite
c. 1350	SANDSTONE: White, fine, sub-rounded well sorted, with good siliceous cement, no visible porosity
c. 1365	CLAYSTONE: Light & dark grey, grey green, occasionally red brown, becoming soft, less indurated

Figure 59: Identification of a doleritic intrusion between 1346 and 1365 mMD in borehole 34/05-1. a) Log responses and location of sidewall cores (SWC). b) Lithology description of sidewall cores and cuttings. c) Model of contact aureoles and CLRsZ from Spacapan et al. (2020).

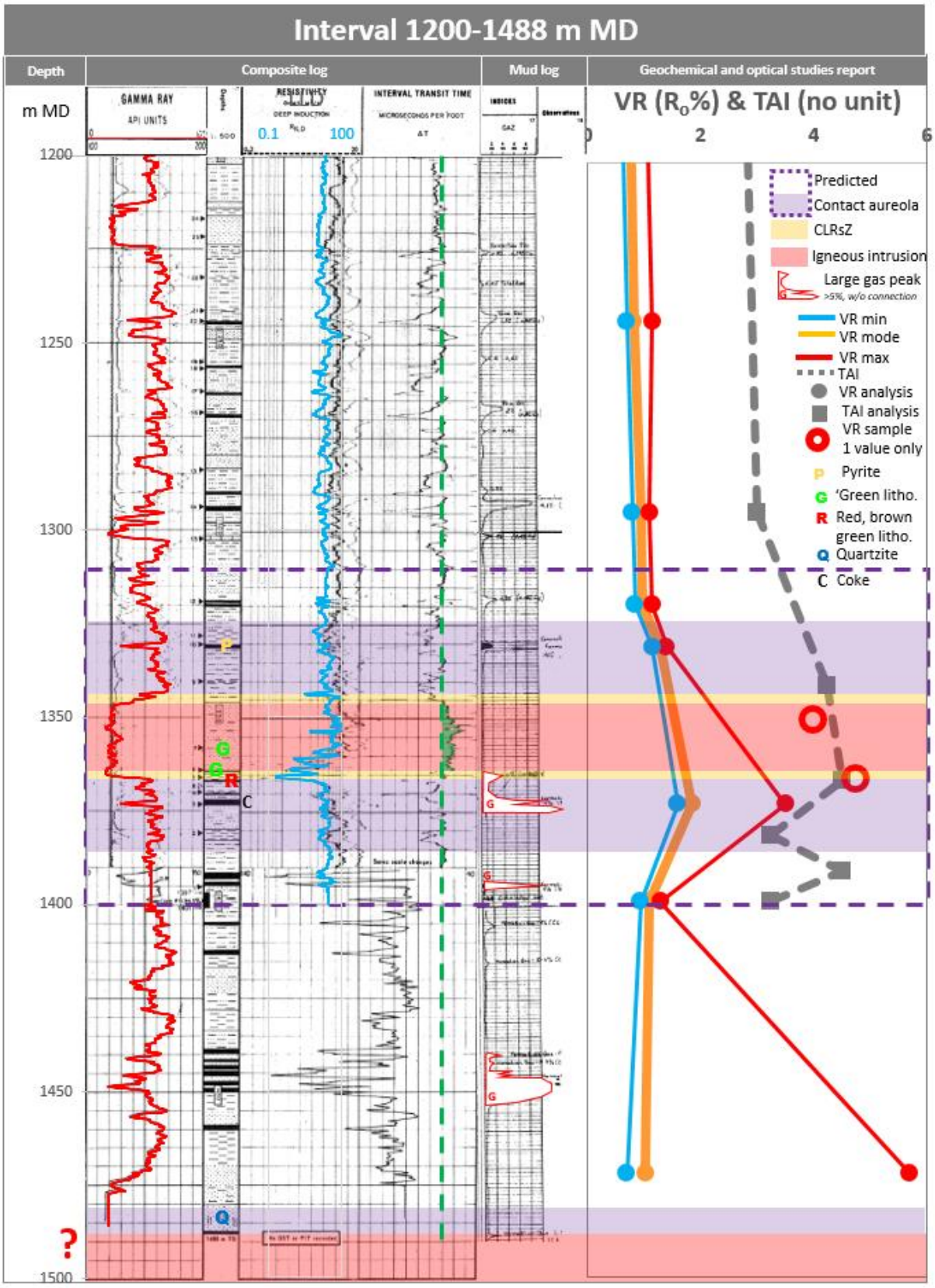

Figure 60: 34/05-1 location of doleritic intrusions between 1200 and 1488 mMD (TD).

1.5.2.2 Low resistivity anomaly

A significant anomaly is the presence of very low resistivity spikes in the resistivity logs between 1361 and 1367 mMD (Figure 59a). No such spikes are present in the remainder of the Carboniferous section (FIGURE 60).

Low resistivity anomalies are sometimes associated with igneous intrusions (Spacapan et al., 2020). The low signal is caused by massive-sulphide deposits (mainly pyrite) that precipitate in the chilled margin of the sills and the host rock, creating in the borehole a zone of spiky low resistivities at the upper and lower boundary of the intrusion (FIGURE 59B), called Contact Low Resistivity Zones (CLRsZ) (Spacapan et al., 2020). Graphite, created by the heating of organic materials, is also a low resistivity material that contributes to the low signal created by the sulphides (Spacapan et al., 2020).

Therefore the low resistivity spikes at the bottom of the low GR unit could actually be the lower CLRsZ of the igneous intrusion. The upper CLRsZ would be marked by only one small low resistivity peak in this case (FIGURE 59A).

1.5.2.3 Formation gas peak

The mud log also records a formation hydrocarbon gas peak of up to 10% between 1365 and 1375 mMD, which is not associated with a drilling pipe connection, which often generates gas peaks due to the idle time spent at a particular depth. No such high values occurs in the Carboniferous section above (only smaller 1-3% peaks due to coal layers) (FIGURE 60). However, two peaks at 7% and 10% occur below at respectively 1395 and 1445-1453 mMD. These peaks are associated with numerous coal layers. While a few coal layers are present at c. 1370 mMD, and certainly contributed to it, the peak seems too high to have been produced *in situ* solely by the coals (when compared with the smaller peak but thicker coal layers at c. 1392 mMD).

Igneous intrusions are known to be sometimes associated with formation gas peaks in the mud log, due to migration of gas generated both at deeper depths and by the heating of the host rock by the igneous intrusion. The gas is stored in open fractures in the igneous rocks (cooling joints) and in the host rock (hydraulic fractures due to fluid escape from the cooling magma) (Rateau et al., 2013).

Therefore the hydrocarbon gas peak at c. 1370 mMD could partly be due to gas coming from fractures present in the lower CLRsZ of the igneous intrusion.

1.5.2.4 Sidewall core and cuttings lithology description

There are two sidewall cores (SWC) located in the low GR interval. Sidewall core #6 is described as a grey green, very silty, well cemented, very fine-grained sandstone with subangular poorly sorted grains including biotite and calcite veins. Sidewall core #7 is described as a medium grey-green,

mottled, argillaceous and very calcareous micaceous tight siltstone (Renoux and Croisile, 1981) (FIGURE 59C).

The colour of the sandstone (grey green) is unusual as all other sandstones in the Carboniferous section are described as white or light grey (except for SWC #46 at 967.5 mMD which is a light grey-green sandstone). The colour (grey green) and texture (very fine-grained) is typical of crushed dolerite. It is likely that the mud logger misinterpreted the dolerite with a green sandstone.

The mud log also notes the presence of pyrite at c. 1330 mMD and grey, green, red and brown claystones at c. 1365 mMD which becomes less indurated with depth (FIGURE 59C). There is no mention of pyrite nor variegated claystones in the remaining section of the Carboniferous (Elf, 1980).

The pyrite could be associated with the hydrothermal activity associated with the intrusion as discussed above (Spacapan et al., 2020) while the variegated claystones could be altered dolerite (Hoshi and Okubo, 2010).

1.5.2.5 Thermal indicators

The thermal anomalies discussed above are in agreement with an igneous intrusion at this depth (Figure 60). Rather than being located very close to the borehole as hypothesized by the operator, the intrusion was actually intercepted by it but misdiagnosed as a sand.

The single VR measurements of 4 and 4.75 R_o% at 1350 and 1366 mMD and the high TAI at 1340.5 and 1366 mMD come from the thin (a few meters) CLRsZ above and below the intrusion, while the samples with values of 1.3 and 1.8 R_o% at c. 1330 and 1372.5 mMD and the TAI of 3.5 at 1372.5 mMD represent zones of the thermal aureole with lower temperatures (FIGURE 60). The high TAI of 4.5 at 1390.5 m is possibly a caved sample from above. Finally both samples at 1318.9 and 1398.9 mMD show no evidence of thermal effects due to the intrusion and represent zones outside the contact aureole (FIGURE 60).

The upper boundary of the contact aureole is therefore located between c. 1319 and 1330.2 mMD (so 16 to 27 meters thick) and the lower boundary between 1372.5 and 1399 mMD (so 9 to 35 meters thick) (FIGURE 60). The average thickness of the lower and upper aureoles is 21 and 22 meters, which is 120% of the thickness of intrusion.

1.5.2.6 Age and lithology of the igneous intrusion

The presence of coke at 1372.5 mMD indicates that the intrusion was emplaced after the thermal maturation of the organic matter to relatively high levels (0.8 to 1.6 R_o% according to Creaney (1980)). Consequently, and assuming that the Carboniferous organic matter reached its highest maturity during the Carboniferous-Permian, the intrusion must be post Carboniferous-Permian and is not

associated with the Carboniferous-Permian magmatism of NW Europe (Monaghan and Parrish, 2006). Based on regional geology constraints, the intrusion is most likely Paleocene-Eocene in age (Á Horni et al., 2017) but could also be Oligocene-Miocene or Cretaceous in age (Tate and Dobson, 1988).

The grey-green colour of the lithology, together with the large amount of doleritic intrusions in other wells offshore west of Ireland point imply the intrusion is basic and likely a dolerite.

In conclusion, the low GR unit between 1346 and 1364 mMD has been misdiagnosed by the operator as a sandstone and is instead an 18 meters thick igneous intrusion associated with a c. 7 meters thick lower CLRsZ, a c. 2 meters thick upper CLRsZ and c. 20 meters thick upper and lower thermal aureoles, which is within the same order of magnitude of the thicknesses predicted by the model of Spacapan et al. (2020).

The igneous intrusion is probably a Paleogene doleritic sill associated with the North-East Atlantic Igneous Province but a younger or older (Mesozoic?) age cannot be excluded.

1.5.2.7 Other intrusions

The indicators which point to the presence of an igneous intrusion (unusual lithology description in cuttings and SWC, blocky GR and high sonic velocity) and its CLRsZ and thermal aureoles (anomalously high TAI, VR, T_{max}, very low and spiky resistivity logs, coke texture in coals, pyrite and variegated clays) have been looked for in the remaining section of the borehole (FIGURE 60).

The presence of relatively high VR measurements at 1048.6 mMD (up to 1.7 R_o%) and 951 mMD (up to 1.4 R_o%) (FIGURE 58) was thought to be an indication of another possible intrusion around these depths. As mentioned above, a light grey-green sandstone at 967.5 mMD (SWC #46) could be a candidate for a misinterpreted doleritic intrusion, which might explains some of the high VR data above and below. At this depth, there is 2.5 m thick low GR unit (967.5-970 mMD), but there is no associated low resistivity spikes, nor a high sonic velocity anomaly.

The geochemists hypothesized that the high VR values in the deepest VR sample at 1472 mMD (FIGURE 58) were due to caving and originated from the thermally-affected interval above (1320-1400 mMD). Another possibility is the presence of a thin intrusion below 1400 mMD and probably close or below the bottom of the well. A white, very fine and very hard quartzite is present at the bottom of the well (1480-1488.5 mMD, FIGURE 60). Although quartzite can be formed by contact metamorphism of texturally mature sandstones (e.g. SUMMER AND AYALON (1995)), this quartzite is believed to belong to the Dalradian basement as discussed above or else to be a pure quartz sandstone from the Westphalian B sediments.

1.5.2.8 Conclusions

A previously unrecognized igneous intrusion has been identified between 1346 and 1364 mMD with a thermal aureole of c. 20 m on either side that explains the thermal indicators anomalies reported in the geochemical report. The intrusion is characterized by a blocky and low GR response, high sonic velocities, a zone of spiky low resistivity at the bottom, a grey-green fine-grained lithology (probably dolerite) and the presence of organic matter affected by high temperatures in the vicinity of the intrusion (coke textures in coal, high VR, TAI and T_{max}). Another thin intrusion might be present at 967.5-970 mMD based on the anomalous colour of cuttings and some high VR values a few tens of meters above and below. However, the existence of this intrusion is more speculative.

1.6 34/05-1 - Age and significance of the red brick clastic unit

The red clastic unit between the Paleocene-Eocene sandstone and Carboniferous clastics is described as a non-carbonaceous, red-brick silty clay, with streaks of very fine to fine-grained white sandstone, occasionally glauconitic. It is tentatively attributed to the Albian (with a question mark) by the operator (Croisile, 1980).

The age of this unit is important because it can yield useful information about the age of its basal unconformity and consequently a better understanding of the timing of uplift and erosion events in the area. The following section reviews and discusses the available data that constrain the possible age of this unit.

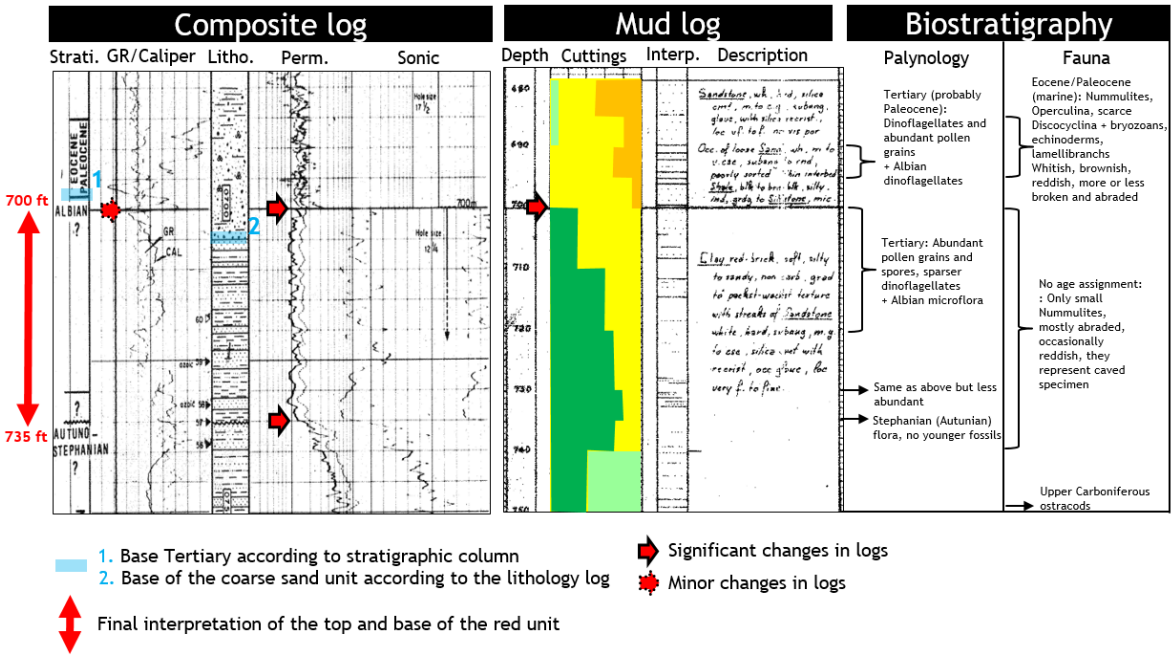

Figure 61: Determination of the top and bottom boundaries of the red unit based on information from the composite log, mud log and biostratigraphical report of borehole 34/05-1.

Upper and lower boundary of the red clastic unit

The upper boundary of the unit is poorly defined on the composite log (Croisile, 1980). On the stratigraphic column of the log, the boundary is at 698 mMD while on the lithology column it seems to be at 705 mMD (FIGURE 61).

There is a shift in the permeability logs at 700 mMD, also observed to a lesser extent in the caliper log (*i.e.* hole diameter) (FIGURE 61). The mud log (one of the logs used to construct the composite log, in particular the lithology and lithologic description columns of the composite log) shows fine-grained sands from 680 to 740 mMD, coarse-grained sands only from 680 to 700 mMD and claystones only from 700 to below 740 mMD (Elf, 1980). This suggests that a lithological transition occurs at c. 700 mMD, from fine and coarse-grained sandstones to a claystones and fine-grained sands (FIGURE 61). The resolution of the mud log at these depths is 5 meters. Therefore, the lithological transition could be anywhere between 695 m and 700 mMD.

The microfauna and microflora are Cenozoic in age at least down to 695 mMD. Between 700 and 740 mMD, the fossils are much rarer and the age is uncertain, while the fossils are definitely Upper Carboniferous in age at least from 735 mMD (FIGURE 61). The biostratigraphical data thus only confirms that the upper boundary of the red unit is below 695 mMD.

Altogether, the changes of character of the lithology, permeability and caliper logs points towards a lithological boundary at 700 mMD (FIGURE 61). This depth will be used for the rest of the discussion.

The lower boundary of the red clastic unit is well defined in the composite at 735 mMD, which is supported by the shift at that depth in the permeability logs, cuttings lithology and biostratigraphical data (FIGURE 61). The unit has therefore a thickness of 35 meters.

Biostratigraphic report data

According to the biostratigraphic report (Ducazeauz et al., 1981), the microfauna is composed of small, mostly abraded, and occasionally reddish *Nummulites*, while the microflora comprises a mixture of Cenozoic and Albian species. The Cenozoic microflora is dominated by abundant pollen grains and spores and rarer dinoflagellates. The Albian microflora is dominated by dinoflagellates with additional species such as *Subtilisphaera sp.* The fossils become rare towards the bottom of the unit but both Cenozoic and Albian fossils are present down to at least 730 mMD (FIGURE 61). The report does not assign any definite age to this unit.

The overlying Cenozoic unit, a white sand, comprises a Paleocene-Eocene marine microfauna (*Nummulites*, *Operculina*, *Discocyclina*, bryozoans, echinoderms, lamellibranch debris). The fossils are whitish, brownish or reddish in colour and are often broken and abraded, which suggests reworking.

The unit also comprises a Cenozoic (probably Paleocene) and Mesozoic (Albian) microflora (Ducazeauz et al., 1981). The underlying Carboniferous unit is composed of abundant Late Carboniferous microfossils with no sign of any cavings (*i.e.* no microfossils younger than Carboniferous) (FIGURE 61).

The part of the report that discusses this biostratigraphic dataset is missing (sections 3 and 4 of the report, Ducazeauz et al. (1981)). The abstract of the report highlights one interpretation but without explaining the underlying reasoning. They suggest that a thin Albian unit might be located between 690 and 700 mMD but they do not rule out the possibility that the unit between 685 and 700 mMD is Paleocene in age with Albian reworking. The abstract does not discuss the age of the red unit, but based on their hypothesis of a possible Albian unit above the red unit, and on the assignment of the red unit to the "Albian?" in the composite log, it is likely that they concluded that the red unit is most probably Albian in age.

Discussion: age of the red unit

The two main hypotheses for the age of the red unit is:

1) Albian with Paleocene-Eocene cavings (the main hypothesis of the operator)
2) Paleocene-Eocene with Albian reworking

The absence of cavings in the Carboniferous section points towards a low probability of cavings in the red unit as well. Also, the Paleocene-Eocene unit comprises reddish and abraded *Nummulites*. This seems to imply that the white sand reworked a unit that comprised red *Nummulites*. Therefore the *Nummulites* must have been emplaced in the red unit before the deposition of the overlying white sand. These observations points towards a Paleocene-Eocene age for the red unit. The abundance of Paleocene pollens and spores in the red unit makes sense since the sediments were most likely deposited in a continental setting.

The stratigraphers suggest that the Cenozoic fossils in both the red unit and the Cenozoic sand are probably cavings because they are broken and abraded. However, the broken and abraded character of the fossils could be explained by the alternation of subaerial exposures and marine transgressions throughout the Paleocene-Eocene: marine transgressions would deposit *Nummulites* and other marine fossils in the area that would be reworked and weathered when exposed to shoreline, subaerial or fluvial conditions.

The presence of Albian fossils throughout the Cenozoic and red units could be explained by reworking of *in-situ* Albian sediments (somewhere between 730 and 735 mMD) and/or the reworking by continental processes (*e.g.* fluvial transport) of Albian sediments located on a paleo-outcrop further away from the borehole (probably on the west towards the highest parts of the Porcupine High)

and/or the reworking by marine transgression of Albian sediments located on the paleo-seabed eastward of the well (in the northern part of the present-day Porcupine Basin).

Glauconite is often present in Lower Cretaceous marine rocks (e.g. the 'greensand'). The red unit is described as occasionally glauconitic which could support the attribution of an Early Cretaceous age. However, the unit is red and not green and glauconite is also described in the overlying Paleocene-Eocene sandstone. Therefore, the presence of glauconite is not sufficiently diagnostic to imply one age or the other.

Based on the available data, there is no reason to discard the hypothesis that the red unit is a mixture of mostly Paleocene-Eocene continental sediments with minor marine sediments and reworked Albian sediments. The unit is overlain by a transgressive marine sand of Paleocene-Eocene age that probably ended the periodic subaerial exposures of this part of the Porcupine High. Therefore for this study, both hypotheses will be considered equally.

The microflora of the Cenozoic and red units are attributed a precise age of 'Paleocene', rather than the less precise Paleocene-Eocene age attributed to the microfauna. Therefore, it is possible that the red unit and overlying white sand could actually be Paleocene in age, rather than Paleocene-Eocene. However, the operator decided to attribute a Paleocene-Eocene age to the Cenozoic unit, rather than a Paleocene age, therefore there must be some uncertainties on the accuracy of the Paleocene attribution. This study will follow the operator choice and employ a Paleocene-Eocene age.

1.7 Discussion: which samples are in-situ?

1.7.1 Introduction

One of the key issues with dredge and ultra-shallow borehole samples is the uncertainty regarding the origin of the sample, as clearly only samples which are *in-situ* or near *in-situ* (originating from a nearby outcrop) can be used to determine the geological/thermal history of a region. The following discussion aims to establish which samples are potentially *in-situ* by using all available information at hand.

One assumption that will be used here is that *in-situ* samples from the same dredged site or region will likely have shared the same thermal history and will therefore have the same AFT/AHe ages and MTL (within errors). Although magmatic activity can invalidate this assumption by creating local thermal disturbances, this assumption is still useful to identify *in-situ vs* non-*in-situ* samples.

The location, lithology, zircon and apatite U/Pb ages, Pb isotopes and thermochronological information for all samples have been summarized in Table 8. The samples in this table are listed in order of AFT age from youngest to oldest.

1.7.2 C-MeBo: In-situ

The first sample which is considered *in-situ* is C-MeBo from shallow borehole 25/7-sb(MeBo)3. The driller considered this core *in-situ* because of 1) the recovery of a uniform lithology over 85 cm of core and 2) the thinner Quaternary cover of the site in comparison to the previous drilling site down dip (Murray and Freudenthal, 2006). Moreover, the dating of the gneiss yielded a Paleoproterozoic age which is in agreement with the prediction of a Paleoproterozic basement in this northern part of the Porcupine High based on K-feldspar Pb isotope analyses from Jurassic sands on the western margin of the Porcupine High (Tyrrell et al., 2007) and magnetic anomalies (Riddihough and Max, 1976).

1.7.3 C-MeBo2: Near in-situ

Sample C-MeBo2 from shallow borehole 25/27-sb(MeBo2) is a clast of deformed granite in a sandy and calcareous conglomerate of Late Quaternary age (Murray and Freudenthal, 2006). The dominance of gneiss clasts in the conglomerate led the campaign geologists to interpret the clasts as being derived from a nearby outcrop and therefore the clasts could be considered as near-*in-situ* (Murray and Freudenthal, 2006). As discussed in the main thesis, this granite might be sourced from an outcrop located south of the inferred FHCBL (at a minimum distance of 10 km from the location of 25/27-sb(MeBo)2). Consequently, this sample is considered to be near *in-situ* and might reflect the thermal history of the basement south of the FHCBL or the thermal history of the fault suture zone itself.

1.7.4 C-PH1 to C-PH14: In-situ

The dredges psammites at the summit of the Porcupine High are also very likely to be *in-situ*, in particular samples PH4 to PH12. These samples all share the same characteristics:

- Lithology: psammite,
- Zircon and apatite U/Pb signature: Neoproterozoic psammites with a Laurentian detrital signature = PHMS,
- AFT age: c. 190 Ma,
- AHe age: c. 100-174 Ma,
- and track length statistics: MTL c. 9.5 µm, minimum and maximum lengths of 2.5 to 15.5 µm, wide distribution peaking at c. 13 µm.

The only sample from this 2011 dredge which is different is sample C-PH1 which is also a PHMS psammite but has a younger LAFT central age of c. 142 Ma. Its MTL is identical to the other samples (9.7 µm) but the length distribution shows a possible bimodality that is not as marked in the other samples (with peaks at c. 9.5 and 12.5 µm).

Table 8: Geological information for all Porcupine High seabed samples, sorted out by AFT ages.

Sample	Lithology	Zircon U/Pb age	Apatite U/Pb age	Kfsp affinity	Basement group	Site	AFT age			AHe	MTL		In-situ?	(If not in-situ) Possible sources
							Ma	±	-	*Ma*	*Ma*	±		
C-PH1	Psammite	c. 0.8-1.8 Ga	c. 0.9-1.8 Ga	Mostly AGC	PHMS	PH	142	8	Base Cretaceous	n/a	9.69	3.01	Yes + hot fluids?	n/a
C-302-1	Psammite	c. 1-1.8 Ga	1-2.8 Ga?	?	PHMS? Other?	302/3	143	5		68-139	12.61	1.62	Possible	n/a
C-MeBo2	Gneiss clast	490 Ma	383 Ma	Caledonian	PHCG	MeBo2	144.1	7.5		51-57	10.29	2.45	Near + hot fluids?	OPWI?
C-MeBo	Gneiss	1.31 Ga	0.88 Ga	Rockall Rhinns	NPHO	MeBo3	157	27	Late Jurassic	186-197	13.03	1.21	Yes	n/a
C-402-11	Gneiss?	c. 2.75 Ga	c. 1.75 Ga	Lewisian	HG1	402	167	5	Middle Jurassic?	88-99	12.58	1.83	No	Probably Lewisian Complex in the Outer Hebrides
C-204-1	Micaschist	Detrital: Moine/ Grampian	Mostly Caledonian	?	LG1	204	180	8	Early Jurassic	78-123	12.46	1.5	Possible	Offshore Mayo, OPWI or Scotland?
C-402-6	Greenschist	Detrital: Upper Dalradian	Mostly Caledonian	?	LG2	402	190	19		51-82	12.49	1.49	Possible + hot fluids	n/a
C-PH4	Psammite	c. 0.8-1.8 Ga	c. 0.9-1.8 Ga	Mostly AGC	PHMS	PH	184	12		98-172	9.86	3.01	Yes	n/a
C-PH12	Psammite						191	20		n/a	9.72	3.08		
C-PH10	Psammite						193	11		n/a	9.76	3.25		
C-PH5	Psammite						194	11		115-162	9.79	2.86		
C-402-9	Gneiss	c. 1.55-2.02 Ga	c. post-Grenville	AGC?	HG3	402	198	7	Late Triassic	313-444	12.67	1.83	Possible	n/a
C-402-4	Gneiss						216	10		n-a	12.69	1.45		
C-402-13	Amphibolite						261	18	Ea.-Mid. Permian	95-99	12.57	1.71		
C-303-1	Amphibolite	c.1.83-1.94 Ga	c. 1.75 Ga	AGC	HG2	302/3	283	9		347-480	12.65	1.81	No	Probably from Central Highlands
C-402-3	Gneiss					402	289	16		n/a	12.03	1.89		
C-402-1	Gneiss	c. 2.75 Ga	c. 1.75 Ga	Lewisian	HG1		425	16	Late Caledonian	0-2	12.05	2.09		Probably Lewisian Complex in the Outer Hebrides, NW Scotland
C-402-8	Gneiss						546	18	Late Cadomian?	379-351	12.2	1.8		

HG1: High-grade metamorphic rock group 1
HG2: High-grade metamorphic rock group 2
HG3: High-grade metamorphic rock group 3
LG1: Low-grade metamorphic rock group 1
LG2: Low-grade metamorphic rock group 2
NPHO: North Porcupine High Orthogneiss
PHMS: Porcupine High Metasedimentary Sequence
PHCG: Porcupine High Caledonian Gneiss
Ap.: apatite
AGC: Annagh Gneiss Complex
Kfsp: K-feldspar
Zr.: zircon

1.7.5 HG1 samples, C-402-1, C-402-8, C-402-11: Not in-situ

These three samples are high-grade metamorphic rocks from the HG1 group of Chew et al. (2019). Based on the regional prediction of the extension of the onshore basement terranes and the presence of Paleoproterozoic crust in the northern part of the Rockall Bank (Daly et al. (1995), Tyrrell et al. (2007)), it is unlikely that the Archean HG1 rocks are *in-situ* since the Archean basement is expected to crop out much further to the north.

Moreover, C-402-1 and C-402-8 have AFT central ages of 425 and 546 Ma. Regionally, such old AFT ages are only found in Northern Ireland, Scotland and the English Midlands (FIGURE 62). The Outer Hebrides and/or the NW coast of Scotland and surrounding offshore platform are a likely source area for these two samples since both Lewisian basement and old AFT ages can be found there. Sample C-402-11 probably also come from the same source area since Mesozic AFT ages are also known there (FIGURE 62).

1.7.6 HG-2 samples, C-303-1, C-402-3: Not in-situ

These two samples are a gneiss and an amphibolite with Paleoproterozoic zircons and apatite ages. The Paleoproterozoic age of the apatites indicates that the basement rock from which these samples originate has not experienced Grenville (c. 1 Ga) orogenesis. In Ireland and Scotland, this type of basement is represented by the Rhinns Complex which occurs offshore north of Ireland (island of Inishtrahull) and in SW Scotland (islands of Islay and Colonsay) within the Colonsay-West Islay Block (Muir et al., 1994).

If these samples were *in-situ*, it would imply that they must be a major Caledonian fault separating this basement unaffected by the Grenville Orogeny from the AGC of Co. Mayo and the NPHO on the Porcupine High, both of which being Proterozoic basements with a Grenville footprint (Daly (1996), Daly et al. (2008)). This fault might represent an extension to the SW of the Loch Gruinart-Leannan Fault in Islay and Ireland (Stewart et al., 1999).

If these samples are not *in-situ* then they must come from further north, probably from the Colonsay-West Islay Block, which might be the case since Proterozoic basement rocks with a Grenville footprint are also found in the dredges (group HG3, see next section Moreover, if they were *in-situ*, a Permian AFT age would imply that they were not affected by the Jurassic-Early Cretaceous rifting and hyper-extension in the Rockall Basin, despite being located at the very edge of the basin where the thermal effects of such geodynamical events are expected to be found.

In conclusion, these three sample are not in-situ and are probably derived from the Archean basement of Scotland.

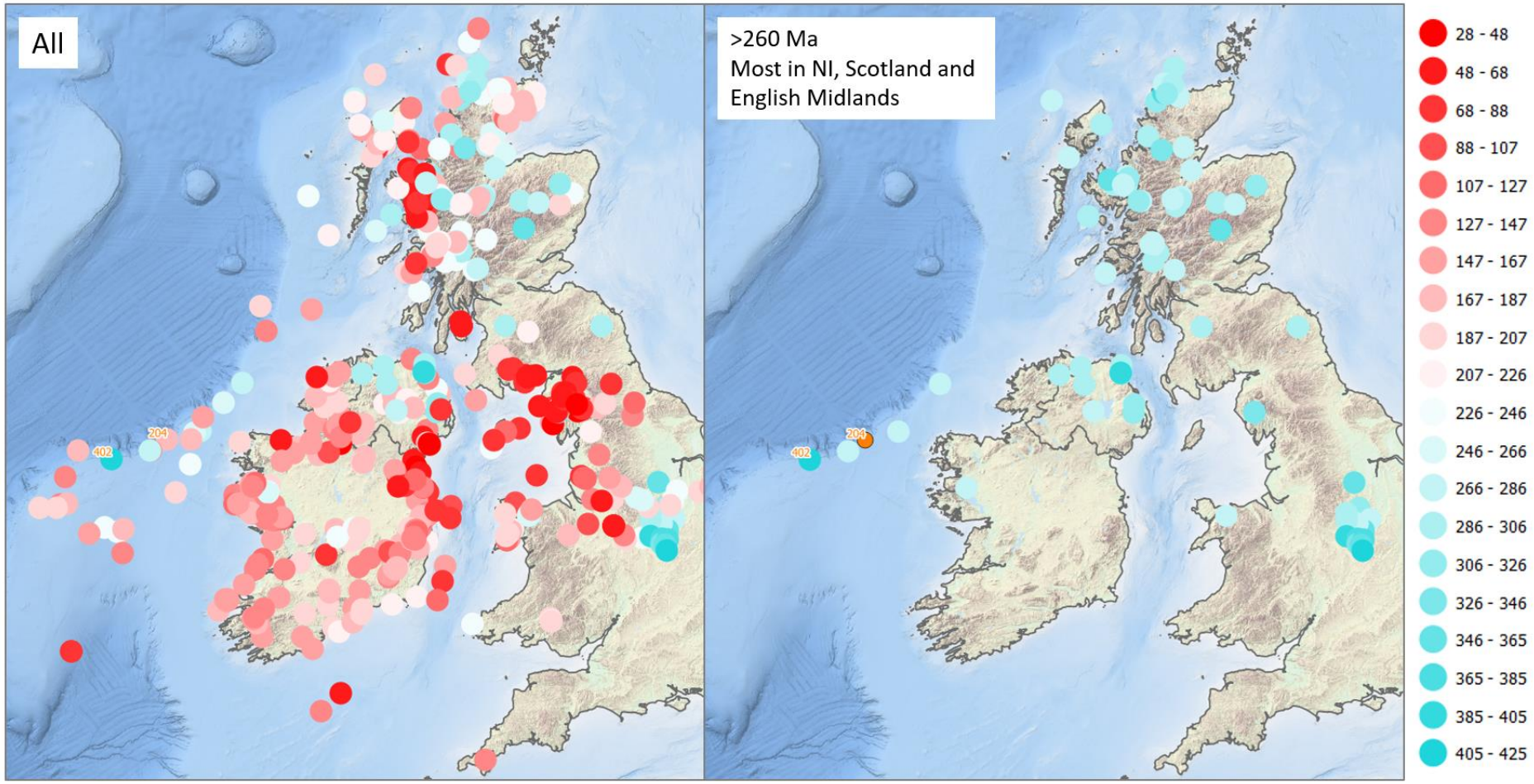

Figure 62: Possible sources of areas with AFT ages > 266 Ma.

Consequently, these two samples are probably not *in-situ* but come from further to the NE (Colonsay-West Islay Block), even though it cannot be excluded that they are indeed *in-situ*.

1.7.7 C-402-4, 9 and 13: Possibly in-situ

These three samples belong to group HG3 of Chew et al. (2019). Unlike the HG2 samples, these samples come from Paleoproterozoic gneissic basement which has been affected by the Grenville Orogeny. Similar Proterozoic basement with a Grenville orogenic footprint are the AGC of Co. Mayo (Daly, 1996) and the NPHO (Daly et al., 2008). Therefore, these samples are likely to be *in-situ* and could represent the offshore extension of the AGC and the connection between the AGC and the NPHO.

These samples have Late Triassic to Middle Permian LAFT central ages. Although somewhat rare based on the regional distribution of surface sample AFT ages (FIGURE 62), such ages are known in the region, with for example a sample from the Cross Point Gneiss of the AGC yielding an AFT age of 199 Ma (Döpke, 2017).

Consequently, based on the geochronological and thermochronological data, these three samples are likely to be *in-situ*.

1.7.8 C-204-1, C-402-6: Possibly in-situ

These two low-grade metamorphic rocks have AFT ages which are similar to the PHMS samples. C-204-1 has AHe ages also very similar to the PHMS AHe ages, while sample C-402-6 has Paleogene AHe ages. Both the geochronological and thermochronological results are plausible if the samples are *in-situ*.

1.7.9 C-302-1: Possibly in-situ

Finally, sample C-302-1 is a psammite with zircon and apatite U/Pb age signatures similar to the PHMS samples. However, this sample has younger AFT and AHe ages (143 Ma and 68-139 Ma respectively) and a longer confined track MTL than PH1-12. This sample could represent *in-situ* Dalradian metasediments that have experienced a different thermal history than the PHMS (located c. 150 km to the SW).

1.7.10 In situ nature of the 2014 dredges - conclusions

To summarize, for the samples of the 2014 campaigns (sites 204, 302/303 and 402), three groups of samples can potentially represent *in-situ* lithologies that crop out on the north side of the Porcupine High (TABLE 8):

1. High-grade metamorphic rocks with late Paleoproterozic zircons and post-Grenville apatites (group HG3, offshore extension of the AGC) and with Late Triassic-Middle Devonian AFT ages (site 402 only)
2. Neoproterozoic low-grade metamorphic rocks (groups LG1 and LG2) with Early Jurassic AFT ages (sites 204 and 402)
3. Neoproterozoic low-grade metamorphic rocks with Early Cretaceous AFT ages (sample C-302-1) (site 302 only)

The large dispersion of AFT ages among the potential *in-situ* groups and the lack of meaningful trends from one site to another prevents the determination of one group as being more likely to be *in-situ* than another one. It is also possible that all three groups are *in-situ* but represent two to three tectonic blocks with different and independent thermal histories and/or sampling of rocks that were at different paleo-altitudes. Due to the large variations in AFT/AHe ages and the difficulty in ascertaining the source of these dredge samples, they will not be used for quantitative modelling.

1.8 References

Á Horni, J., Hopper, J. R., Blischke, A., Geisler, W. H., Stewart, M., McDermott, K., Judge, M., Erlendsson, Ö., and Árting, U., 2017, Regional distribution of volcanism within the North Atlantic Igneous Province: Geological Society, London, Special Publications, v. 447, no. 1, p. 105.

Barker, C. E., 1988, Geothermics of petroleum systems: Implications of the stabilization of kerogen thermal maturation after a geologically brief heating duration at peak temperature, *in* Magoon, L. B., ed., Petroleum Systems of the United States, U.S. Geological Survey, p. 26-29.

Blackmore, R., 1995, Low-Grade Metamorphism in the Upper Palaeozoic Munster Basin, Southern Ireland: Irish Journal of Earth Sciences, v. 14, p. 115-133.

Cailleaux, P., and Robert, P., 1981, Geochemical and optical studies of organic matter: SNEA (P) Direction Exploration, Laboratoire de Géologie de Boussens.

Chew, D., O'Sullivan, G., Caracciolo, L., Mark, C., and Tyrrell, S., 2020, Sourcing the sand: Accessory mineral fertility, analytical and other biases in detrital U-Pb provenance analysis: Earth-Science Reviews, v. 202, p. 103093.

Chew, D., Tyrrell, S., Daly, J. S., Cogné, N., Sun, K., and Badenszki, E., 2019, The basement geology of the Porcupine High - A key transatlantic link between the Caledonides and Appalachians, GSA 2019, Volume 51: Phoenix, Arizona, USA, GSA.

Church, J. W., Denison, C. N., Footitt, R., Harrison, D. J., Haskins, C. W., and Neville, R. S. W., 1981, Phillips 35/15-1 offshore Ireland well: Biostratigraphy of the interval 2050'-12096' T.D.: Robertson Research International Limited.

Cohen, K. M., Harper, D. A. T., and Gibbard, P. L., 2020, ICS International Chronostratigraphic Chart 2020/01, International Commission on Stratigraphy, IUGS.

Corcoran, D. V., and Clayton, G., 2001, Interpretation of vitrinite reflectance profiles in sedimentary basins, onshore and offshore Ireland: Geological Society, London, Special Publications, v. 188, no. 1, p. 61-90.

Corcoran, D. V., and Doré, A. G., 2005, A review of techniques for the estimation of magnitude and timing of exhumation in offshore basins: Earth-Science Reviews, v. 72, no. 3–4, p. 129-168.

Corcoran, D. V., and Mecklenburgh, R., 2005, Exhumation of the Corrib Gas Field, Slyne Basin, offshore Ireland: Petroleum Geoscience, v. 11, no. 3, p. 239-256.

Creaney, S., 1980, Petrographic texture and vitrinite reflectance variation on the ALston block, North-East England: Proceedings of the Yorkshire Geological Society, v. 42, no. 4, p. 553-580.

Croisile, M., 1980, 34/05-1 composite log: Elf Aquitaine Ireland Ltd.

Daly, J. S., 1996, Pre-Caledonian History of the Annagh Gneiss Complex North-Western Ireland, and Correlation with Laurentia-Baltica: Irish Journal of Earth Sciences, v. 15, p. 5-18.

Daly, J. S., Heaman, L. M., Fitzgerald, R. C., Menuge, J. F., Brewer, T. S., and Morton, A. C., 1995, Age and crustal evolution of crystalline basement in western Ireland and Rockall: Geological Society, London, Special Publications, v. 93, no. 1, p. 433-434.

Daly, J. S., Tyrrell, S., Badenszki, E., Haughton, P., and Shannon, P., 2008, IS06/10: Petrographic and geochemical characterisation of the Porcupine High using recently recovered MeBo shallow cores.

De Geyter, G., De Man, E., Herman, J., Jacobs, P., Moorkens, T., Steurbaut, E., and Vandenberghe, N., 2006, Disused Paleogene regional stages from Belgium: Montian, Heersian, Landenian, Paniselian, Bruxellian, Laekenian, Ledian, Wemmelian and Tongrian: Geologica Belgica (online), v. 9, no. 1-2.

Deschamps, A., Grigné, C., Le Saout, M., Soule, S. A., Allemand, P., Van Vliet-Lanoe, B., and Floc'h, F., 2014, Morphology and dynamics of inflated subaqueous basaltic lava flows: Geochemistry, Geophysics, Geosystems, v. 15, no. 6, p. 2128-2150.

Donelick, R. A., O'Sullivan, P. B., and Ketcham, R. A., 2005, Apatite Fission-Track Analysis: Reviews in Mineralogy and Geochemistry, v. 58, no. 1, p. 49-94.

Döpke, D., 2017, Modelling the thermal history of onshore Ireland, Britain and its offshore basins using low-temperature thermochronology [PhD PhD thesis]: Trinity College Dublin, 263 p.

Doran, T., Roveda, V. L., Lowe, S. P., and Whitbread, D. R., 1982, Geochemical evaluation of cuttings samples and sidewall cores from the Porcupine Basin well: 26/30-1, offshore Eire.

Ducazeauz, J., SJardine, S., Durif, P., and Grosdidier, E., 1981, Biostratigraphic report of well 34/05-1: SNEA.

Elf, 1980, Elf: Elf Aquitaine Ireland Ltd.

Flowers, R. M., and Kelley, S. A., 2011, Interpreting data dispersion and "inverted" dates in apatite (U–Th)/He and fission-track datasets: An example from the US midcontinent: Geochimica et Cosmochimica Acta, v. 75, no. 18, p. 5169-5186.

Fügenschuh, B., Froitzheim, N., Capdevila, R., and Boillot, G., 2003, Offshore granulites from the Bay of Biscay margins: fission tracks constrain a Proterozoic to Tertiary thermal history: Terra Nova, v. 15, no. 5, p. 337-342.

Gerneck, J. R., Saguiez, P., Brewster, J., McAdoo, R., and Luck, B. J., 1980, 35/15-1 composite log: Phillips Petroleum Company Ireland Limited.

Goodhue, R., and Clayton, G., 1999, Organic maturation levels, thermal history and hydrocarbon source rock potential of the Namurian rocks of the Clare Basin, Ireland: Marine and Petroleum Geology, v. 16, no. 7, p. 667-675.

Graham, J. R., 2009, Variscan deformation and metamorphism, *in* Holland, C. H., and Sanders, I., eds., The geology of Ireland, Dunedin Academic, p. 295-310.

Green, P., and Duddy, I., 2018, Apatite (U-Th-Sm)/He thermochronology on the wrong side of the tracks: Chemical Geology, v. 488, p. 21-33.

Green, P. F., 2001, Thermal history reconstruction in Irish Rockall trough boreholes 16/28-sb01, 83/20-sb01, 83/24-sb02 using AFTA, VR and fluid inclusion data GEOTRACK REPORT #777.

Green, P. F., Duddy, I. R., Gleadow, A. J. W., Tingate, P. R., and Laslett, G. M., 1986, Thermal annealing of fission tracks in apatite: 1. A qualitative description: Chemical Geology: Isotope Geoscience section, v. 59, no. Supplement C, p. 237-253.

Harris, A. J. L., and Allen III, J. S., 2008, One-, two- and three-phase viscosity treatments for basaltic lava flows: Journal of Geophysical Research: Solid Earth, v. 113, no. B9.

Henderson, P., 1980, The igneous rocks drilled from the Porcupine Basin.

Henrichs, I. A., O'Sullivan, G., Chew, D. M., Mark, C., Babechuk, M. G., McKenna, C., and Emo, R., 2018, The trace element and U-Pb systematics of metamorphic apatite: Chemical Geology, v. 483, p. 218-238.

Hoshi, K., and Okubo, S., 2010, Hydrothermally dissolved dolerite reservoir in the Akita Basin, Japan, Search and Discovery Article: AAPG International Conference and Exhibition: Calgary, Alberta, Canada, AAPG.

Ketcham, R. A., Beek, P., Barbarand, J., Bernet, M., and Gautheron, C., 2018a, Reproducibility of Thermal History Reconstruction From Apatite Fission-Track and (U-Th)/He Data: Geochemistry, Geophysics, Geosystems, v. 19, no. 8, p. 2411-2436.

Ketcham, R. A., van der Beek, P., Barbarand, J., Bernet, M., and Gautheron, C., 2018b, Reproducibility of Thermal History Reconstruction From Apatite Fission-Track and (U-Th)/He Data: Geochemistry, Geophysics, Geosystems, v. 19, no. 8, p. 2411-2436.

Ludwig, K. R., 1998, On the Treatment of Concordant Uranium-Lead Ages: Geochimica et Cosmochimica Acta, v. 62, no. 4, p. 665-676.

McCulloch, A. A., 1993, Apatite fission track results from Ireland and the Porcupine basin and their significance for the evolution of the North Atlantic: Marine and Petroleum Geology, v. 10, no. 6, p. 572-590.

Monaghan, A. A., and Parrish, R. R., 2006, Geochronology of Carboniferous–Permian magmatism in the Midland Valley of Scotland: implications for regional tectonomagmatic evolution and the numerical time scale: Journal of the Geological Society, v. 163, no. 1, p. 15-28.

Muir, R. J., Fitches, W. R., and Maltman, A. J., 1994, The Rhinns Complex: Proterozoic basement on Islay and Colonsay, Inner Hebrides, Scotland, and on Inishtrahull, NW Ireland: Transactions of the Royal Society of Edinburgh: Earth Sciences, v. 85, no. 1, p. 77-90.

Murray, B., and Freudenthal, T., 2006, Report from cruise CE0619 with R/V Celtic Explorer on the Porcupine Bank: PAD.

Nielsen, S. B., Clausen, O. R., and McGregor, E., 2017, basin%Ro: A vitrinite reflectance model derived from basin and laboratory data: Basin Research, v. 29, no. S1, p. 515-536.

Rateau, R., Schofield, N., and Smith, M., 2013, The potential role of igneous intrusions on hydrocarbon migration, West of Shetland: Petroleum Geoscience, v. 19, no. 3, p. 259-272.

Renoux, J., and Croisile, M., 1981, Completion report well 34/5-1: Elf Aquitaine (Ireland) Ltd.

Riddihough, R. P., and Max, M. D., 1976, A geological framework for the continental margin to the west of Ireland: Geological Journal, v. 11, no. 2, p. 109-120.

Smallwood, J. R., and Maresh, J., 2002, The properties, morphology and distribution of igneous sills: modelling, borehole data and 3D seismic from the Faroe-Shetland area: Geological Society, London, Special Publications, v. 197, no. 1, p. 271-306.

Spacapan, J. B., D´Odorico, A., Palma, O., Galland, O., Senger, K., Ruiz, R., Manceda, R., and Leanza, H. A., 2020, Low resistivity zones at contacts of igneous intrusions emplaced in organic-rich formations and their implications on fluid flow and petroleum systems: A case study in the northern Neuquén Basin, Argentina: Basin Research, v. 32, no. 1, p. 3-24.

Stacey, J. S., and Kramers, J. D., 1975, Approximation of terrestrial lead isotope evolution by a two-stage model: Earth and Planetary Science Letters, v. 26, no. 2, p. 207-221.

Steiger, R. H., and Jäger, E., 1977, Subcommission on geochronology: Convention on the use of decay constants in geo- and cosmochronology: Earth and Planetary Science Letters, v. 36, no. 3, p. 359-362.

Stewart, M., Strachan, R. A., and Holdsworth, R. E., 1999, Structure and early kinematic history of the Great Glen Fault Zone, Scotland: Tectonics, v. 18, no. 2, p. 326-342.

Suggate, R. P., 1998, RELATIONS BETWEEN DEPTH OF BURIAL, VITRINITE REFLECTANCE AND GEOTHERMAL GRADIENT: Journal of Petroleum Geology, v. 21, no. 1, p. 5-32.

Summer, N. S., and Ayalon, A., 1995, Dike intrusion into unconsolidated sandstone and the development of quartzite contact zones: Journal of Structural Geology, v. 17, no. 7, p. 997-1010.

Sweeney, J., and Burnham, A. K., 1990, Evaluation of a simple model of vitrinite reflectance based on chemical kinetics: AAPG Bulletin, v. 74, no. 10, p. 1559-1570.

Szymanski, E., Stockli, D., Johnson, P., and Hager, C., 2016, Thermochronometric Evidence for Diffuse Extension and Two-Phase Rifting within the Central Arabian Margin of the Red Sea Rift: Central Arabian Rift Flank, Red Sea Rift: Tectonics, v. 35.

Tate, M. P., and Dobson, M. R., 1988, Syn- and post-rift igneous activity in the Porcupine Seabight Basin and adjacent continental margin W of Ireland: Geological Society, London, Special Publications, v. 39, no. 1, p. 309-334.

Tyrrell, S., Haughton, P. D. W., and Daly, J. S., 2007, Drainage reorganization during breakup of Pangea revealed by in-situ Pb isotopic analysis of detrital K-feldspar: Geology, v. 35, no. 11, p. 971-974.

Van der Veen, F. M., 1981, Evaluation of source rock properties: Shell.

Vermeesch, P., 2017, Statistics for LA-ICP-MS based fission track dating: Chemical Geology, v. 456, p. 19-27.

Vermeesch, P., Seward, D., Latkoczy, C., Wipf, M., Günther, D., and Baur, H., 2007, α-Emitting mineral inclusions in apatite, their effect on (U–Th)/He ages, and how to reduce it: Geochimica et Cosmochimica Acta, v. 71, no. 7, p. 1737-1746.

Ware, P. D., and Turner, J. P., 2002, Sonic velocity analysis of the Tertiary denudation of the Irish Sea basin: Geological Society, London, Special Publications, v. 196, no. 1, p. 355-370.

Wilkinson, C. M., Ganerød, M., Hendriks, B. W. H., Eide, E. A., Péron-Pinvidic, G., Hopper, J. R., Funck, T., Stoker, M. S., Gaina, C., Doornenbal, J. C., and Árting, U. E., 2017, Compilation and appraisal of geochronological data from the North Atlantic Igneous Province (NAIP), The NE Atlantic Region. A Reappraisal of Crustal Structure, Tectonostratigraphy and Magmatic Evolution, Volume 447, Geological Society of London, p. 0.

2 Annexe 2 - Thermal history models

2.1 Introduction

The results of each thermal history inverse modelling for each scenario are summarized according to the following format:

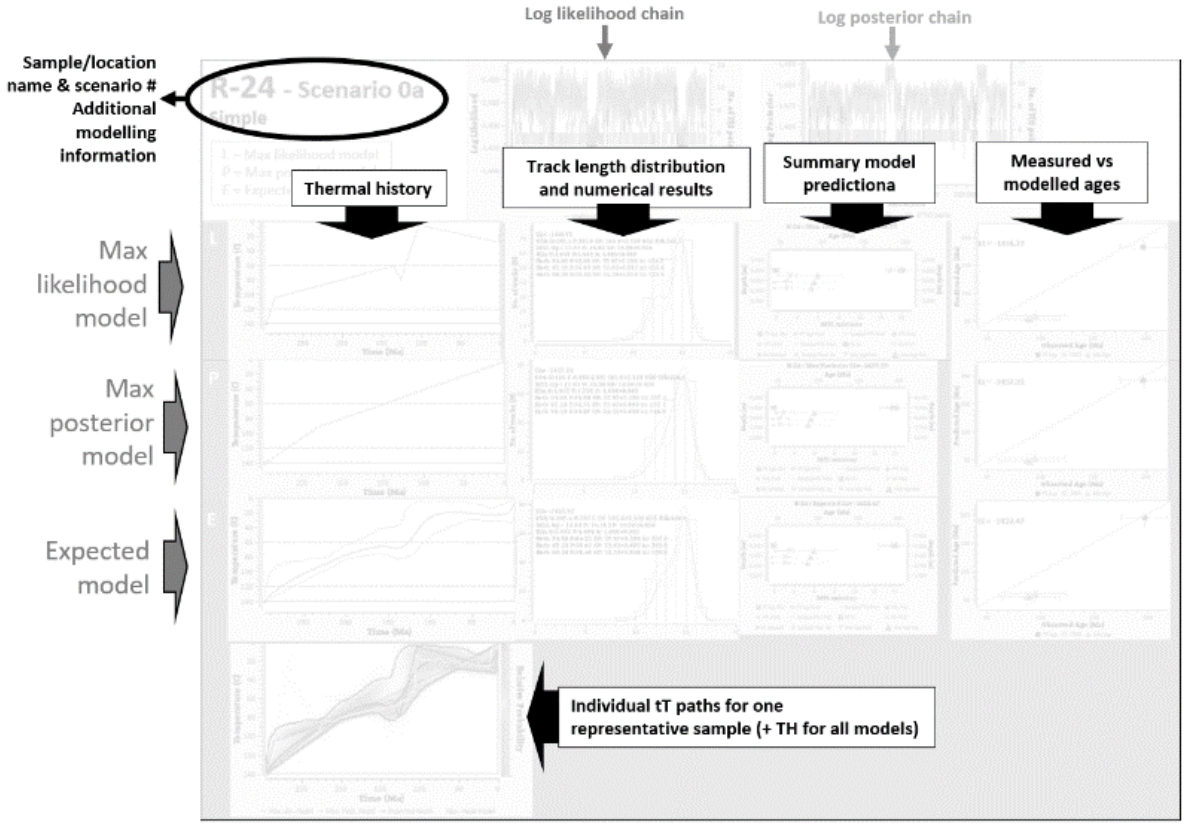

Note: The main goal of these figures is to offer a rapid visual check of measured *vs* modelled/predicted data. Some of the legends of the figures are not readable due to the requirement of gathering all the relevant figures on one page only for each model. Each figure can be investigated in better details in a digital annex located on the FT Lab SSD drive (folder 'Digital Annexe Thesis Rateau, 2021/Thermal History Modelling (THM) results'). Colour figures can be found in the PDF version.

2.2 Northern zone

2.2.1 13/03-1

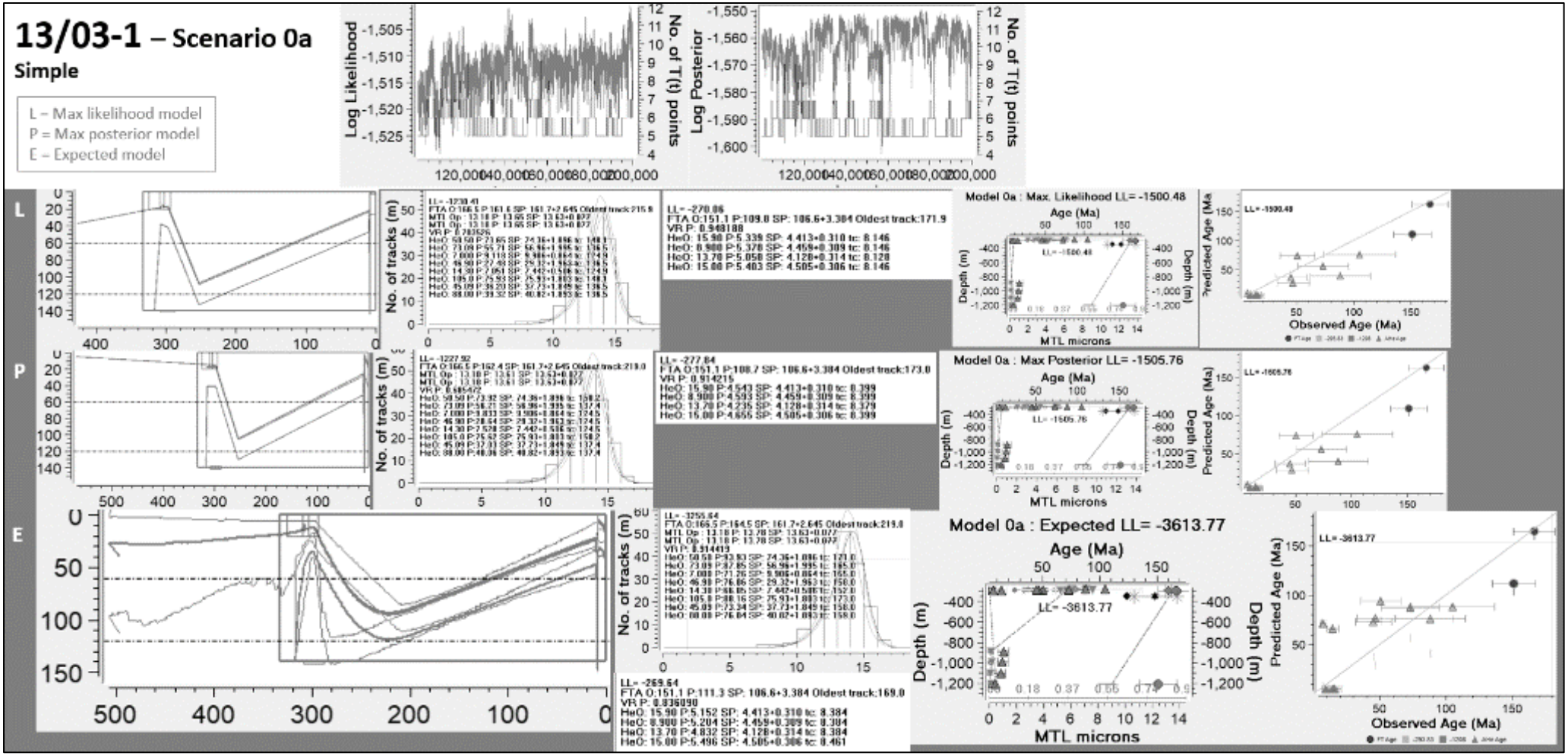

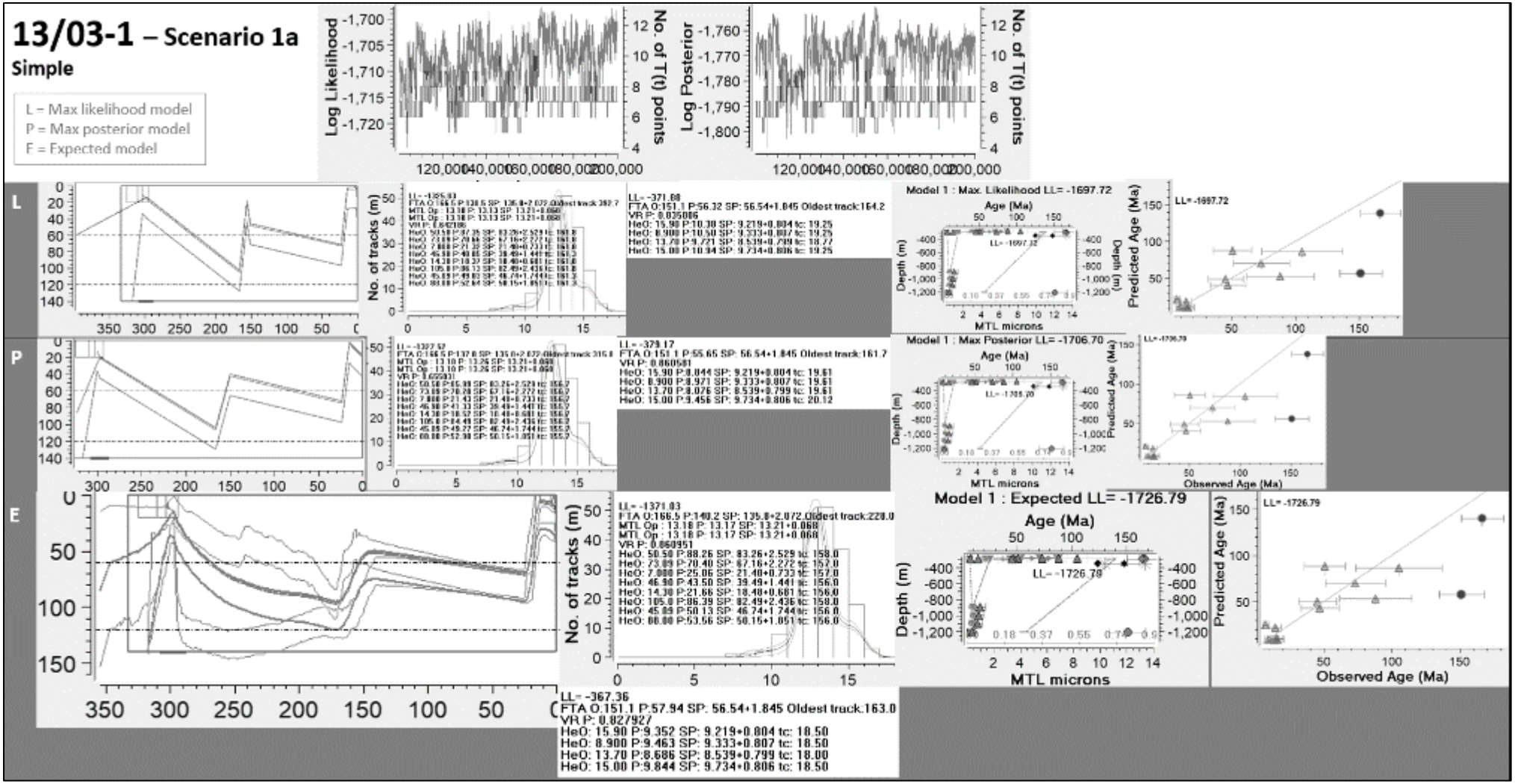
13/03-1 – Scenario 1a
Simple
L = Max likelihood model
P = Max posterior model
E = Expected model
Log Likelihood
No. of T(t) points
Log Posterior
No. of T(t) points
L
P
E
No. of tracks (m)
Depth (m)
MTL microns
Age (Ma)
Predicted Age (Ma)
Observed Age (Ma)
Model 1 : Max. Likelihood LL= -1697.72
Model 1 : Max Posterior LL= -1706.70
Model 1 : Expected LL= -1726.79
LL= -371.08
FTA O:151.1 P:56.32 SP: 56.54+1.845 Oldest track:164.2
VR P: 0.835086
HeO: 15.90 P:10.30 SP: 9.219+0.804 tc: 19.25
HeO: 8.900 P:10.50 SP: 9.333+0.807 tc: 19.25
HeO: 13.70 P:9.721 SP: 8.539+0.799 tc: 18.77
HeO: 15.00 P:10.94 SP: 9.734+0.806 tc: 19.25
LL= -379.17
FTA O:151.1 P:55.65 SP: 56.54+1.845 Oldest track:161.7
VR P: 0.860581
HeO: 15.90 P:8.044 SP: 9.219+0.804 tc: 19.61
HeO: 8.900 P:8.971 SP: 9.333+0.807 tc: 19.61
HeO: 13.70 P:8.076 SP: 8.539+0.799 tc: 19.61
HeO: 15.00 P:9.456 SP: 9.734+0.806 tc: 20.12
LL= -1371.83
FTA O:166.5 P:140.2 SP: 135.8+2.072 Oldest track:228.0
MTL Op : 13.18 P: 13.17 SP: 13.21+0.068
MTL Op : 13.18 P: 13.17 SP: 13.21+0.068
VR P: 0.860951
HeO: 50.50 P:88.26 SP: 83.26+2.529 tc: 158.0
HeO: 73.89 P:70.40 SP: 67.16+2.272 tc: 157.0
HeO: 7.888 P:25.06 SP: 21.48+0.733 tc: 157.0
HeO: 46.90 P:43.50 SP: 39.49+1.441 tc: 156.0
HeO: 14.30 P:21.66 SP: 18.48+0.681 tc: 156.0
HeO: 105.8 P:86.39 SP: 82.49+2.436 tc: 158.0
HeO: 45.85 P:50.13 SP: 46.74+1.744 tc: 156.0
HeO: 88.88 P:53.56 SP: 50.15+1.851 tc: 156.0
LL= -367.36
FTA O:151.1 P:57.94 SP: 56.54+1.845 Oldest track:163.0
VR P: 0.827927
HeO: 15.90 P:9.352 SP: 9.219+0.804 tc: 18.50
HeO: 8.900 P:9.463 SP: 9.333+0.807 tc: 18.50
HeO: 13.70 P:8.686 SP: 8.539+0.799 tc: 18.00
HeO: 15.00 P:9.844 SP: 9.734+0.806 tc: 18.50

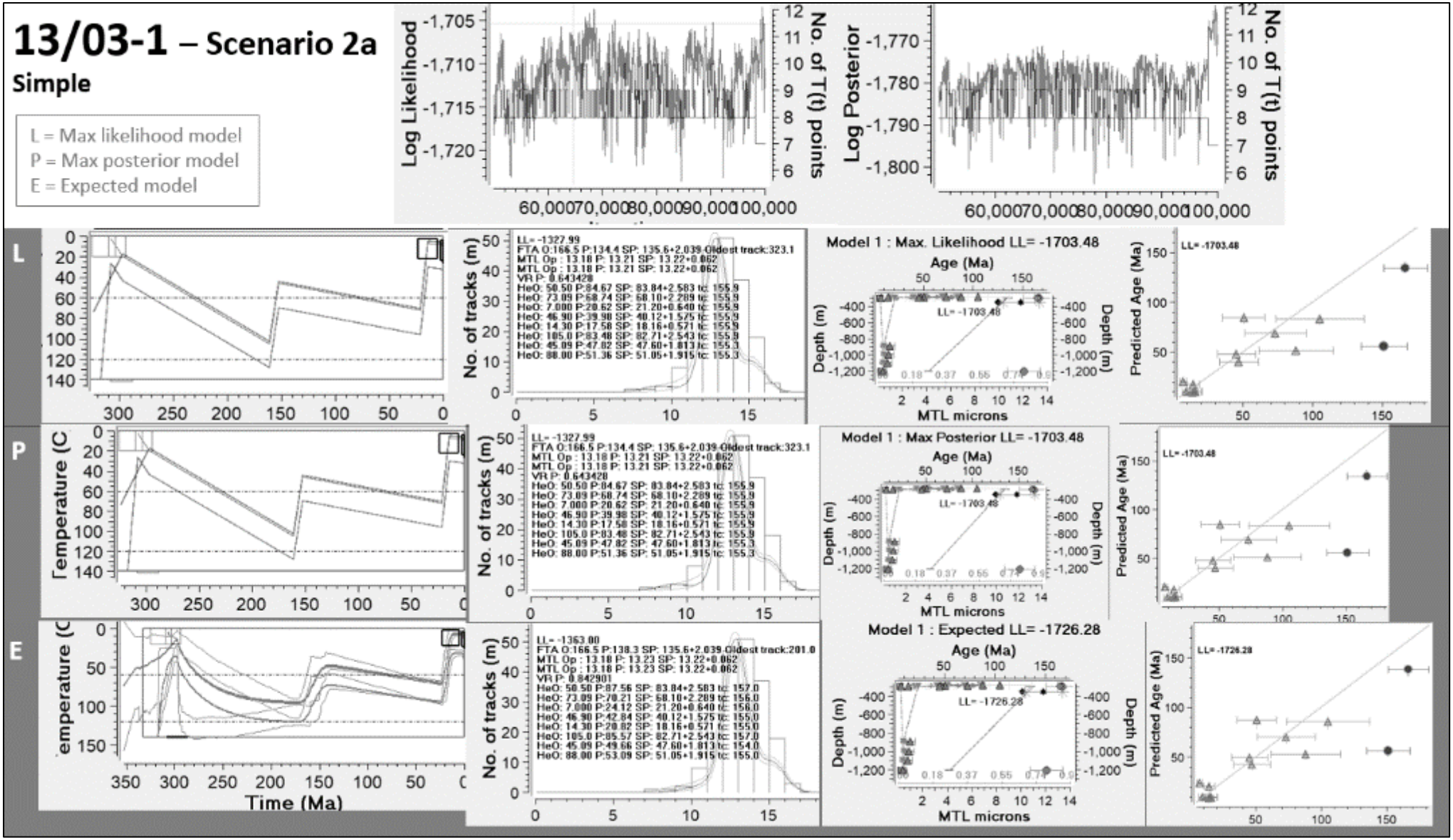
13/03-1 – Scenario 2a
Simple
L = Max likelihood model
P = Max posterior model
E = Expected model
Log Likelihood
No. of T(t) points
Log Posterior
No. of T(t) points
L
P
E
Temperature (C
Time (Ma)
No. of tracks (m)
Model 1 : Max. Likelihood LL= -1703.48
Model 1 : Max Posterior LL= -1703.48
Model 1 : Expected LL= -1726.28
Age (Ma)
Depth (m)
MTL microns
Predicted Age (Ma)

13/03-1 – Scenario 3a

Simple

L = Max likelihood model
P = Max posterior model
E = Expected model

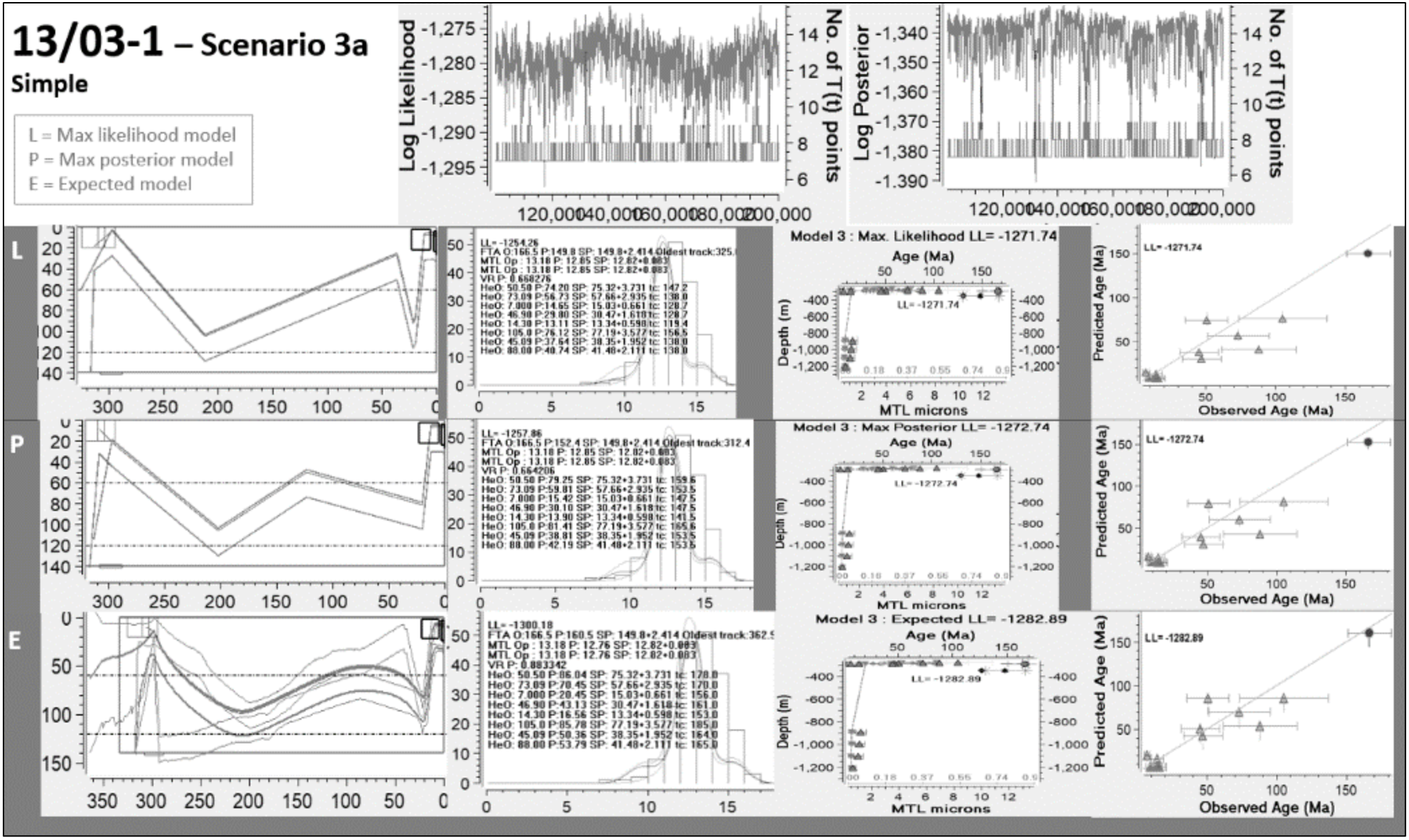

13/03-1 – Scenario 4a

Simple

L = Max likelihood model
P = Max posterior model
E = Expected model

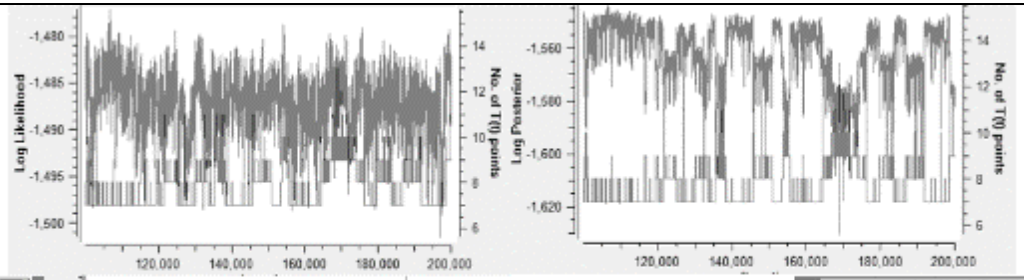

L

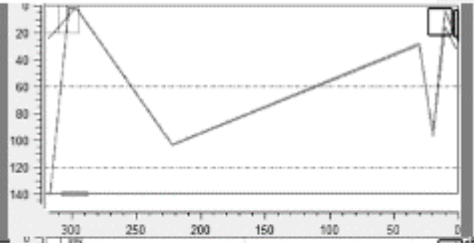

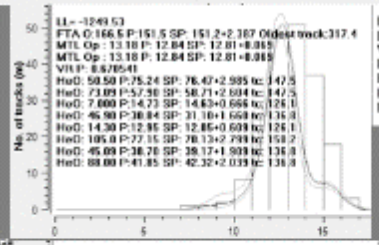

LL= -227.60
FTA O:151.1 P:144.3 SP: 137.5+4.776 Oldest track:226.2
VR P: 0.676853
HeO: 15.90 P:10.27 SP: 9.832+0.669 tc: 16.62
HeO: 8.900 P:10.36 SP: 9.921+0.673 tc: 16.62
HeO: 13.70 P:9.768 SP: 9.331+0.645 tc: 16.15
HeO: 15.00 P:10.74 SP: 10.31+0.672 tc: 16.62

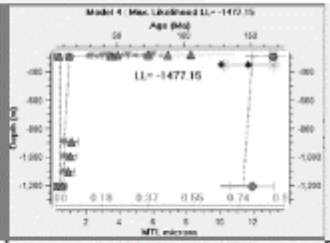

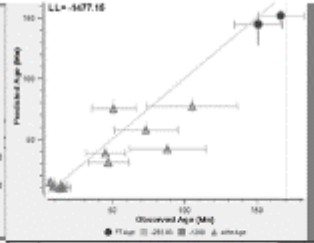

P

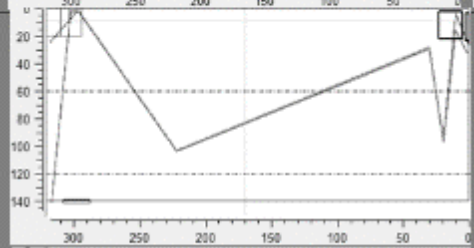

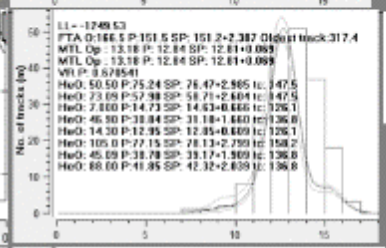

LL= -227.60
FTA O:151.1 P:144.3 SP: 137.5+4.776 Oldest track:226.2
VR P: 0.676853
HeO: 15.90 P:10.27 SP: 9.832+0.669 tc: 16.62
HeO: 8.900 P:10.36 SP: 9.921+0.673 tc: 16.62
HeO: 13.70 P:9.768 SP: 9.331+0.645 tc: 16.15
HeO: 15.00 P:10.74 SP: 10.31+0.672 tc: 16.62

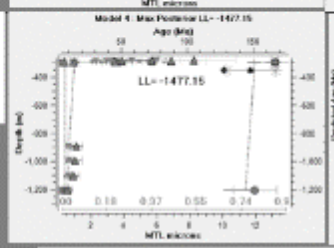

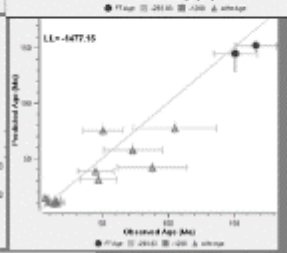

E

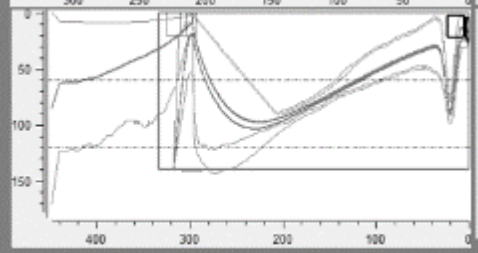

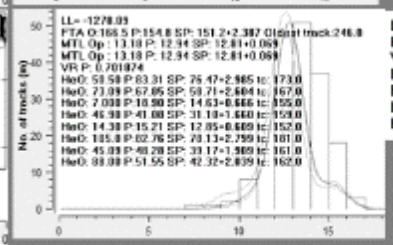

LL= -229.31
FTA O:151.1 P:141.2 SP: 137.5+4.776 Oldest track:217.0
VR P: 0.736051
HeO: 15.90 P:9.710 SP: 9.832+0.669 tc: 15.00
HeO: 8.900 P:9.799 SP: 9.921+0.673 tc: 15.00
HeO: 13.70 P:9.210 SP: 9.331+0.645 tc: 15.00
HeO: 15.00 P:10.22 SP: 10.31+0.672 tc: 16.00

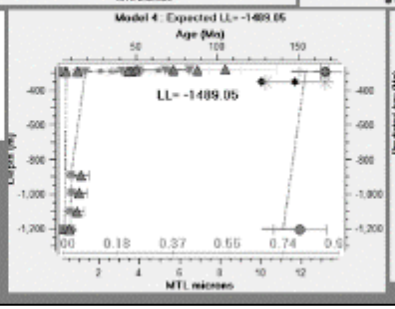

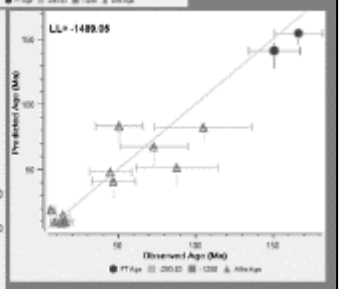

2.3 Central zone

2.3.1 16/28-sb01

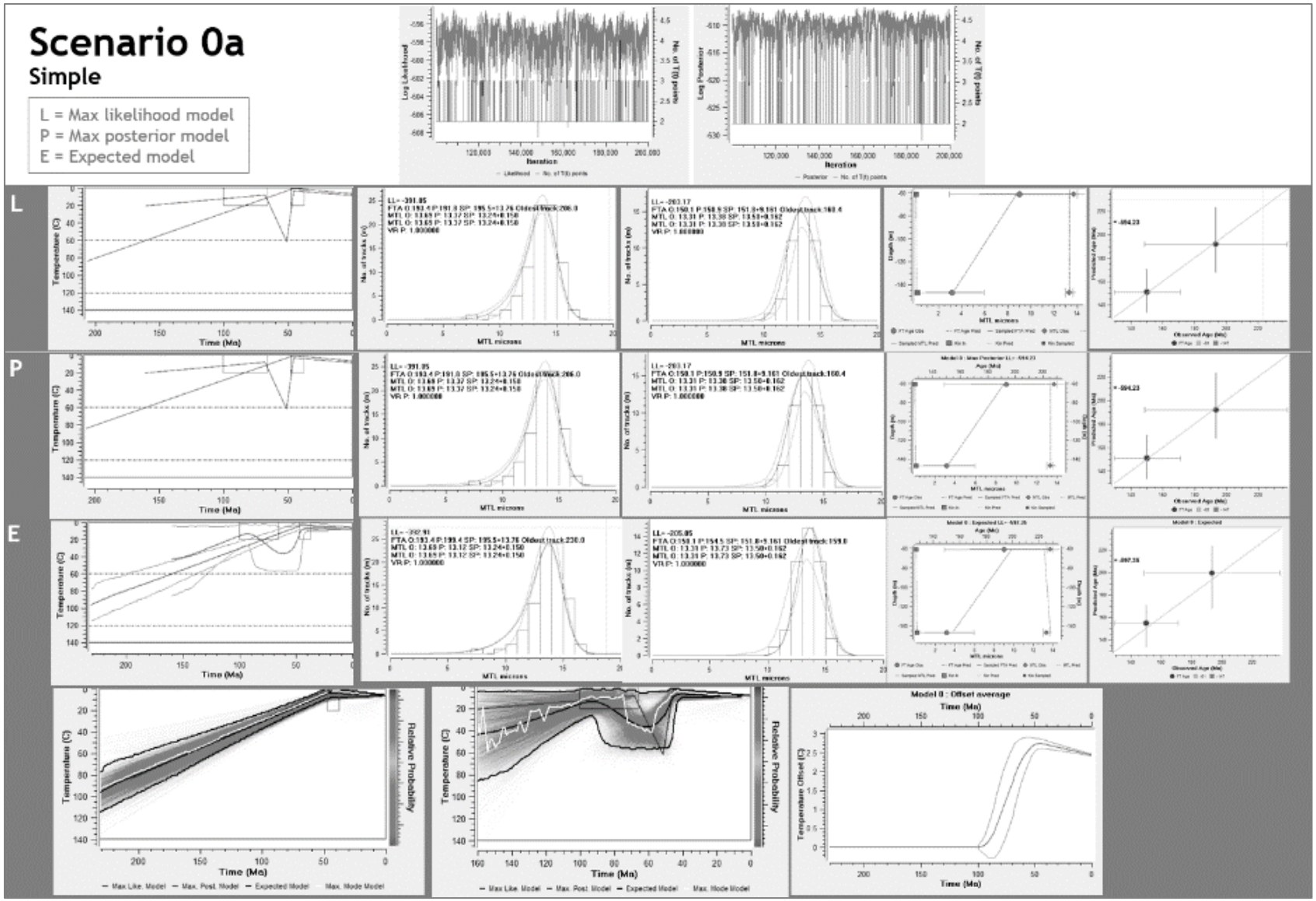

Scenario 0b

Complex

L = Max likelihood model
P = Max posterior model
E = Expected model

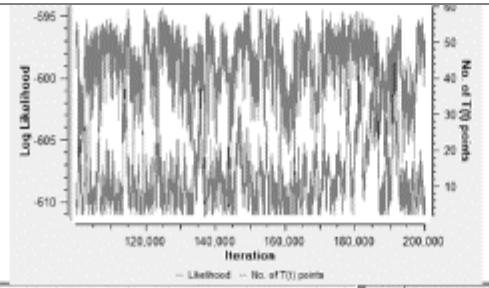

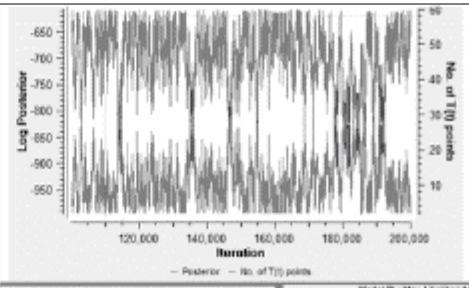

L

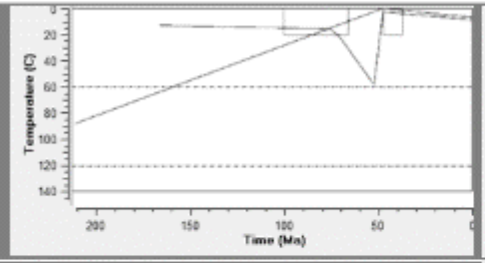

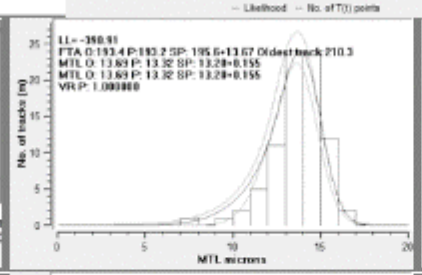

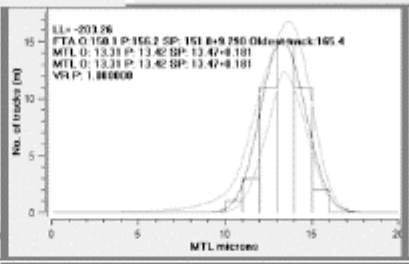

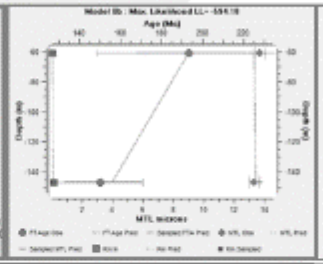

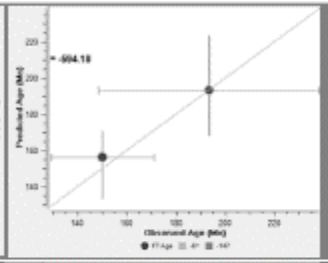

P

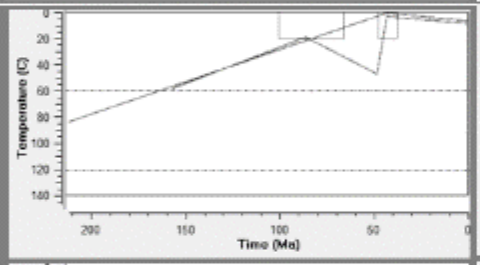

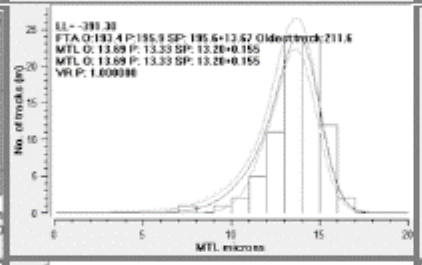

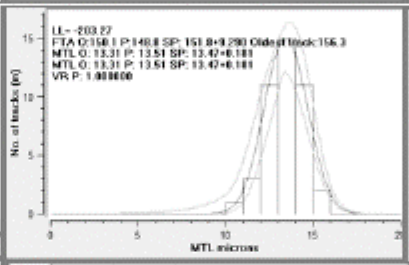

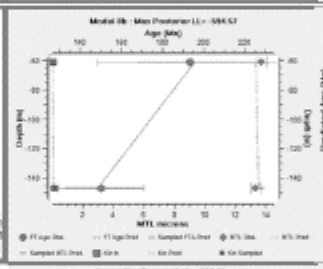

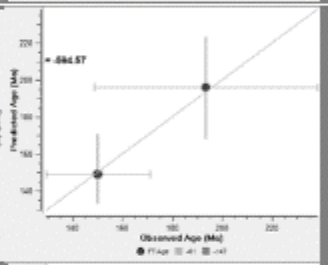

E

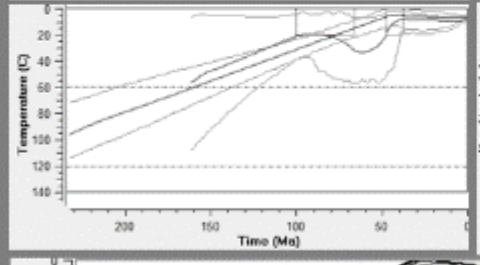

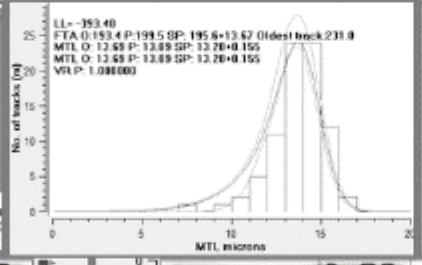

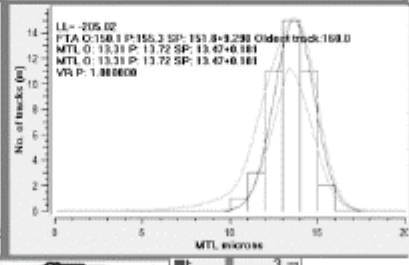

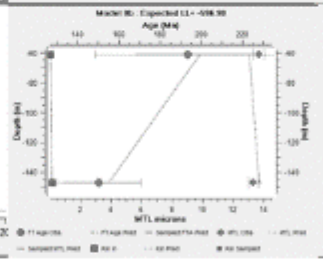

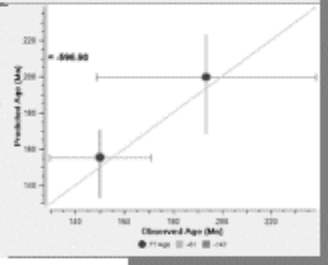

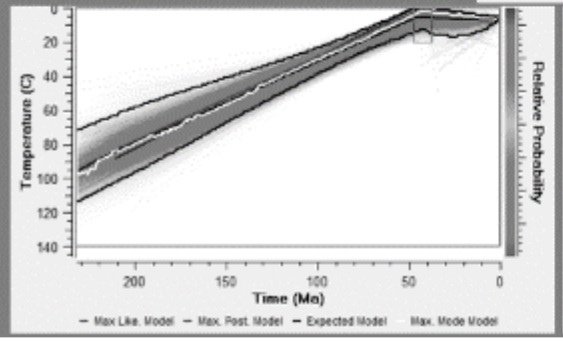

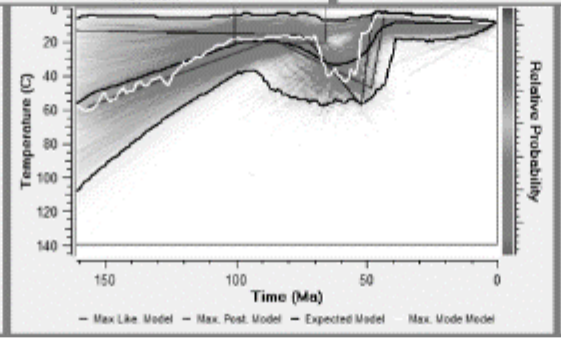

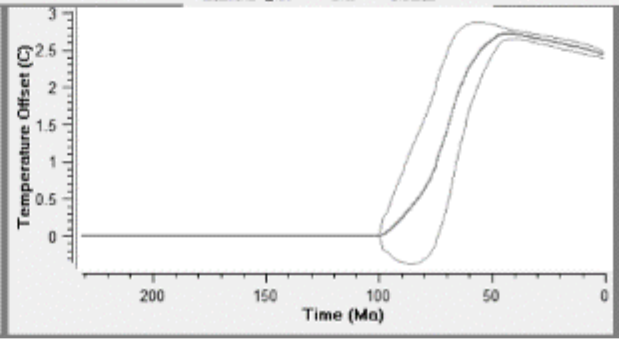

Scenario 1a

Simple

L = Max likelihood model
P = Max posterior model
E = Expected model

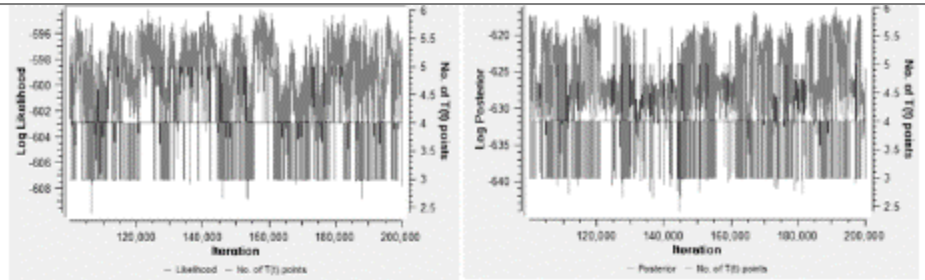

L

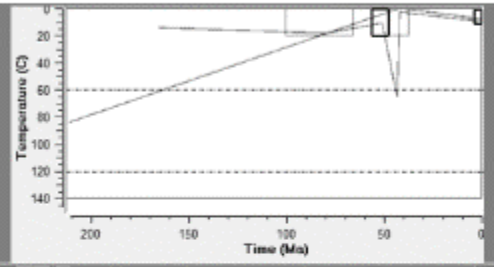

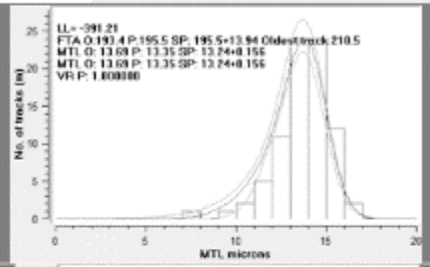

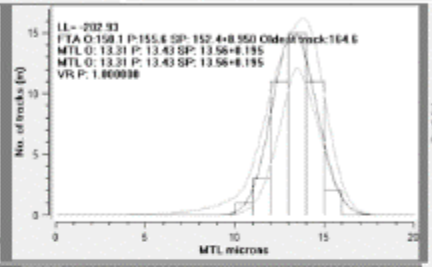

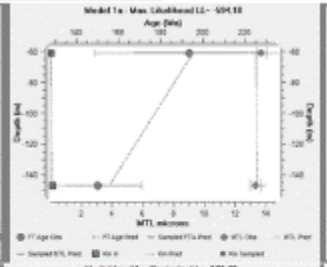

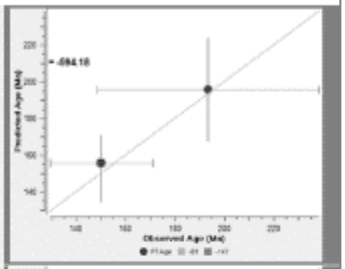

P

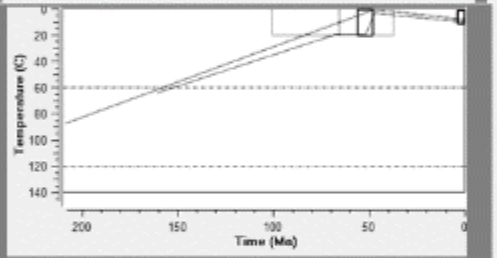

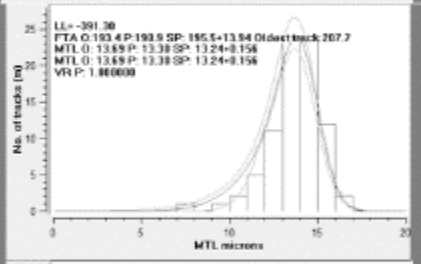

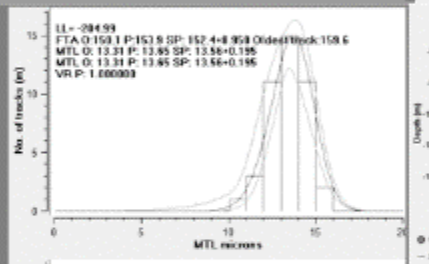

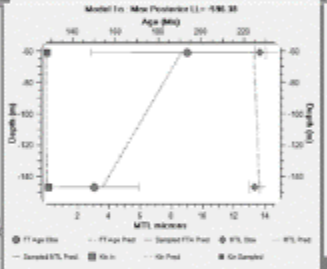

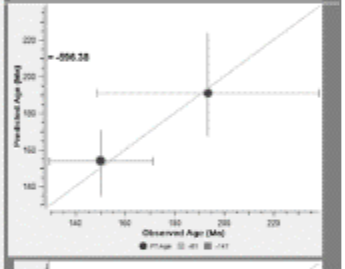

E

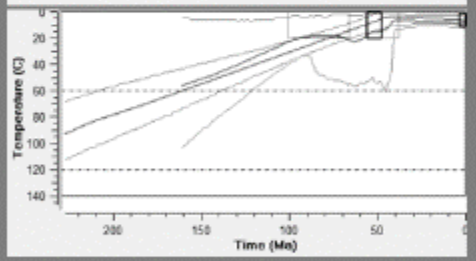

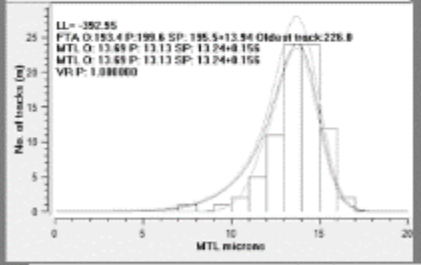

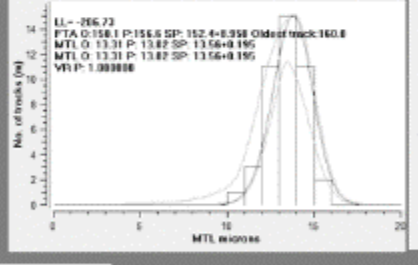

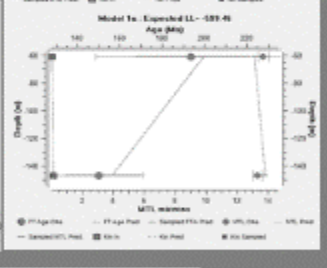

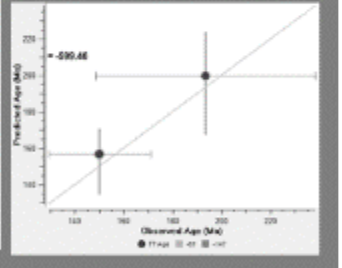

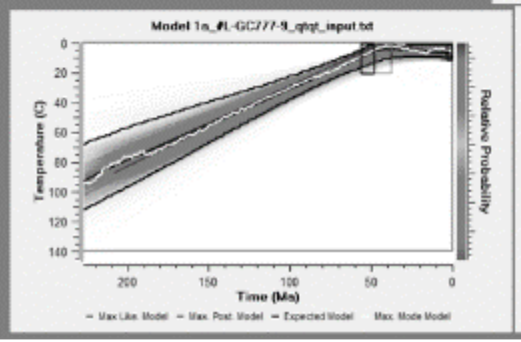

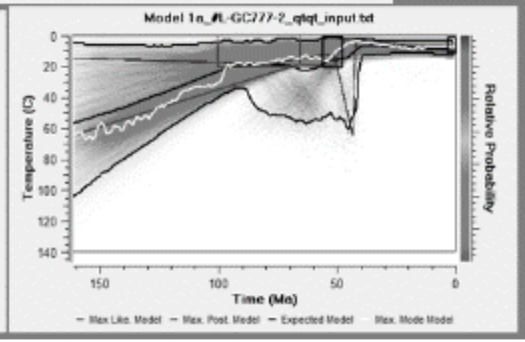

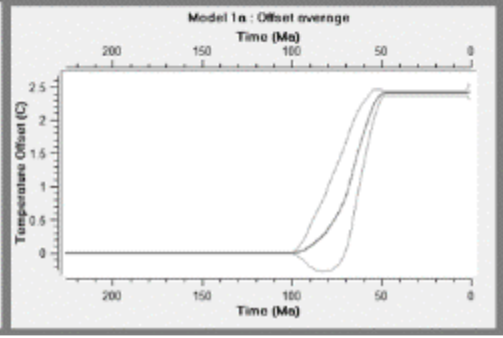

Scenario 1b

Complex

L = Max likelihood model
P = Max posterior model
E = Expected model

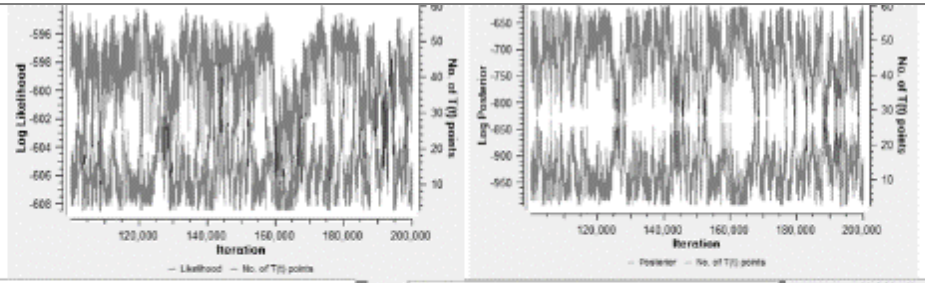

L

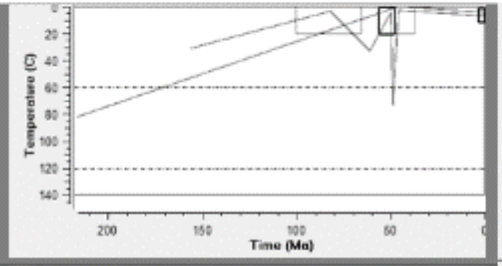

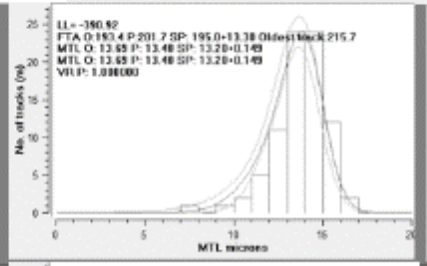

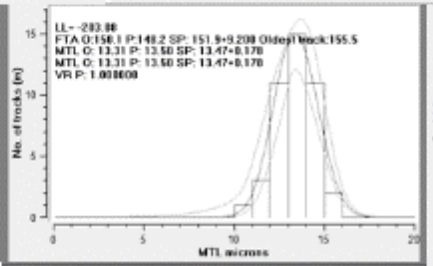

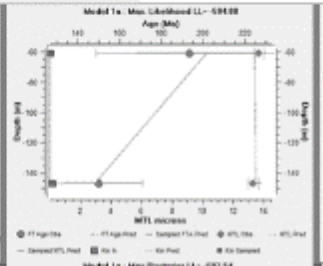

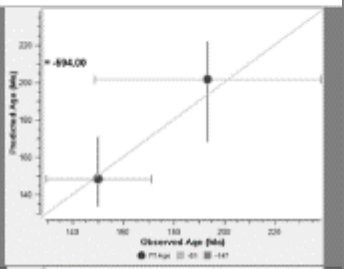

P

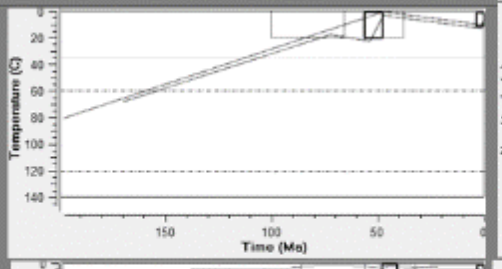

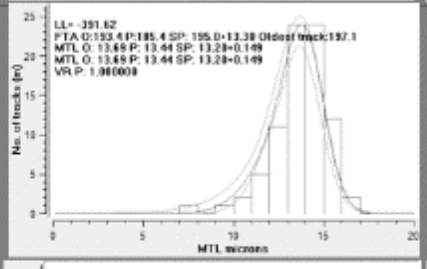

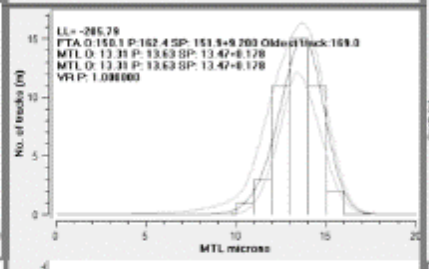

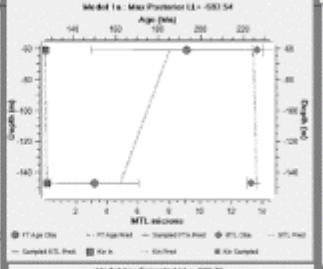

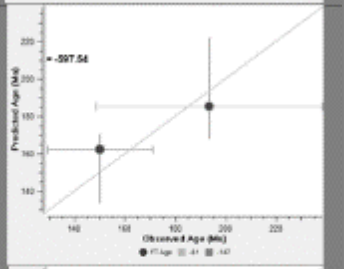

E

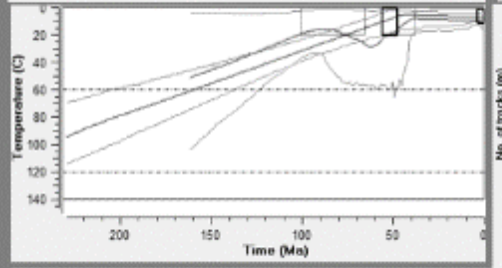

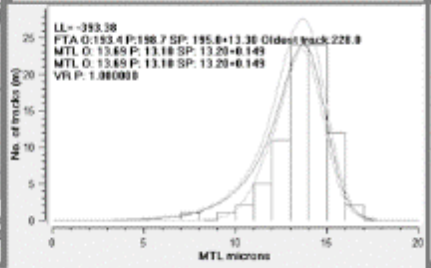

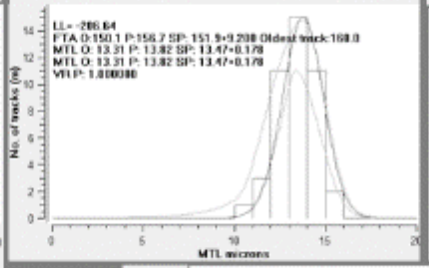

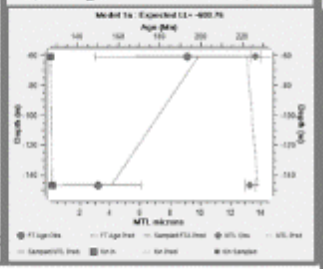

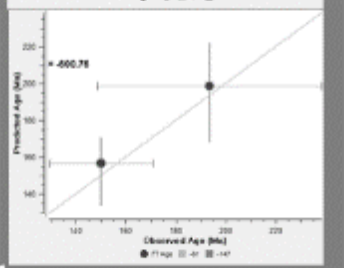

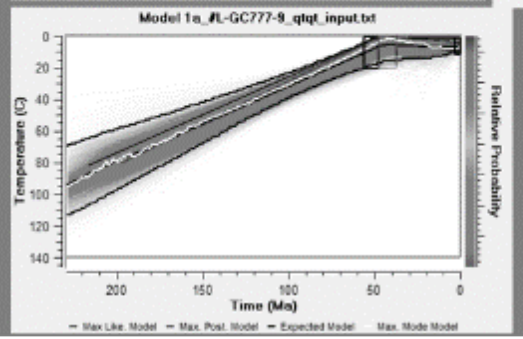

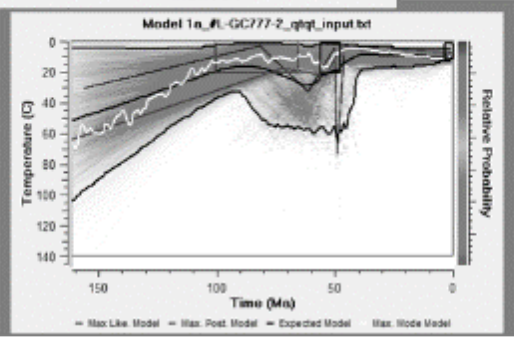

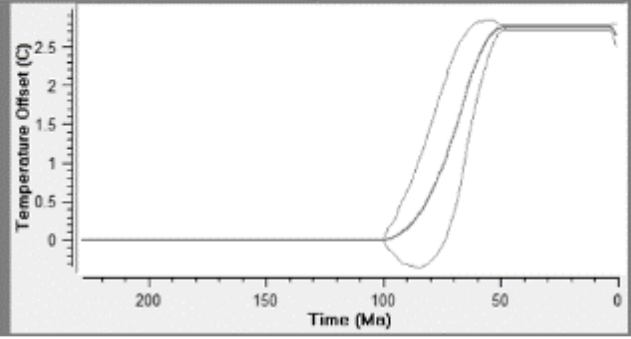

Scenario 2a

Simple

L = Max likelihood model
P = Max posterior model
E = Expected model

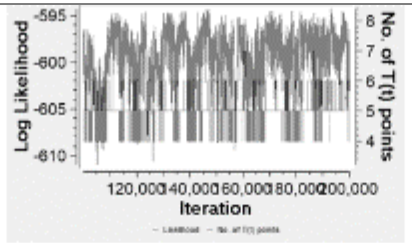

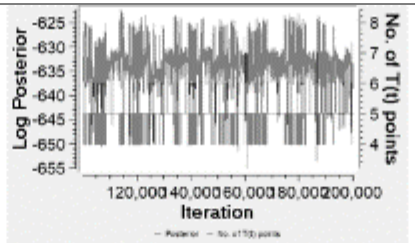

L

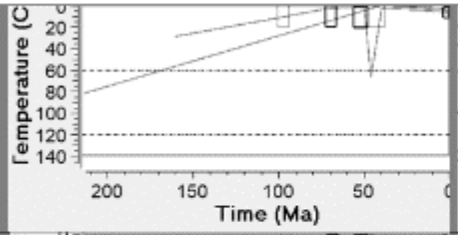

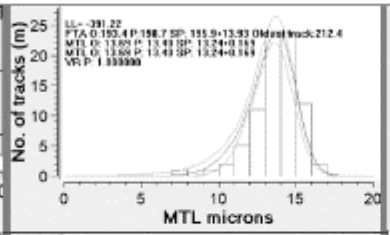

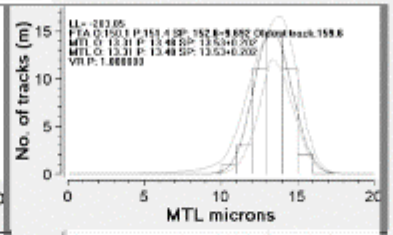

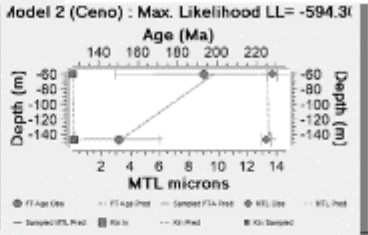

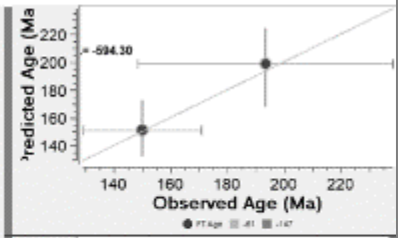

P

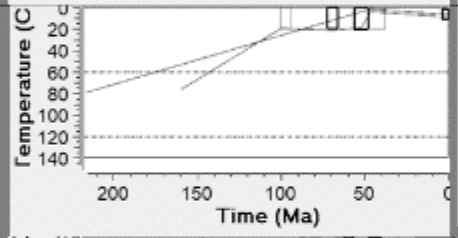

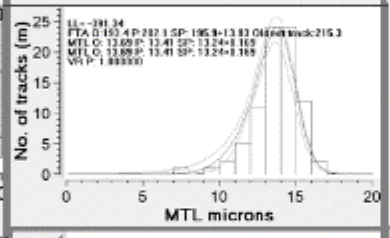

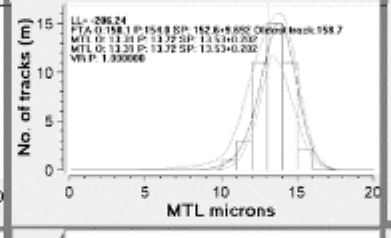

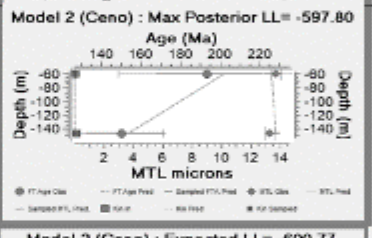

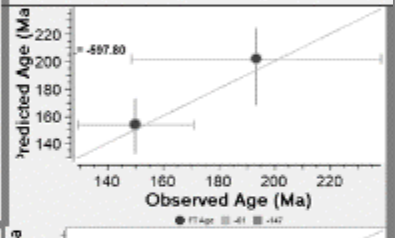

E

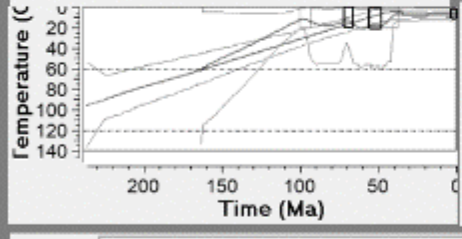

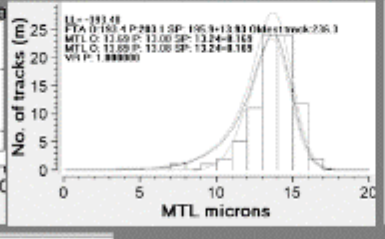

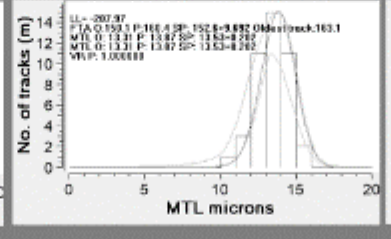

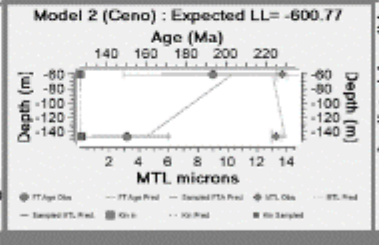

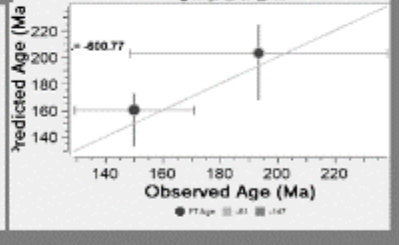

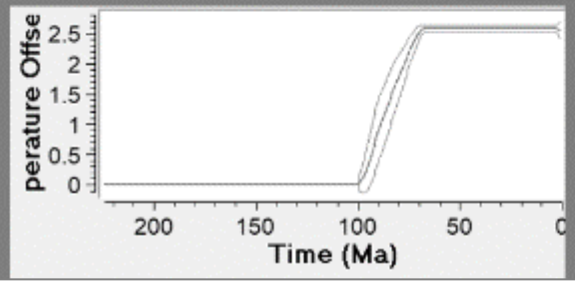

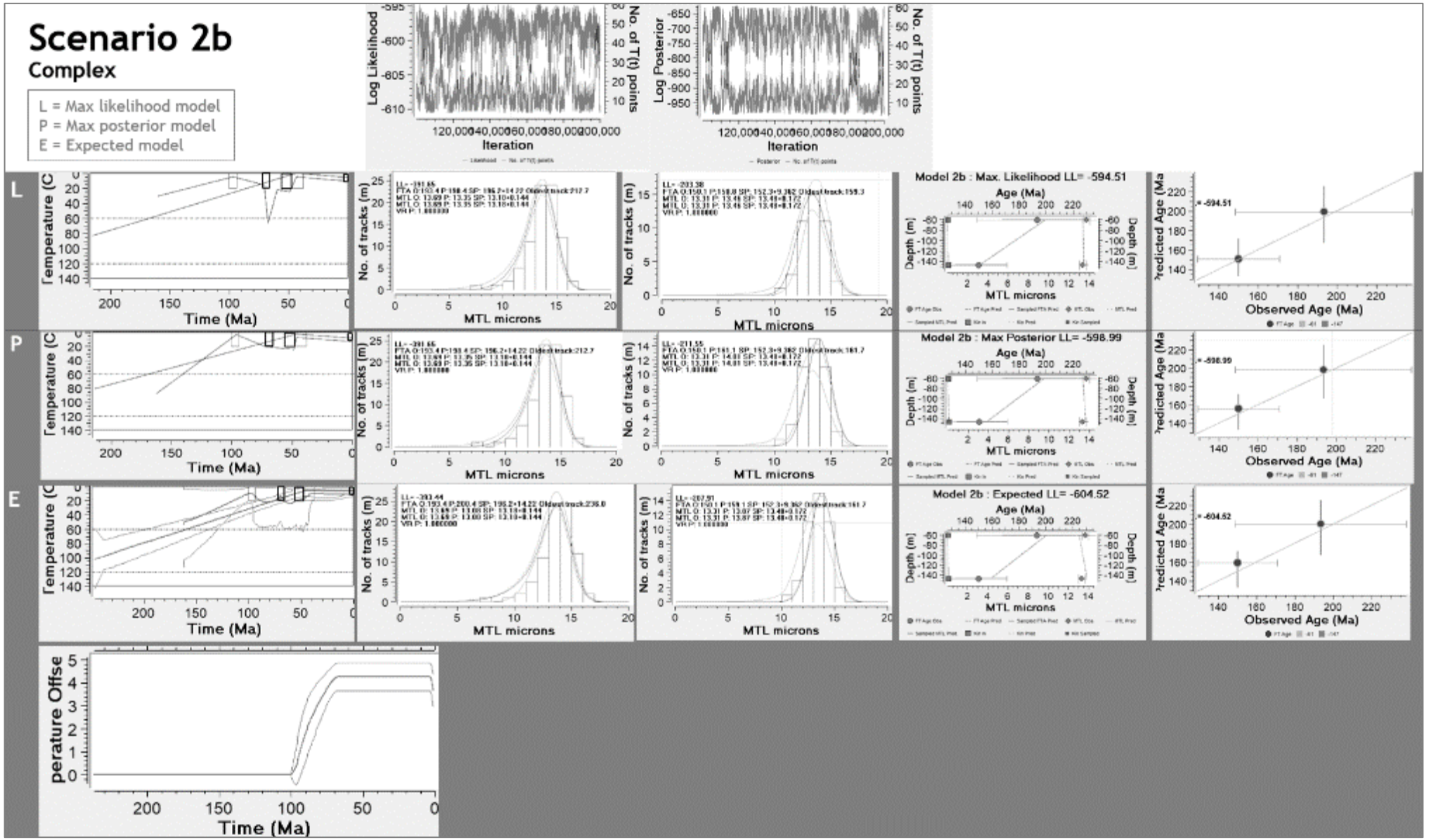
Scenario 2b
Complex
L = Max likelihood model
P = Max posterior model
E = Expected model
Log Likelihood
No. of T(t) points
Iteration
Log Posterior
No. of T(t) points
Iteration
L
P
E
Temperature (C
Time (Ma)
No. of tracks (m)
MTL microns
Model 2b : Max. Likelihood LL= -594.51
Model 2b : Max Posterior LL= -598.99
Model 2b : Expected LL= -604.52
Age (Ma)
Depth (m)
MTL microns
Predicted Age (Ma)
Observed Age (Ma)
-594.51
-598.99
-604.52
perature Offse
Time (Ma)

Scenario 3a

Simple

L = Max likelihood model
P = Max posterior model
E = Expected model

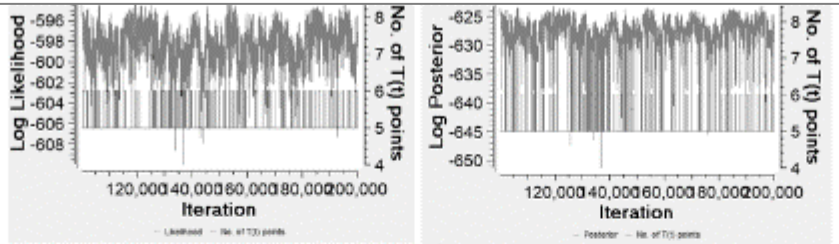

L

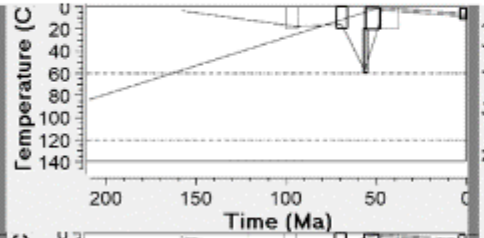

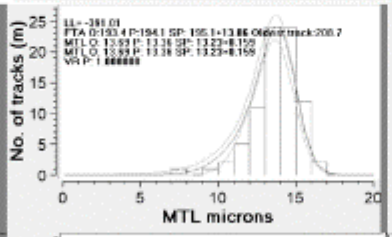

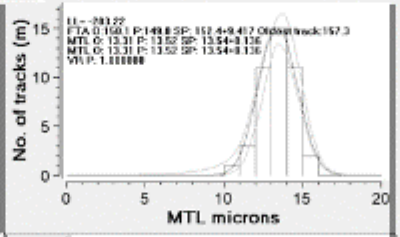

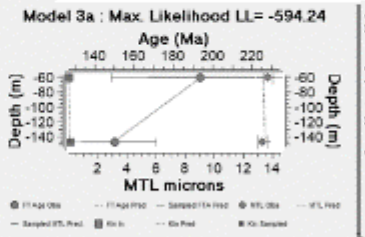

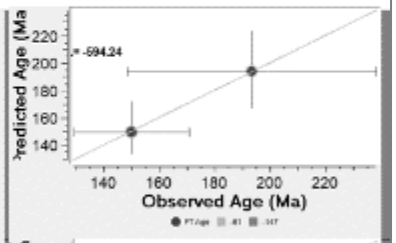

P

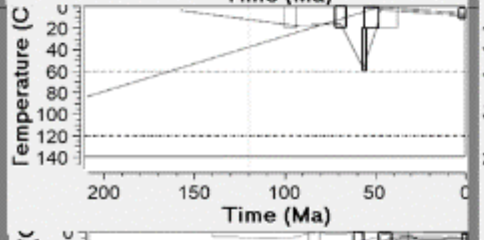

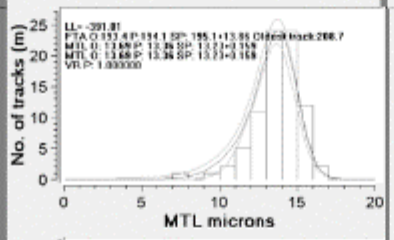

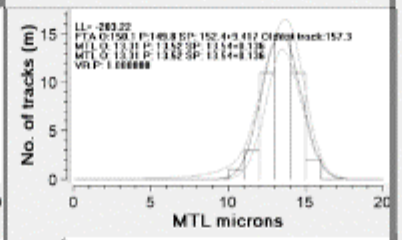

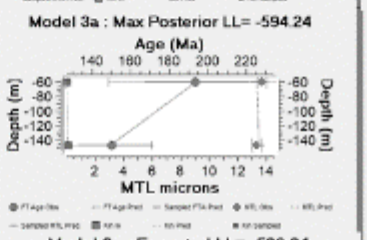

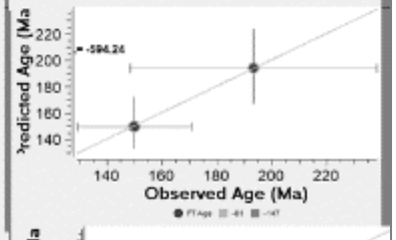

E

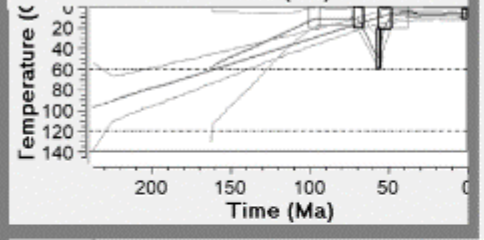

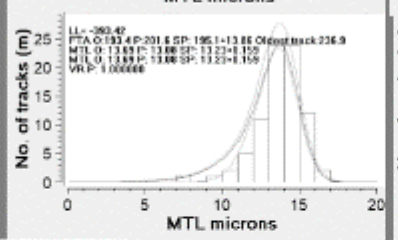

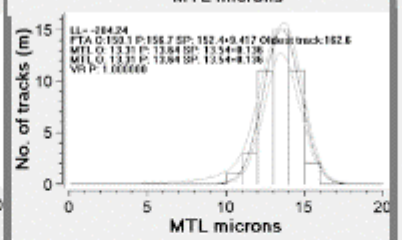

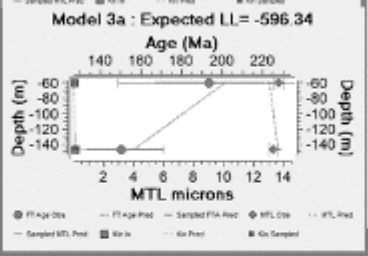

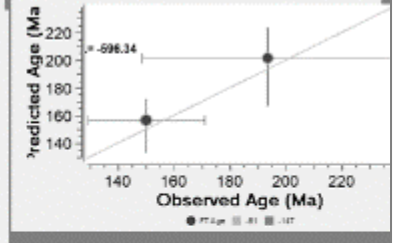

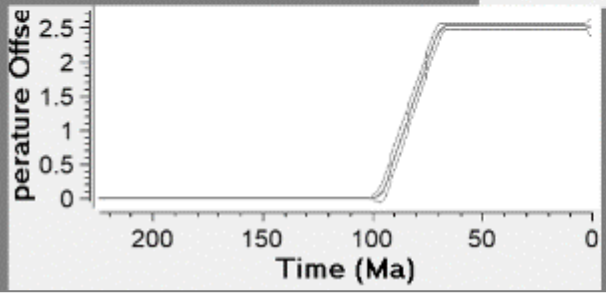

Scenario 3b

Simple

L = Max likelihood model
P = Max posterior model
E = Expected model

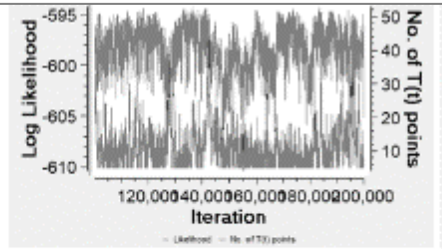

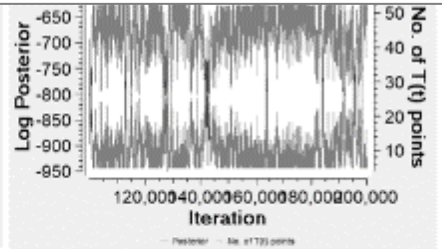

L

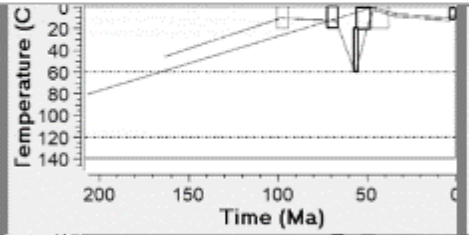

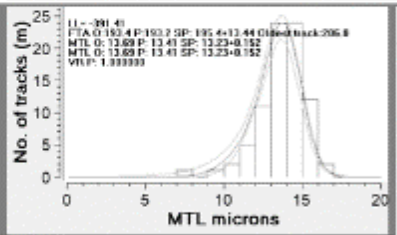

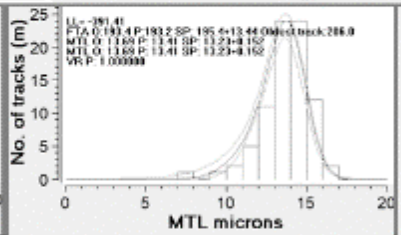

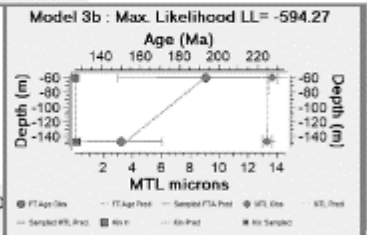

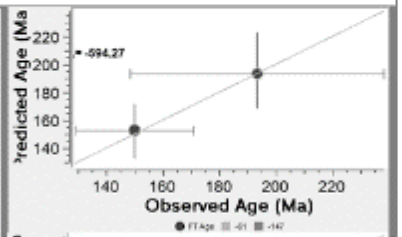

P

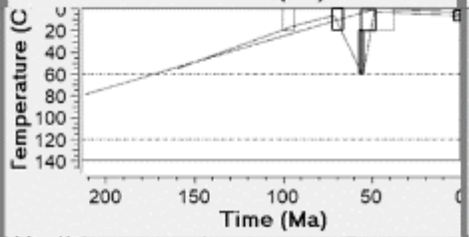

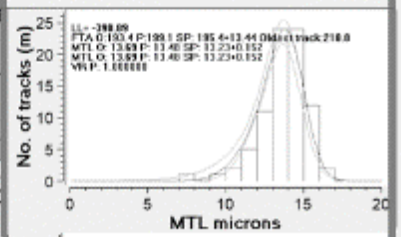

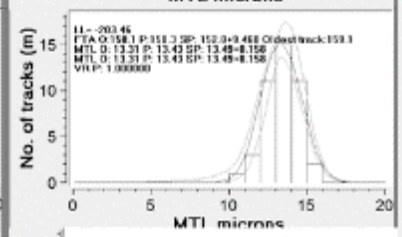

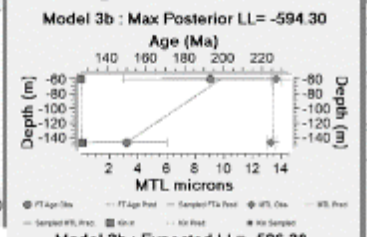

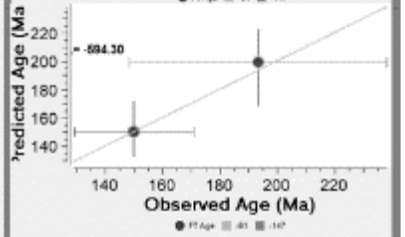

E

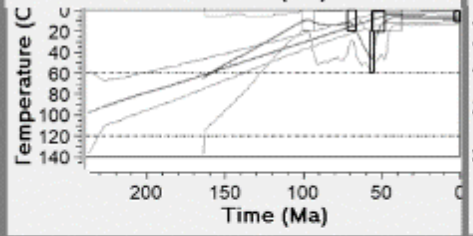

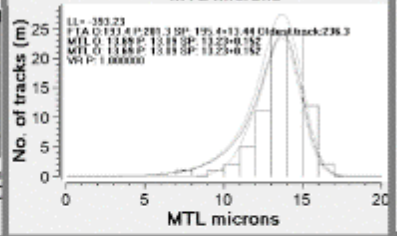

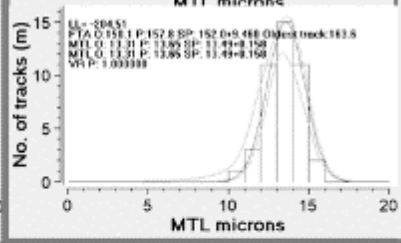

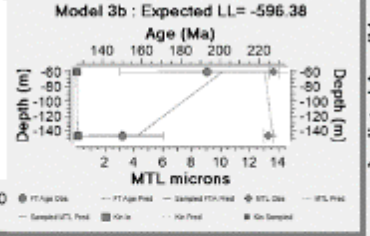

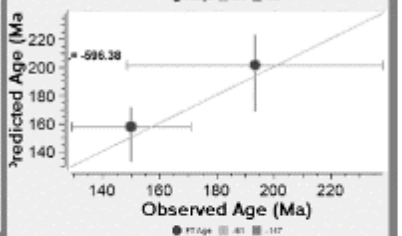

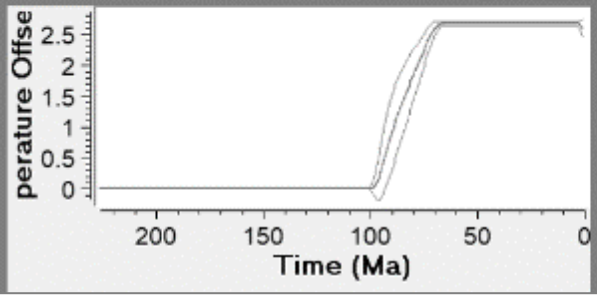

2.3.2 26/26-1

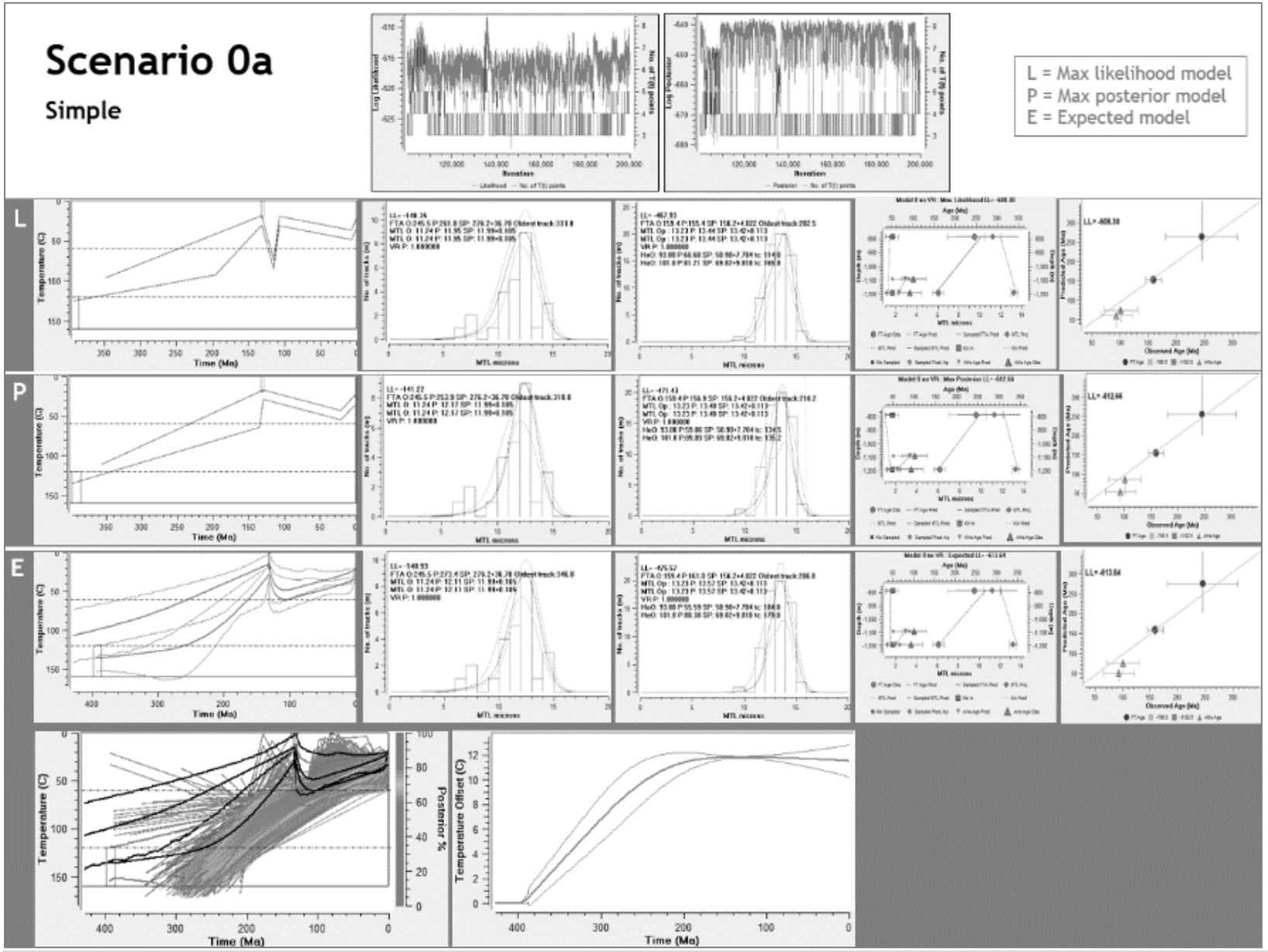
Scenario 0a
Simple
L = Max likelihood model
P = Max posterior model
E = Expected model
L
P
E
Temperature (C)
Time (Ma)
MTL microns
Observed Age (Ma)
Predicted Age (Ma)
Temperature Offset (C)
% Posterior

Scenario 0b

Complex

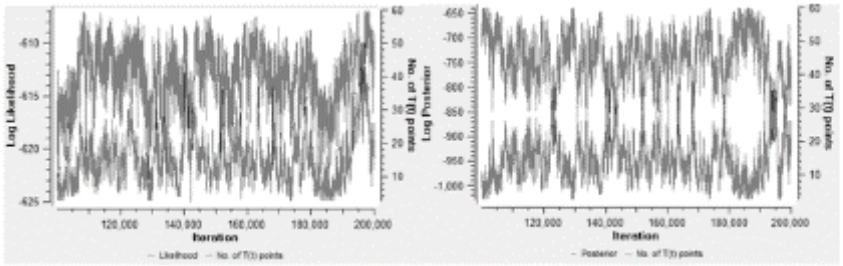

L = Max likelihood model
P = Max posterior model
E = Expected model

L

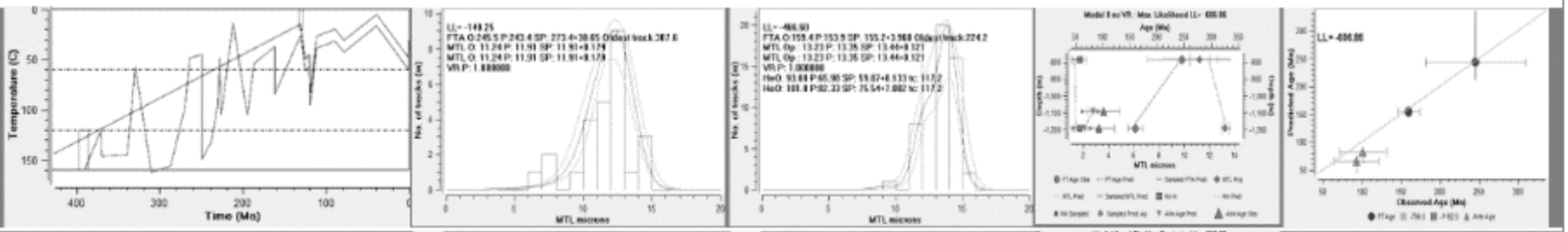

P

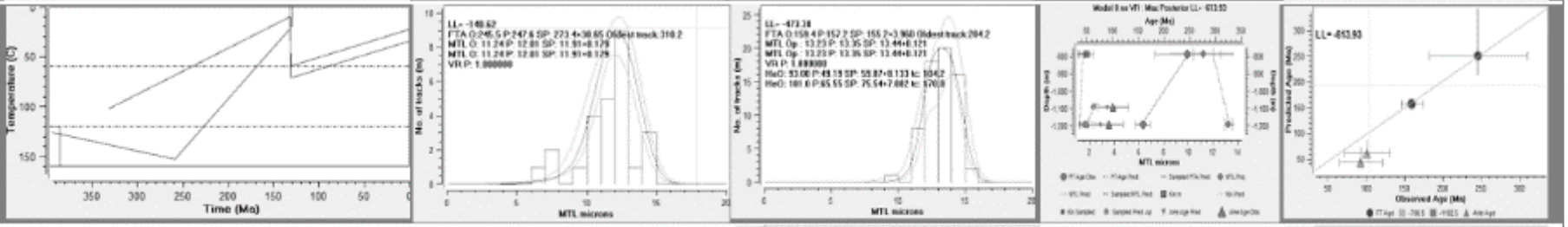

E

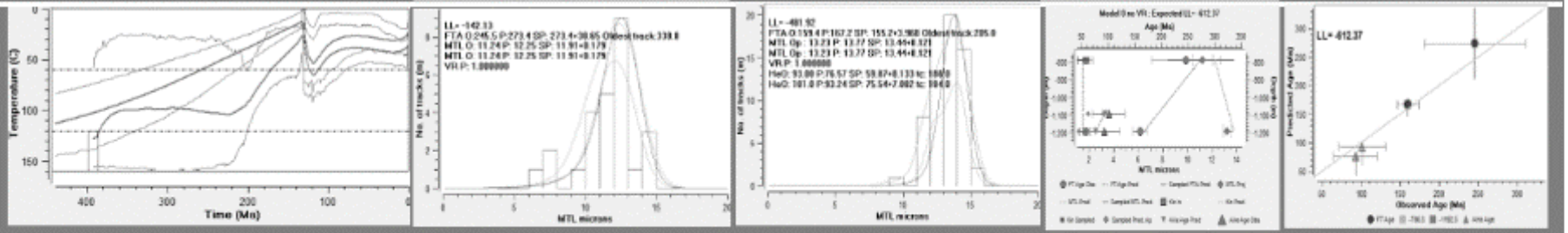

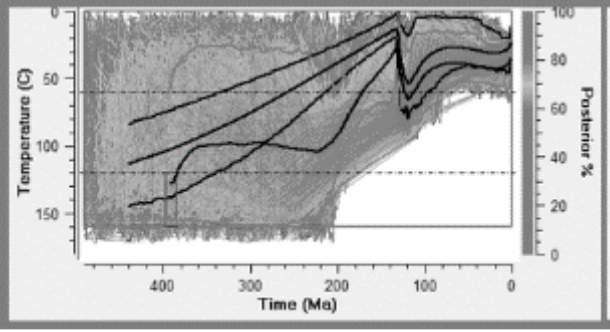

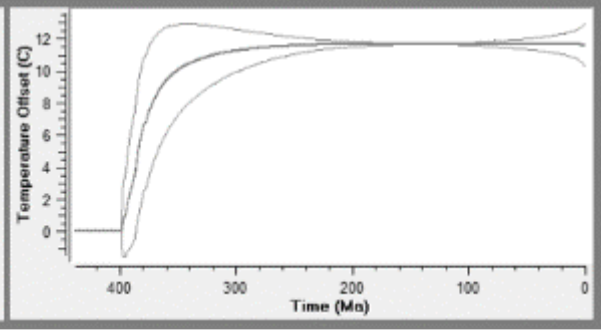

Scenario 1a

Simple

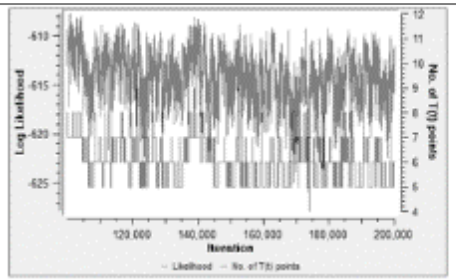

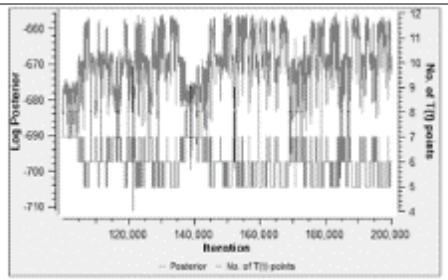

L = Max likelihood model
P = Max posterior model
E = Expected model

L

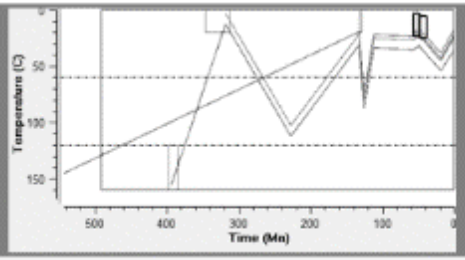

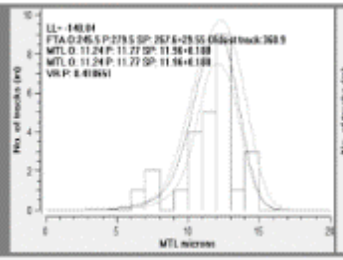

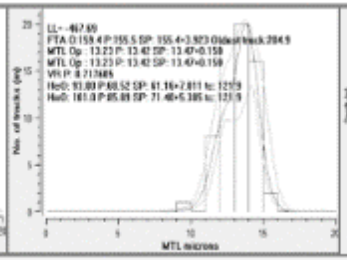

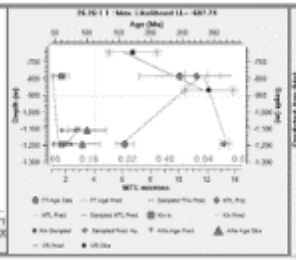

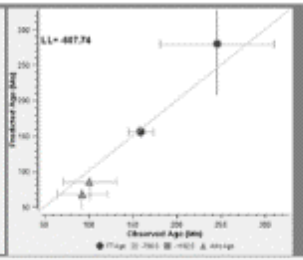

P

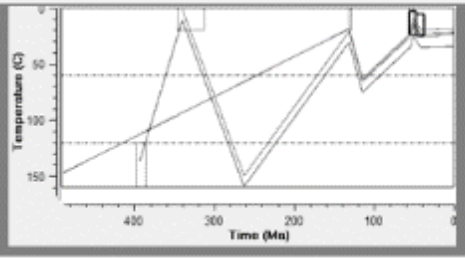

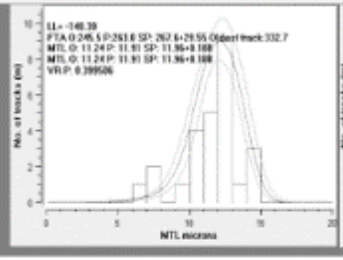

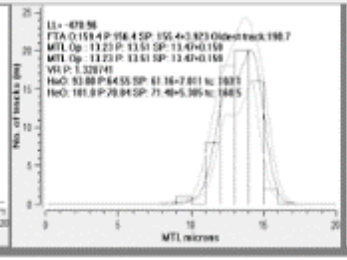

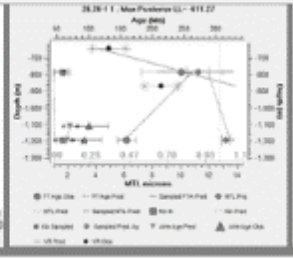

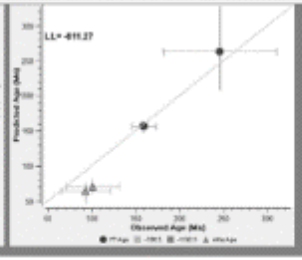

E

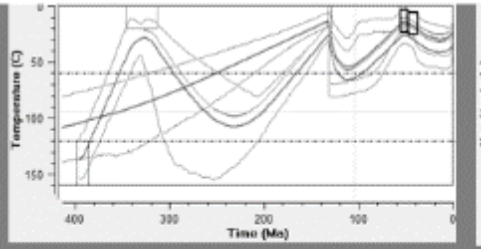

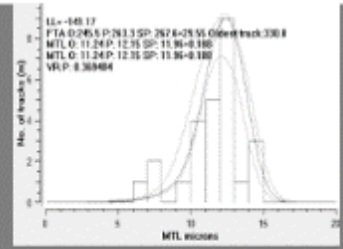

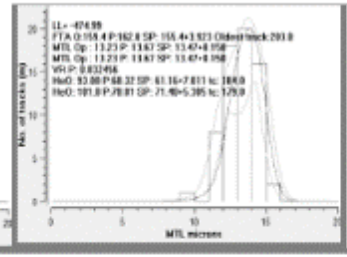

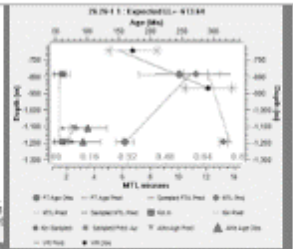

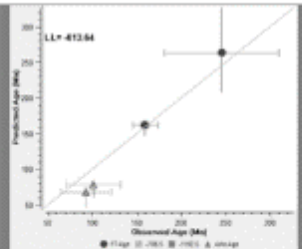

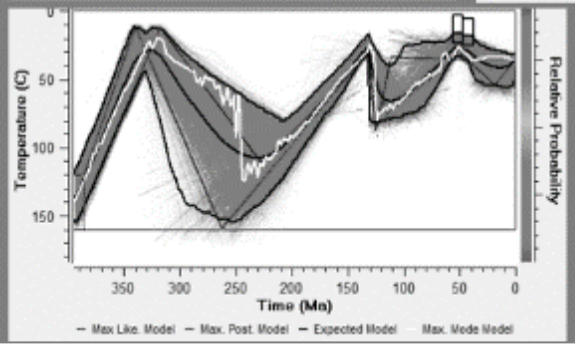

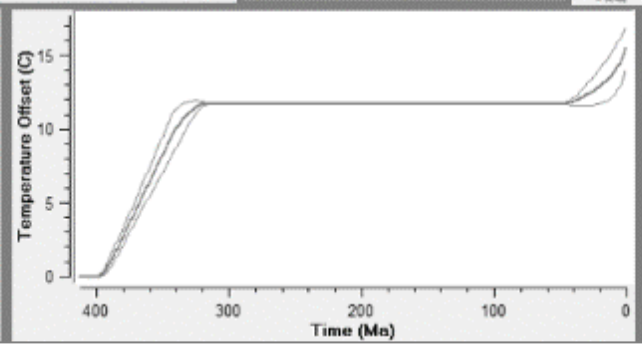

Scenario 1b

Complex

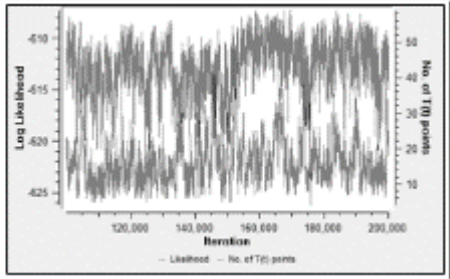

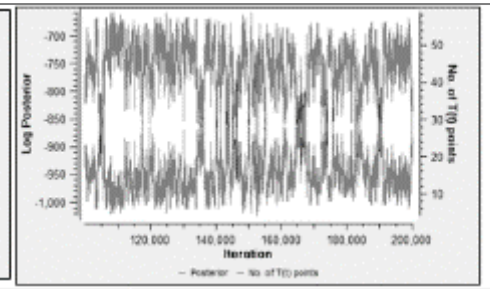

L = Max likelihood model
P = Max posterior model
E = Expected model

L

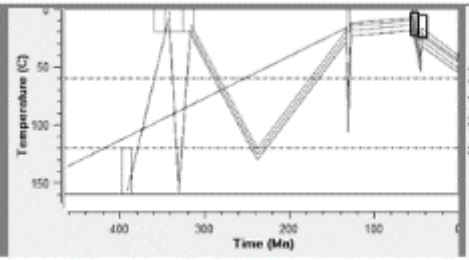

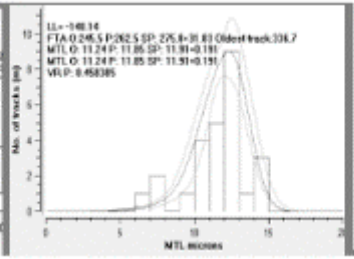

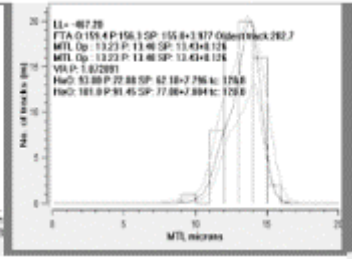

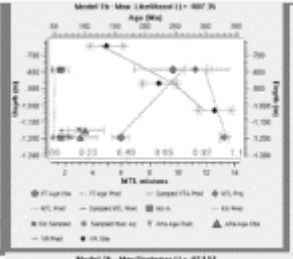

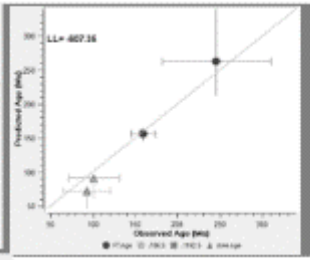

P

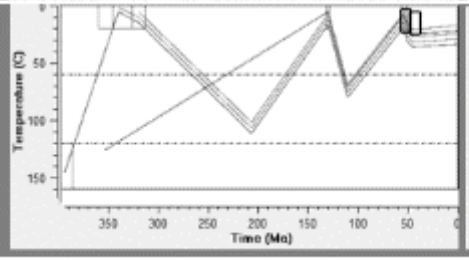

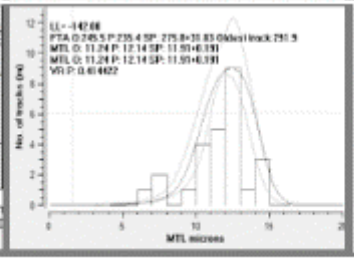

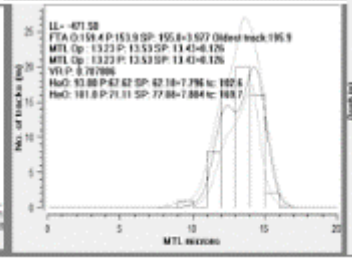

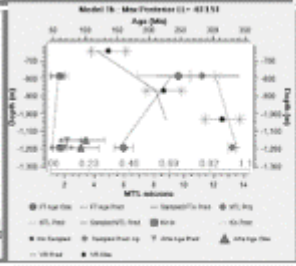

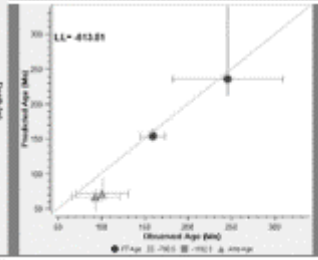

E

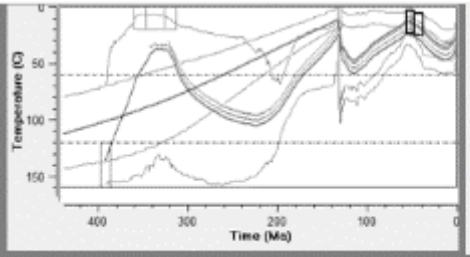

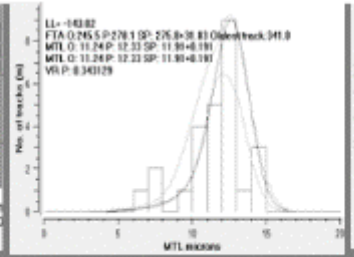

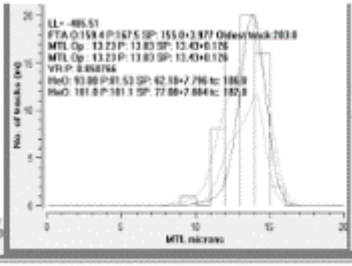

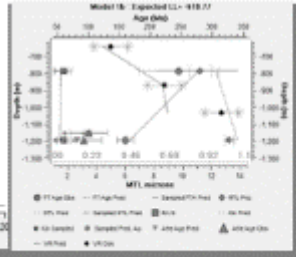

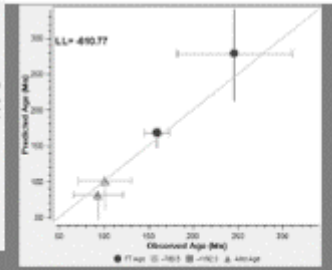

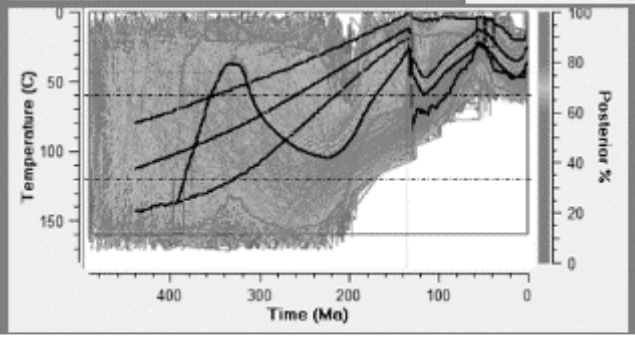

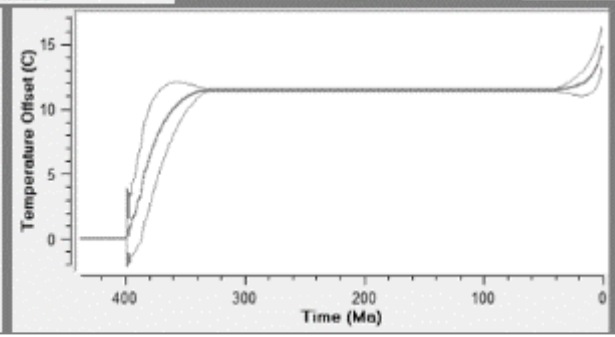

Scenario 2a

Simple

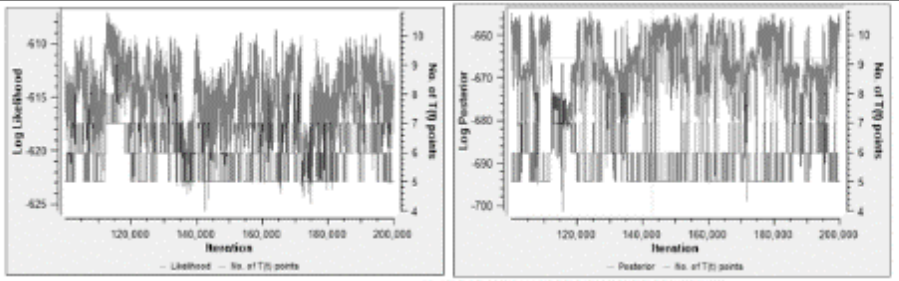

L = Max likelihood model
P = Max posterior model
E = Expected model

L

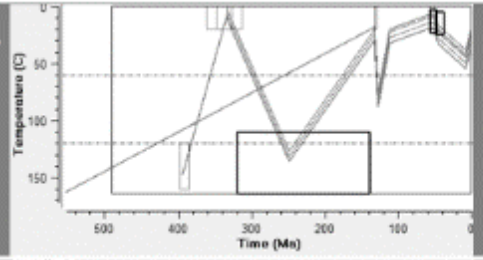

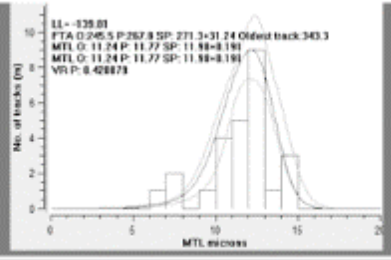

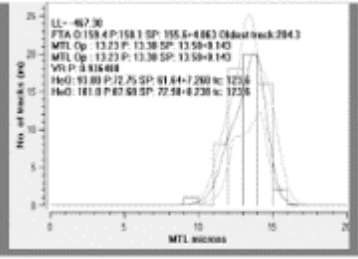

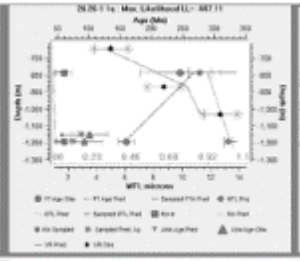

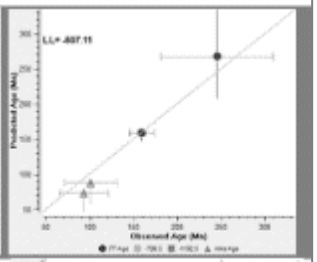

P

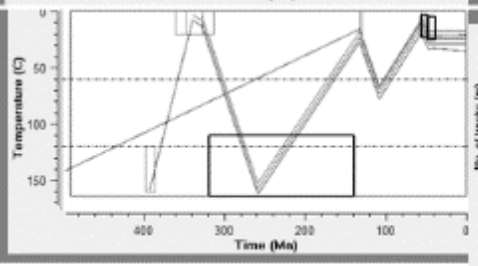

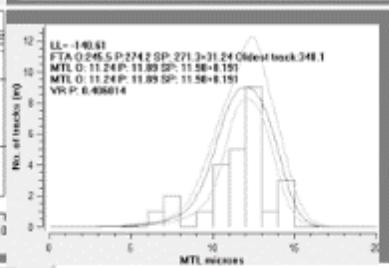

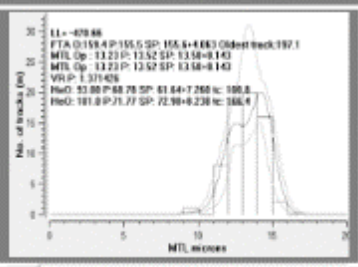

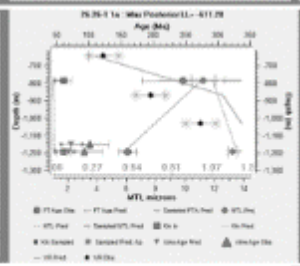

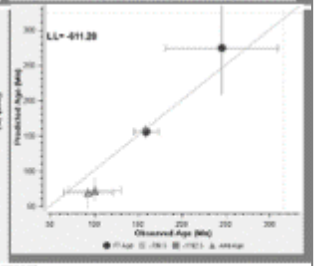

E

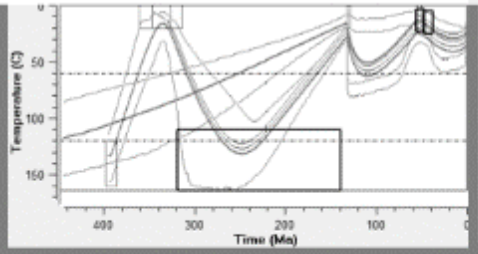

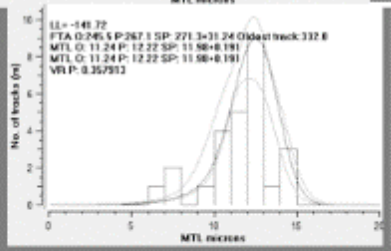

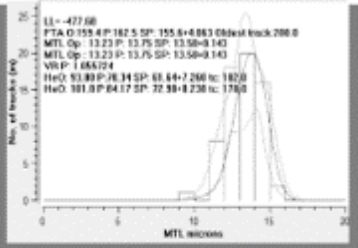

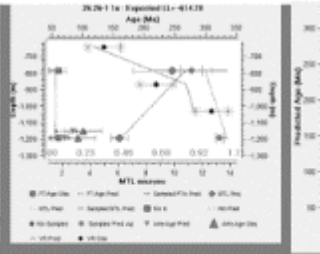

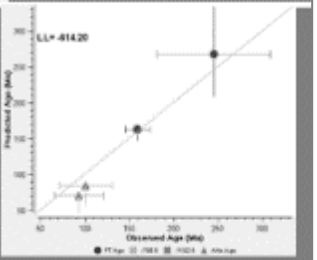

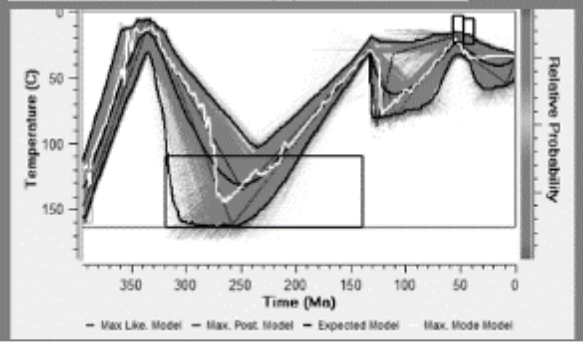

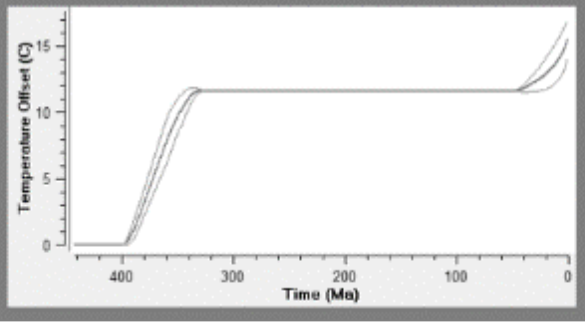

Scenario 2b

No lengths in top sample
Complex

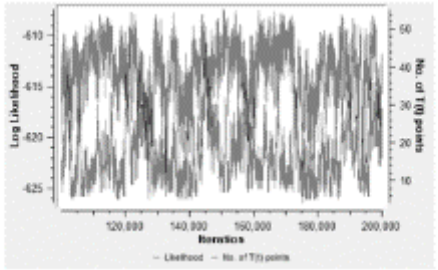

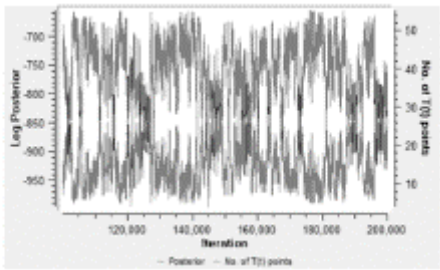

L = Max likelihood model
P = Max posterior model
E = Expected model

L

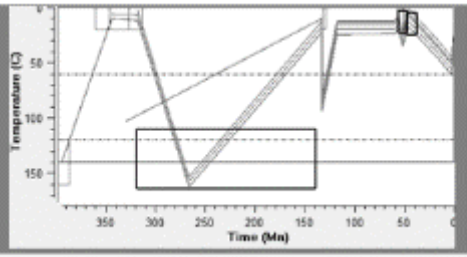

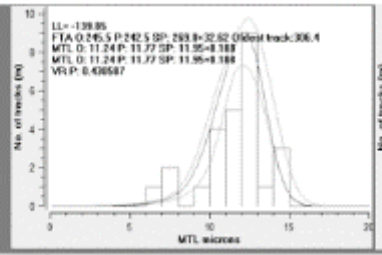

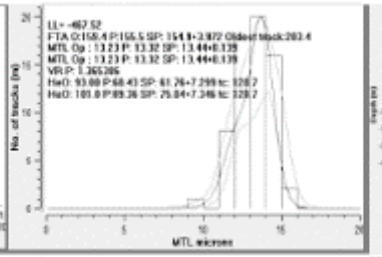

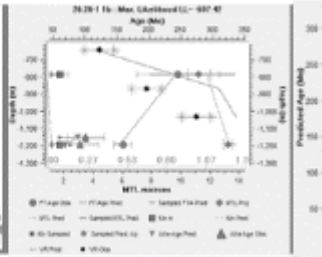

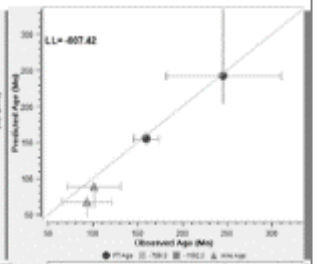

P

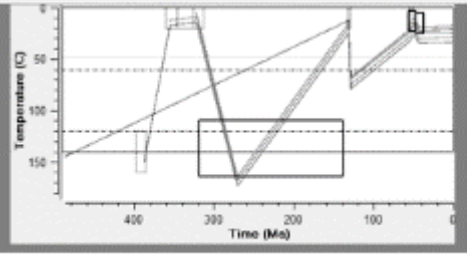

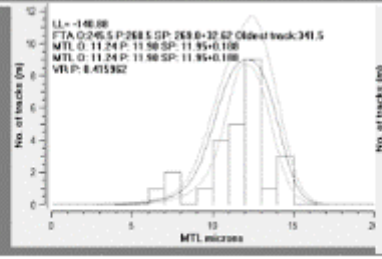

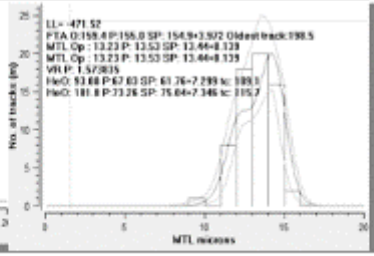

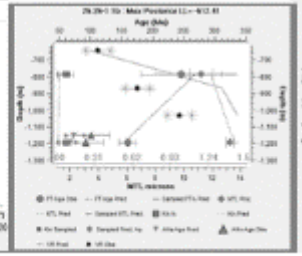

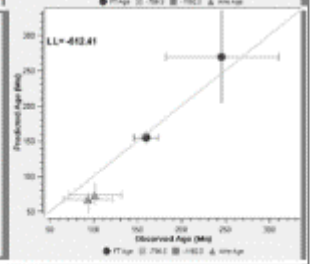

E

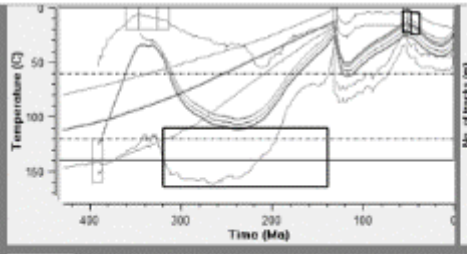

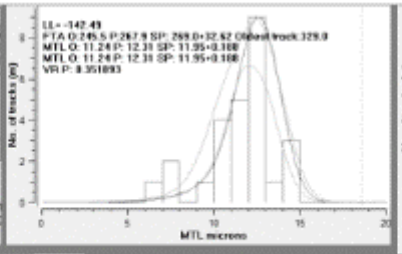

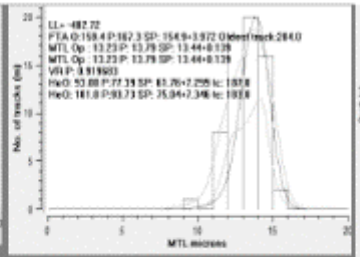

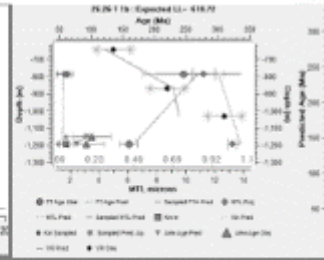

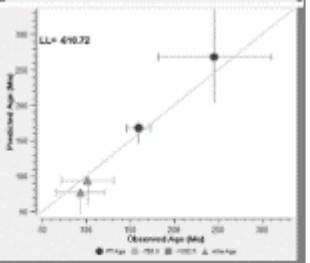

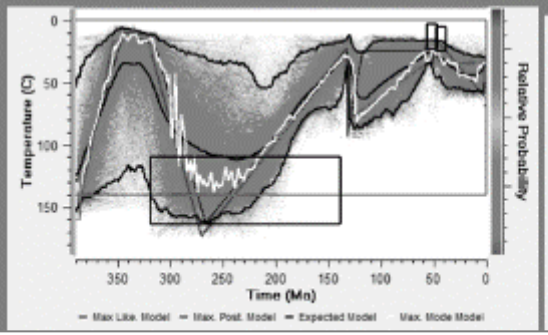

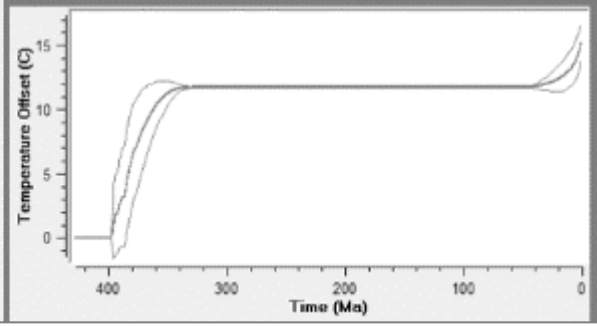

Scenario 3a

No lengths in top sample
Simple

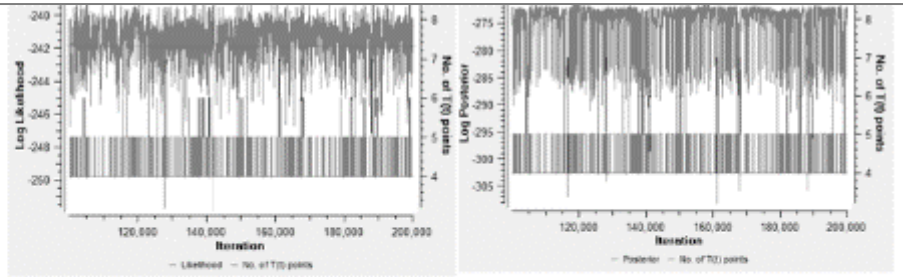

L = Max likelihood model
P = Max posterior model
E = Expected model

L

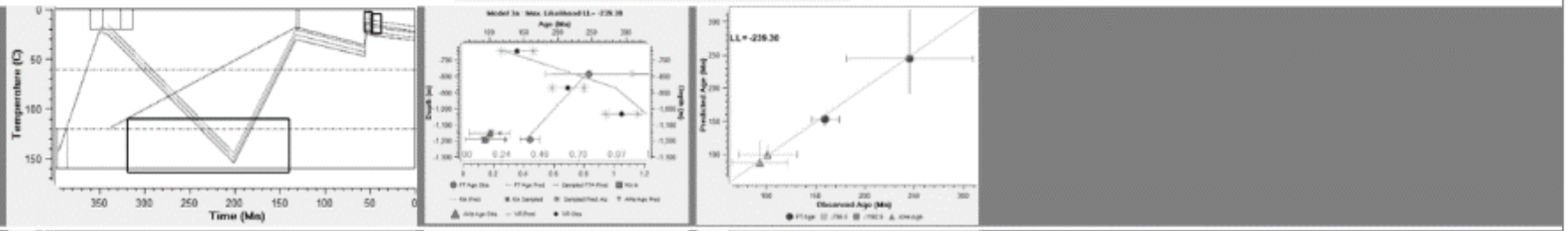

P

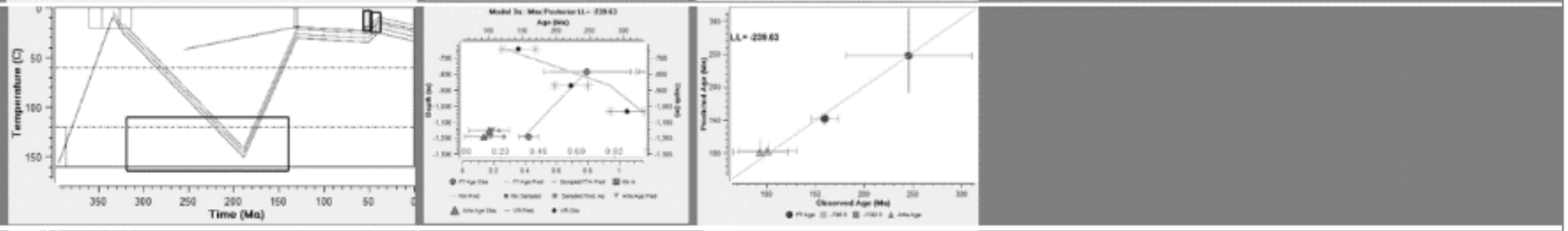

E

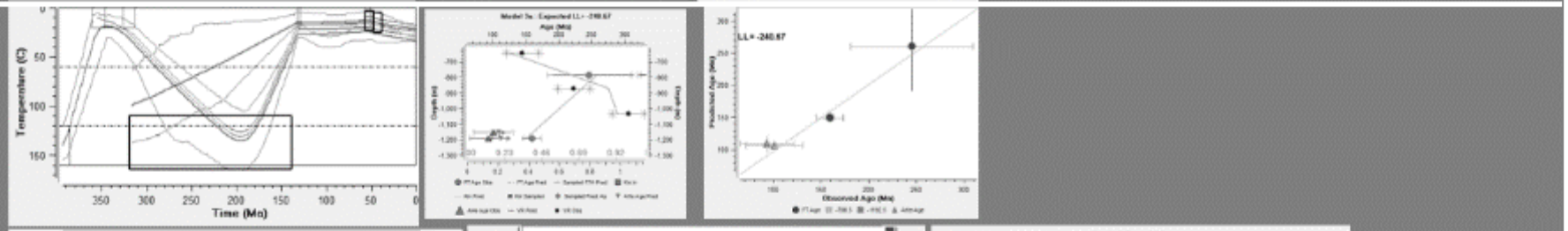

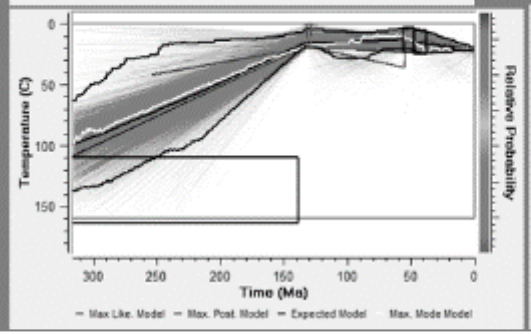

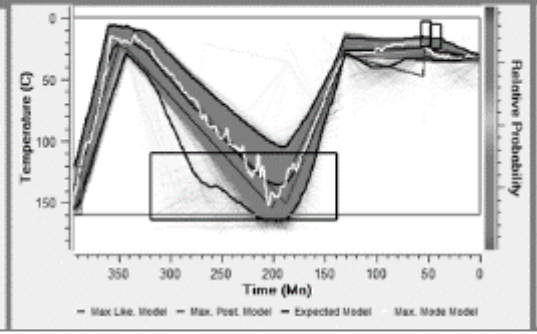

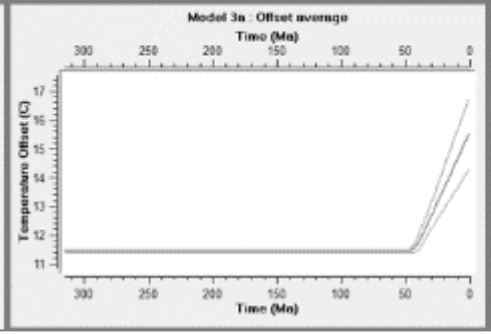

Scenario 3b

No lengths in top sample
Complex

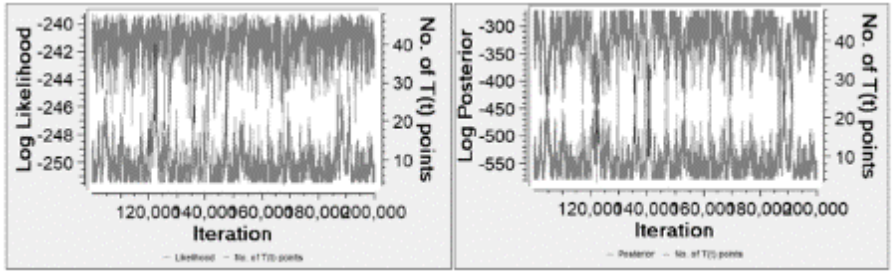

L = Max likelihood model
P = Max posterior model
E = Expected model

L

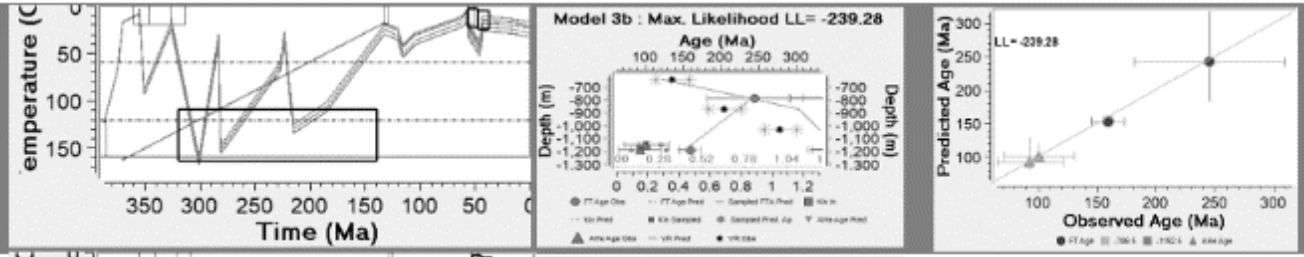

P

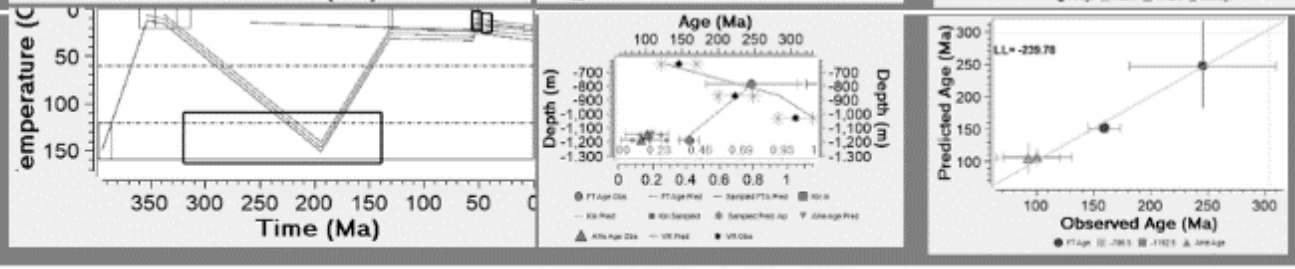

E

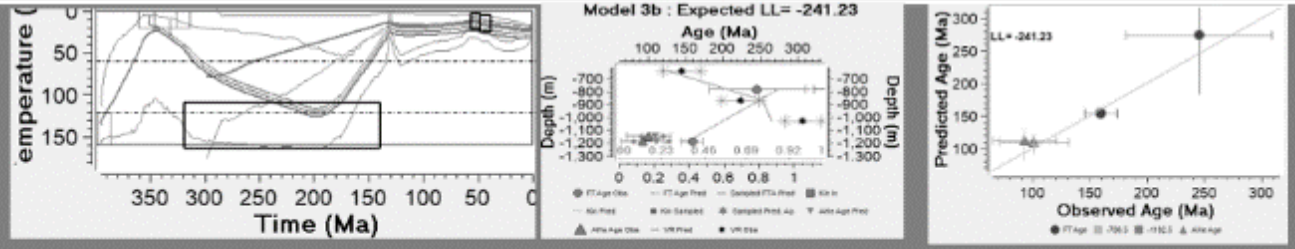

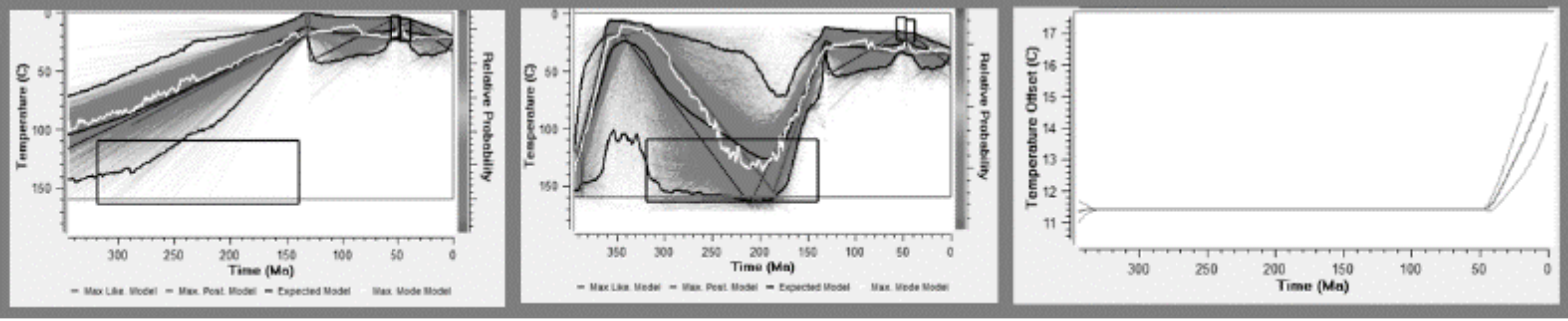

2.3.3 34/05-1

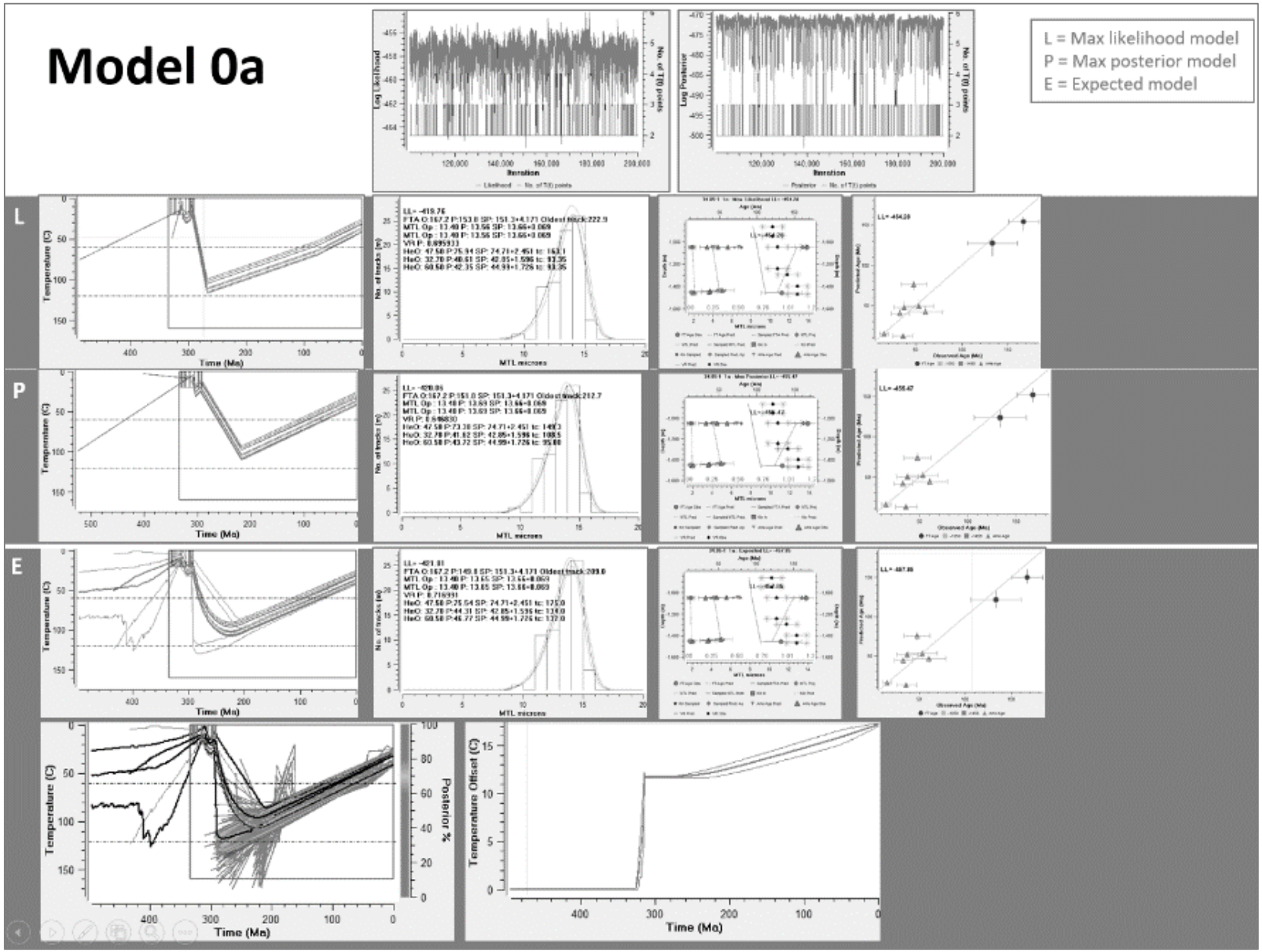
Model 0a
L = Max likelihood model
P = Max posterior model
E = Expected model
L
P
E
Temperature (C)
Time (Ma)
MTL microns
No. of tracks (n)
Temperature Offset (C)
Posterior %

Model 0b

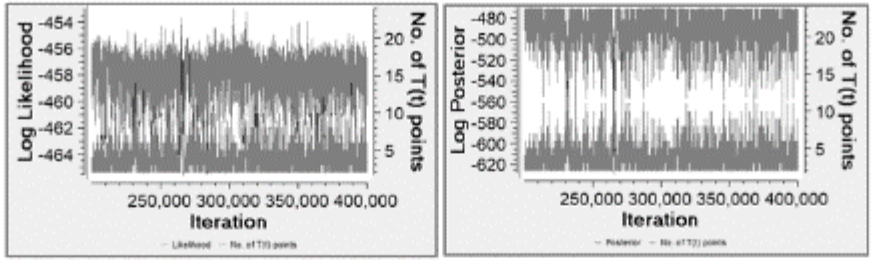

L = Max likelihood model
P = Max posterior model
E = Expected model

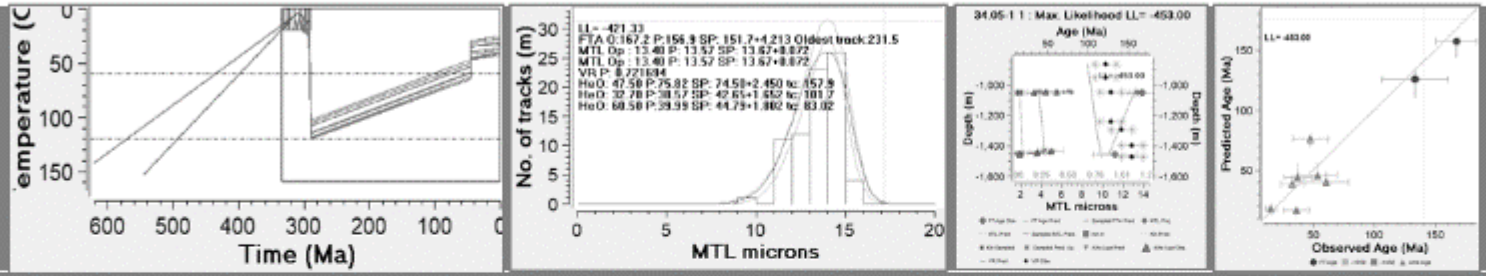

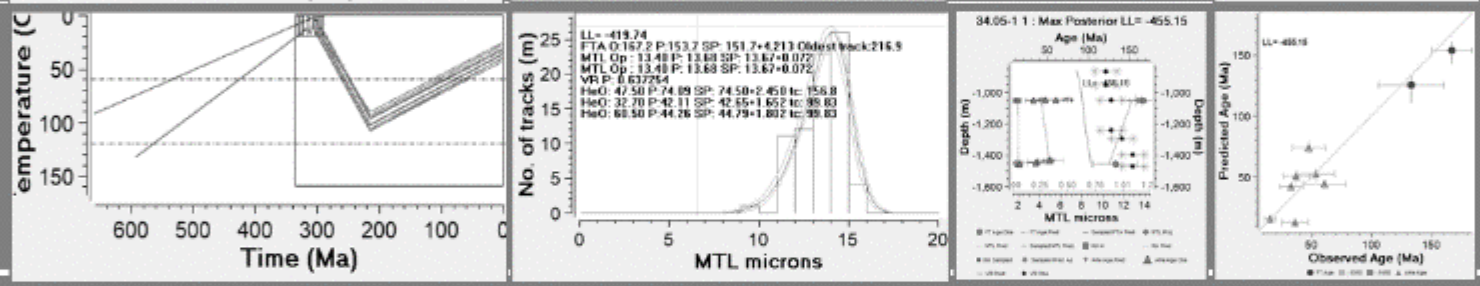

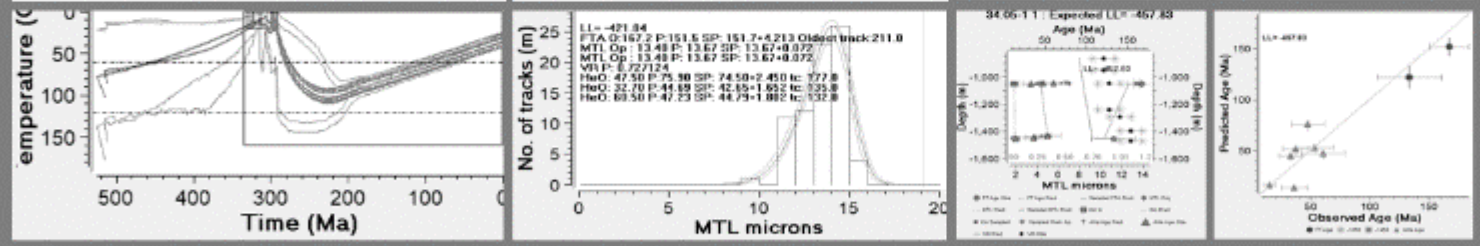

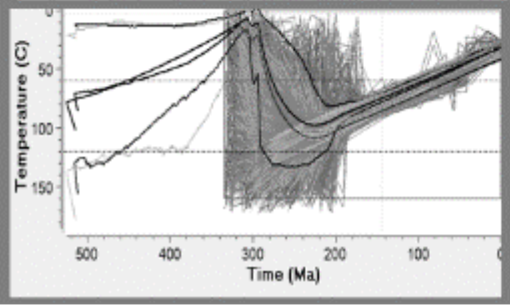

Model 1a

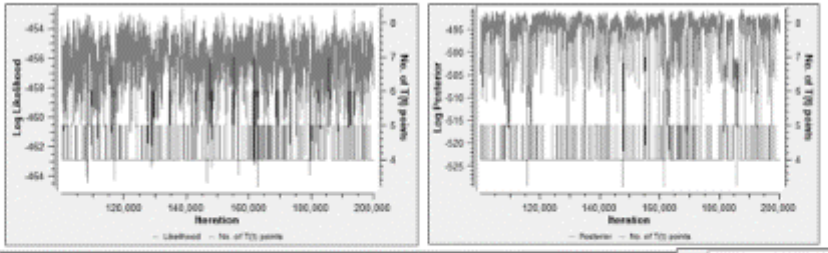

L = Max likelihood model
P = Max posterior model
E = Expected model

L

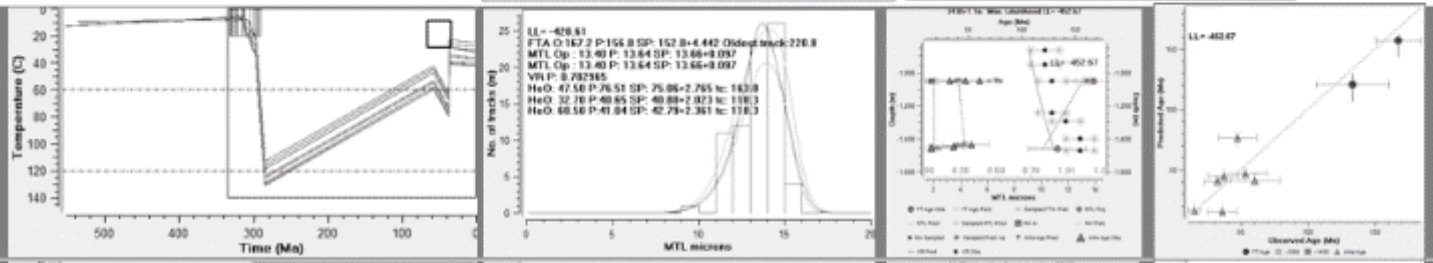

P

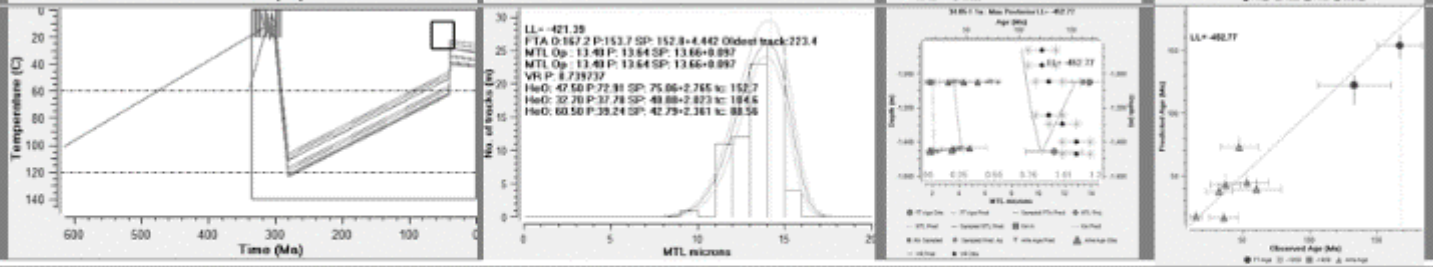

E

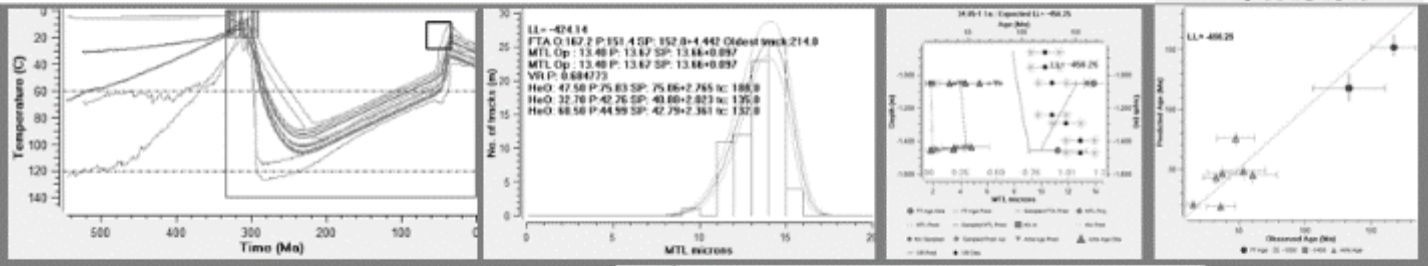

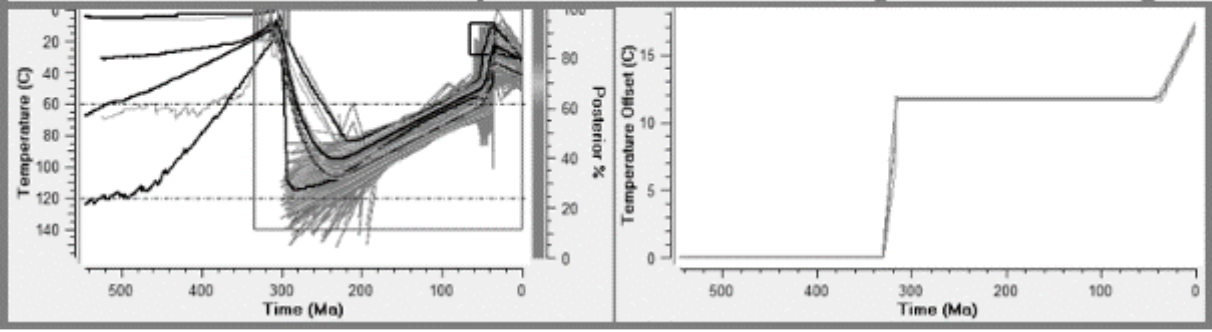

Model 1b

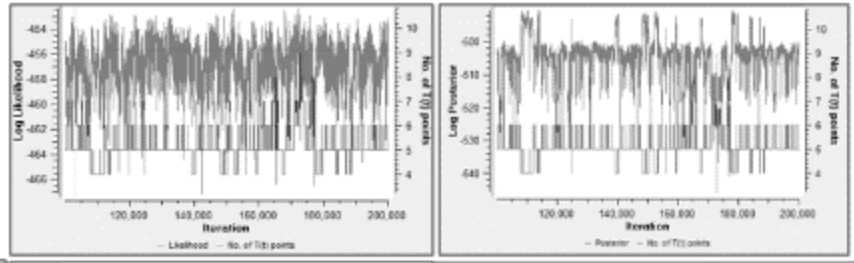

L = Max likelihood model
P = Max posterior model
E = Expected model

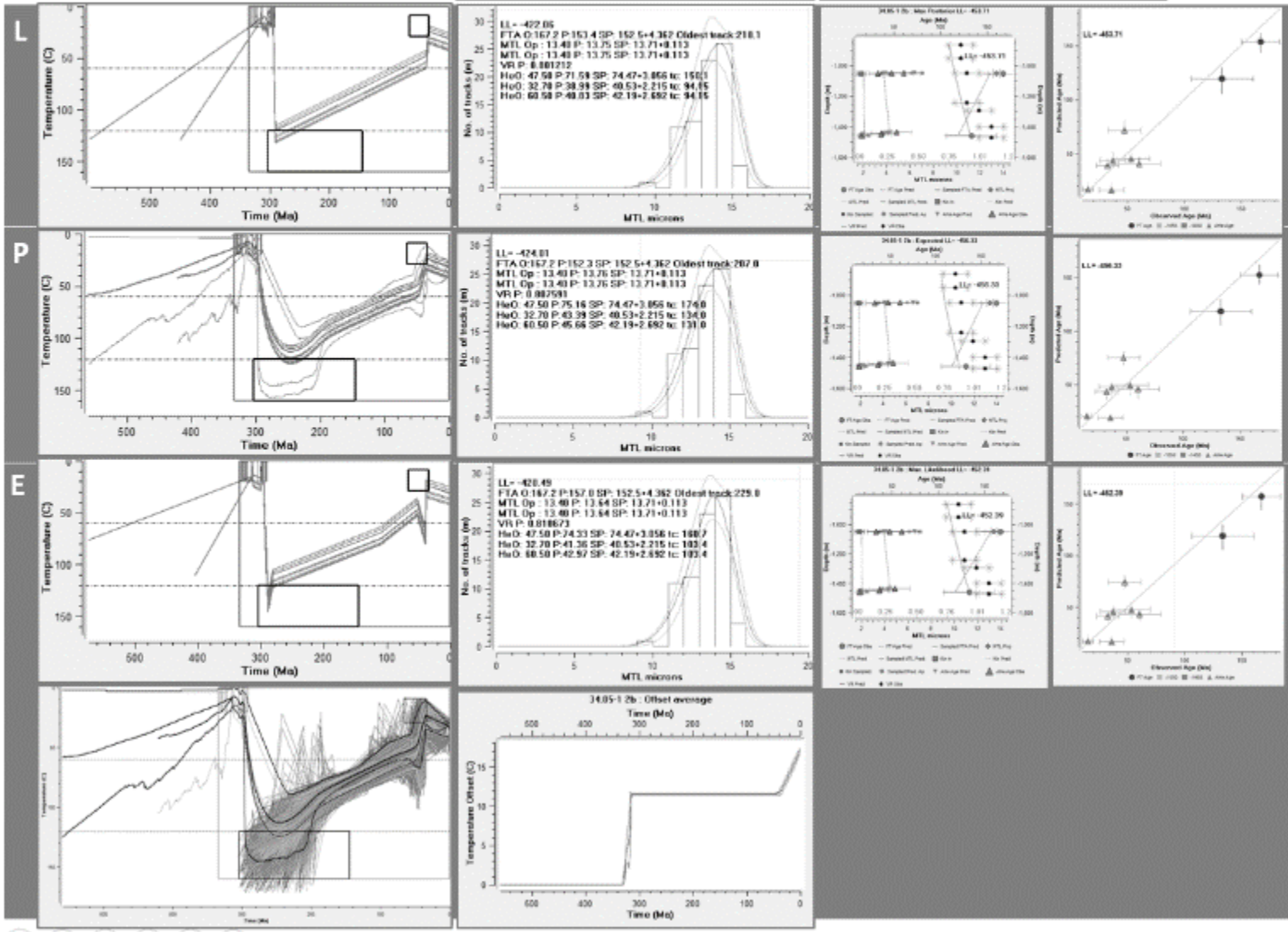

Model 1c

L = Max likelihood model
P = Max posterior model
E = Expected model

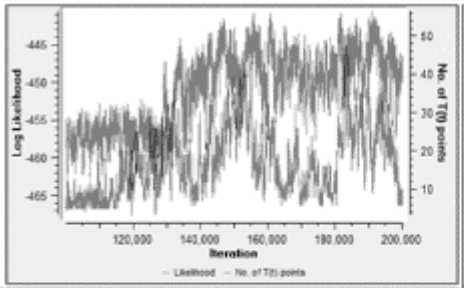

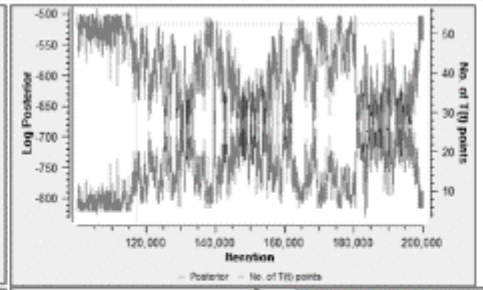

L

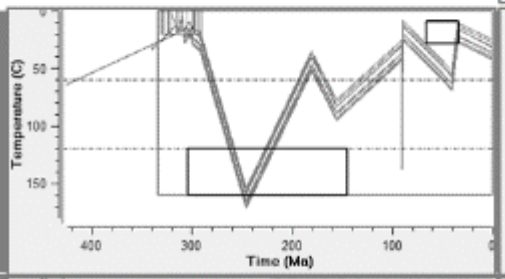

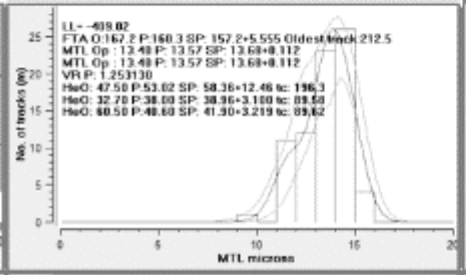

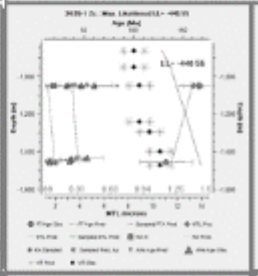

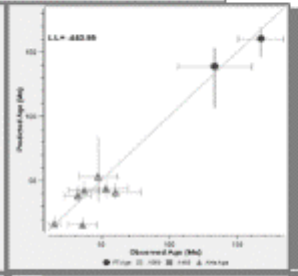

P

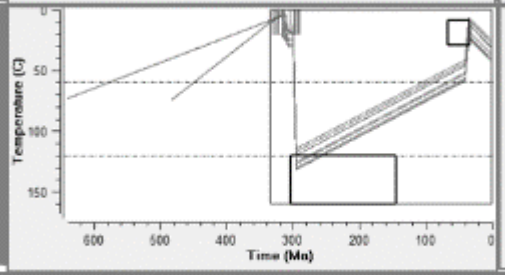

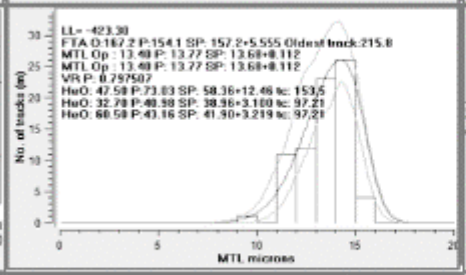

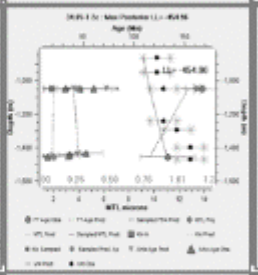

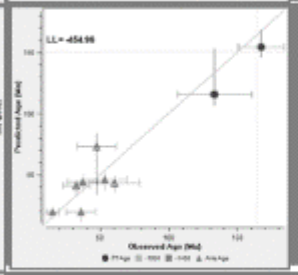

E

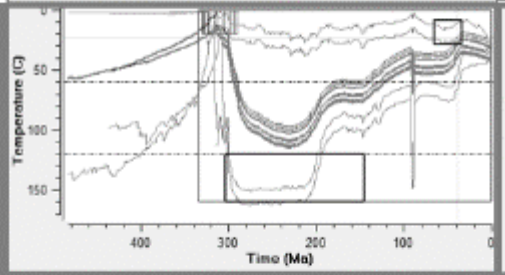

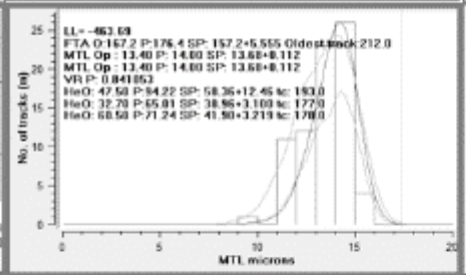

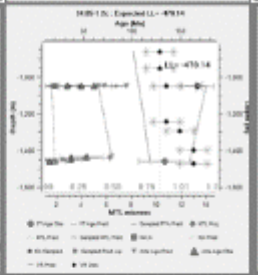

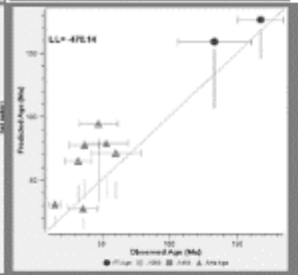

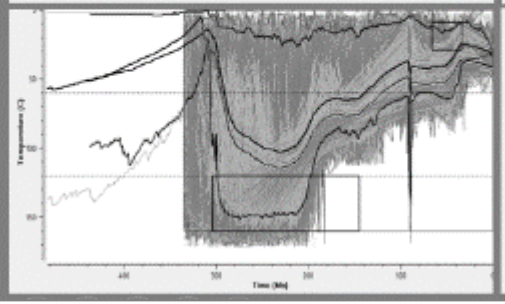

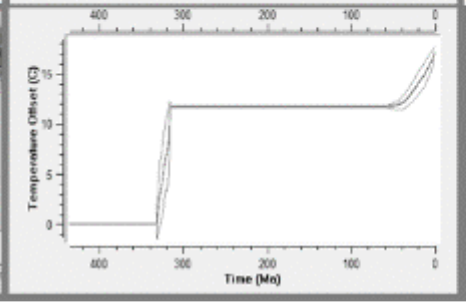

Model 2a

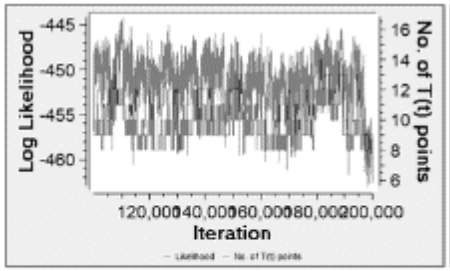

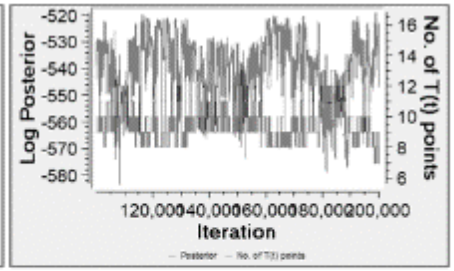

L = Max likelihood model
P = Max posterior model
E = Expected model

L

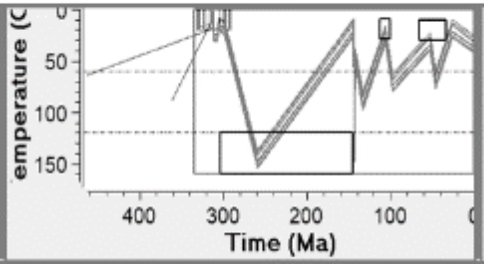

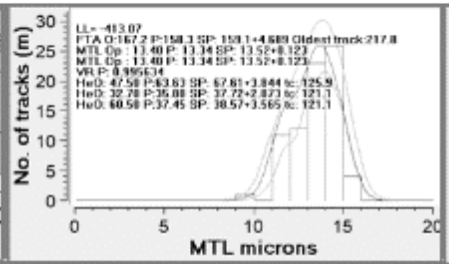

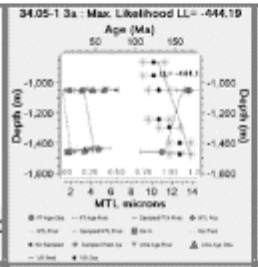

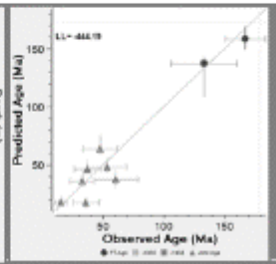

P

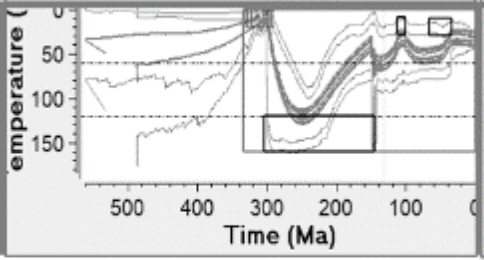

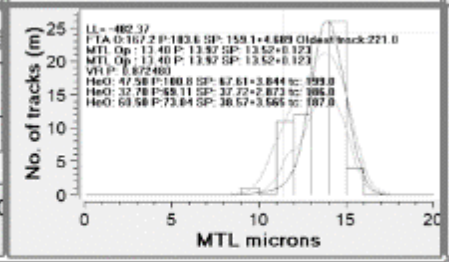

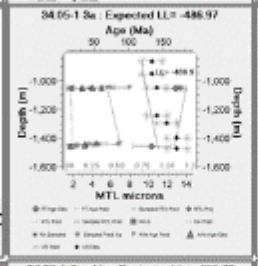

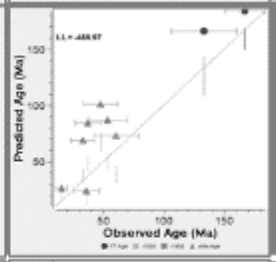

E

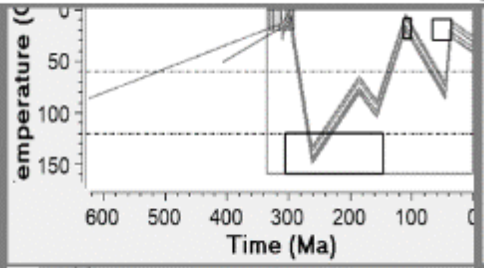

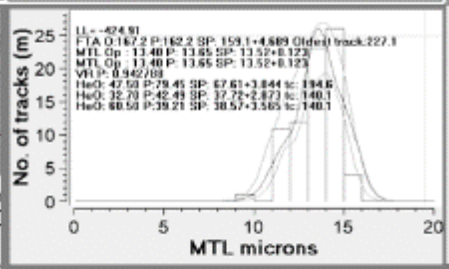

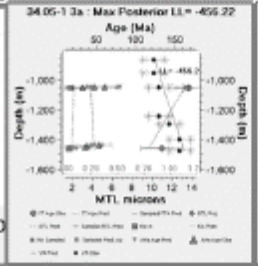

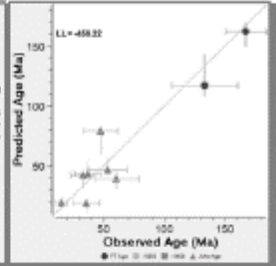

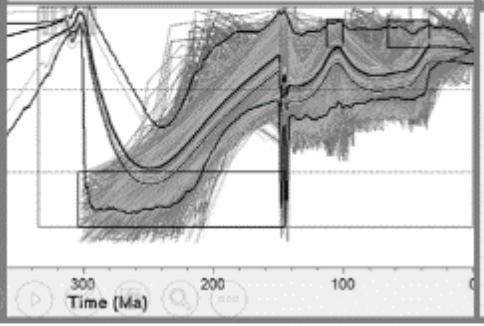

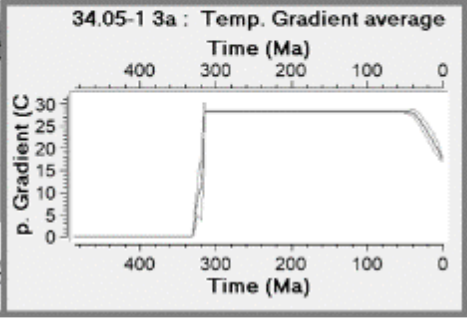

Model 2b

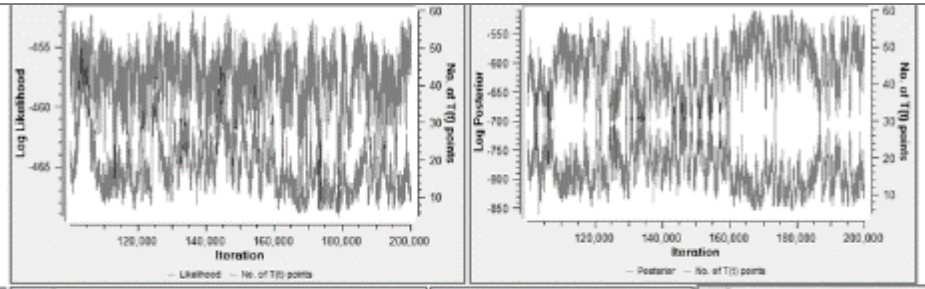

L = Max likelihood model
P = Max posterior model
E = Expected model

L

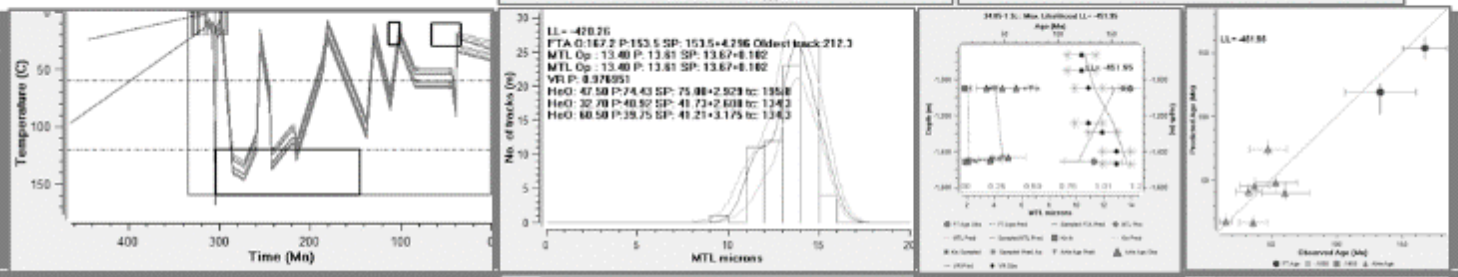

P

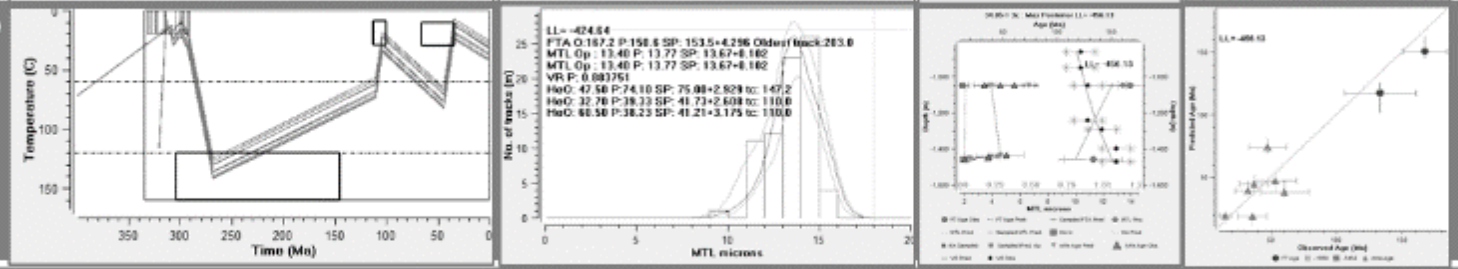

E

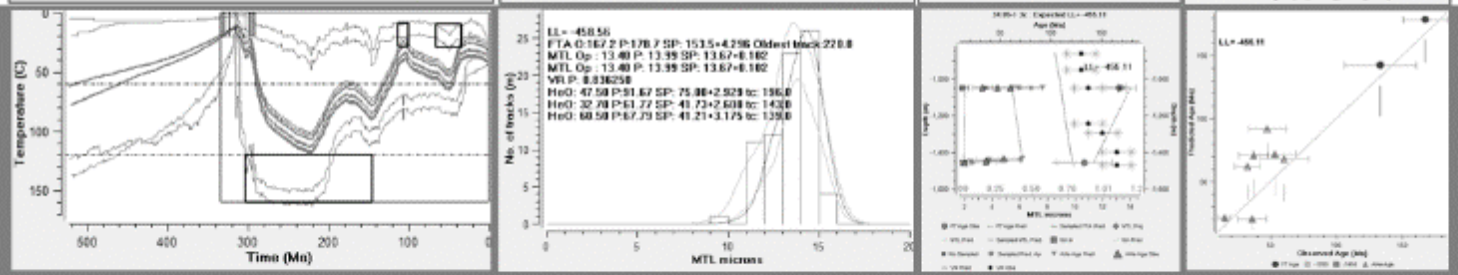

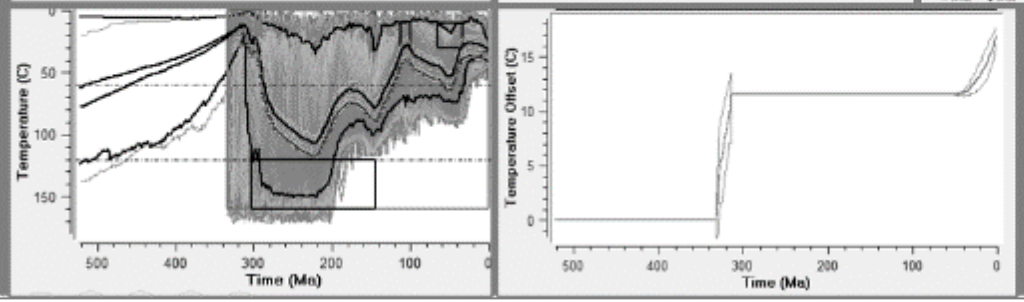

Model 2c

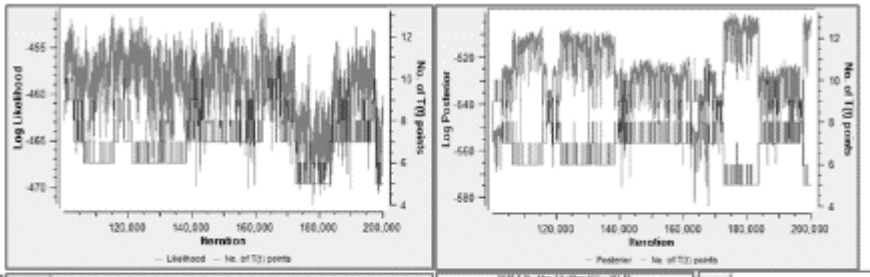

L = Max likelihood model
P = Max posterior model
E = Expected model

L

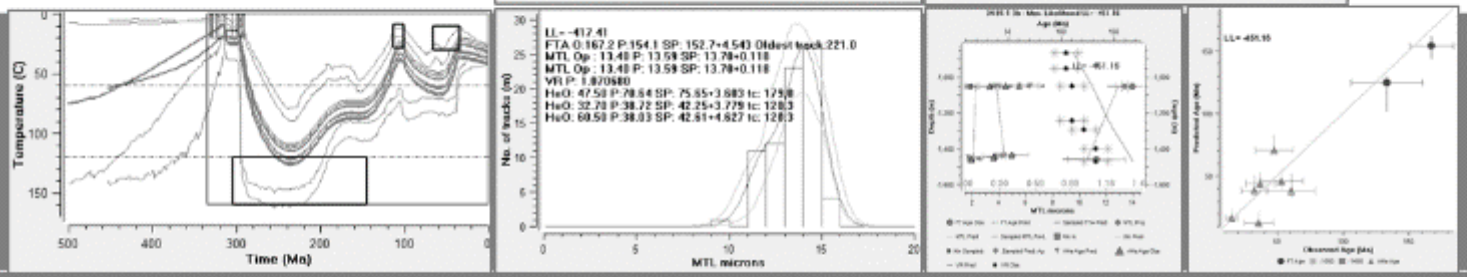

P

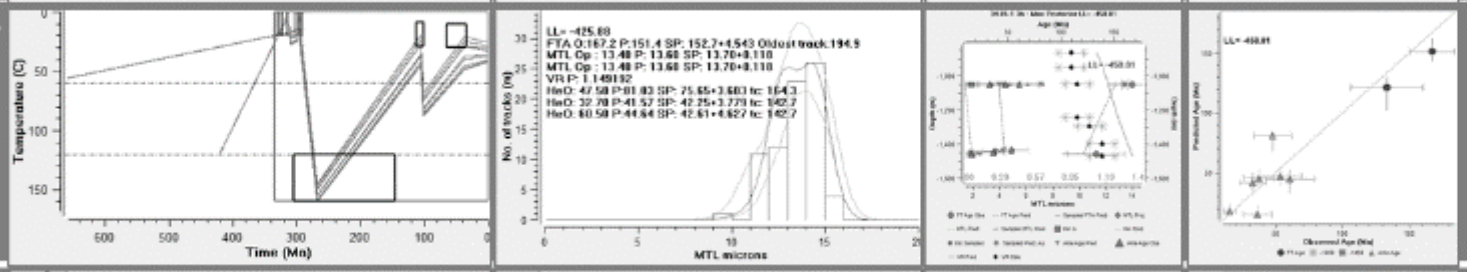

E

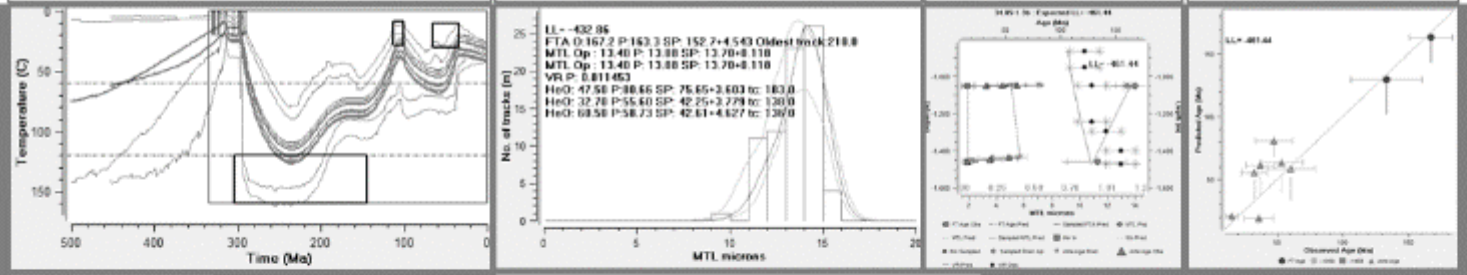

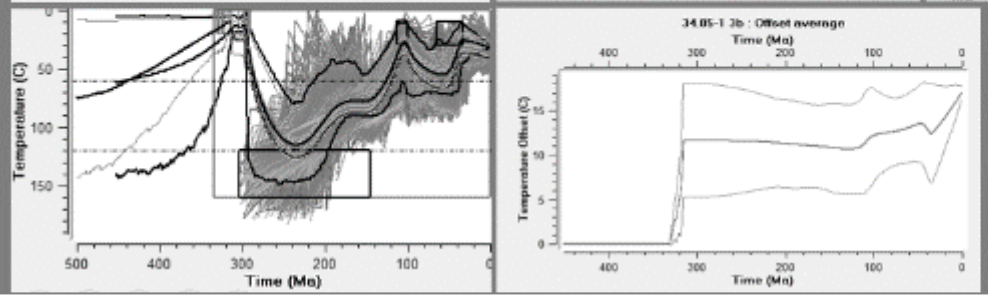

2.3.4 C-PH4-12

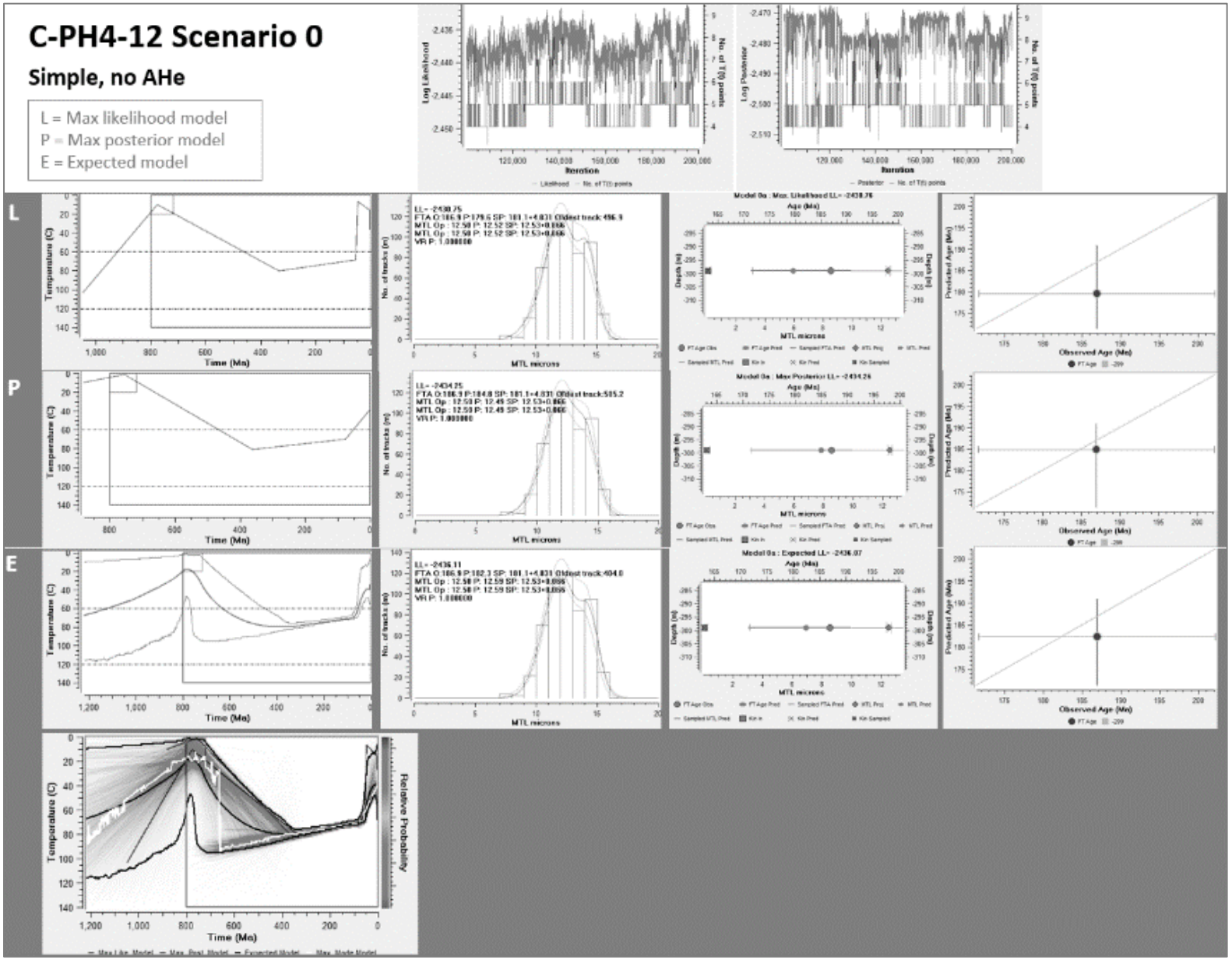
C-PH4-12 Scenario 0
Simple, no AHe
L = Max likelihood model
P = Max posterior model
E = Expected model
L
P
E
Temperature (C)
Time (Ma)
MTL microns
Observed Age (Ma)
Predicted Age (Ma)
Depth (m)
Iteration
Log Likelihood
Log Posterior
No. of T(t) points
Relative Probability

C-PH4-12 Scenario 1

Simple, no lengths

L = Max likelihood model
P = Max posterior model
E = Expected model

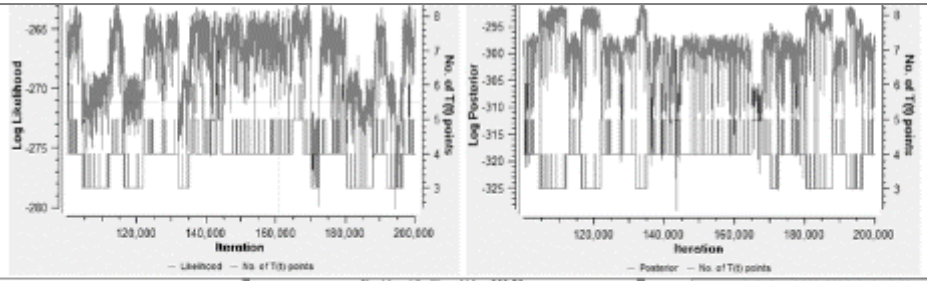

L

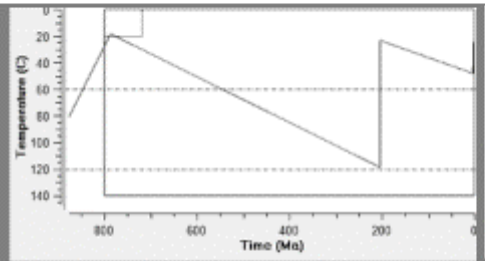

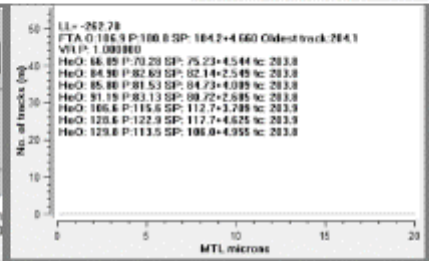

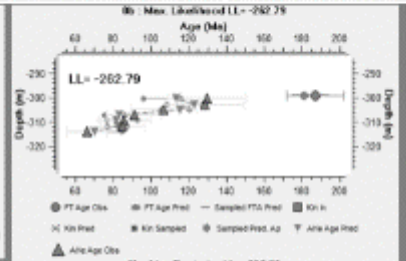

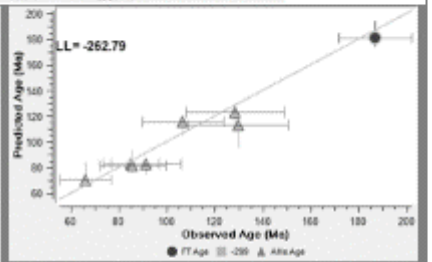

P

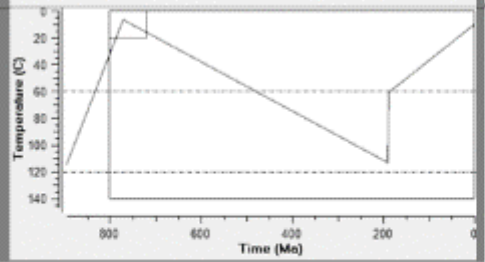

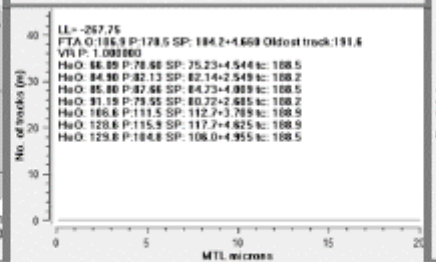

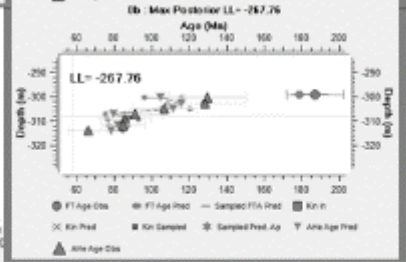

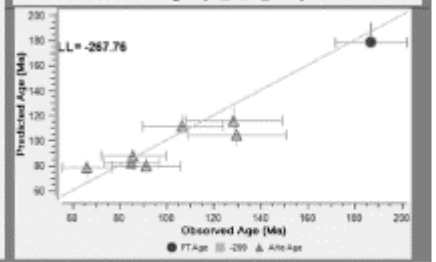

E

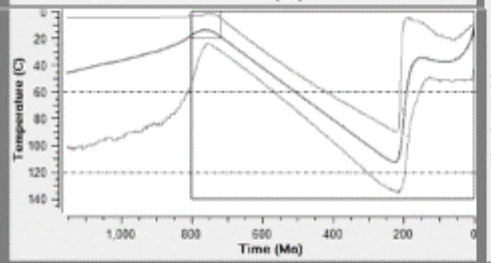

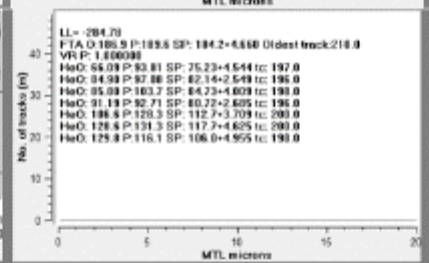

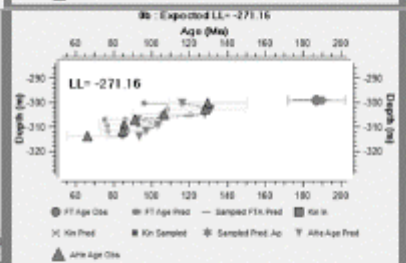

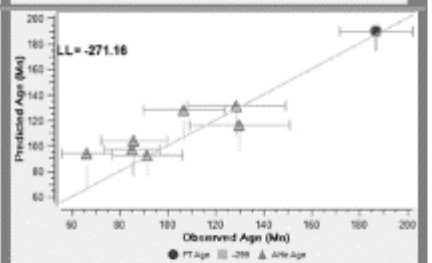

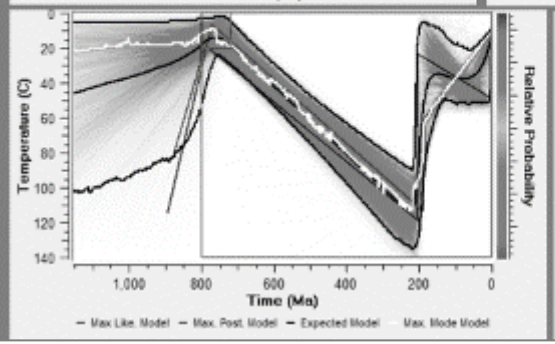

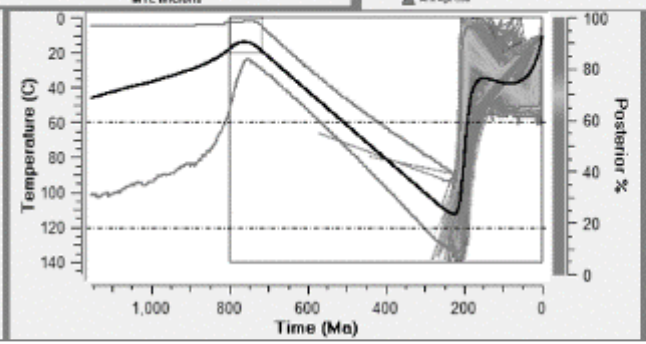

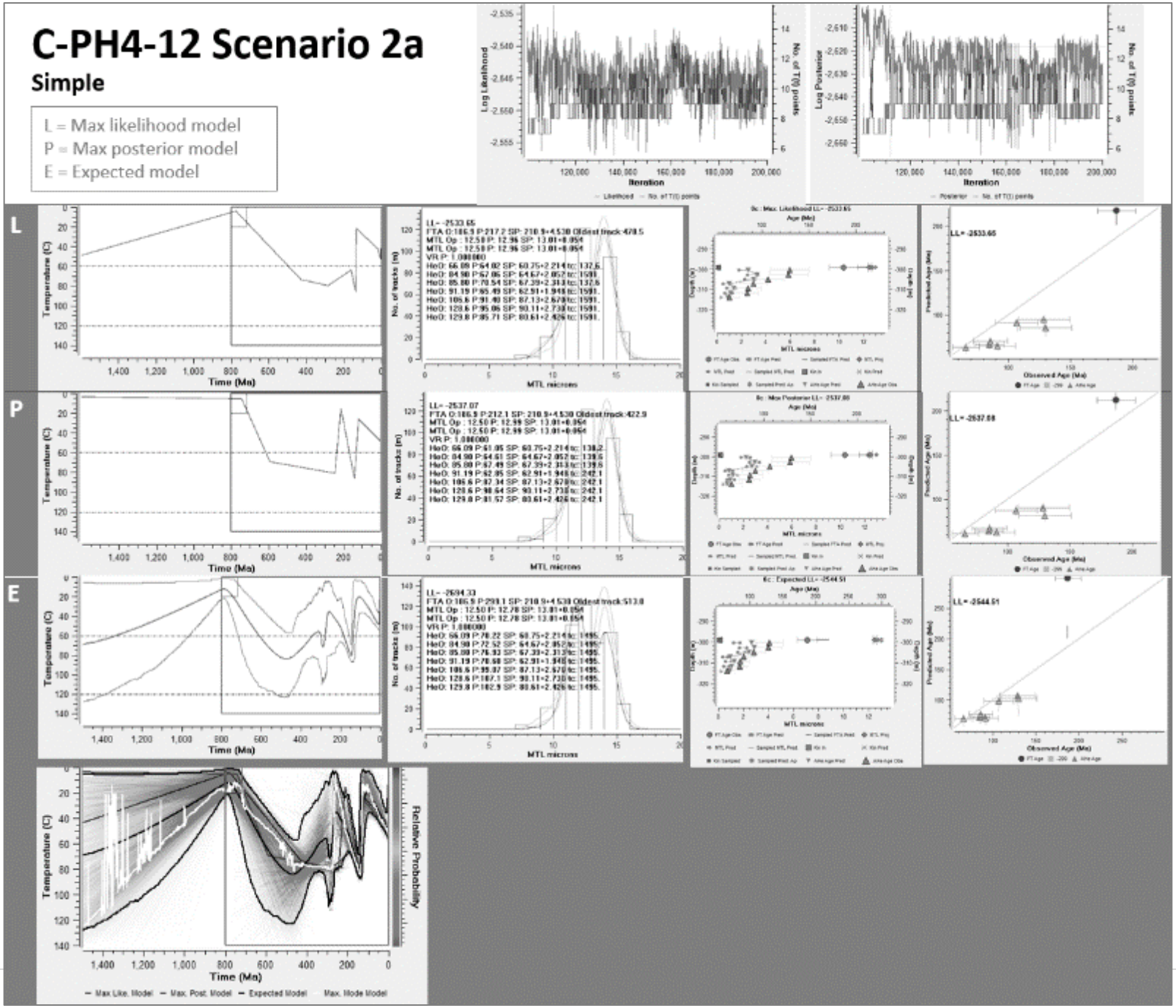
C-PH4-12 Scenario 2a
Simple
L = Max likelihood model
P = Max posterior model
E = Expected model
L
P
E
Log Likelihood
Log Posterior
No. of T(t) points
Iteration
Temperature (C)
Time (Ma)
No. of tracks (n)
MTL microns
Observed Age (Ma)
Predicted Age (Ma)
Relative Probability
Max. Like. Model
Max. Post. Model
Expected Model
Max. Mode Model

C-PH4-12 Scenario 2b

Simple 16.3

L = Max likelihood model
P = Max posterior model
E = Expected model

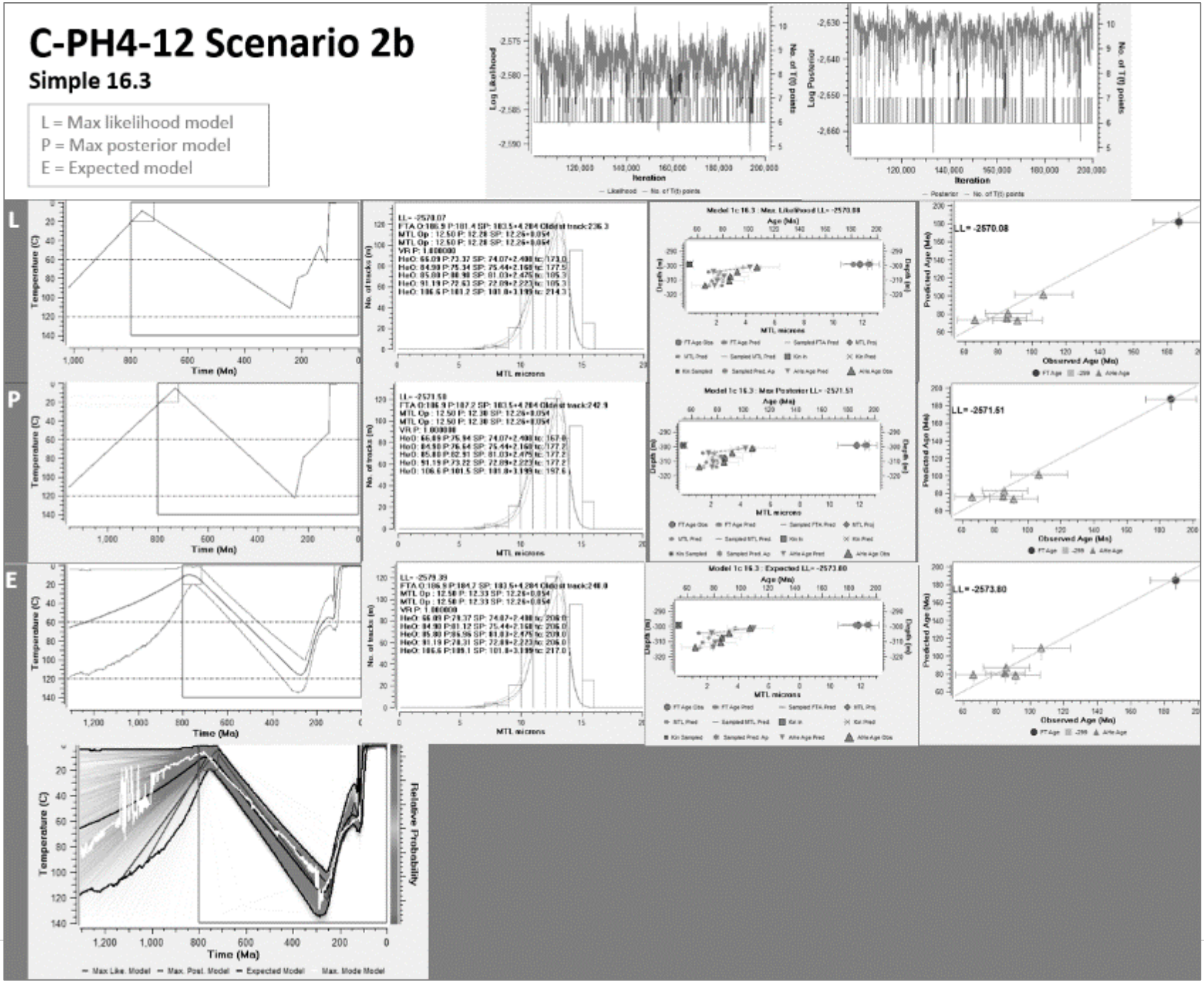

2.3.5 C-MeBo

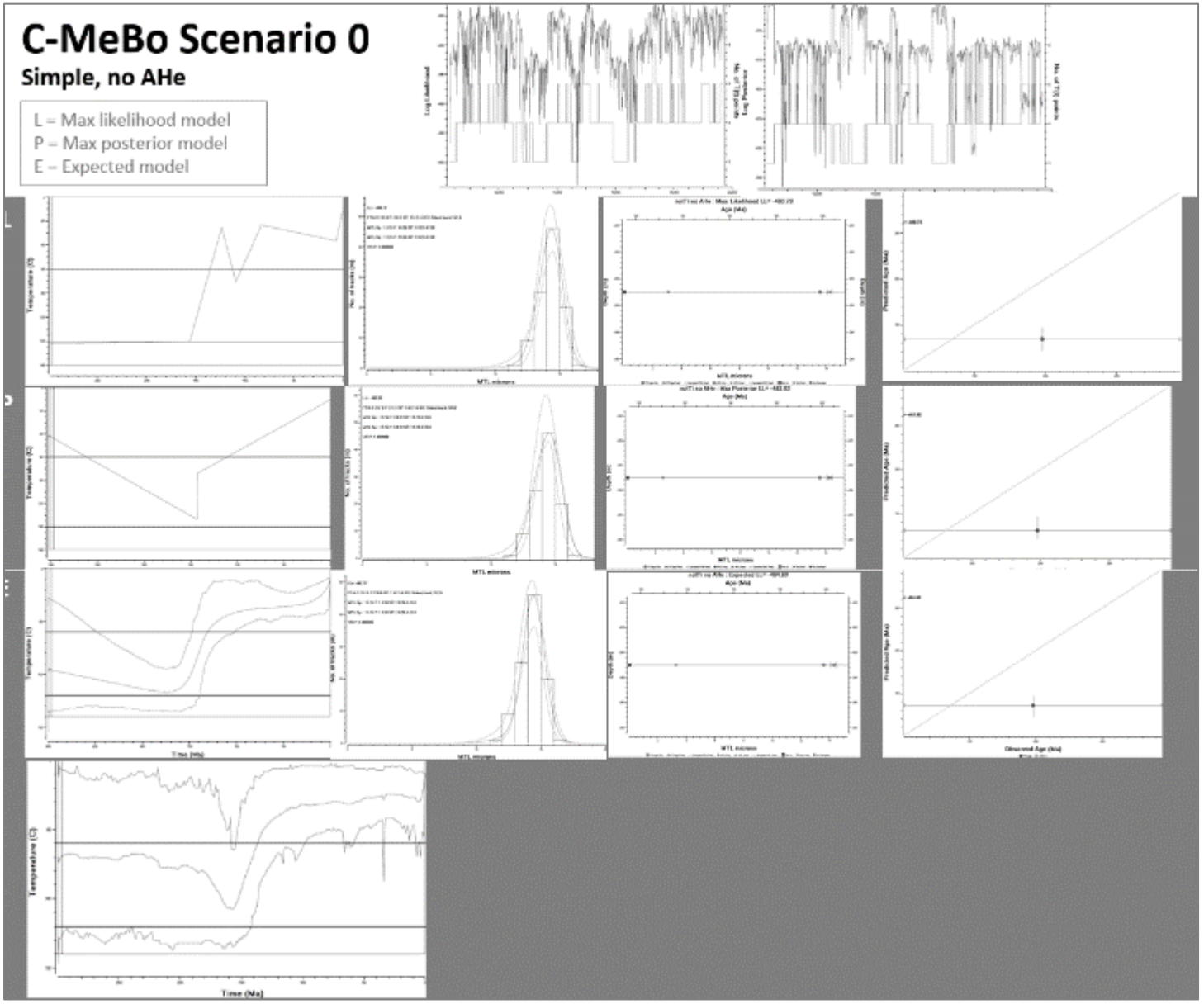
C-MeBo Scenario 0
Simple, no AHe
L = Max likelihood model
P = Max posterior model
E = Expected model

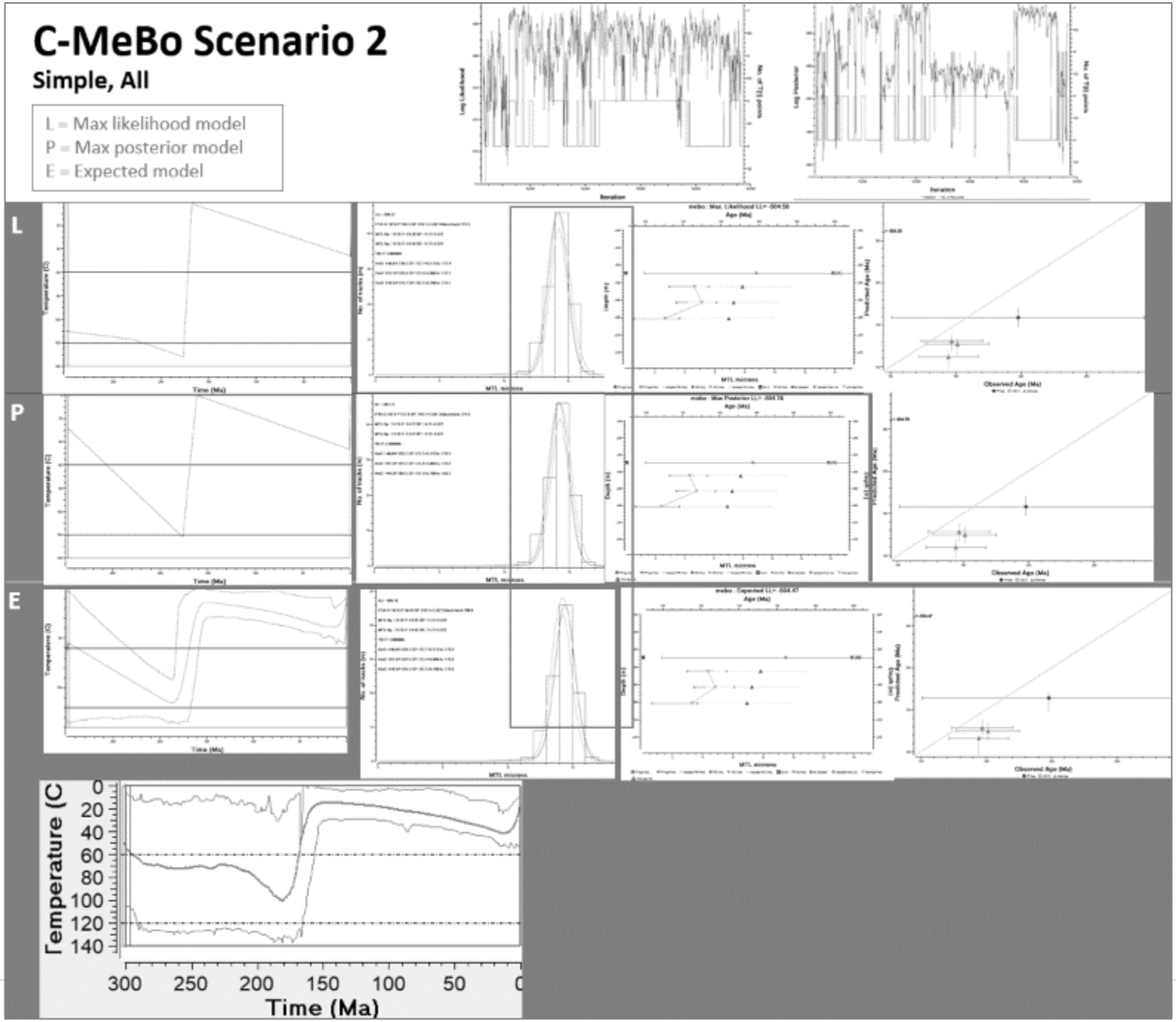
C-MeBo Scenario 2
Simple, All
L = Max likelihood model
P = Max posterior model
E = Expected model
L
P
E
Temperature (C
0
20
40
60
80
100
120
140
300
250
200
150
100
50
Time (Ma)

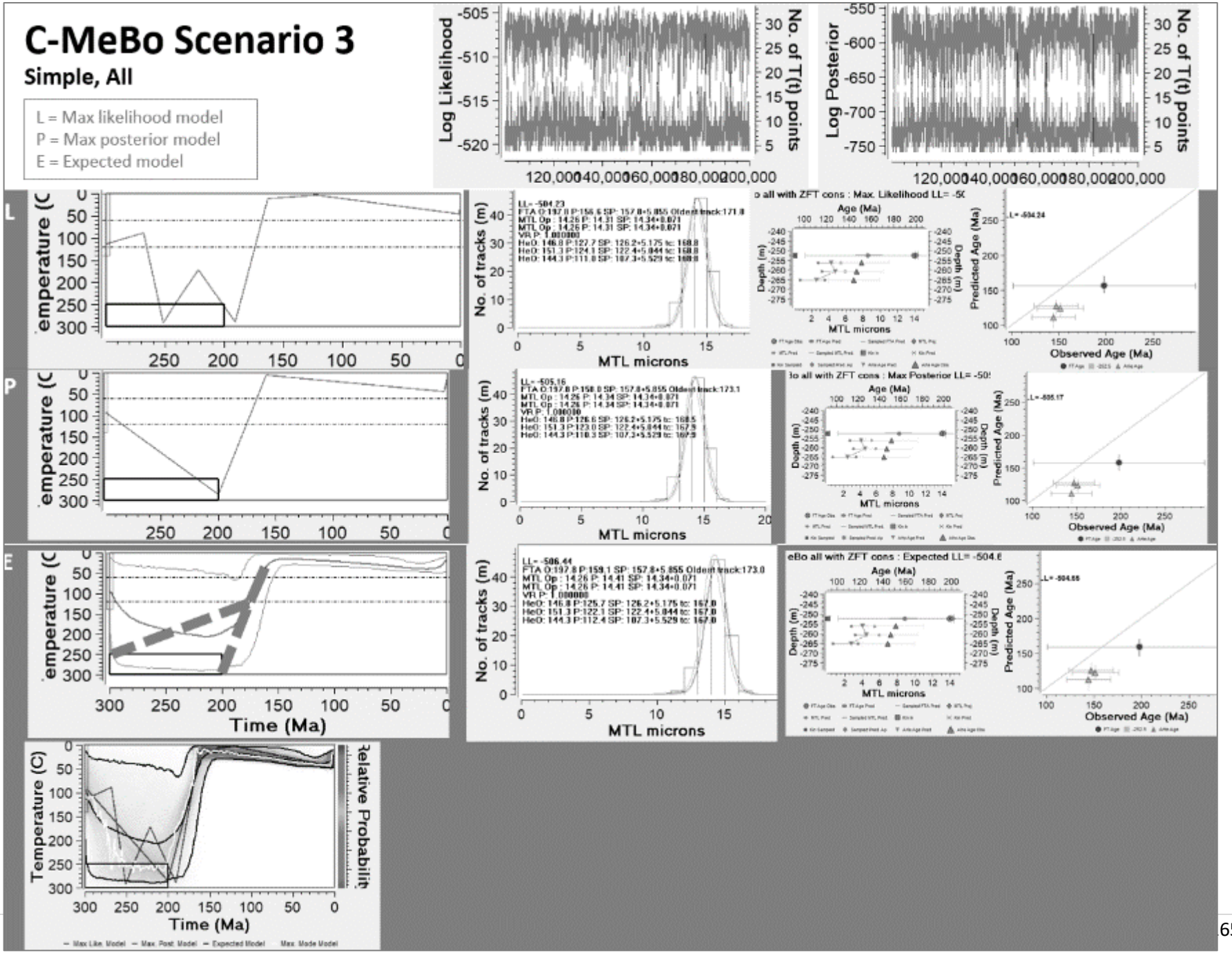
C-MeBo Scenario 3
Simple, All
L = Max likelihood model
P = Max posterior model
E = Expected model
Log Likelihood
No. of T(t) points
Log Posterior
No. of T(t) points
Age (Ma)
Depth (m)
MTL microns
Predicted Age (Ma)
Observed Age (Ma)
No. of tracks (m)
MTL microns
Temperature (C)
Time (Ma)
Relative Probability

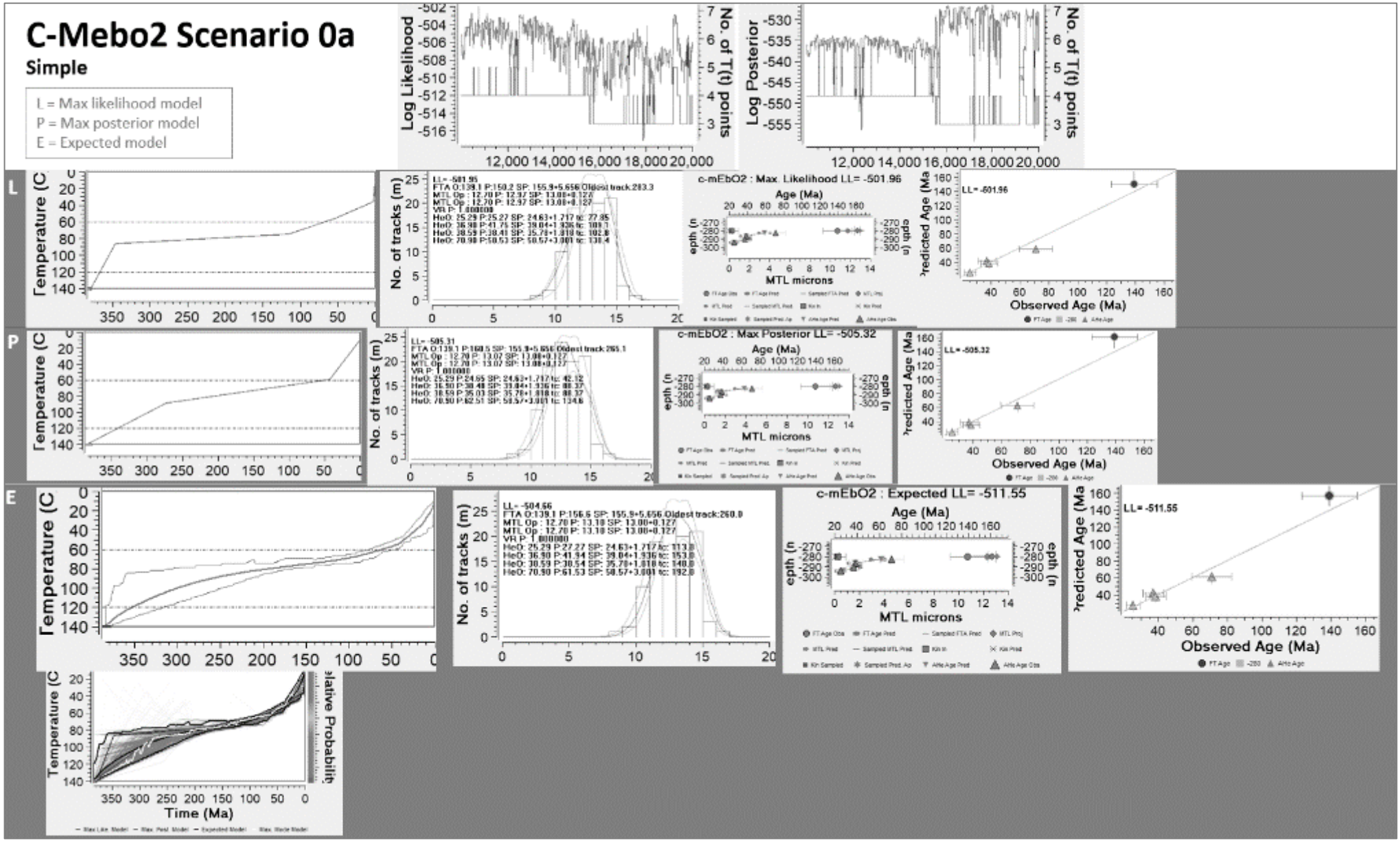
C-Mebo2 Scenario 0a
Simple
L = Max likelihood model
P = Max posterior model
E = Expected model
Log Likelihood
No. of T(t) points
Log Posterior
No. of T(t) points
12,000 14,000 16,000 18,000 20,000
L
P
E
Temperature (C
No. of tracks (m)
MTL microns
Age (Ma)
Predicted Age (Ma)
Observed Age (Ma)
c-mEbO2 : Max. Likelihood LL= -501.96
c-mEbO2 : Max Posterior LL= -505.32
c-mEbO2 : Expected LL= -511.55
LL= -501.96
LL= -505.31
LL= -504.66
LL= -505.32
LL= -511.55
Temperature (C
Time (Ma)
Relative Probability

C-Mebo2 Scenario 0b

Complex

L = Max likelihood model
P = Max posterior model
E = Expected model

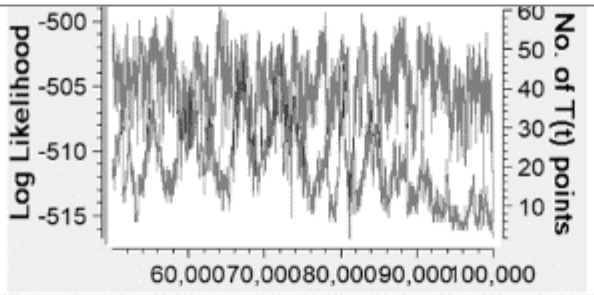

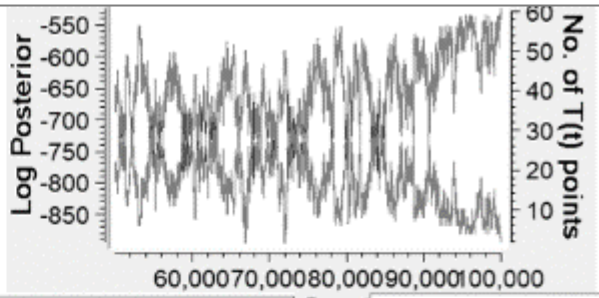

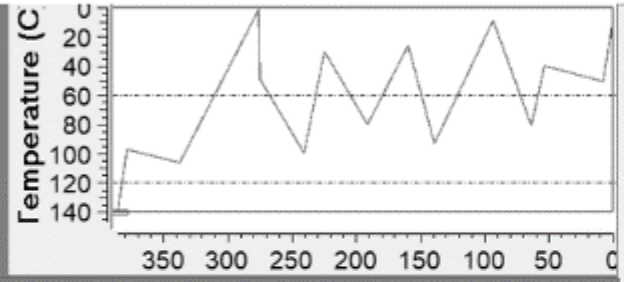

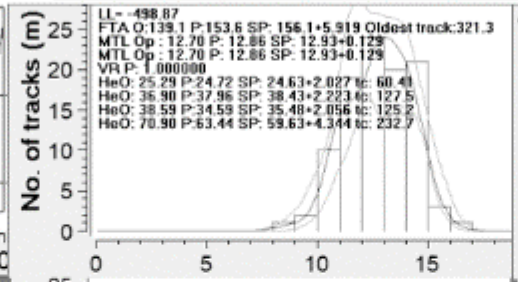

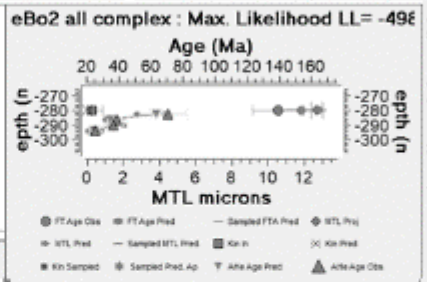

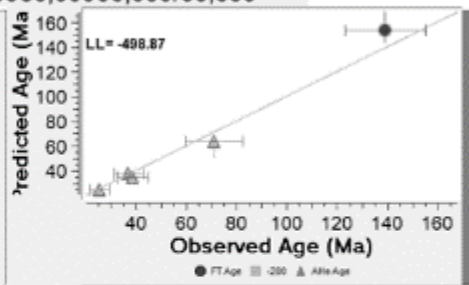

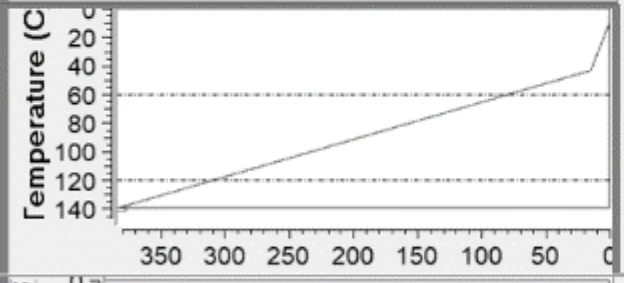

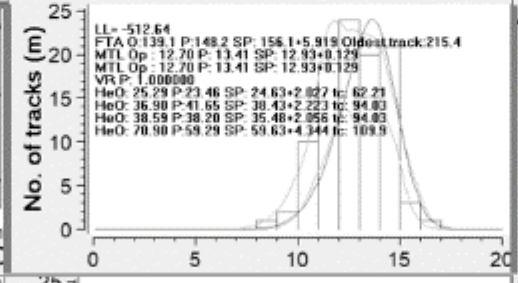

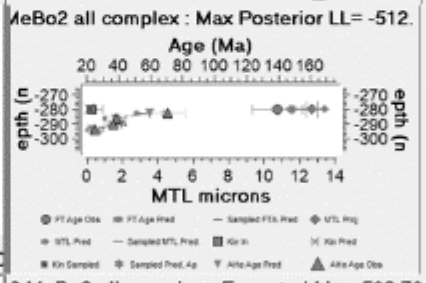

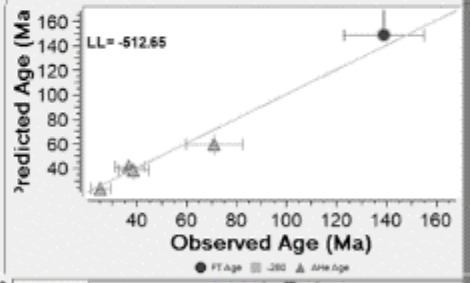

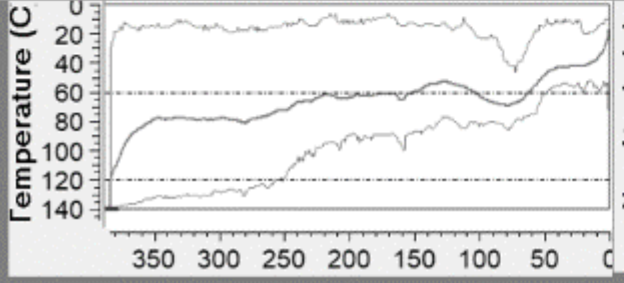

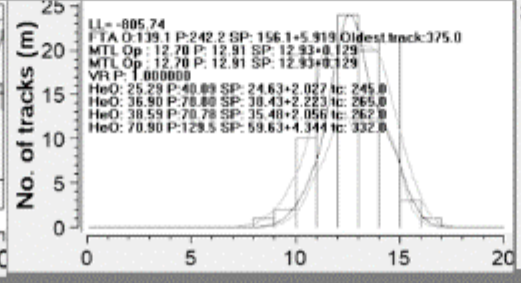

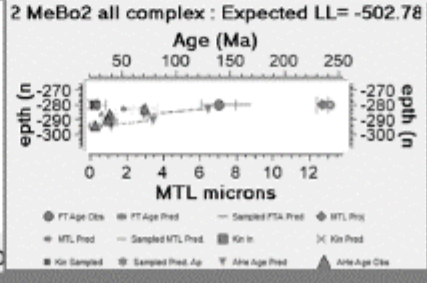

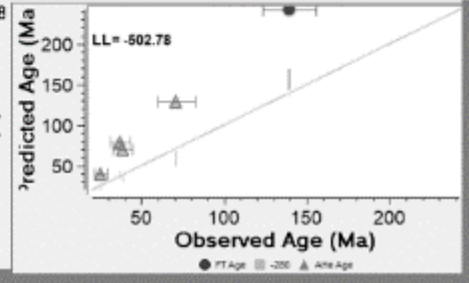

C-Mebo2 Scenario 1a

Simple No Ahe ages

L = Max likelihood model
P = Max posterior model
E = Expected model

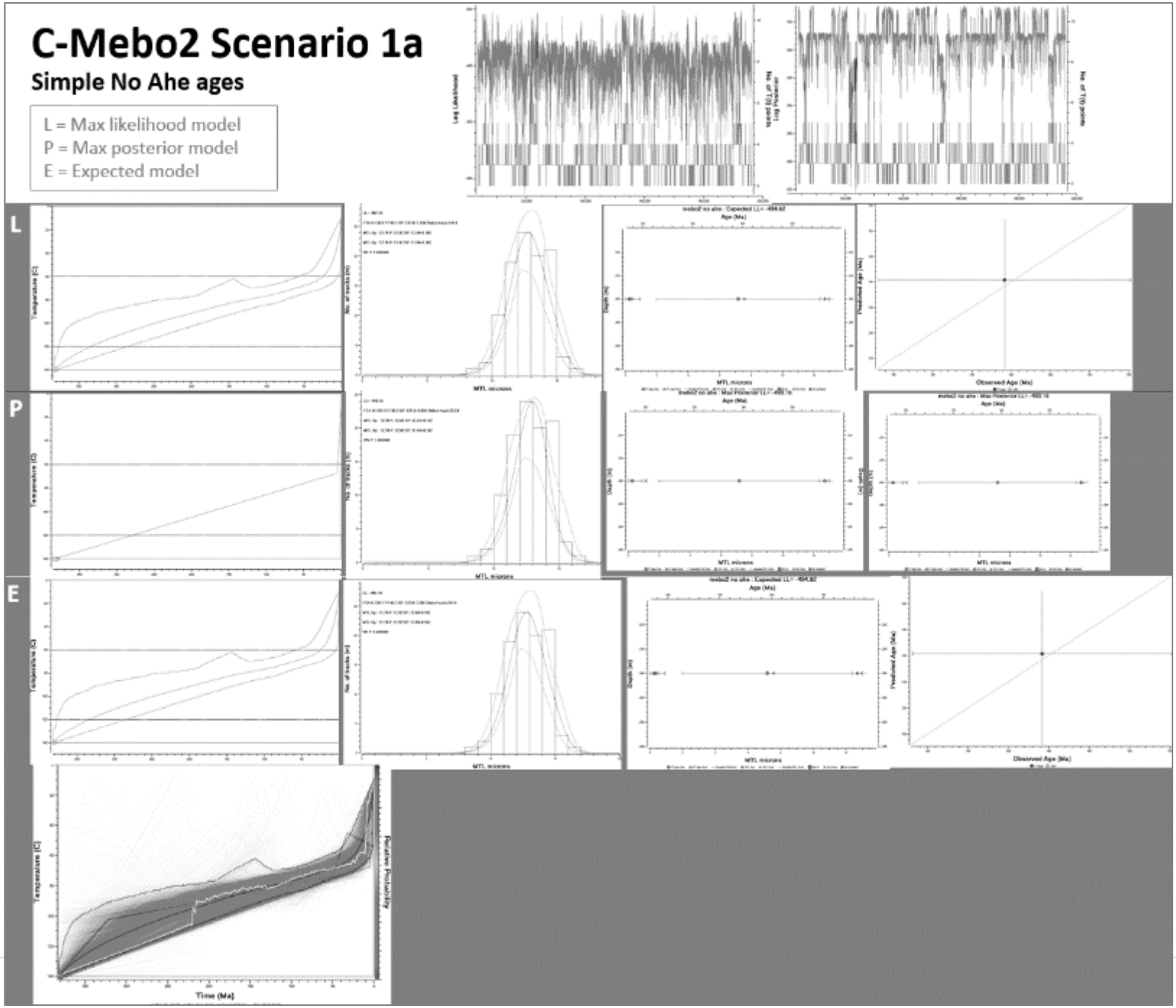

C-Mebo2 Scenario 1b

Complex No Ahe ages

L = Max likelihood model
P = Max posterior model
E = Expected model

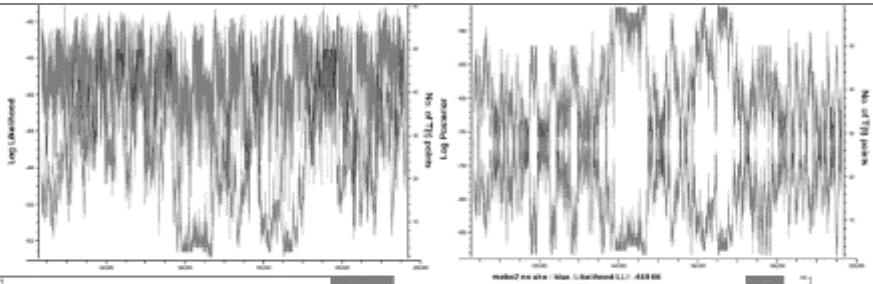

L

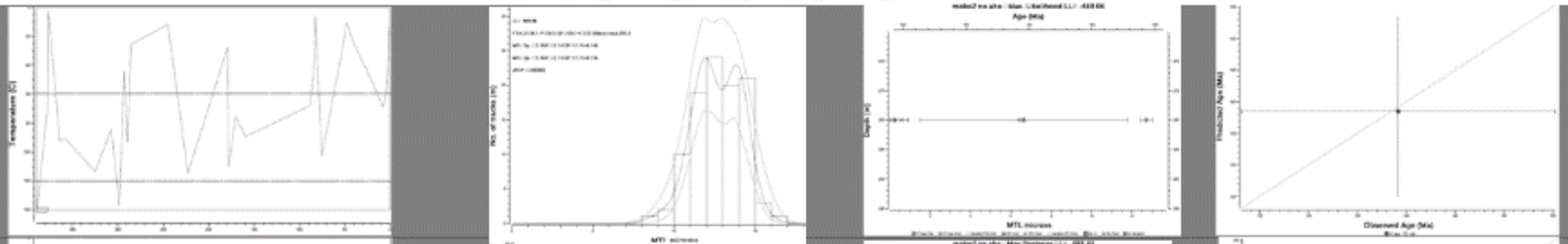

P

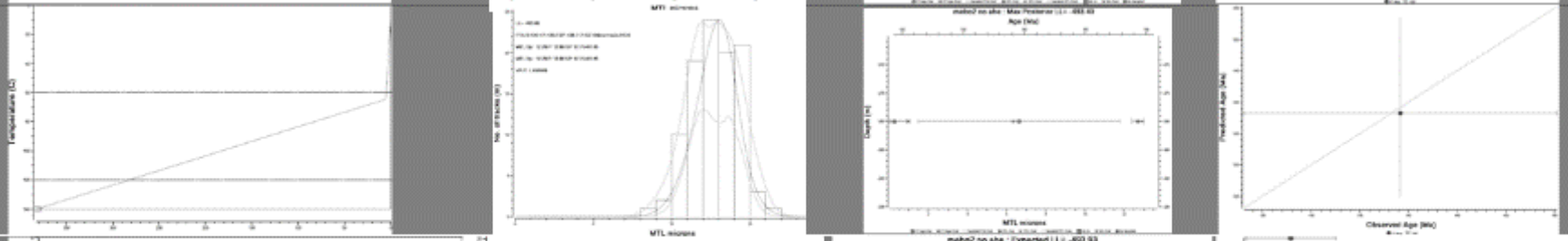

E

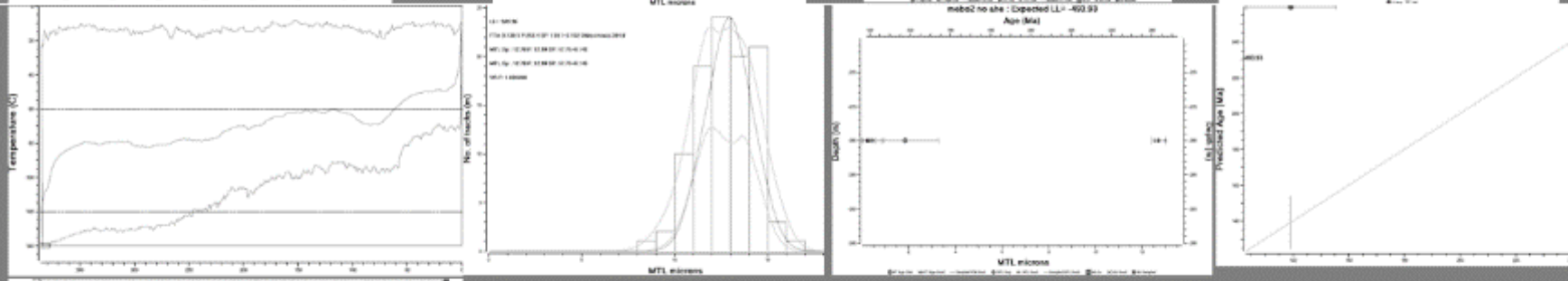

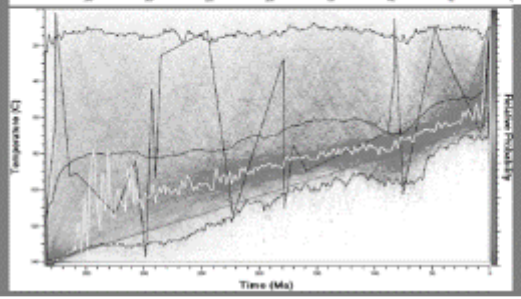

C-Mebo2 Scenario 2a

Simple L0 16.3

L = Max likelihood model
P = Max posterior model
E = Expected model

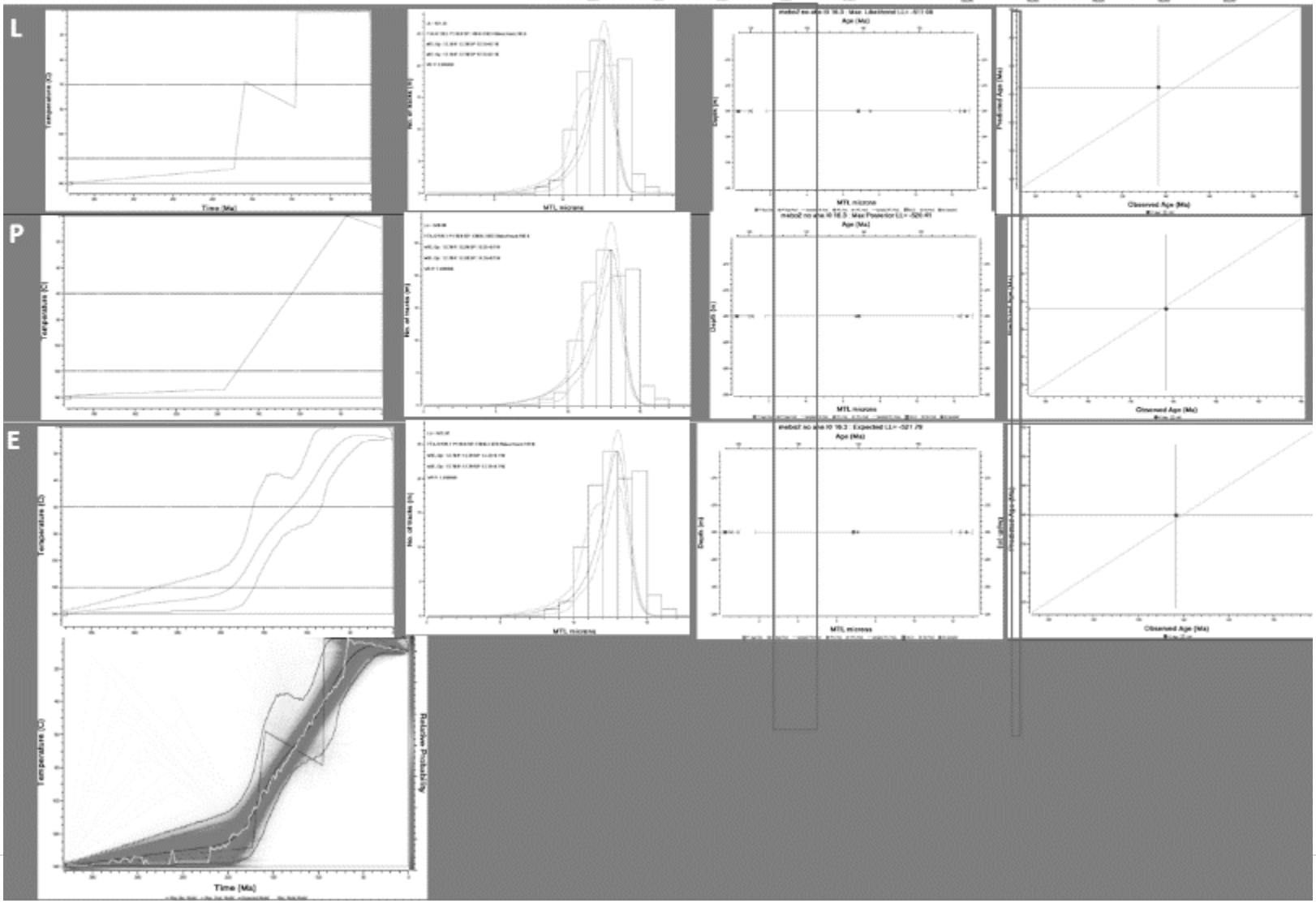

C-Mebo2 Scenario 3a

Simple, All, L0 16.3

L = Max likelihood model
P = Max posterior model
E = Expected model

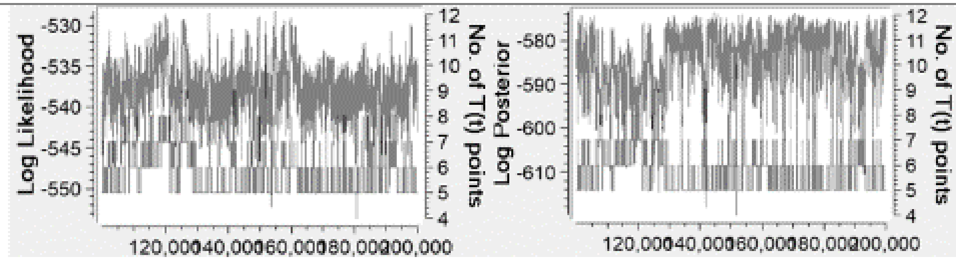

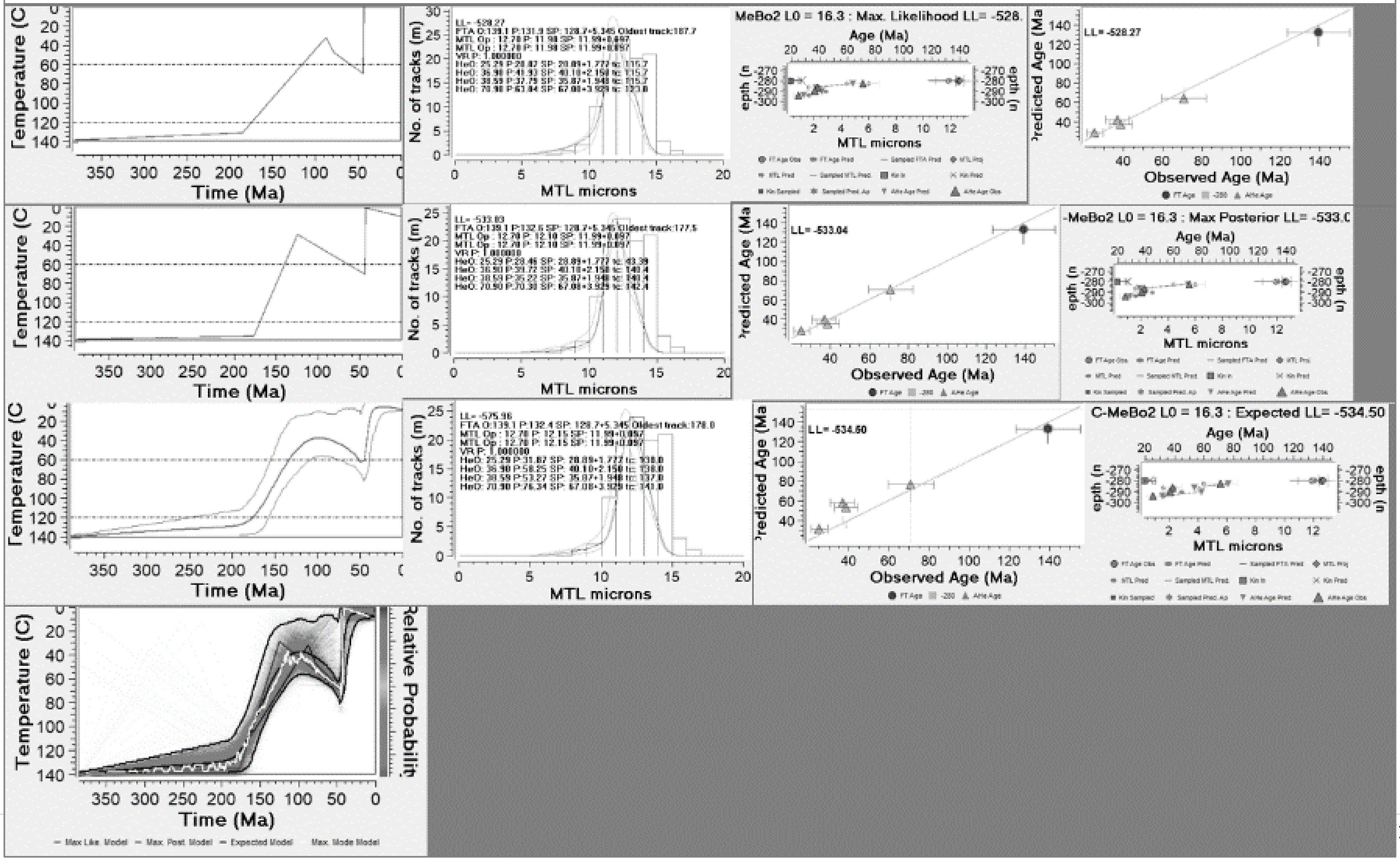

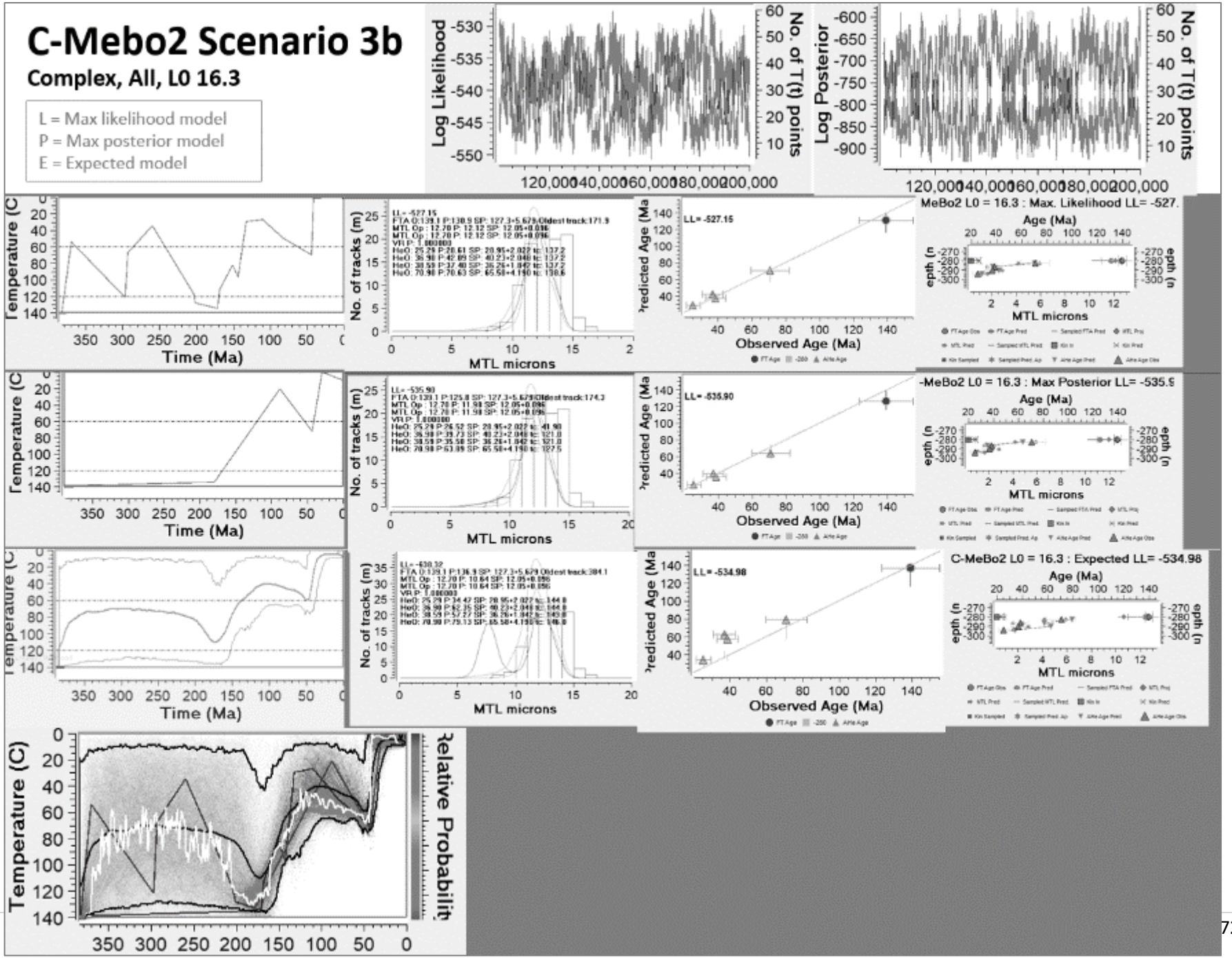
C-Mebo2 Scenario 3b
Complex, All, L0 16.3
L = Max likelihood model
P = Max posterior model
E = Expected model
Log Likelihood
No. of T(t) points
Log Posterior
No. of T(t) points
Temperature (C)
Time (Ma)
No. of tracks (m)
MTL microns
Predicted Age (Ma)
Observed Age (Ma)
LL= -527.15
MeBo2 L0 = 16.3 : Max. Likelihood LL= -527.
Age (Ma)
MTL microns
LL= -535.90
-MeBo2 L0 = 16.3 : Max Posterior LL= -535.9
LL= -534.98
C-MeBo2 L0 = 16.3 : Expected LL= -534.98
Temperature (C)
Relative Probability

2.3.6 26/30-1

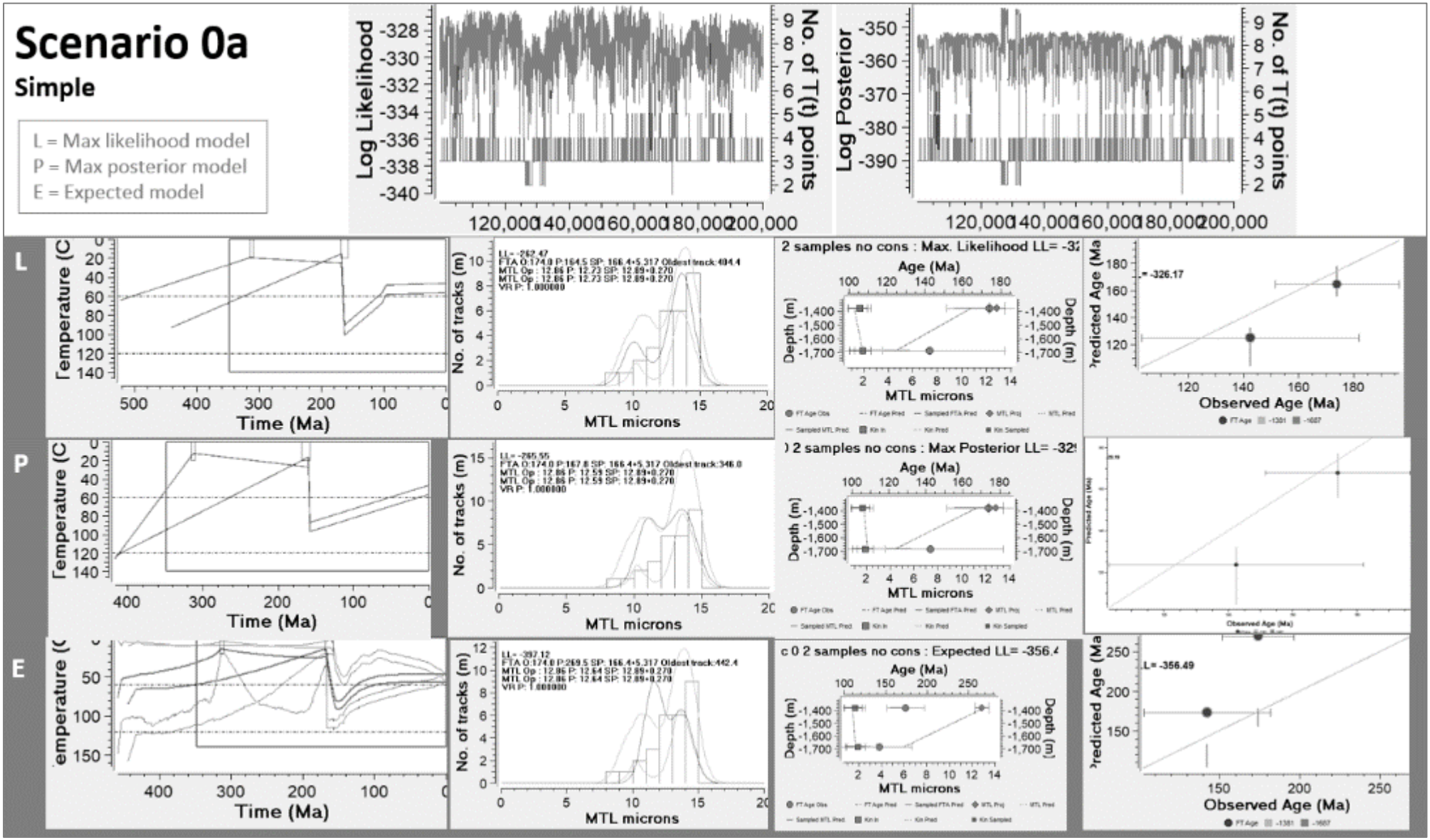
Scenario 0a
Simple
L = Max likelihood model
P = Max posterior model
E = Expected model
Log Likelihood
No. of T(t) points
Log Posterior
No. of T(t) points
L
P
E
Time (Ma)
No. of tracks (m)
MTL microns
2 samples no cons : Max. Likelihood LL= -32
) 2 samples no cons : Max Posterior LL= -32
c 0 2 samples no cons : Expected LL= -356.4
Age (Ma)
Depth (m)
MTL microns
Predicted Age (Ma)
Observed Age (Ma)
= -326.17
L= -356.49

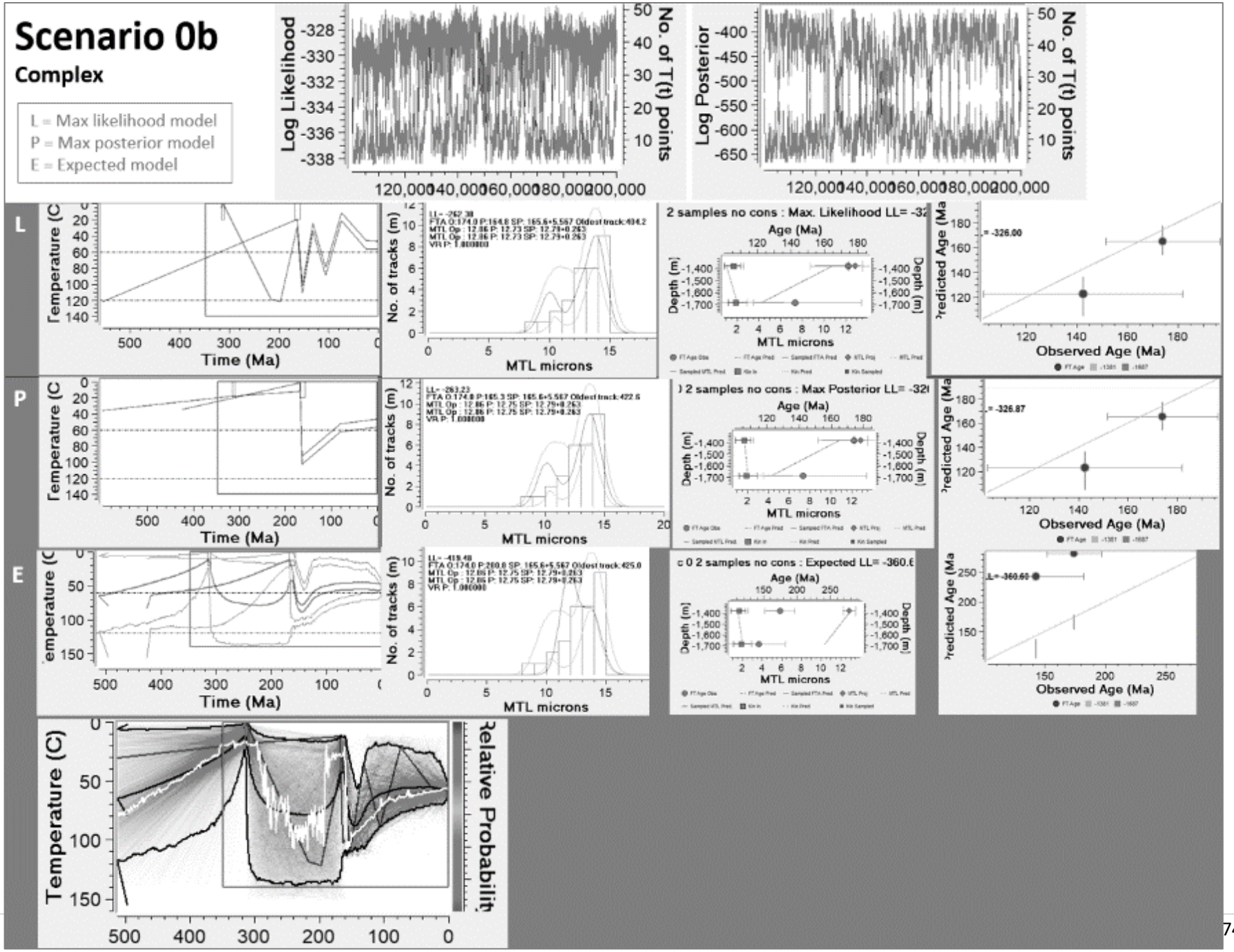
Scenario 0b
Complex
L = Max likelihood model
P = Max posterior model
E = Expected model
Log Likelihood
No. of T(t) points
Log Posterior
No. of T(t) points
L
P
E
Temperature (C)
Time (Ma)
No. of tracks (m)
MTL microns
2 samples no cons : Max. Likelihood LL= -32
2 samples no cons : Max Posterior LL= -32
c 0 2 samples no cons : Expected LL= -360.6
Age (Ma)
Depth (m)
Predicted Age (Ma)
Observed Age (Ma)
= -326.00
= -326.87
L= -360.60
Temperature (C)
Relative Probabilit

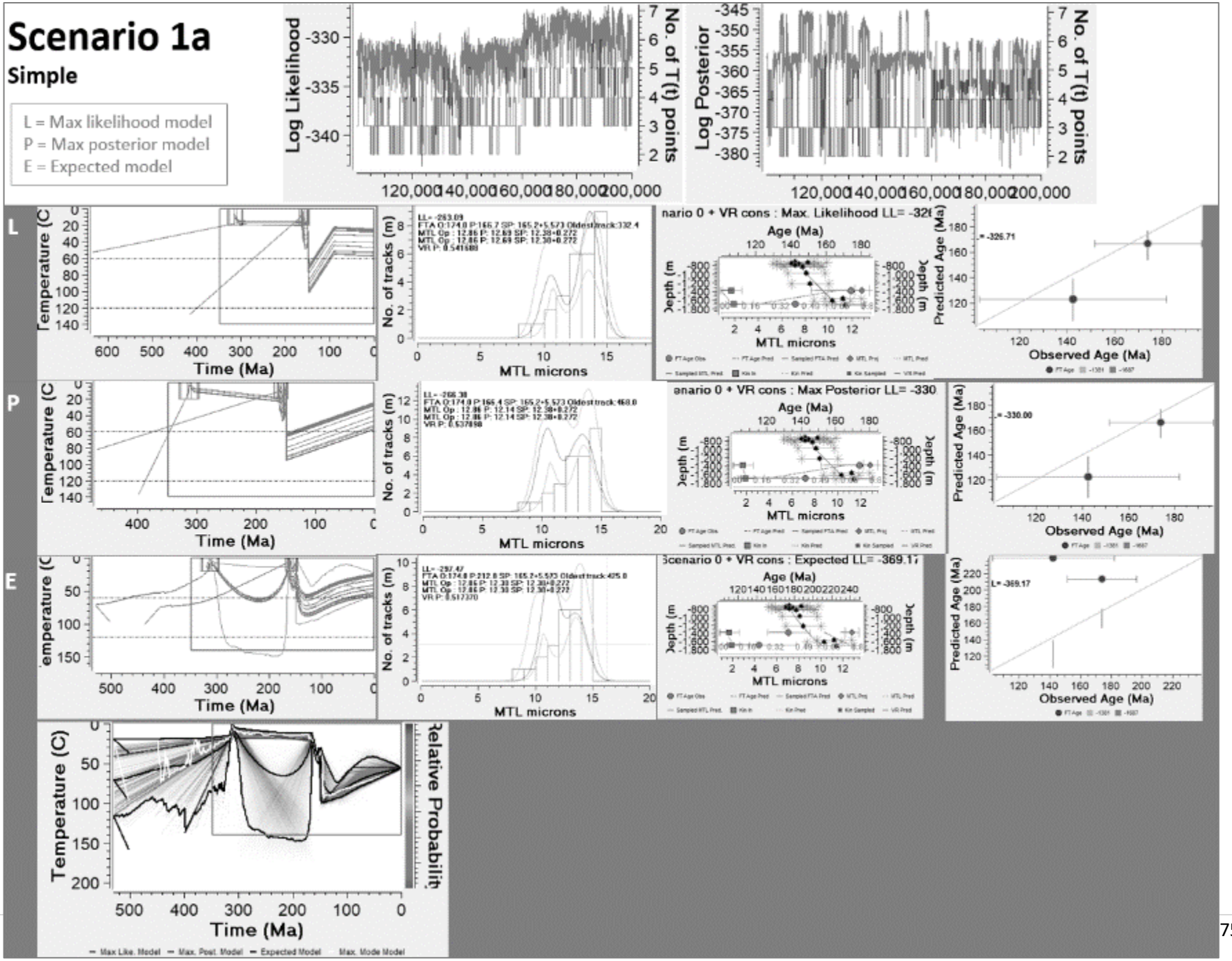
Scenario 1a
Simple
L = Max likelihood model
P = Max posterior model
E = Expected model
Log Likelihood
No. of T(t) points
Log Posterior
No. of T(t) points
L
P
E
Temperature (C)
Time (Ma)
No. of tracks (m)
MTL microns
Age (Ma)
Depth (m)
MTL microns
Predicted Age (Ma)
Observed Age (Ma)
Relative Probability
Max Like. Model
Max. Post. Model
Expected Model
Max. Mode Model

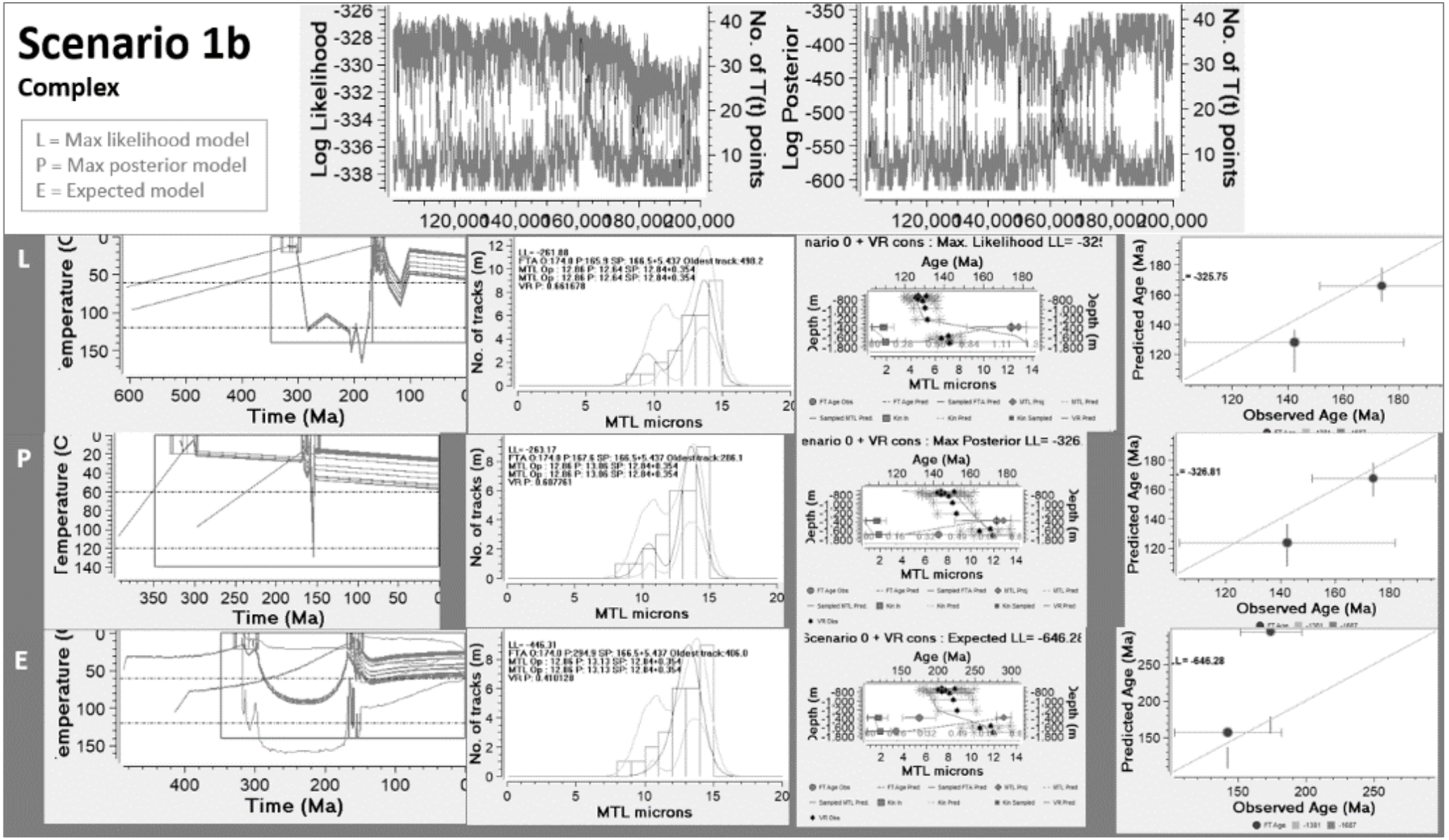
Scenario 1b
Complex
L = Max likelihood model
P = Max posterior model
E = Expected model
Log Likelihood
No. of T(t) points
Log Posterior
No. of T(t) points
120,000 140,000 160,000 180,000 200,000
L
P
E
Time (Ma)
No. of tracks (m)
MTL microns
Age (Ma)
Depth (m)
MTL microns
Predicted Age (Ma)
Observed Age (Ma)
= -325.75
= -326.81
L= -646.28

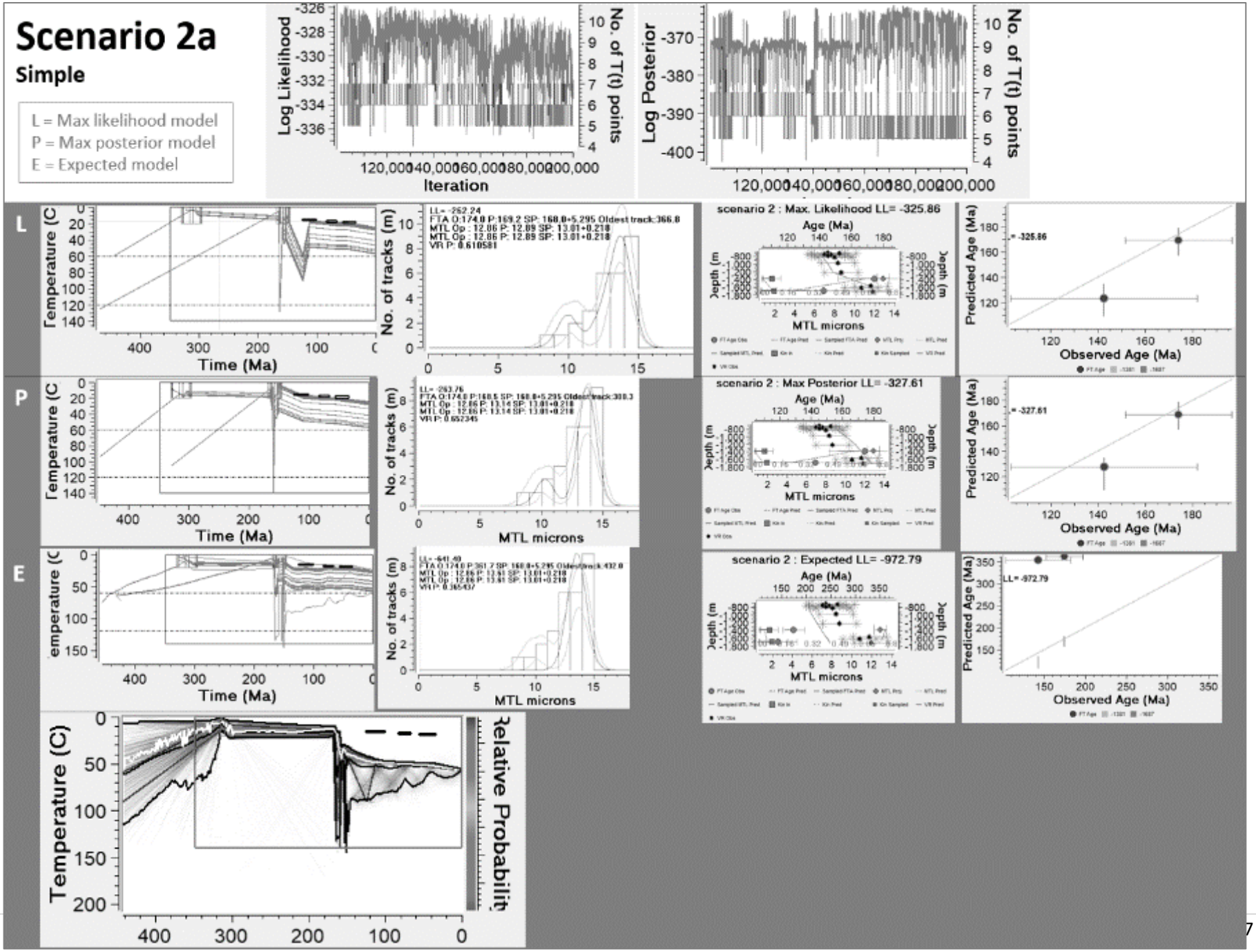
Scenario 2a
Simple
L = Max likelihood model
P = Max posterior model
E = Expected model
Log Likelihood
No. of T(t) points
Iteration
Log Posterior
No. of T(t) points
L
P
E
Temperature (C
Time (Ma)
No. of tracks (m)
MTL microns
scenario 2 : Max. Likelihood LL= -325.86
scenario 2 : Max Posterior LL= -327.61
scenario 2 : Expected LL= -972.79
Age (Ma)
Depth (m)
Predicted Age (Ma)
Observed Age (Ma)
Temperature (C)
Relative Probabilit

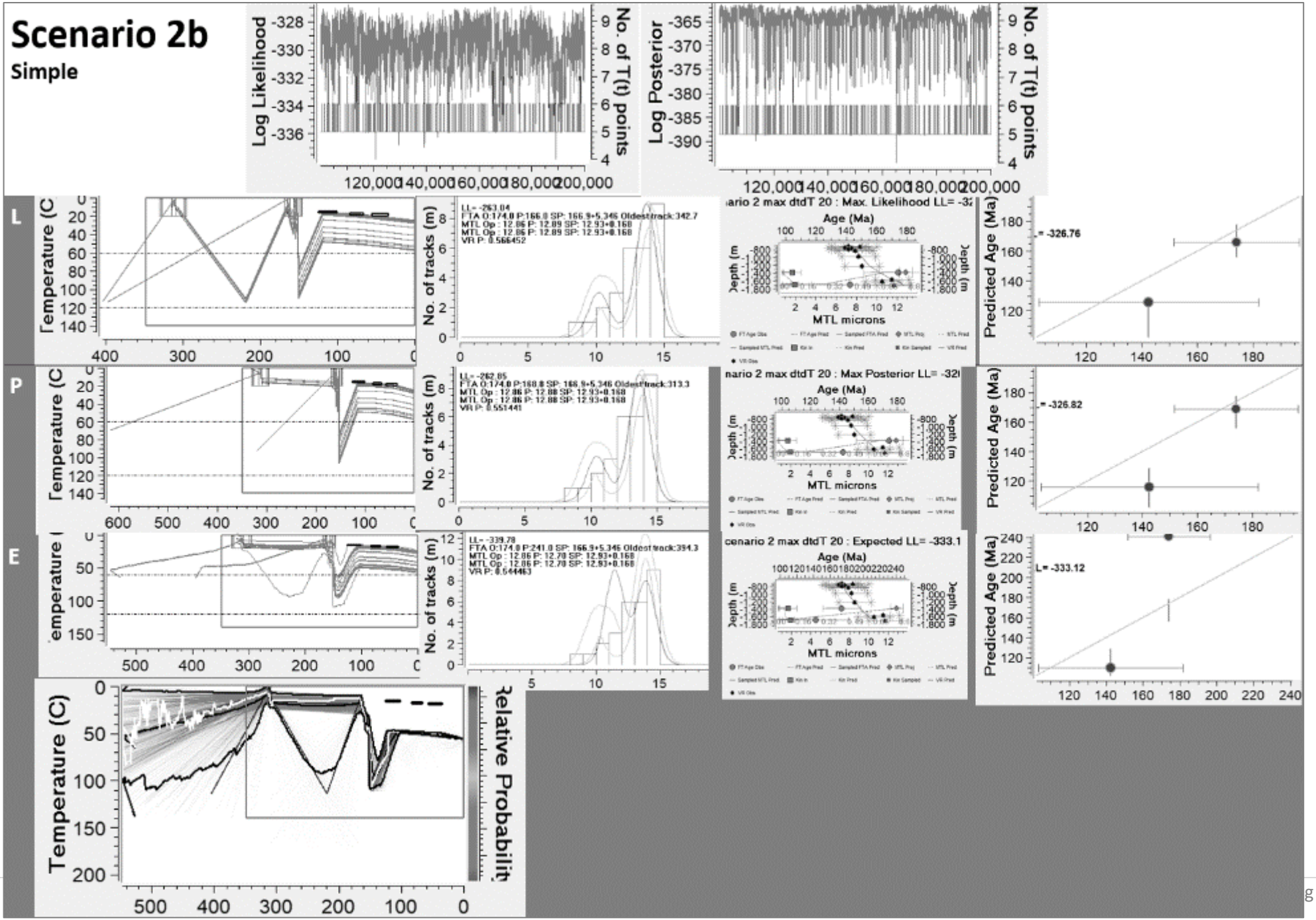
Scenario 2b
Simple
Log Likelihood
No. of T(t) points
Log Posterior
No. of T(t) points
L
P
E
Temperature (C)
No. of tracks (m)
MTL microns
Age (Ma)
Predicted Age (Ma)
= -326.76
= -326.82
L= -333.12
Temperature (C)
Relative Probability

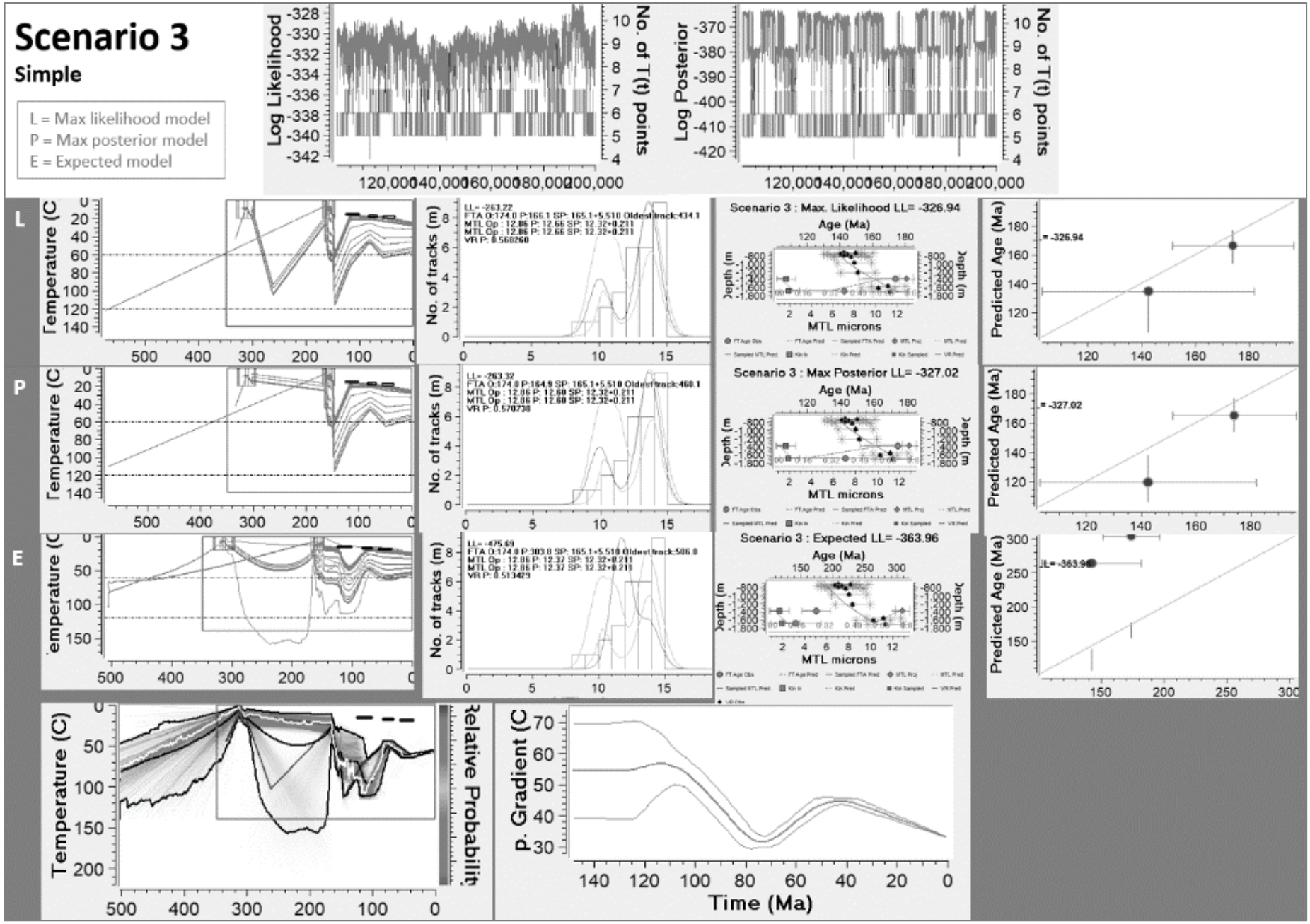
Scenario 3
Simple
L = Max likelihood model
P = Max posterior model
E = Expected model
Log Likelihood
No. of T(t) points
Log Posterior
No. of T(t) points
L
P
E
Temperature (C
No. of tracks (m)
Scenario 3 : Max. Likelihood LL= -326.94
Scenario 3 : Max Posterior LL= -327.02
Scenario 3 : Expected LL= -363.96
Age (Ma)
Depth (m
MTL microns
Predicted Age (Ma)
Temperature (C)
Relative Probabilit
p. Gradient (C
Time (Ma)

2.4 Southern zone

2.4.1 Stability of the log likelihood and posterior chains

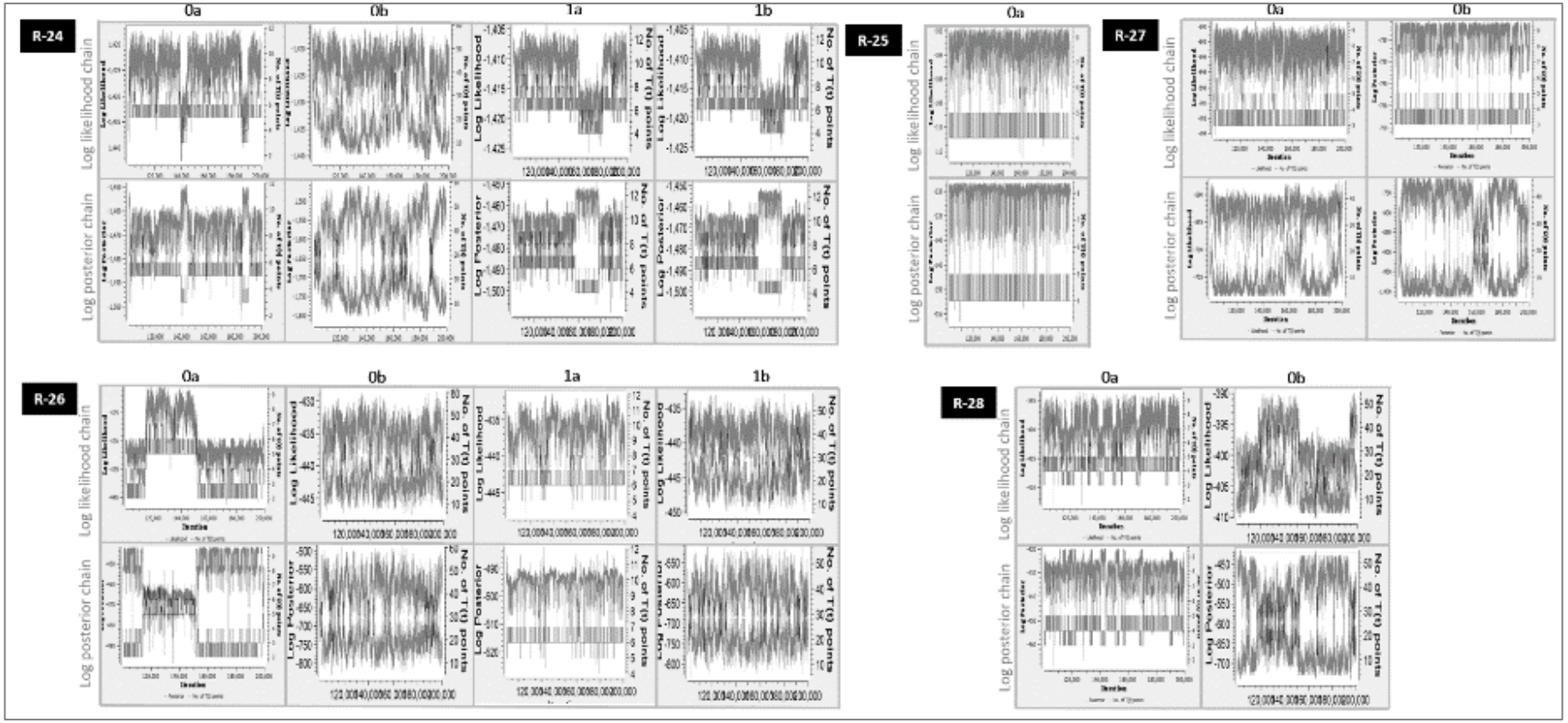

2.4.2 R-24

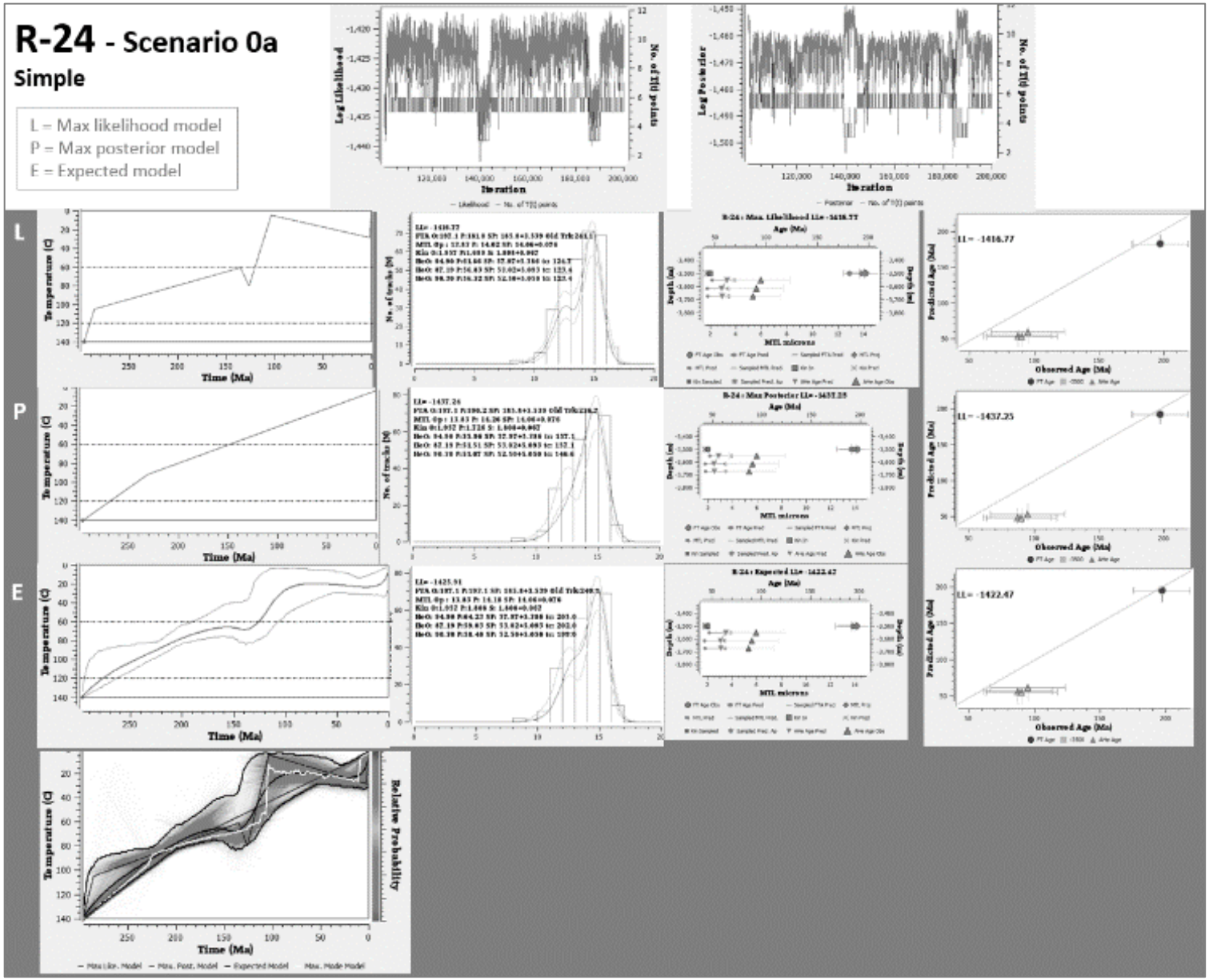
R-24 - Scenario 0a
Simple
L = Max likelihood model
P = Max posterior model
E = Expected model
Iteration
Log Likelihood
Log Posterior
No. of T[t] points
L
P
E
Temperature (C)
Time (Ma)
No. of tracks (N)
Depth (m)
MTL microns
Age (Ma)
Predicted Age (Ma)
Observed Age (Ma)
Relative Probability
Max Lik. Model
Max. Post. Model
Expected Model
Max. Mode Model

R-24 - Scenario 0b

Complex

L = Max likelihood model
P = Max posterior model
E = Expected model

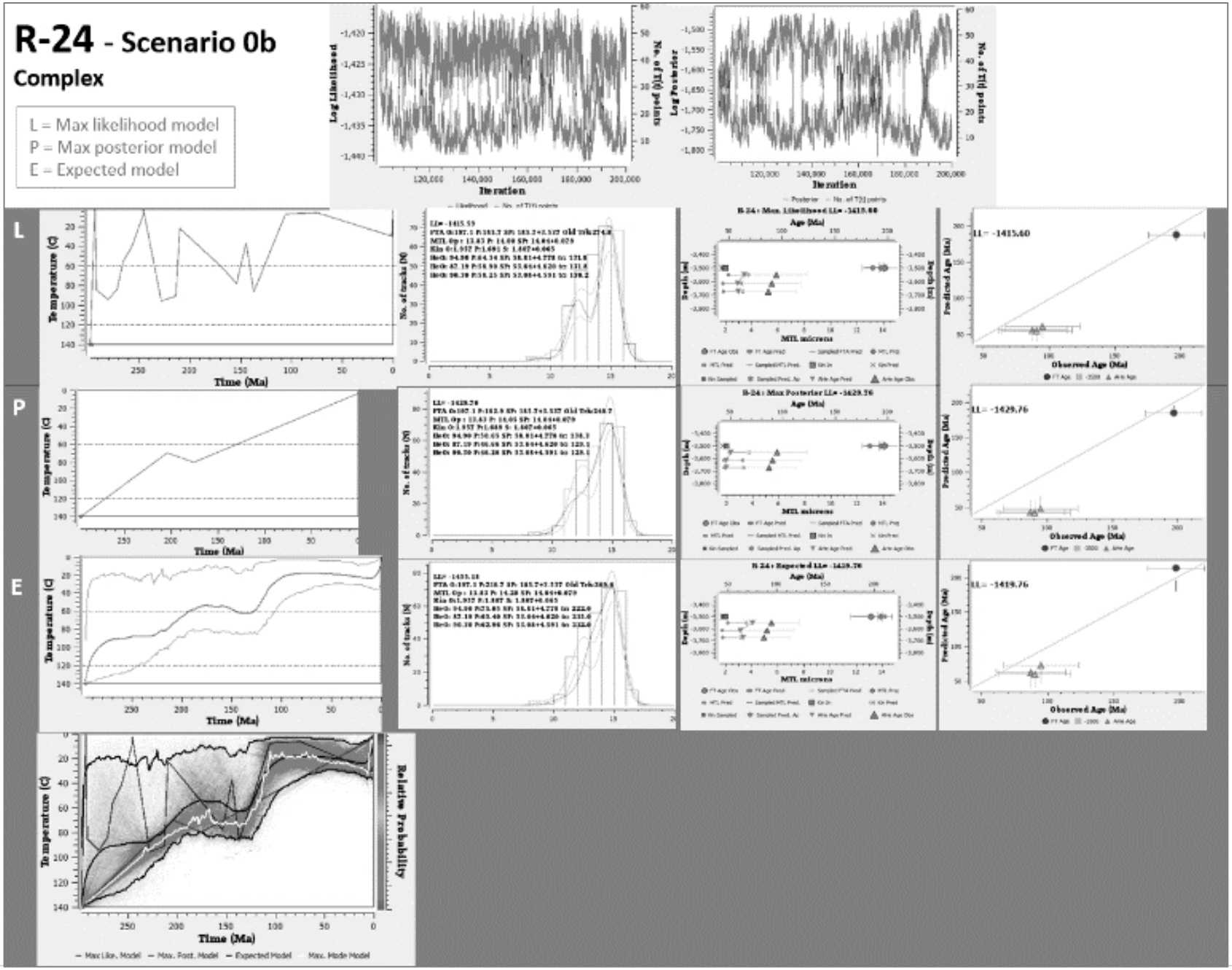

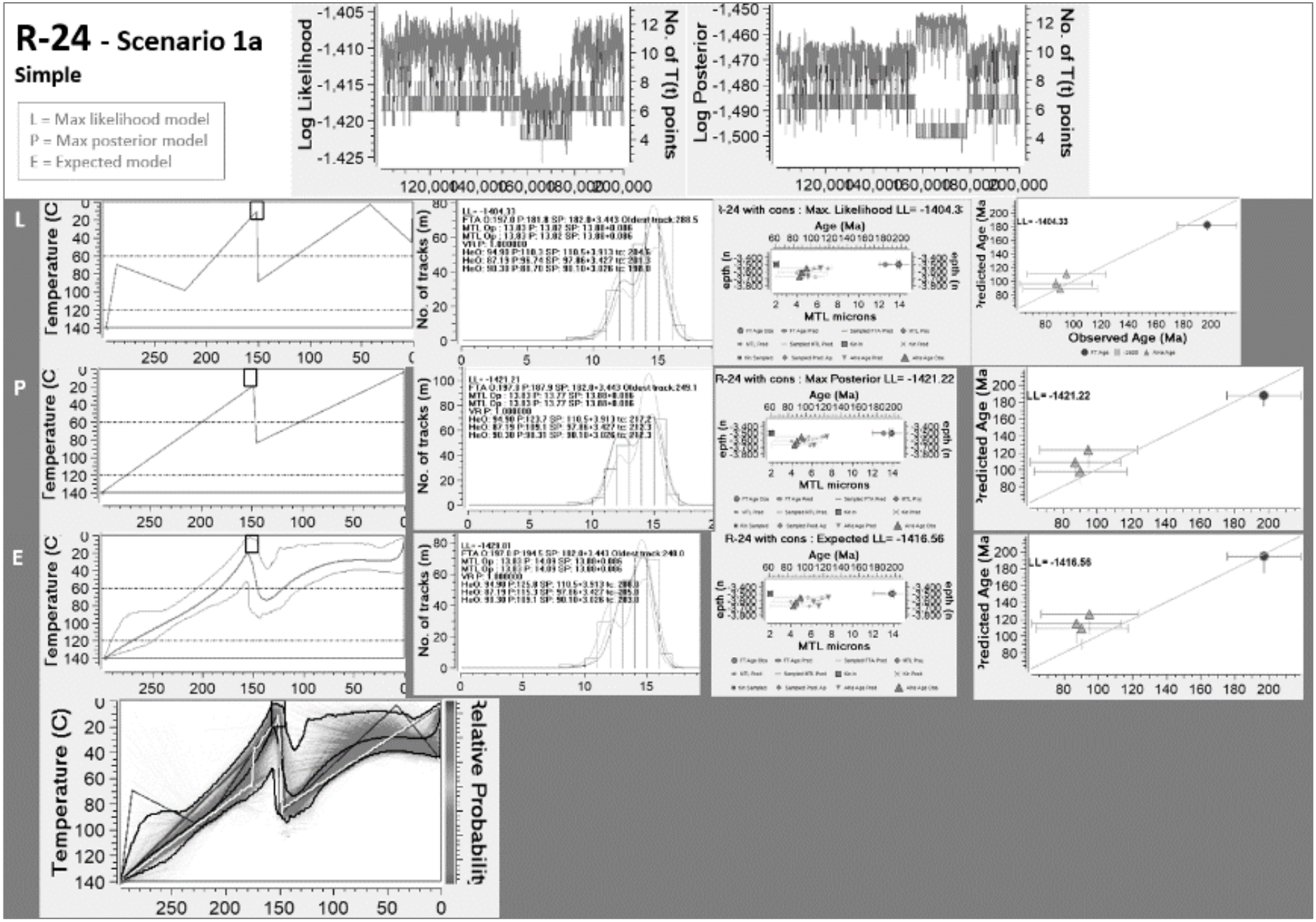
R-24 - Scenario 1a
Simple
L = Max likelihood model
P = Max posterior model
E = Expected model
Log Likelihood
No. of T(t) points
Log Posterior
No. of T(t) points
L
P
E
Temperature (C)
No. of tracks (m)
R-24 with cons : Max. Likelihood LL= -1404.33
R-24 with cons : Max Posterior LL= -1421.22
R-24 with cons : Expected LL= -1416.56
Age (Ma)
MTL microns
Predicted Age (Ma)
Observed Age (Ma)
LL= -1404.33
LL= -1421.22
LL= -1416.56
Temperature (C)
Relative Probability

R-24 - Scenario 1b

Complex

L = Max likelihood model
P = Max posterior model
E = Expected model

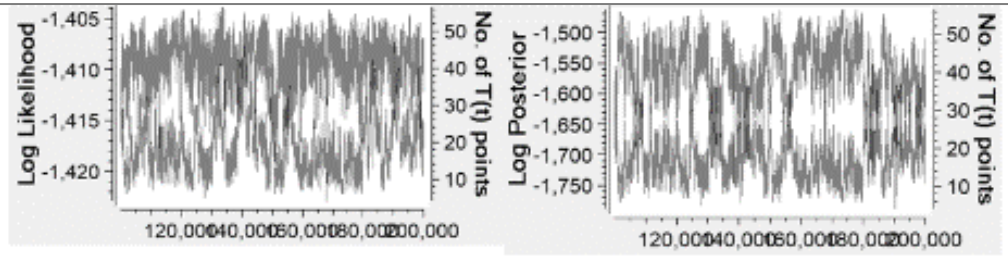

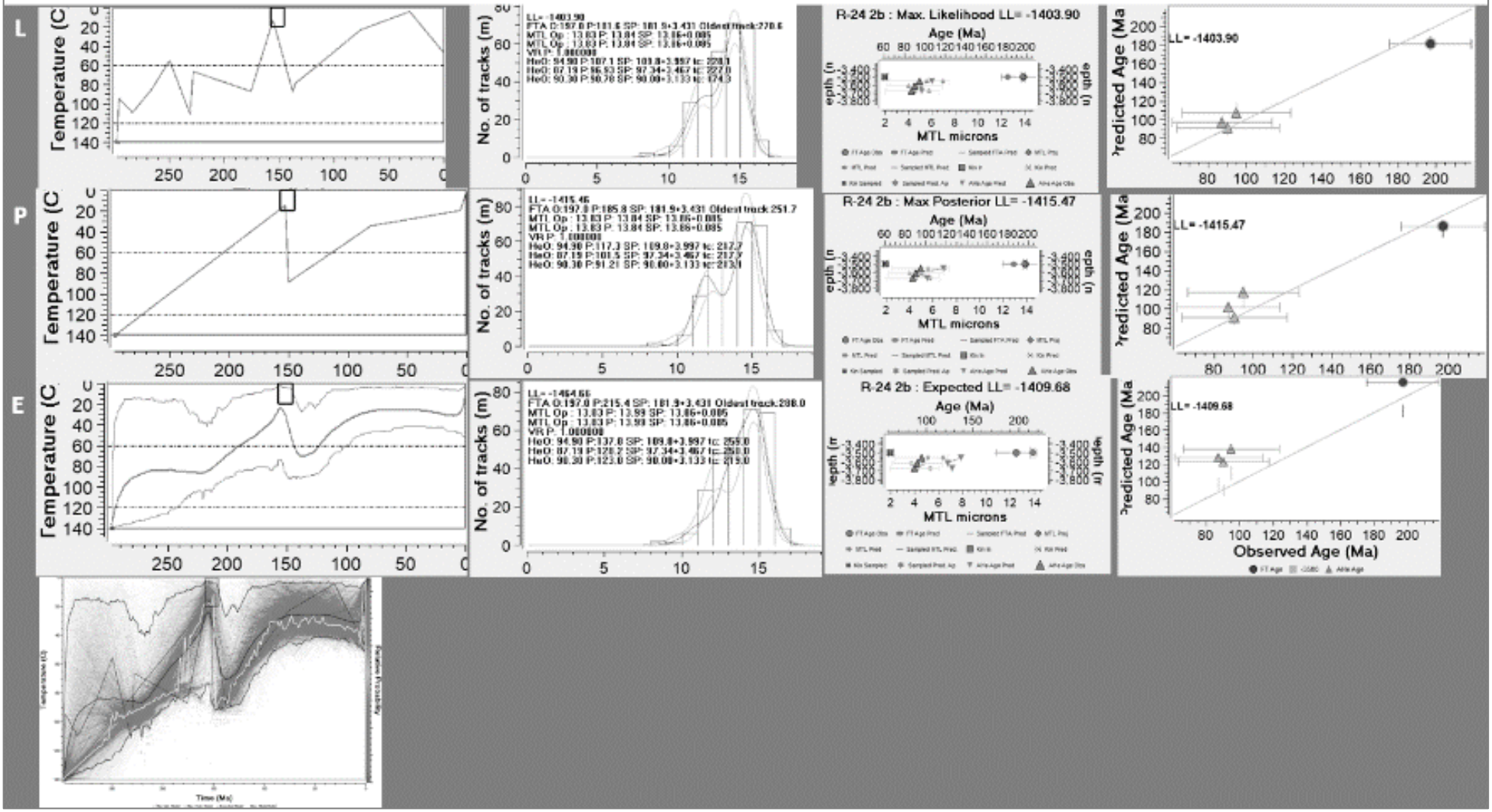

2.4.3 R-25

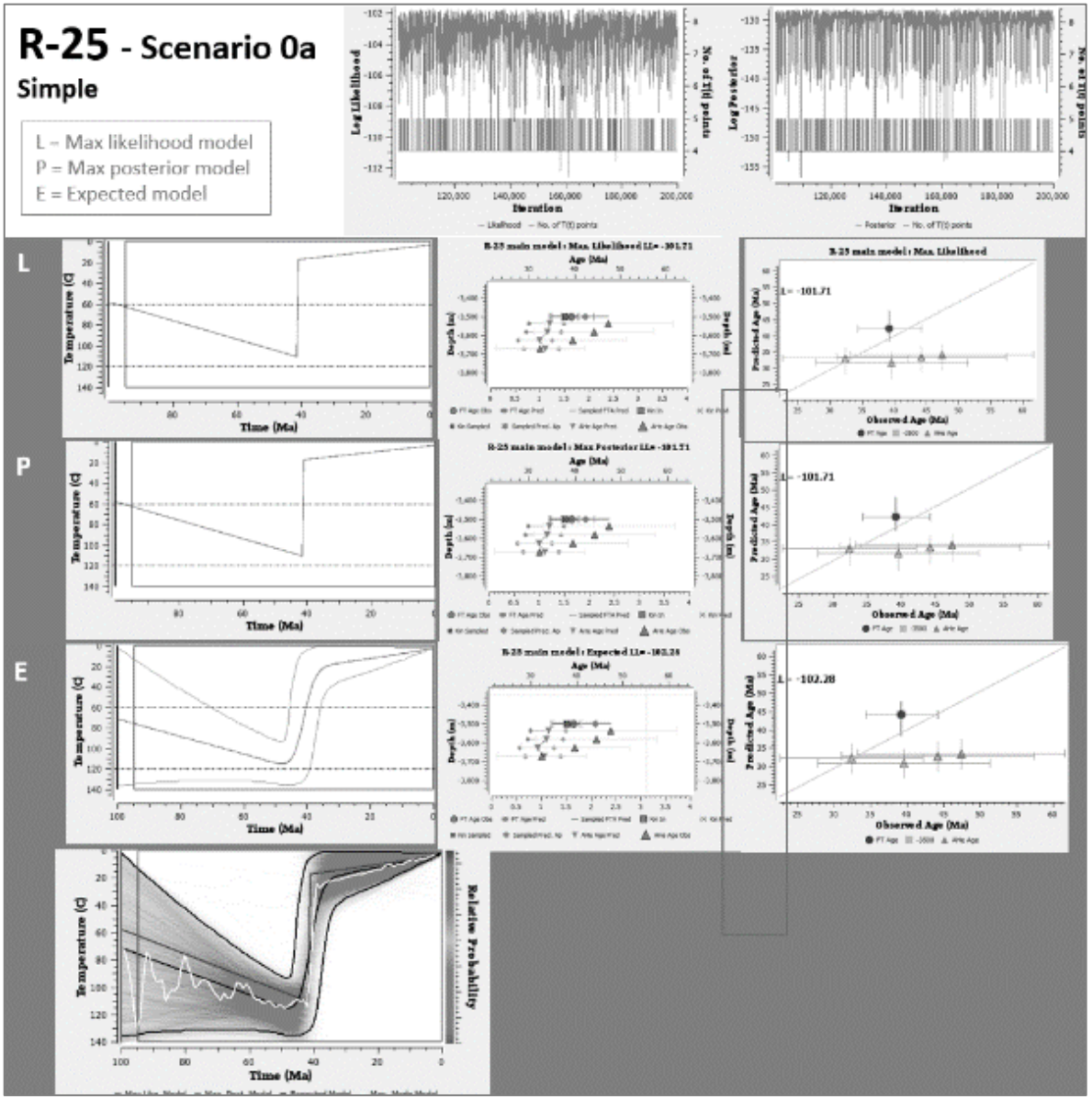
R-25 - Scenario 0a
Simple
L = Max likelihood model
P = Max posterior model
E = Expected model
Log Likelihood
No. of T(i) points
Iteration
Log Posterior
L
P
E
Temperature (C)
Time (Ma)
Depth (m)
Age (Ma)
Predicted Age (Ma)
Observed Age (Ma)
L = -101.71
L = -102.28
Relative Probability

2.4.4 R-26

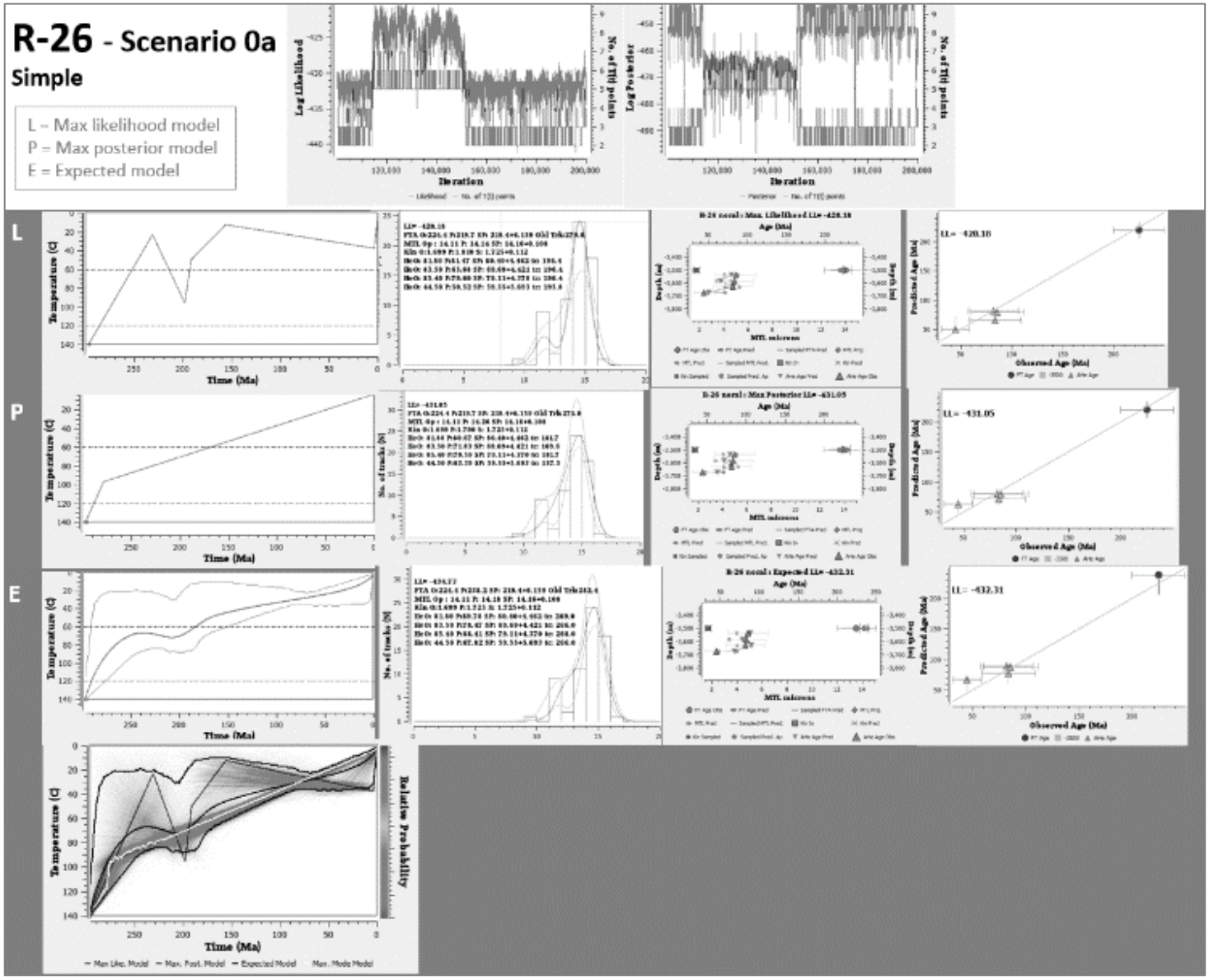
R-26 - Scenario 0a
Simple
L = Max likelihood model
P = Max posterior model
E = Expected model
Log Likelihood
Log Posterior
No. of TH points
Iteration
L
P
E
Temperature (C)
Time (Ma)
No. of tracks (N)
Depth (m)
MTL inkorrect
Predicted Age (Ma)
Observed Age (Ma)
Relative probability
Max Like. Model
Max. Post. Model
Expected Model
Max. Mode Model

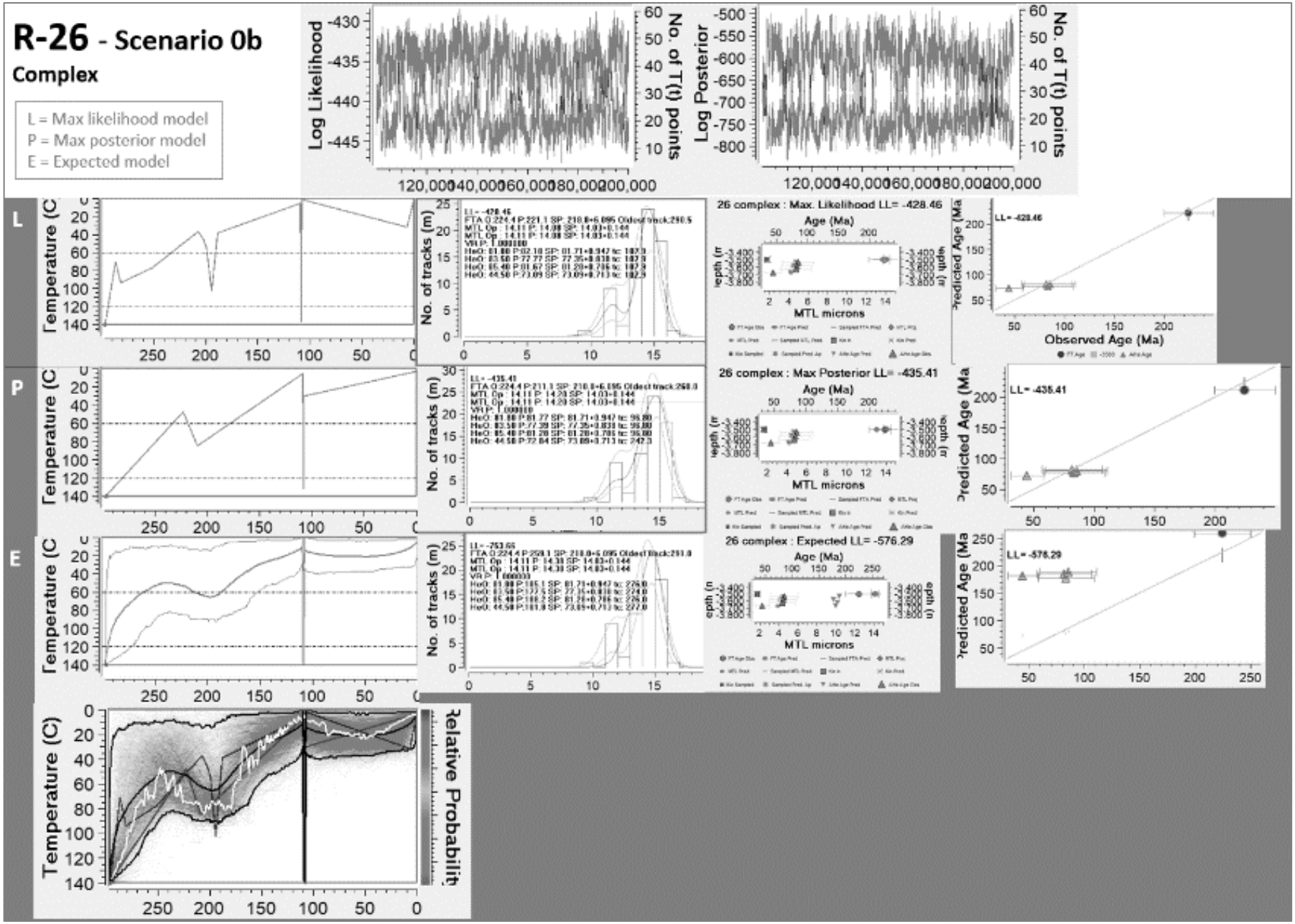
R-26 - Scenario 0b
Complex
L = Max likelihood model
P = Max posterior model
E = Expected model
Log Likelihood
No. of T(t) points
Log Posterior
No. of T(t) points
120,000
140,000
160,000
180,000
200,000
L
P
E
Temperature (C
No. of tracks (m)
26 complex : Max. Likelihood LL= -428.46
26 complex : Max Posterior LL= -435.41
26 complex : Expected LL= -576.29
Age (Ma)
MTL microns
Predicted Age (Ma)
Observed Age (Ma)
LL= -428.46
LL= -435.41
LL= -576.29
Temperature (C)
Relative Probabilit

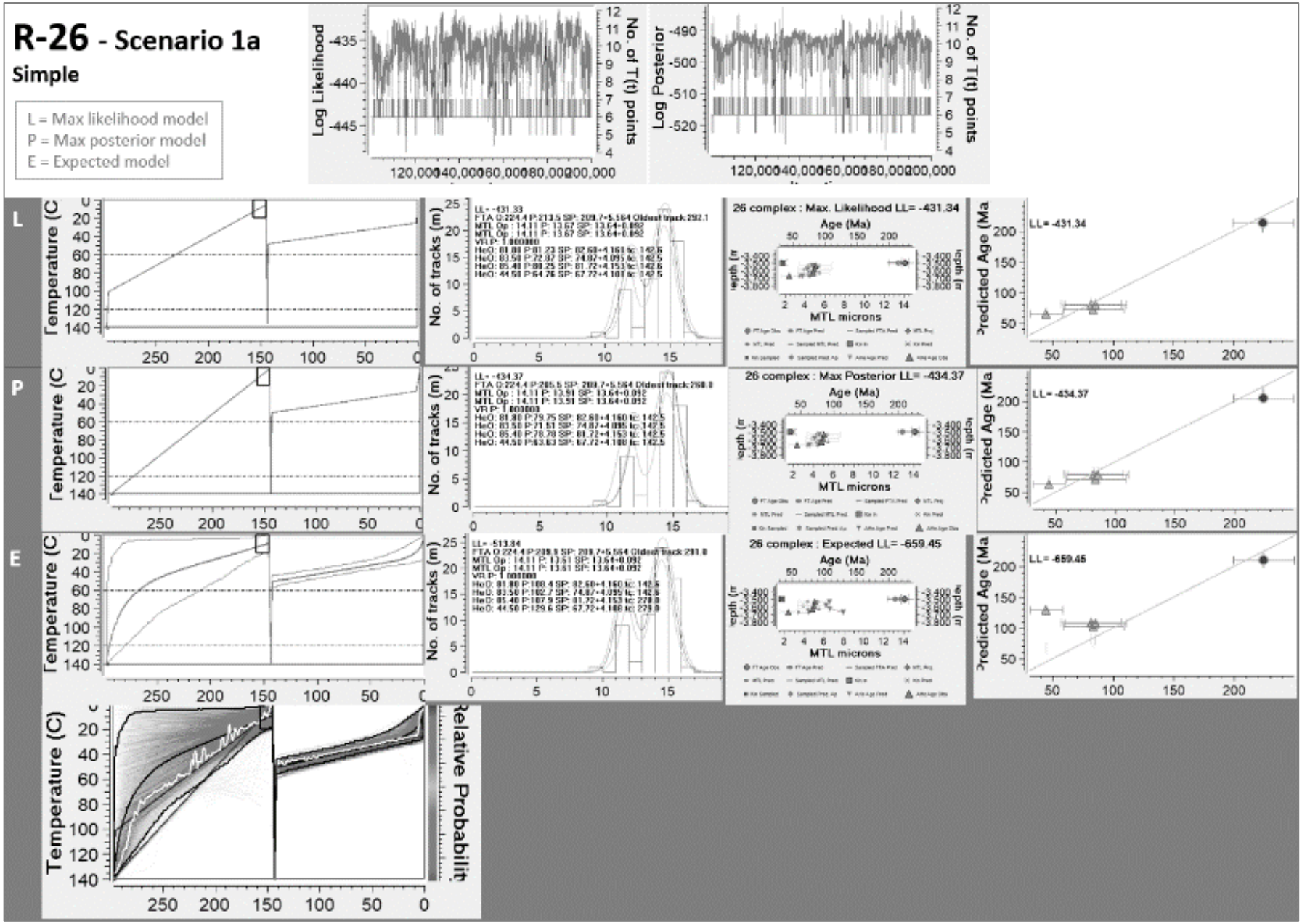
R-26 - Scenario 1a
Simple
L = Max likelihood model
P = Max posterior model
E = Expected model
Log Likelihood
No. of T(t) points
Log Posterior
No. of T(t) points
L
P
E
Temperature (C
No. of tracks (m)
26 complex : Max. Likelihood LL= -431.34
26 complex : Max Posterior LL= -434.37
26 complex : Expected LL= -659.45
Age (Ma)
MTL microns
Predicted Age (Ma
LL= -431.34
LL= -434.37
LL= -659.45
Temperature (C)
Relative Probabilit

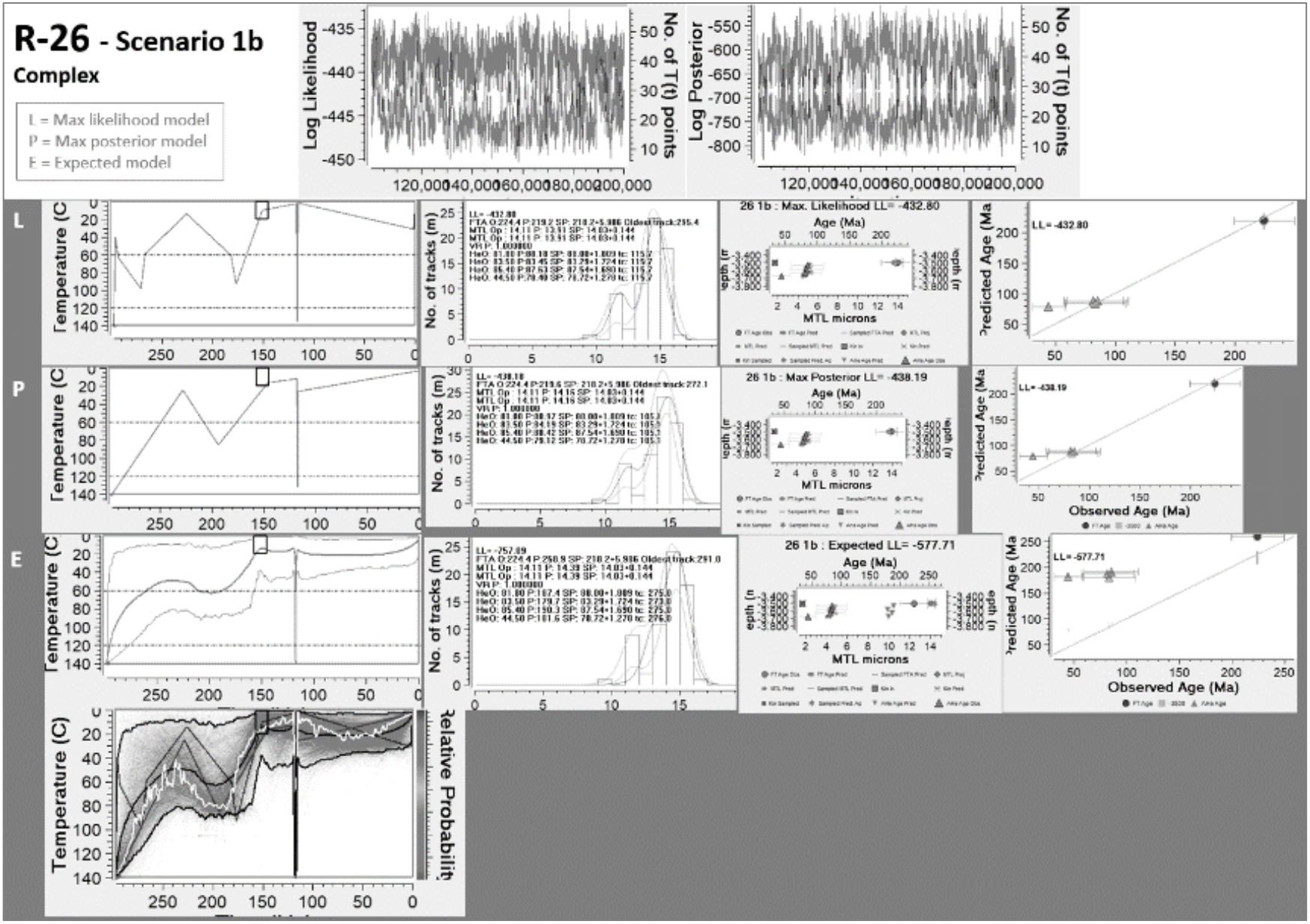
R-26 - Scenario 1b
Complex
L = Max likelihood model
P = Max posterior model
E = Expected model
Log Likelihood
No. of T(t) points
Log Posterior
No. of T(t) points
120,000 40,000 60,000 80,000 100,000
L
P
E
Temperature (C)
No. of tracks (m)
26 1b : Max. Likelihood LL= -432.80
26 1b : Max Posterior LL= -438.19
26 1b : Expected LL= -577.71
Age (Ma)
MTL microns
Predicted Age (Ma)
Observed Age (Ma)
LL= -432.80
LL= -438.19
LL= -577.71
Relative Probability

2.4.5 R-27

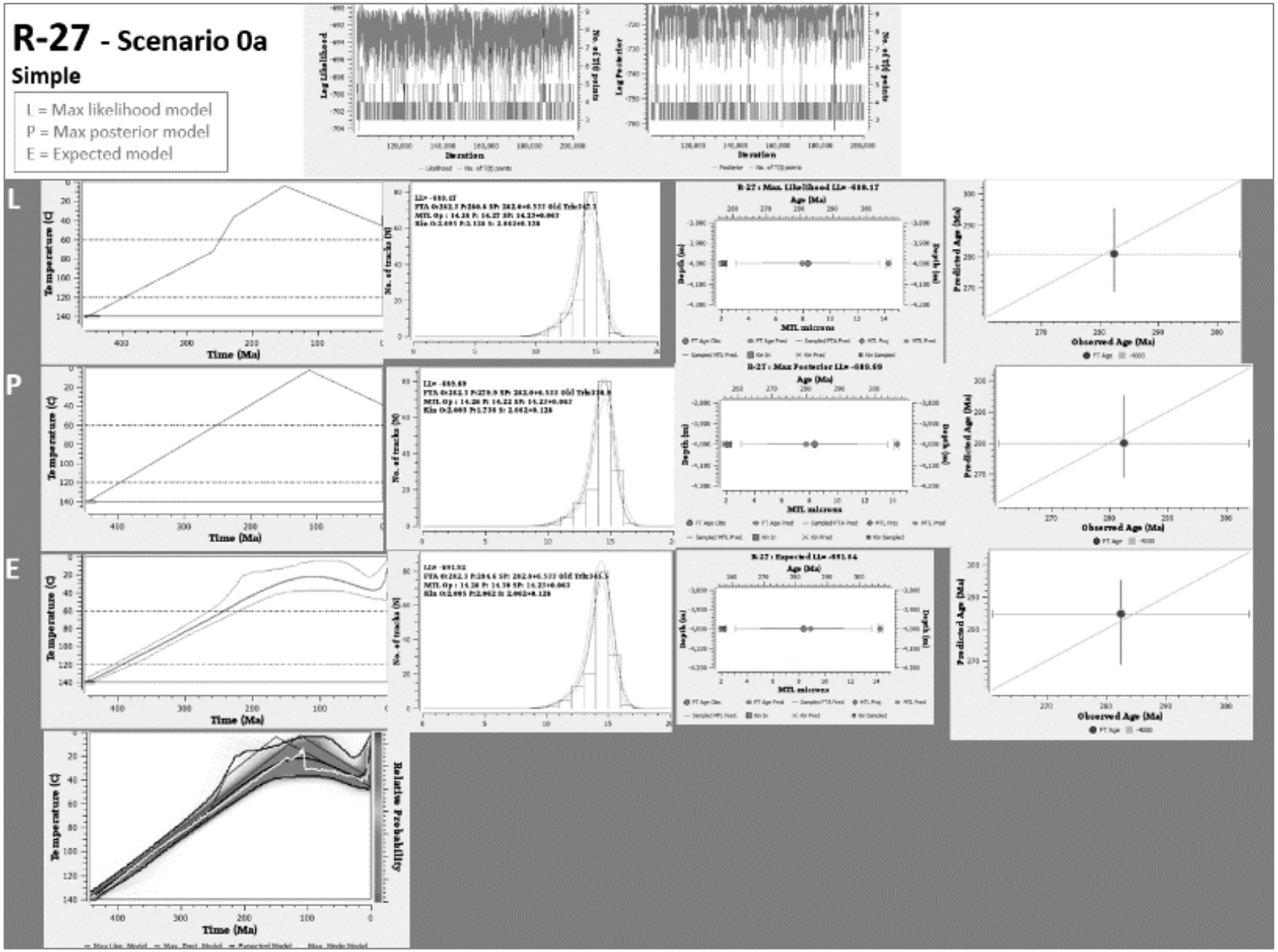
R-27 - Scenario 0a
Simple
L = Max likelihood model
P = Max posterior model
E = Expected model
L
P
E
Temperature (C)
Time (Ma)
No. of tracks (N)
Depth (m)
MIL microns
Predicted Age (Ma)
Observed Age (Ma)
Relative Probability

R-27 - Scenario 0b

Complex

L – Max likelihood model
P – Max posterior model
E – Expected model

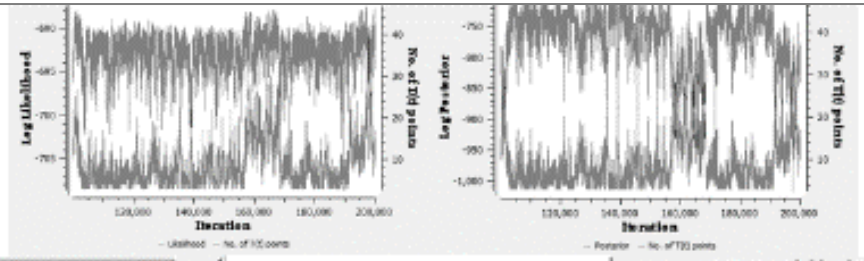

L

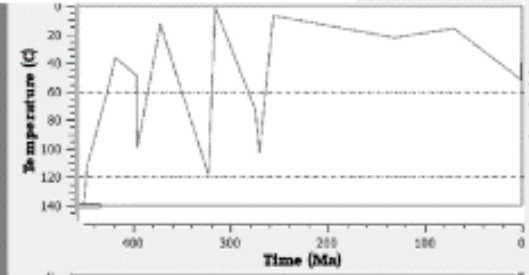

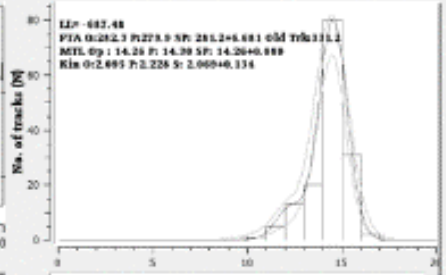

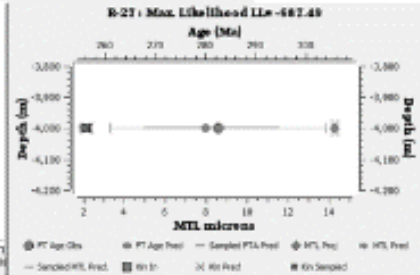

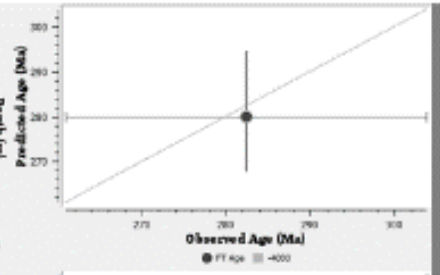

P

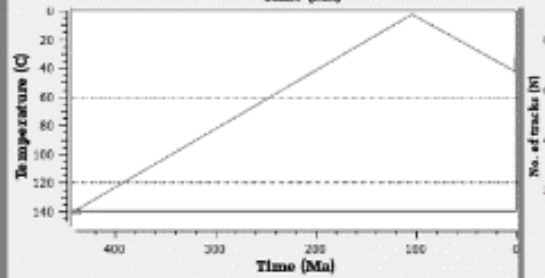

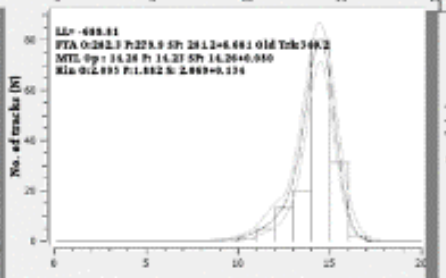

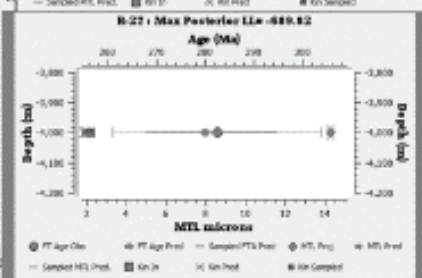

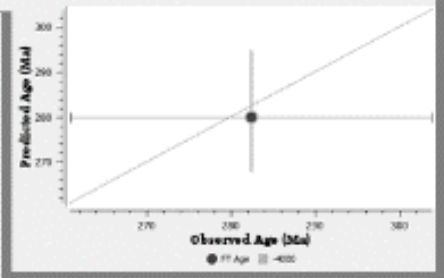

E

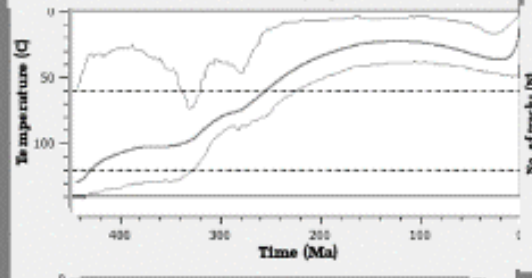

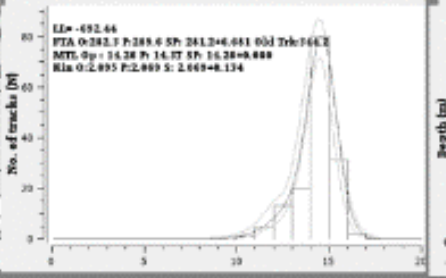

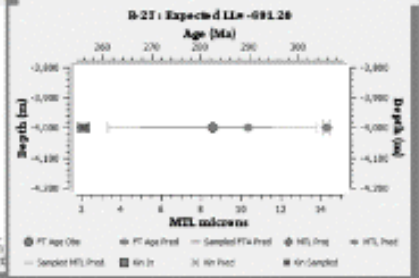

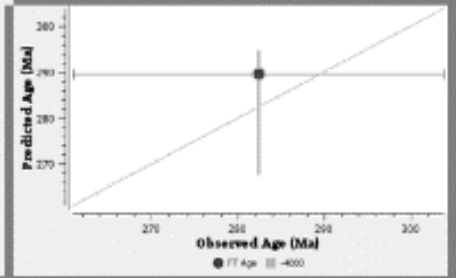

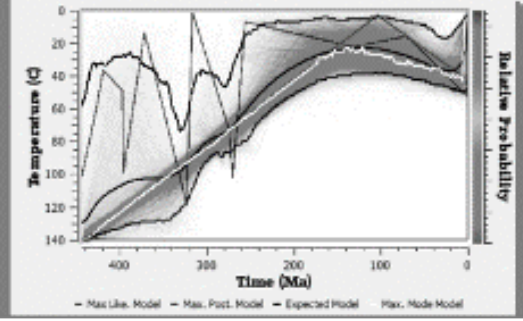

2.4.6 R-28

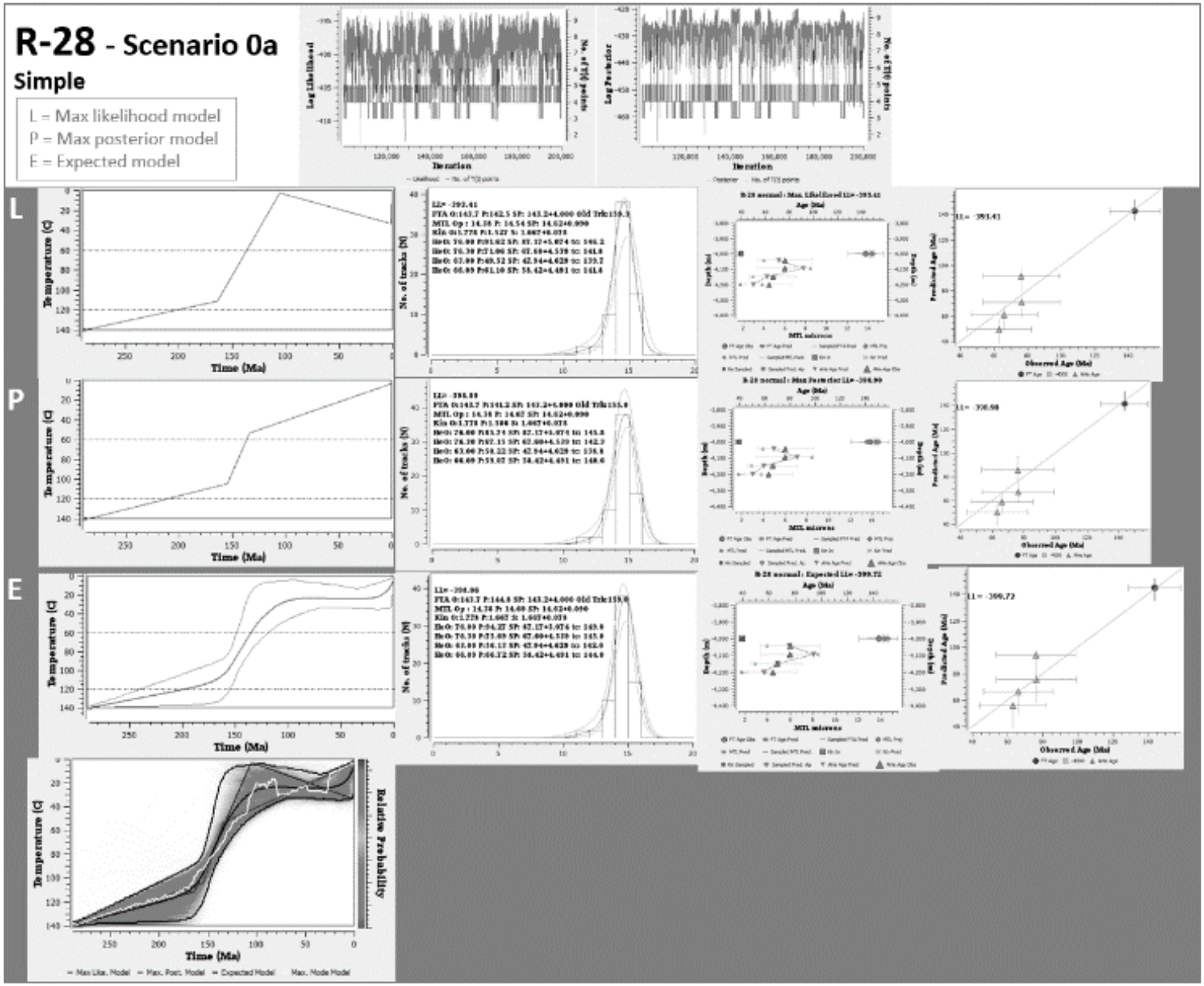
R-28 - Scenario 0a
Simple
L = Max likelihood model
P = Max posterior model
E = Expected model
L
P
E
Temperature (C)
Time (Ma)
No. of tracks (N)
Log Likelihood
Log Posterior
Iteration
No. of T(t) points
Observed Age (Ma)
Predicted Age (Ma)
MTL microns
Relative Probability

R-28 - Scenario 0b

Complex

L = Max likelihood model
P = Max posterior model
E = Expected model

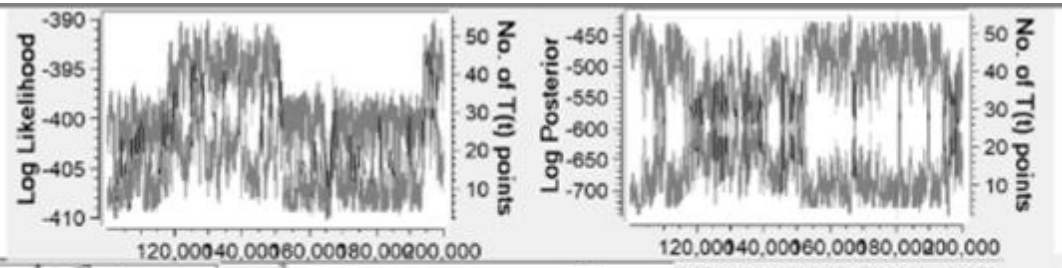

L

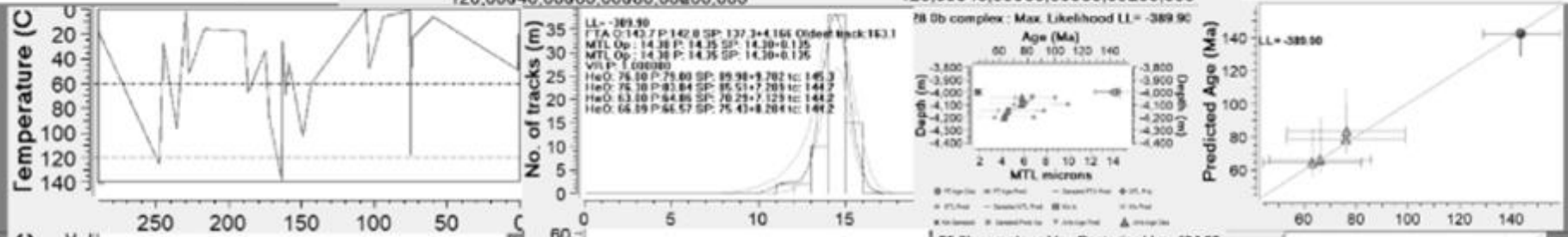

P

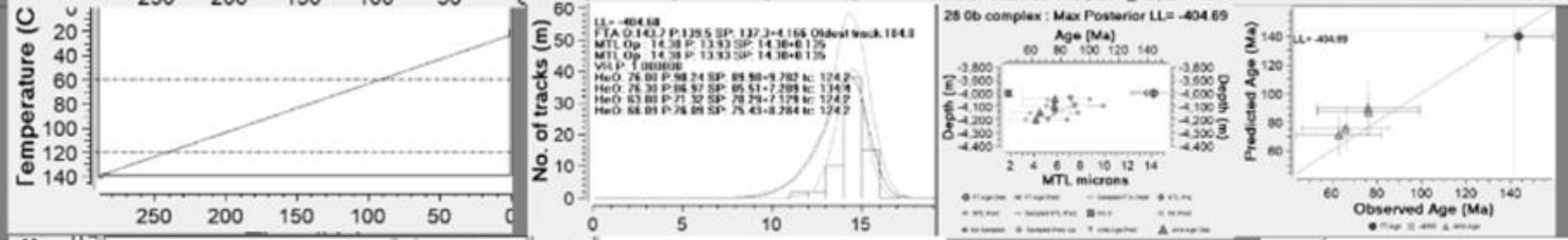

E